

**Electrical restitution and action potential  
repolarisation studies in acutely isolated  
cardiac ventricular myocytes**

**Thesis submitted for the degree of  
Doctor of Philosophy  
at the University of Leicester**

**By**

**Rawan A. Khuwaileh, MD  
Department of Molecular and Cell Biology  
University of Leicester**

**2016**

**Electrical restitution and action potential repolarisation studies in acutely isolated cardiac ventricular myocytes**

Cardiac death is a major clinical problem that most commonly results from ventricular arrhythmias. Electrical restitution, which is the relationship between action potential duration (APD) and diastolic interval (DI), is a determinant of the risk of ventricular fibrillation (VF), a leading cause of sudden cardiac death. The maximum slope of the electrical restitution curve is an indicator of the risk of VF. Steep maximum slopes indicate an increased risk of arrhythmia. The aim of the project was to study electrical restitution in single cells and investigate the effect modulators of the nitric oxide (NO) pathways have on action potentials. Experiments were done on acutely isolated left ventricular guinea-pig myocytes at 37<sup>0</sup>C using the perforated patch clamp technique. The diurnal variation in electrical restitution was also studied by isolating myocytes during the active or resting periods for guinea-pigs. The active period myocytes were more prone to arrhythmias than the resting period cells as the maximum slope of the electrical restitution curve was steeper in the active period myocytes under basal conditions ( $P \leq 0.01$ ). Inhibition of NO synthases (NOS) caused substantial shortening of APD<sub>90</sub> at high stimulation frequencies (4 and 5 Hz) by 35 ms, 39 ms respectively, in active compared to resting period cells but only following  $\beta$ -adrenergic receptor ( $\beta$ -AR) stimulation with isoprenaline (ISO). These effects are consistent with NO inhibiting effects of ISO on cardiac repolarisation (a protective effect) seen on whole heart studies. While comparing the response to ISO of the active versus resting period myocytes at each stimulation frequency, showed that there was a statistically significant shortening at 1 Hz by 18 ms ( $P \leq 0.001$ ) and at 2 Hz by 19 ms ( $P \leq 0.05$ ); with the resting period myocytes being more responsive. Applying NO signalling pathway modulators failed to modulate the electrical restitution curve. However, during constant pacing (2 Hz) experiments, NO signalling pathway modulators changed action potential (AP) duration in the presence of ISO. Enhancing the effect of cGMP-dependent pathway by adding the soluble guanylyl cyclase activatore BAY 60-2770 prolonged APD<sub>90</sub> by 20.5 ms ( $P \leq 0.05$ ), while enhancing S-nitrosylation by inhibiting S-nitrosoglutathione reductase with N6022 shortened APD<sub>90</sub> by 49.2 ms which was statistically significant ( $P \leq 0.05$ ). In conclusion, NO modulate cardiac repolarization of single cells in the presence of  $\beta$ -AR stimulation through a complex interplay of both cGMP-dependent and nitrosylation dependent mechanisms. However, NO modulation did not affect the electrical restitution slope in single myocytes.

The effect of the bradycardiogenic drug ivabradine on AP repolarization was also studied ivabradine had variable effect on AP repolarization. However, the main finding was shortening of APD<sub>90</sub> which suggests it affects predominantly currents other than I<sub>Kr</sub>.

## **Acknowledgements**

First, I would like to thank my supervisor Dr John Mitcheson, and my committee members Dr Kieran Brack and Dr Volko Straub for their advice; guidance and support that helped me produce this work. In particular, I am grateful to John for his endless support and help through my PhD. My thanks also go to Professor André Ng for his valuable comments on my data. Many thanks to Dr Noel Davies for creating software that made my data analysis much easier. I would also like to extend my gratefulness to Dr Richard Rainbow for teaching me how to isolate myocytes. I would also like to thank Rachel Caves and other members of the laboratory for their assistance throughout the course of my PhD.

My thanks go to my Father (Abdulla), Mother (Entisar) for making me smile when things got tough, Tareq, Bassam, Difaf, Hamza, and Bakir. I'm eternally grateful for your support, especially during the last few months. My warmest thanks go to my father-in-law and mother-in-law for encouraging me to do my best. Last, but certainly not least, my sincerest appreciation goes to Muneer, without whom it would be difficult to reach this point. Thanks for believing in me and supporting me. Thanks for putting up with me working countless late nights.

## **Contents**

Title	i
Abstract	ii
Acknowledgements	iii
Contents	iv
Publications	ix
Abbreviations	x

## **Chapter 1. Introduction**

1.1	Electrophysiology of the heart.....	1
1.1.1	Background.....	1
1.1.2	The action potential.....	2
1.1.2.1	Ionic equilibrium potentials of cardiac cells.....	2
1.1.2.2	Regional heterogeneity of the cardiac action potential.....	4
1.1.2.3	Phases of the ventricular action potential.....	5
1.1.2.4	Refractoriness of the ventricular action potential.....	6
1.1.2.5	Phases of the pacemaker action potential.....	8
1.1.3	Cardiac ion channels.....	9
1.1.3.1	Channels nomenclature.....	9
1.1.3.2	Cardiac ion channels and gating subtypes.....	10
1.1.3.3	Overview of the structure and kinetics of the main ion channels in cardiac muscle.....	12
1.1.4	Cardiac excitation-contraction coupling.....	20
1.1.4.1	Cardiac relaxation.....	22
1.2	Cardiac electrophysiology abnormalities.....	22
1.2.1	Background of cardiac arrhythmia and sudden cardiac death.....	25
1.2.2	Electrical restitution.....	27
1.2.2.1	Electrical restitution definition and link to arrhythmia.....	27
1.2.3	Ionic mechanisms of electrical restitution.....	29
1.3	Autonomic control of the heart.....	33
1.3.1	The effects of ANS on electrical restitution curve and VF risk.....	33
1.3.2	Role of NO in electrical restitution and VF risk.....	35
1.4	Nitric Oxide.....	37

1.4.1	Nitric oxide synthesis.....	37
1.4.1.1	Nitric oxide synthase isoforms.....	40
1.4.1.1.1	Neuronal nitric oxide synthase.....	40
1.4.1.1.2	Endothelial nitric oxide synthase.....	41
1.4.1.1.3	Inducible nitric oxide synthase.....	41
1.4.2	NO signalling pathways.....	42
1.4.2.1	cGMP-dependent NO signalling pathway.....	43
1.4.2.1.1	Soluble guanylyl cyclase.....	43
1.4.2.1.1.1	sGC inhibition and activation.....	45
1.4.2.1.2	Phosphodiesterases.....	46
1.4.2.1.3	cGMP-dependent protein kinase.....	47
1.4.2.2.	cGMP-independent NO signalling pathways.....	48
1.4.3	NO effects on heart.....	52
1.4.3.1	Effects of NO on the QT interval.....	52
1.4.3.2	Effects of NO on cardiac ion currents.....	53
1.4.4	NO role in the accentuated antagonism .....	54
	effect of the vagus nerve on the sympathetic system	
1.4.5	Role of NO in sympathetic regulation of cardiac function.....	56
1.4.5.1	Regulation of adrenergic pathway by nNOS.....	56
1.4.5.2	$\beta$ 3-ARs are coupled to eNOS.....	56
1.4.5.2.1	eNOS reduces cardiac responses to $\beta$ 3-ARs.....	57
1.5	Diurnal variation of cardiac electrophysiology.....	59
1.6	Rationale behind ivabradine studies.....	62
1.7	Aims.....	63

## **Chapter 2. Materials and Methods**

2.1	Guinea pig housing.....	64
2.2	Isolation of guinea pig ventricular myocytes.....	65
2.3	Electrophysiology.....	67
2.3.1	Electrophysiology apparatus.....	67
2.3.2	Patch-clamp recording techniques.....	68
2.3.3	Perforated patch-clamp of guinea pig ventricular myocytes.....	69
2.3.4	Recording solutions.....	72

2.3.5	Data acquisition.....	72
2.4	Action potential recording.....	73
2.5	Electrical restitution protocols.....	74
2.5.1	Electrical restitution data analysis..... and APD <sub>90</sub> repolarization measurement	75
2.5.2	Fitting the electrical restitution curve.....	77
2.6	Constant pacing data analysis and APD <sub>25,50,90</sub> measurement.....	78

**Chapter 3. Diurnal variation of electrical restitution properties of acutely isolated guinea-pig left ventricular cardiac myocytes**

3.1	Introduction.....	80
3.2	Electrical restitution experimental design.....	81
3.3	Results.....	84
3.3.1	Is there diurnal variation in APD <sub>90</sub> under basal..... conditions at each stimulation frequency?	87
3.3.2	Are there differences in how active and resting..... period myocytes respond to $\beta$ -AR stimulation (ISO) and the role of NO in regulating the ISO response?	89
3.3.3	Is there diurnal variation in electrical restitution curve?.....	95
3.3.3.1	APD <sub>90Max</sub> .....	96
3.3.3.2	Slope.....	98
3.3.3.3	Time constant.....	100
3.3.3.4	Maximum stimulation frequency.....	102
3.3.4	Is there diurnal variation between the two time period..... myocytes in developing arrhythmic activity, such as alternans, EADs, DADs	104
3.4	Discussion.....	106
3.4.1	Diurnal variation of APD <sub>90</sub> .....	106
3.4.1.1	APD <sub>90</sub> values are similar in active and resting..... period myocytes under basal conditions	106
3.4.1.2	APD <sub>90</sub> responses to ISO are larger in resting..... than active period myocytes	107
3.4.2	Blocking NO production.....	109

in the continued presence of ISO shortens APD<sub>90</sub> and this effect was more pronounced in the active period myocytes

3.4.3	The molecular basis for NO regulation of cardiac APD.....	110
3.4.3.1	NO signalling is known to be linked to $\beta$ -AR.....	110
3.4.3.2	Ionic currents other than $I_{Ca,L}$ ..... that regulate APD	111
3.4.4	Diurnal variation of electrical restitution parameters.....	112
3.4.4.1	Active period myocytes are more..... arrhythmic under basal conditions	112

**Chapter 4. How is action potential repolarization regulated by NO signalling pathways in acutely isolated guinea-pig active ventricular myocytes**

4.1	Introduction.....	114
4.2	Results.....	117
4.2.1	Does the shortening effect of L-NNA depends..... on the presence of $\beta$ -AR?	117
4.2.2	Is there any effect of the NO donor SNAP on..... the APD or electrical restitution parameters?	118
4.2.3	The effect of sGC activation on electrical restitution.....	123
4.2.4	Does L-NNA shorten APD <sub>90</sub> in presence of ISO..... while stimulation at constant frequency at 2 Hz?	130
4.2.5	Is there any effect of potentiation of sGC ..... with BAY on AP properties measured in the presence of ISO?	131
4.2.6	What is the effect of blocking the cGMP-dependent..... NO signalling pathway on APD in the presence of ISO?	133
4.2.7	Does modulating S-nitrosylation affect AP repolarization?.....	134
4.2.7.1	Are the effects of N6022 specific and NO mediated?.....	136
4.3	Discussion.....	141
4.3.1	The electrophysiological effect of L-NNA on AP..... is dependent on the presence of $\beta$ -AR stimulation (ISO)	141
4.3.2	SNAP has no effect on ventricular myocytes APs.....	142
4.3.3	Activation of sGC lengthens cardiac APD..... whereas inhibiting sGC shortens APD, but the effects	144

	are only observed in the presence of $\beta$ -AR stimulation	
4.3.4	APD is substantially shortened.....	146
	by upregulation of cGMP-independent NO signalling	

**Chapter 5. The electrophysiological effects of ivabradine in guinea-pig left**

**ventricular myocytes**

5.1	Introduction.....	148
5.2	Results.....	149
5.2.1	What is the effect of 0.5 and 1 $\mu$ M ivabradine.....	149
	on single cell electrical restitution curve?	
5.2.2	The effect of 1 and 3 $\mu$ M Ivabradine on APD <sub>25,50,90</sub> .....	156
	with constant pacing at 2Hz	
5.2.3	The effect of applying I <sub>Kr</sub> blocker E4031 before.....	161
	1 and 3 $\mu$ M Ivabradine on APD <sub>25,50,90</sub>	
	in constant paced cells	
5.3	Discussion.....	163
5.3.1	Ivabradine showed variable effects on AP properties.....	164
5.3.2	Blocking I <sub>Kr</sub> with E4031 and then apply.....	165
	ivabradine obliterated the variable	
	effect of Ivabradine on APD	
5.3.3	Ivabradine shortened APD in some cells.....	166

**Chapter 6. Conclusions, clinical significance, and future works**

6.1	Conclusions.....	167
6.2	Clinical significance of the findings in the heart.....	168
6.3	Future works.....	170

**Chapter 7. Bibliography**

<b><u>Appendix</u></b>	.....	204
------------------------	-------	-----

## **Publication:**

In addition to the work presented in this thesis, I've contributed to the following publication:

-Gasparoli, L., D'Amico, M., Masselli, M., Pillozzi, S., Caves, R., **Khuwaileh, R.**, Tiedke, W., Mugridge, K., Pratesi, A., Mitcheson, J.S. and Basso, G., 2015. **New pyrimido-indole compound CD-160130 preferentially inhibits the KV11.1B isoform and produces antileukemic effects without cardiotoxicity.** *Molecular pharmacology*, 87(2), pp.183-196.

## **Abstracts:**

### **Physiological Society Meeting, London, UK, July 2014 (poster):**

Diurnal variation of the electrical restitution properties of acutely isolated guinea-pig left ventricular cardiac myocytes.

## **Abbreviations**

8-Br-cGMP	8-bromo-cyclic guanosine monophosphate
AC	adenylyl cyclase
ACh	acetylcholine
ANOVA	analysis of variance
AP	action potential
APD	action potential duration
APD <sub>90</sub>	action potential duration to 90% repolarisation
BAY 60-2770	(4-((4-carboxybutyl)[2-(5-fluoro-2-{{4'(trifluoromethyl)bi phenyl-4-yl]methoxy} phenyl)ethyl]amino)methyl)benzoic acid)
BH <sub>4</sub>	tetrahydrobiopterin
CaM	calmodulin
cAMP	cyclic adenosine monophosphate
CAPON	carboxy-terminal PDZ ligand of neuronal nitric oxide synthase
cGMP	cyclic guanosine monophosphate
CNB	cyclic nucleotide binding
DAF-2 DA	4,5-diaminofluorescein diacetate
DI	diastolic interval
DMSO	dimethyl sulfoxide
e <sup>-</sup>	electron
E4031	N-[4-[[1-[2-(6-Methyl-2-pyridinyl)ethyl]-4- piperidinyl]carbonyl]phenyl] methane sulfonamide dihydrochloride
ECC	excitation-contraction coupling
EDTA	ethylene diamine tetraacetic acid
EGTA	ethylene glycol tetraacetic acid
E <sub>k</sub>	equilibrium potential for potassium
eNOS	endothelial nitric oxide synthase/NOS3
FAD	flavin adenine dinucleotide
FMN	flavin mononucleotide

$I_{Ca,L}$	L-type calcium current
$I_{CNG}$	cyclic nucleotide-gated current
$I_{K1}$	inward rectifier potassium current
$I_{Kr}$	rapid delayed rectifier potassium current
$I_{Ks}$	slow delayed rectifier potassium current
$I_{Kur}$	ultra-rapid delayed rectifier potassium current
$I_{Na}$	sodium current
iNOS	inducible nitric oxide synthase/NOS2
ISO	isoprenaline
$I_{To}$	transient outward potassium current
L-NNA	N-Nitro-L-arginine
LQTS	long QT syndrome
mRNA	messenger ribonucleic acid
nNOS	neuronal nitric oxide synthase/NOS1
NO	nitric oxide
NOS	nitric oxide synthase
ns	no significance
ODQ	1H-[1,2,4]Oxadiazolo[4,3-a]quinoxalin-1-one
PDE	phosphodiesterase
PDZ	post-synaptic density-protein, discs-large, ZO-1
PKA	protein kinase A/cAMP-dependent protein kinase
PKG	protein kinase G/cGMP-dependent protein kinase
PLB	phospholamban
SEM	standard error of the mean
SERCA	sarcoplasmic/endoplasmic reticulum calcium ATPase
sGC	soluble guanylyl cyclase
SNAP	S-nitroso-N-acetylpenicillamine
SR	sarcoplasmic reticulum
VF	ventricular fibrillation
VS	vagus nerve stimulation

## **Chapter 1** **Introduction**

### **1.1 Electrophysiology of the heart**

#### **1.1.1 Background**

The heart is the muscular organ of the circulatory system that continually pumps blood throughout the body. The heart is composed of cardiac muscle tissue that is strong and able to contract and relax rhythmically throughout a person's life. The heart has four separate chambers. The upper chamber on each side of the heart, the atrium, receives and collects the blood coming to the heart. The atrium then delivers blood to the lower chamber, the ventricle, which pumps blood away from the heart through powerful, rhythmic contractions.

The right side receives oxygen-poor blood from the various regions of the body and delivers it to the lungs where the blood becomes oxygenated. The left side of the heart receives the oxygen-rich blood from the lungs and delivers it to the rest of the body. The key function of the cardiovascular system is to provide rapid and efficient transport of oxygen, nutrients, waste and heat around the body. In this system, the heart acts as a pump providing the driving force for the movement of blood around the body (Tortora and Derrickson, 2008).

The rhythm of the heart is normally determined by a pacemaker site called the sinoatrial node (SAN) located in the posterior wall of the right atrium near the superior vena cava. The SAN consists of specialized cells that undergo spontaneous generation of action potentials at a resting rate of 60-100 action potentials ("beats") per minute in human. Sinus rates below this range are termed sinus bradycardia and sinus rates above this range are termed sinus tachycardia. This intrinsic rhythm is strongly influenced by autonomic nerves, with the vagus nerve being dominant over sympathetic influences at rest (Guyton and Hall, 2015).

The sinus rhythm normally controls both atrial and ventricular rhythm. Action potentials generated by the SAN spread throughout the atria, depolarizing this tissue and causing atrial contraction. The impulse then travels into the ventricles via the atrioventricular node (AVN). Specialized conduction pathways (bundle branches and

Purkinje fibers) within the ventricle rapidly conduct the wave of depolarization throughout the ventricles to elicit ventricular contraction.

Myocardial cells that make up the conduction system of the heart have specialisations to enable them to contract and conduct electrical impulses quickly and efficiently. Myocytes are connected by intercalated discs which hold the cells close together at desmosomes and provide an electrical connection through gap junctions to allow the rapid spread of electrical impulses which take the form of action potentials (Figure 1.1). It is these action potentials that are responsible for the contraction of myocytes, resulting in contraction of the whole heart.

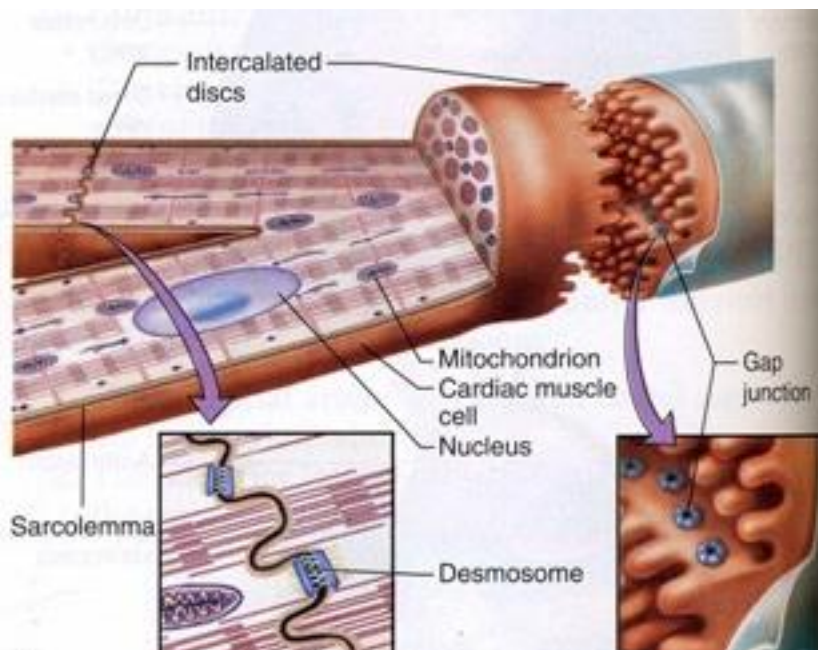


**Figure 1.1: Myocytes and intercalated discs.** Modified from Saladin, (2004).

## **1.1.2 The Action potential**

### **1.1.2.1 Ionic equilibrium potentials of cardiac cells**

The action potential (AP) is a change in the electrical potential ( $E_m$ ) of the cell membrane which leads to propagation of electrical impulses from one cell to another via gap junctions and the specialized conducting system.  $E_m$  is the difference in electrical potential of the interior relative to the exterior of a biological cell. Typical values of membrane potential range from  $-40$  mV to  $-80$  mV according to the cell type (Bers, 2002). At rest, sodium ( $\text{Na}^+$ ) and calcium ( $\text{Ca}^{2+}$ ) ions are more

concentrated in the extracellular solution, while potassium (K<sup>+</sup>) is more concentrated intracellularly (Bers, 2002).

The equilibrium potential for an ion (E<sub>ion</sub>) is described by the Nernst equation which calculates, for defined intra and extracellular ion concentrations, the theoretical membrane potential if the membrane was 100% perfectly selective for that ion (Levick, 2010, see table 1).

Ion	Intracellular (mM)	Extracellular (mM)	Equilibrium potential (mV)
K <sup>+</sup>	140	4	-94
Na <sup>+</sup>	10	140	+70
Ca <sup>2+</sup>	10 <sup>-7</sup>	2	+129
Cl <sup>-</sup>	5	120	-83

**Table 1:** Intracellular and extracellular concentrations and Nernst equilibrium potential values for a typical mammalian myocardial cell in its natural environment (37°C) of few ions of physiological importance.

Nernst Equation:

$$E_{ion} = \frac{RT}{zF} \ln \frac{[ion]_o}{[ion]_i}$$

E<sub>ion</sub> -Equilibrium potential for the ion (mV).

R- Gas constant (8.3 joule.K<sup>-1</sup>.mol<sup>-1</sup>).

T- Temperature in Kelvin.

F- Faraday's constant (96500 coulombs. mol<sup>-1</sup>).

z- Valency of ion (e.g. +1 for monovalent cations).

E<sub>ion</sub> is a theoretical value when there is no net movement across the membrane of the ion at that membrane potential because the concentration gradient is equally opposed by the electrical gradient and the net electrochemical driving force on the ion is zero. For K<sup>+</sup> ions the large concentration gradient allows K<sup>+</sup> ion to efflux, however increasing K<sup>+</sup> efflux increases intracellular negative charge. The potential where these opposing movements are equal is termed as the equilibrium potential

for  $K^+$  ( $E_K$ ). Most cells in the resting state reside close to  $E_K$  as this is the predominant permeating ion at rest; however, they do not have a resting membrane potential at  $E_K$  due to the fact that the membrane is not 100% selectively permeable to a single ion. Permeability to other ions, particularly  $Na^+$  and  $Ca^{2+}$  causes a depolarisation of the membrane potential relative to  $E_K$  (Levick, 2010).

### **1.1.2.2 Regional heterogeneity of the cardiac action potential**

Different regions of the heart have different shapes of action potentials due to the expression levels of different ion channels and transporters. The rate of depolarisation during the upstroke is rapid in ventricles due to the large amplitude and fast kinetics of  $Na^+$  current which mediates the upstroke of the ventricular action potential. While it is slow in SAN due to the absence of  $Na^+$  channels; instead it is the  $Ca^{2+}$  current that carries the action potential upstroke which activates rapidly but not as fast as the  $Na^+$  current (DiFrancesco, 2010). Repolarisation in atria occurs earlier than in ventricles. The long action potential duration (APD) in the ventricle (Figure 1.2) helps in preventing re-excitation by keeping membrane potential depolarised and thus  $Na^+$  and  $Ca^{2+}$  channels inactivated. It also allows contraction to relax before the next beat so the ventricles can fill with blood between beats.

Likewise different layers of the left ventricle have different distribution of ionic currents (Wickenden *et al.*, 1999). Transmural wall of the heart is composed of three layers: epicardium, midmyocardium and endocardium. The midmyocardium consists of specialised cells known as M cell which naturally have longer APD than epicardial and endocardial cells (Liu *et al.*, 1995). In guinea-pigs, the delayed rectifier  $K^+$  currents ( $I_{Kr}$ : Rapidly activating  $K^+$  current and  $I_{Ks}$ : Slow activating  $K^+$  current) are smaller in ventricular endocardial cells than in epicardial cells (Bryant *et al.*, 1998). Smaller  $I_{Ks}$  in left ventricle apex versus ventricular basal myocytes may underlie longer apical APD, although  $I_{Kr}$  appears larger at the ventricular apex in isolated ventricular rabbit myocytes (Cheng *et al.*, 1999). Therefore, this is crucial as it underlies differences in APD and morphology in cells isolated from different ventricular layers.

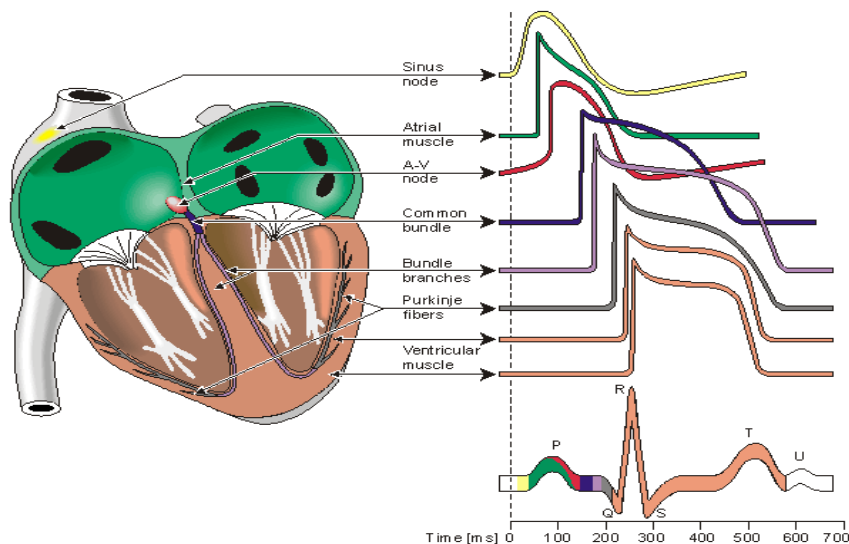


**Figure 1.2: Electrophysiology of the heart.** The different action potential waveforms for each of the specialized cells found in the heart are shown. Also it demonstrates how repolarisation in atria occurs after a shorter delay and is faster than in ventricles and a long plateau appears in the action potential of ventricular cells. A normal electrocardiogram (ECG) is also shown. Modified from Fozzard *et al.* (1991).

### **1.1.2.3 Phases of the ventricular action potential**

The ventricular action potential in humans is more than 200 ms in duration (Eldstrom and Fedida, 2011) and characterized by having 5 different phases that are controlled by different ionic currents. For AP phases refer to Figure 1.3.

**Phase (0)** is the rapid upstroke of the AP. Depolarization is initiated by passive current spread from neighbouring active regions. The rapid upstroke of AP in the ventricular myocytes is due to the voltage dependent opening (activation) of  $\text{Na}^+$  channels. Depolarization stops as the membrane potential approaches  $E_{\text{Na}}$  at which there is no driving force for  $\text{Na}^+$  influx (Eldstrom and Fedida, 2011).

**Phase (1)** is the early repolarization phase in which activation of the transient outward  $\text{K}^+$  current ( $I_{\text{to}}$ ) occurs. The ultra-rapid  $\text{K}^+$  current ( $I_{\text{kur}}$ ) also activates very rapidly and may contribute to the early repolarization in atria.

**Phase (2)** is the plateau phase in which the Inward and outward currents are nearly balanced. During this phase the inward current is mostly the L-type  $\text{Ca}^{2+}$  current

( $I_{Ca,L}$ ) and the outward current is the delayed rectifier  $K^+$  currents ( $I_{Kr}$  and  $I_{Ks}$ ) (Gussak *et al.*, 2008).

**Phase (3)** is the late repolarization phase which is characterized by further repolarization by the outward  $K^+$  currents.

**Phase (4)** is the resting membrane potential, which is the membrane potential when the cell is not being stimulated. The normal resting membrane potential in the ventricular myocardium is about -85 to -95 mV, which is largely determined by the selective permeability of the cell membrane to  $K^+$  ions by inward rectifier  $K^+$  channels ( $I_{K1}$ ).  $I_{K1}$  remains active to maintain the negative resting membrane potential.

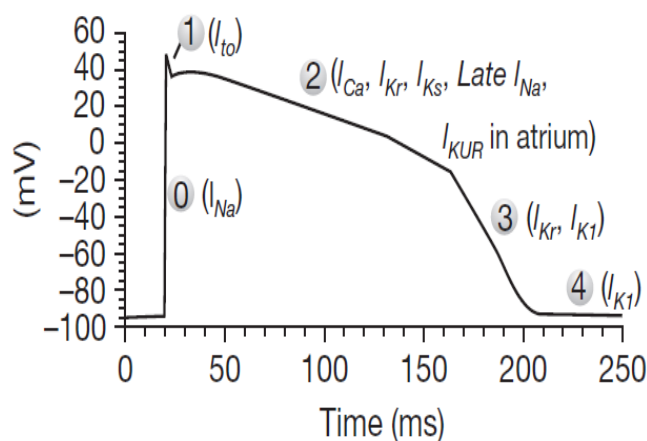


**Figure 1.3: Human ventricular action potential.**  $I_{Na}$ :  $Na^+$  current;  $I_{to}$ : Transient outward  $K^+$  current;  $I_{Ca}$ :  $Ca^{2+}$  current;  $I_{Kr}$ : Rapidly activating  $K^+$  current;  $I_{Ks}$ : Slow activating  $K^+$  current;  $I_{Kur}$ : Ultra-rapid activating  $K$  current;  $I_{K1}$ : Inward rectifier  $K^+$  current. Modified from Eldstrom and Fedida, (2011).

#### 1.1.2.4 Refractoriness of the ventricular AP

The refractory period of a cell is a period of time when another action potential cannot be fired as the cell is still recovering from the previous AP. This occurs because  $Na^+$  channels and  $Ca^{2+}$  channels involved in the generation of an AP are inactivated. This mechanism is protective as it prevents the generation of an ectopic beats.

The refractory period can be divided into the effective refractory period (ERP) and the relative refractory period (RRP) (Figure 1.4). In the ERP, the majority of the ion channels are inactivated and therefore the threshold to fire an AP cannot be

reached. However, in the RRP some ion channels are responsive to a stimulus and an action potential could be generated, if the stimulus is large enough (Conrath *et al.*, 2006). The ERP extends into phase 3 (Conrath *et al.*, 2006). Interestingly, the prolongation of ERP without significant changes in APD decreases incidence of arrhythmogenesis (Ng, G.A, *et al.*, 2007). Moreover, drugs which prolongs phase 3 such as amiodarone and sotalol reduce ventricular arrhythmias (Singh, 1993).

In the RRP, depolarization will reach the threshold required to generate another AP but a greater magnitude of stimulus is required in this period. RRP usually occurs in phase 3 and 4 (Klabunde, 2011).

E4031, a drug that blocks  $I_{Kr}$  channels, has been shown to increase ERP of cardiac myocytes in humans (Naitoh *et al.*, 1998) which Sanguinetti *et al.* (1991) have also confirmed in guinea-pig myocytes. HMR-1556, a blocker of  $I_{Ks}$  channels, has also been shown to increase ERP in cardiac myocytes. This suggests a role of  $K^+$  currents in the refractory periods as blocking  $I_{Kr}$  or  $I_{Ks}$  is reported to change ERP (Conrath *et al.*, 2006).

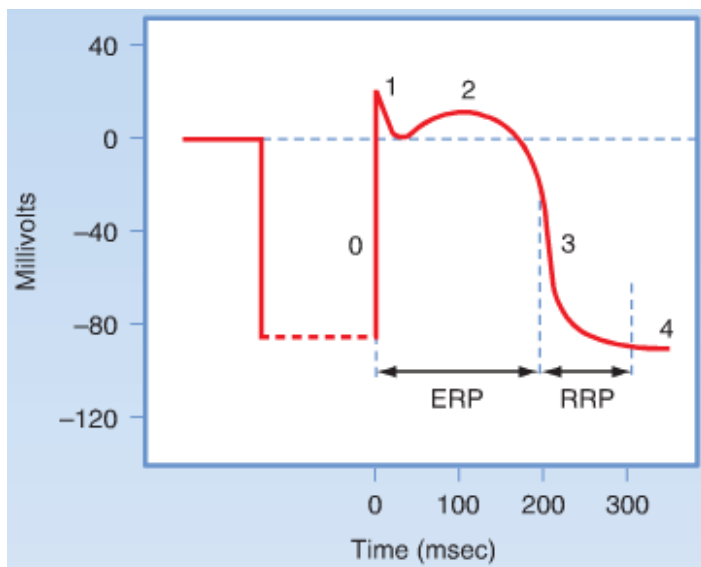


**Figure 1.4: Refractory period of a ventricular action potential.** Diagram showing the effective refractory period (ERP) and the relative refractory period (RRP) of the ventricular action potential. Modified from Koeppen *et al.* (2010).

### **1.1.2.5 Phases of the pacemaker action potential**

The pacemaker AP is seen in the SAN and AVN. Pacemaker cells do not have a stable resting AP, and it is the spontaneous depolarization of the pacemaker potential that gives the heart its auto-rhythmicity.

Figure 1.5 shows the pacemaker AP phases. At **phase 4** the membrane potential is around -60mV. The  $K^+$  channels begin to close, depolarizing the cell. The hyperpolarised state triggers the hyperpolarization-activated cyclic-nucleotide-gated (HCN)-channel, which mediates the “funny” current ( $I_f$ ) to open.  $I_f$  current originally described in SAN myocytes as a small  $Na^+$  current created which allows the SAN to spontaneously depolarise, making it the natural pacemaker of the heart. As  $Na^+$  enters, the cell begins to depolarise. At around -50mV, the transient opening  $Ca^{2+}$  channels (T-type  $Ca^{2+}$  channels) open, allowing  $Ca^{2+}$  into the cell, causing further depolarisation. The long lasting openings  $Ca^{2+}$  channels (L-type  $Ca^{2+}$  channels) open at around -40mV. T-type  $Ca^{2+}$  channels close just prior to reaching threshold (between -40 to -30 mV). The influx of  $Ca^{2+}$  from L-type  $Ca^{2+}$  channels depolarises the cell to threshold (-40 to -30mV), thus generating an AP (Park *et al.*, 2011).

In **phase 0**, the combination of  $I_f$  channels closing and increase in  $Ca^{2+}$  influx via the  $I_{Ca,L}$ ,  $Na^+/Ca^{2+}$  exchanger, and from the sarcoplasmic reticulum (SR) causes further depolarisation.

In **phase 3**, L-type  $Ca^{2+}$  channels become inactivated, decreasing  $I_{Ca,L}$  whilst delayed rectifier  $K^+$  channels open. Consequently,  $E_m$  shifts towards  $E_k$ , leading to repolarisation and later hyperpolarisation of the cell. Then opening of  $I_f$  channels. Without hyperpolarisation,  $I_f$  channels will be inactivated, which will in turn create a shallower slope during phase 4, and a bradycardia effect (Park *et al.*, 2011). Therefore, the degree of activation of  $I_f$  determines the steepness of phase 4 of SAN action potential; hence, the heart rate which explains the autorhythmicity properties of cardiac muscle in the SAN (Zagotta *et al.*, 2003). Phase 1 and 2 are absent in the pacemaker AP.

Ivabradine is a bradycardiac drug which inhibits the pacemaker current  $I_f$  in the SAN; thus increasing the time required for the diastolic depolarization to reach the threshold for action potential firing. Ivabradine treatment has been used to treat

patients with coronary artery disease and heart failure to lowering heart rate and thus reducing oxygen demand and wall stress (Scicchitano *et al.*, 2014). Studies have suggested that ivabradine prolongs ventricular repolarization and alters electrical restitution properties (Hancox *et al.*, 2008; Melgari *et al.*, 2015).

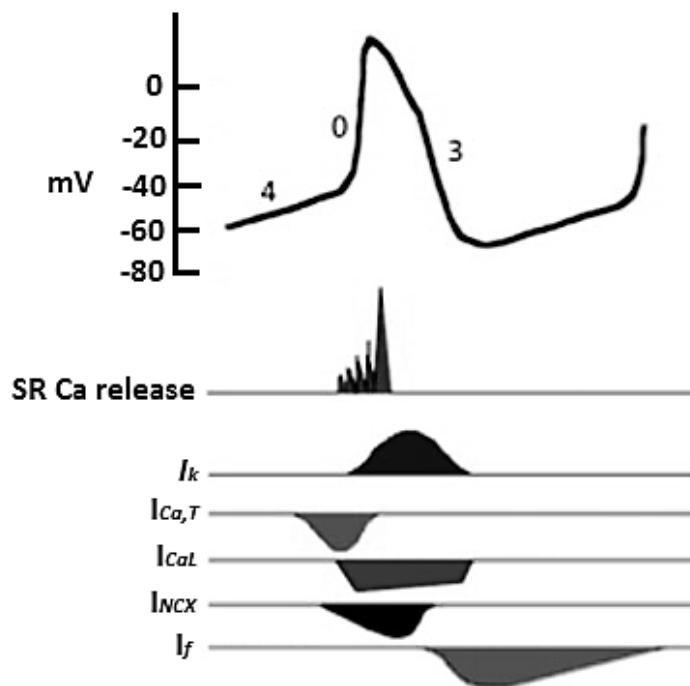


**Figure 1.5: The pacemaker action potential in the sinoatrial node and its ionic constituents.** Illustration of a pacemaker potential demonstrating the different phases and its corresponding activity of ionic currents. SR  $\text{Ca}^{2+}$  release (sarcoplasmic reticulum calcium release),  $I_k$  (delayed rectifier  $\text{K}^+$  currents),  $I_{Ca,T}$  (T-type calcium current),  $I_{Ca,L}$  (L-type calcium current), NCX ( $\text{Na}^+/\text{Ca}^{2+}$  exchanger),  $I_f$  (funny current). Modified from Park *et al.* (2011).

Detailed discussion of the different ionic currents/channels that shape the cardiac action potential will be discussed next.

### 1.1.3 Cardiac ion channels

#### 1.1.3.1 Channel nomenclature

Different ion channels have been identified using electrophysiological recording techniques and cloning. The nomenclature has recently been made more consistent

using an alpha numerical system to define subfamilies and subtypes based on similarities between the amino acid sequences of the channels. In the nomenclature system, the name of an individual channel consists of the chemical symbol of the ion (Na, Ca or K) with the principal type of the channel, for example voltage gated channels have the subscripted 'v' (e.g. Na<sub>v</sub>, Ca<sub>v</sub> or K<sub>v</sub>). The number following the subscript demonstrates the gene subfamily (e.g Na<sub>v</sub>1), and the number following the gene subfamily identifies the specific channel isoform (e.g. Na<sub>v</sub>1.1). The number for each isoform was assigned depending on the proximity of the gene when identified; 'a' is the most proximal gene when identified. Variants of each family member are identified by letters following the numbers (e.g. Na<sub>v</sub>1.1a) (Alexander *et al.*, 1999).

### **1.1.3.2 Cardiac Ion channels and gating subtypes**

Ion channels have 2 main properties, ion permeation and gating. During the action potential, the conductance of ion channels changes and ions move passively down their electro-chemical gradients. Ion permeation describes the movement through the open channel. Most ion channels are selectively permeable to particular ions (e.g Na<sup>+</sup>, K<sup>+</sup>, Ca<sup>2+</sup>, Cl<sup>-</sup>. etc) or to groups of ions (e.g cations or anions). Size, valency, and hydration energy of the ion are important factors that determine the channel selective permeability.

Ion channels are also sub classified by their mechanism of gating into three types; voltage-gated, ligand gated and mechano-sensitive channels (Pinnell *et al.*, 2007). Voltage-gated ion channels change their conductance according to variations in membrane potential. Voltage-dependent gating is the commonest mechanism of gating observed in ion channels. Ligand-dependent gating is the second gating mechanism of cardiac ion channels. An example is the acetylcholine (ACh)-activated K<sup>+</sup> channel in which ACh binds to the M<sub>2</sub>-muscarinic ACh receptor and activates a G protein–signaling pathway that results in the activation of ACh activated K<sup>+</sup> channels (I<sub>KACH</sub>) (Perozo *et al.*, 2002). The mechano-sensitive or the so called stretch-activated channels are the least studied. These channels can transduce a physical stimulus like stretch into an electrical signal (Grant, 2009).

Figure 1.6 summarizes the gating states of voltage gated channels in general. Typically, channels exist in three main states; close (deactivated), opened, and

inactivated. The closed and inactivated states are non-conducting states and ions only move through the pore in the open state. Inactivation reduces outward conductance at depolarized potentials while deactivation reduces inward currents (Nerbonne and Kass, 2005).

The conformational change from closed to open is known as activation and the reverse process is known as deactivation. Activation and inactivation of the channels are favoured with depolarization, while deactivation and recovery from inactivation are favoured with repolarization. These gating processes are critical to the functional role of the ion channel. Channel specific voltage and time dependent kinetics, along with permeation properties; determine when and how channels contribute to action potentials and resting membrane potential (Sanguinetti and Tristani-Firouzi, 2006).

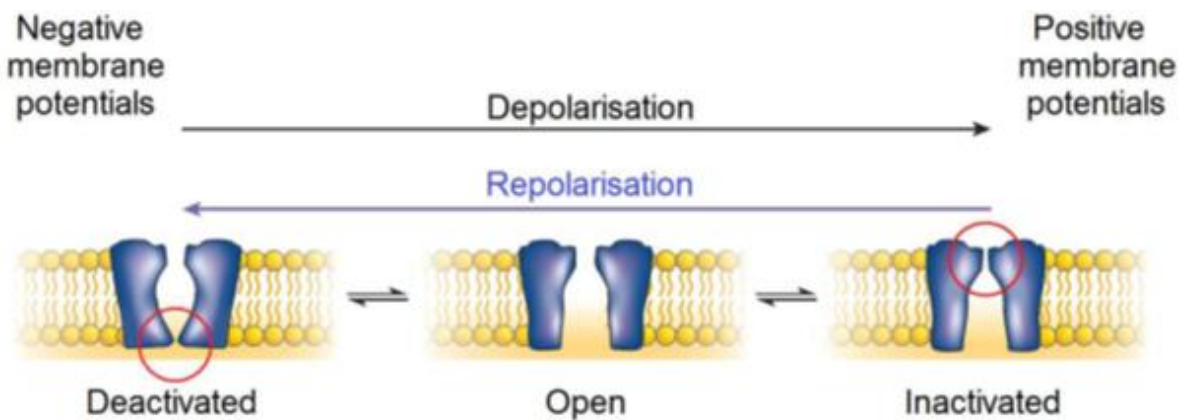


**Figure 1.6: Gating of ion channels.** Modified from Sanguinetti and Tristani-Firouzi, (2006).

### 1.1.3.3 Overview of the structure and kinetics of the main ion channels in cardiac muscle

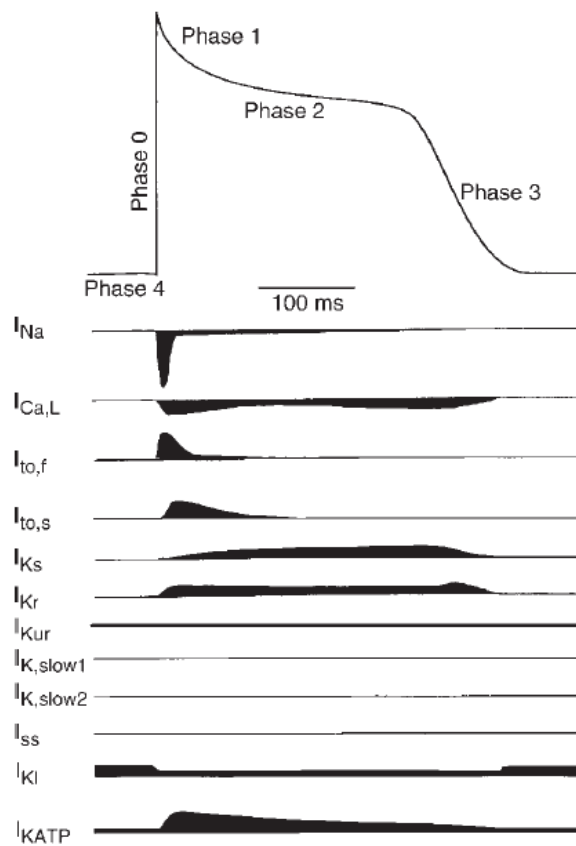


**Figure 1.7: Ventricular AP and its major ionic constituents.** Action potential (Top) and graphical representation of the time courses of the underlying ionic currents in adult human ventricular myocytes. Currents amplitudes are not drawn to scale. Modified from Nerbonne and Kass, (2005).

**Cardiac  $K^+$  channels** mainly are classified into two categories: 1) Voltage-gated  $K^+$  channels which are activated by depolarisation. The currents of these channels are the  $I_{to}$  (transient outward  $K^+$  current),  $I_{Kur}$ ,  $I_{Kr}$ , and  $I_{Ks}$ , for ultra-rapid, rapid and slow activating delayed rectifier  $K^+$  currents respectively (Shinagawa *et al.*, 2000). 2) The inward rectifier  $K^+$  channels ( $I_{K1}$ ,  $I_{K(Ach)}$  and  $I_{K(ATP)}$ ), which are mostly ligand gated channels and have fewer transmembrane segments (Hille, 2001). Inward rectification is a term that means that the channel conducts inward current better than outward current (Zobel *et al.*, 2003).

**Transient outward K<sup>+</sup> current (I<sub>to</sub>).** This current contributes to the early repolarization phase of the AP. It exhibits rapid activation and inactivation gating and is divided into two components I<sub>to</sub> (fast) and I<sub>to</sub> (slow). Both I<sub>to</sub> (fast) and I<sub>to</sub> (slow) activate rapidly but I<sub>to</sub> (fast) inactivates faster than I<sub>to</sub> (slow). I<sub>to</sub> (fast) is carried by K<sub>V</sub>4.3 and K<sub>V</sub>4.2 channels and I<sub>to</sub> (slow) by K<sub>V</sub>1.4 channels (Niwa and Nerbonne, 2010). I<sub>to</sub> is absent in guinea-pig ventricular myocytes (Rosati *et al.*, 2008). Referring to Figure 1.7 it is noticeable that I<sub>to</sub> has large amplitude during the AP notch (Phase 1).

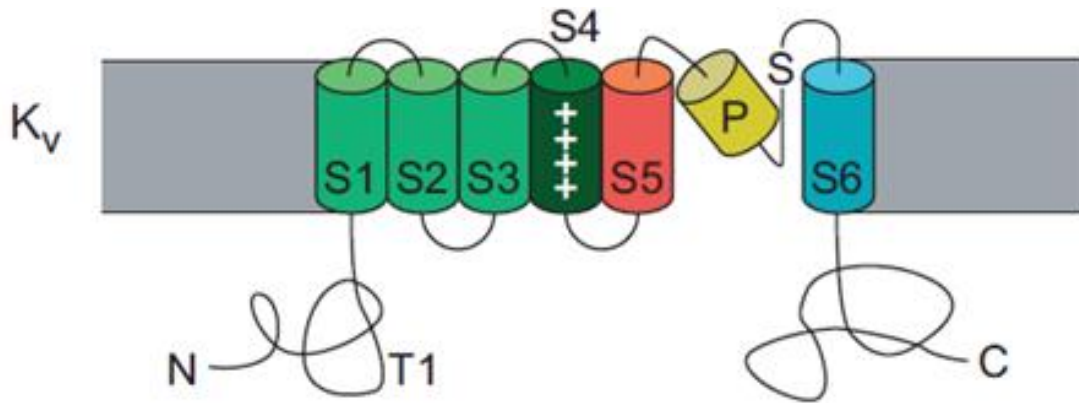
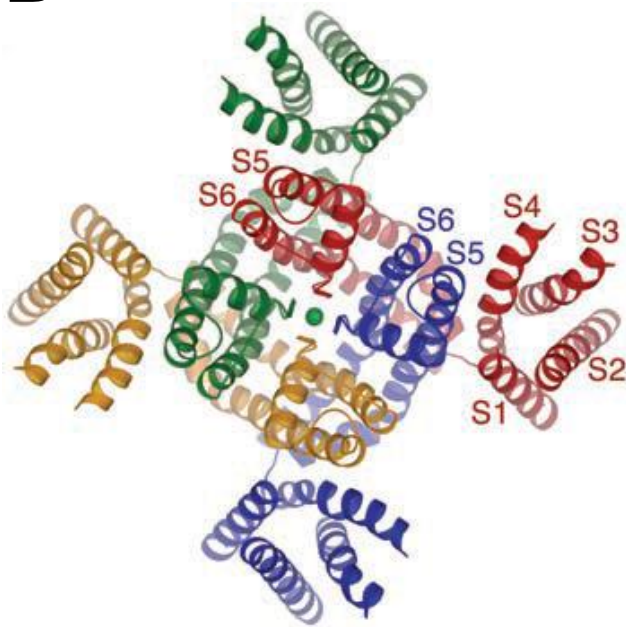
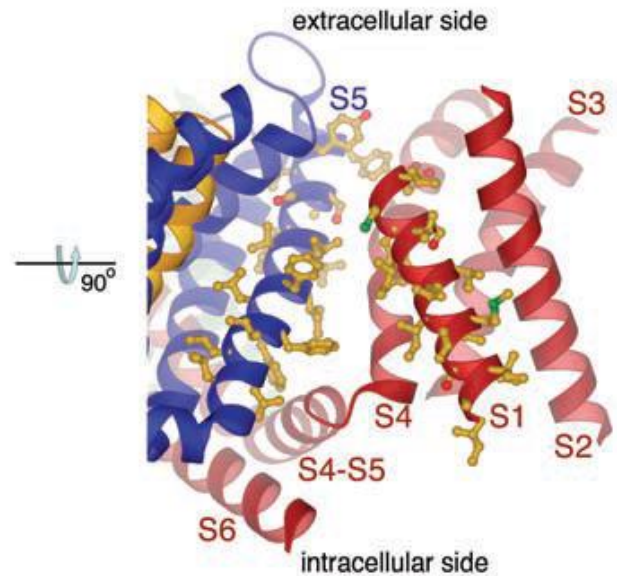
**The delayed rectifier K<sup>+</sup> currents (I<sub>Kur</sub>, I<sub>Kr</sub>, and I<sub>Ks</sub>).** The delayed rectifier K<sup>+</sup> currents are fundamental in repolarisation and are named according to the rate of activation, ultra-rapid (I<sub>Kur</sub>), rapid (I<sub>Kr</sub>) and slow (I<sub>Ks</sub>). These channels share the same basic structure, a tetramer of four pore-forming  $\alpha$  subunits. Each subunit consists of six  $\alpha$  helical transmembrane spanning domains, known as S1-S6, and intracellular NH<sub>2</sub>- and COOH-termini. The voltage sensing domains are S1-S4, with the S4 domain containing regular spaced positively charged lysine or arginine residues. The S5-S6 domains from each of the four subunits collect together centrally to form the pore and the selectivity filter of the channel (Vandenberg *et al.*, 2004; Long *et al.*, 2005) (Figure 1.8).

I<sub>Kr</sub> is conducted by K<sub>V</sub>11.1 channels encoded by the human ether-a-go-go related gene (*hERG*), also known as *KCNH2* (Trudeau *et al.*, 1995). I<sub>Kr</sub>, contrary to its name, activates relatively slowly, although faster than I<sub>Ks</sub>, with a time constant of  $72 \pm 4$  ms in guinea-pig ventricular myocytes under basal conditions at 37°C (Lu *et al.*, 2001). In spite of the relative slow activation, I<sub>Kr</sub> is fundamental in the plateau and repolarisation phases of the ventricular AP. As shown in Figure 1.7; at the resting membrane potential, shown as phase 4, I<sub>Kr</sub> channels are deactivated, thus I<sub>Kr</sub> is absent. Upon initiation of an AP, membrane depolarisation activates I<sub>Kr</sub> channels resulting in a slow increase in I<sub>Kr</sub> due to the slow opening of the activation gate. However, due to the fact that I<sub>Kr</sub> rapidly inactivate (time constant is  $< 2$  ms in guinea-pig ventricular myocytes under basal conditions at 37°C), I<sub>Kr</sub> is small during the plateau phase of the ventricular AP (Sanguinetti and Jurkiewicz, 1990). As the membrane potential becomes more negative during repolarisation, I<sub>Kr</sub> increases further and peaks, as channels rapidly recover from inactivation but also begin to

slowly deactivate. The combination of rapid and voltage dependent recovery from inactivation and slow kinetics of deactivation; results in a window current which is fundamental in repolarization of the ventricular AP (Hancox *et al.*, 1998).

$I_{Ks}$  activates more slowly than  $I_{Kr}$  in response to membrane depolarisation with a activation time constants of  $447 \pm 2$  ms in guinea-pig ventricular myocytes under basal conditions at  $37^{\circ}\text{C}$  (Lu *et al.*, 2001). The deactivation of  $I_{Ks}$  has a fast component and a slow component with time constants of  $203 \pm 11$ ms and  $741 \pm 58$  ms respectively, which is slower than deactivation of  $I_{Kr}$ .  $I_{Ks}$  is also a fundamentally important repolarising current.  $I_{Ks}$  channels are hetero-multimeric proteins composed of both  $K_v7.1$  (encoded by *KCNQ* gene) and minK (encoded by *KCNE* gene). The time course of  $I_{Ks}$  during the phases of the AP is shown in Figure 1.7. In guinea-pig ventricular myocytes it is likely that  $I_{Ks}$  and  $I_{Kr}$  are the predominant repolarising currents (Zicha *et al.*, 2003). Augmentation of  $I_{Ks}$ , due to phosphorylation of  $K_v7.1$ , is fundamental in the shortening of APD during  $\beta$ -AR stimulation (Marx *et al.*, 2002).

$I_{Kur}$  is conducted by  $K_v1.5$  channels in humans and is present in the atria and contributes to rapid, early repolarisation of the atrial AP (Wagoner *et al.*, 1997; Gaborit *et al.*, 2007). Repolarisation of ventricular myocytes does not involve  $I_{Kur}$ .

**A****B****C**

**Figure 1.8: Views of the voltage gated  $K^+$  channels structure. A)** Six  $\alpha$  helical transmembrane spanning domains (S1-S6) of each subunit and intracellular  $NH_2$ - and  $COOH$ - termini. S1-S4 are the voltage sensing domains. The S5-S6 domains from each of the four subunits collect together centrally to form the pore and the selectivity filter of the channel. Modified from Miller, (2000). **B)** Overall structure of the tetramer, viewed from extracellular side. Each of the four subunits is coloured distinctively. **C)** Close-up view of a voltage sensor and its relationship to the pore, viewed from the side. Modified from Long *et al.* (2005).

**Inward rectifier K<sup>+</sup> current (I<sub>K1</sub>).** I<sub>K1</sub> is responsible for establishing the resting membrane potential and contributes more to the final stages of repolarisation. I<sub>K1</sub> is passed by K<sub>ir</sub>2.1 channels that are constitutively open and expressed in ventricular and atrial myocytes (Cho *et al.*, 2003). As shown in Figure 1.7; I<sub>K1</sub> is large at rest and towards the latter stage of repolarisation, phase 4 and 3. In contrast, during the plateau phase I<sub>K1</sub> is smaller due to voltage-dependent block of the channels by Mg<sup>2+</sup> and polyamines (Fakler *et al.*, 1995). The channels are a tetrameric assembly of four subunits; each subunit is composed of only 2 transmembrane domains (TM<sub>1</sub> and TM<sub>2</sub>) which resemble S5 - S6 in K<sub>v</sub> channels and which form the K<sup>+</sup> selective pore of the channel. Four TM<sub>1</sub>-P-TM<sub>2</sub> regions form a narrow selectivity filter and internal aqueous cavity which lowers the electrostatic barrier for K<sup>+</sup> ions and thus ensure a low resistance passage of the ions (Hiroshi Hibino *et al.*, 2010) (Figure 1.9).

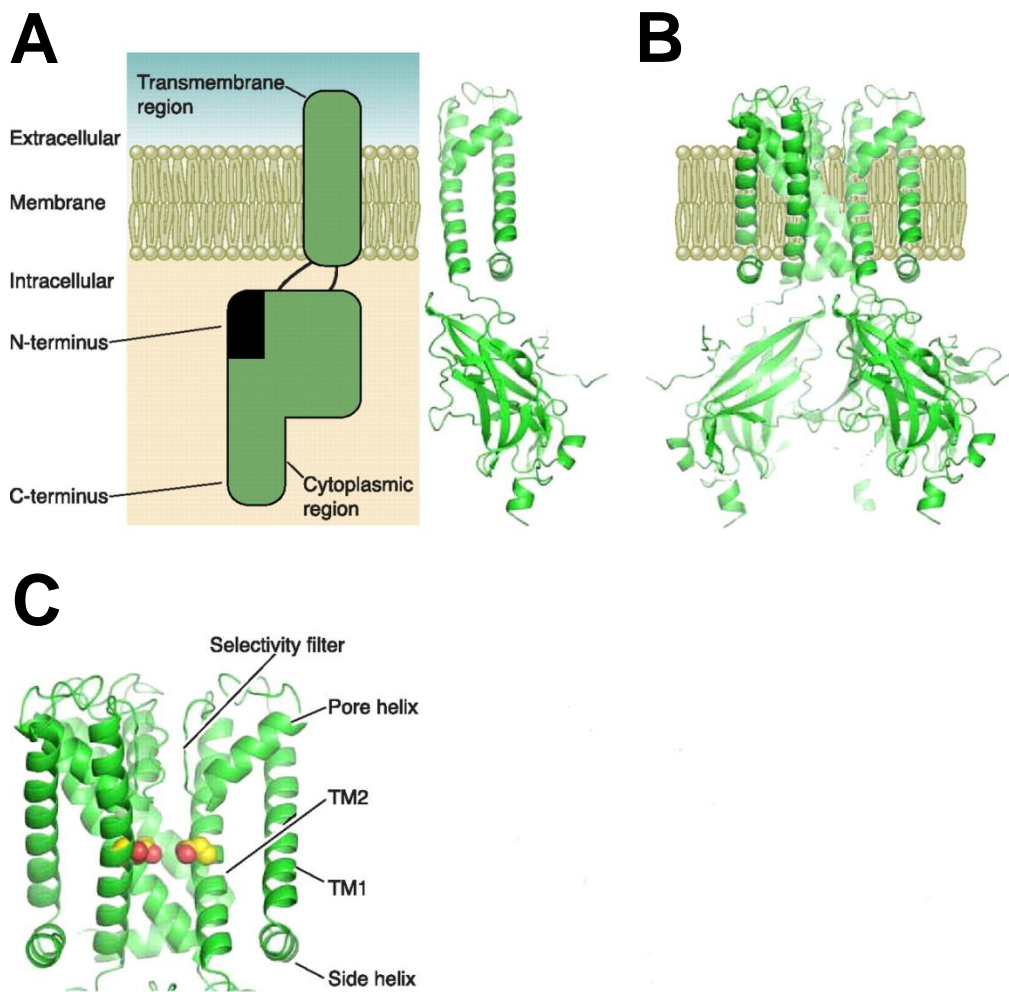


**Figure 1.9: Molecular architecture of inward rectifying (K<sub>ir</sub>) channels.** **A)** A schematic representation of the structure of K<sub>ir</sub> channel. The K<sub>ir</sub> channel is divided into transmembrane and cytoplasmic domains. The cytoplasmic domain is composed of the NH<sub>2</sub>- and COOH-termini. **B)** The tetrameric assembly of K<sub>ir</sub> channels. **C)** The transmembrane domain which comprises three helices: TM1, pore, and TM2; the residue that is largely responsible for the interaction with polyamines and Mg<sup>2+</sup> and thus inward rectification is indicated by the red/yellow spheres. Modified from Hiroshi Hibino *et al.* (2010).

**Cardiac Na<sup>+</sup> channels** generate a large inward Na<sup>+</sup> current and cause rapid upstroke of action potentials. In the ventricle, as the membrane potential depolarises this leads to rapid opening of Na<sub>v</sub>1.5 channels when the membrane potential is around -55mV (Nerbonne and Kass, 2005). This results in a fast inward of Na<sup>+</sup> current (I<sub>Na</sub>) which pushes the membrane potential towards the equilibrium potential for Na<sup>+</sup> (E<sub>Na</sub>), which is typically around +70 mV. Depolarisation of the membrane

potential initiates the rapid upstroke of the ventricular AP (phase 0). However, the membrane potential does not reach  $E_{Na}$  because the membrane is not perfectly selective for  $Na^+$ .  $I_{Na}$  rapidly activates ( $\sim 1$  ms; in guinea-pig Purkinji cells at  $37^\circ C$ ) and deactivates ( $< 0.2$  ms; in guinea-pig Purkinji cells at  $37^\circ C$ ) (Kay *et al.*, 1998). The  $Na^+$  channels become inactivated after a few milliseconds. The channels recover from inactivation as the membrane potential repolarises but  $Na^+$  channels availability takes time to fully recover, contributing to an increased threshold for activation of a new AP which avoids the triggering of another AP before the end of the ongoing AP.  $Na^+$  channels recovery from inactivation is one important contributing mechanism underlying the refractory periods of cardiac cells (Irisawa *et al.*, 1993).

**Cardiac  $Ca^{2+}$  channels** Membrane depolarisation also activates the L-type  $Ca^{2+}$  current ( $I_{Ca,L}$ ) which plays a fundamental role in the plateau phase of the ventricular AP as shown in phase 2 in Figure 1.7. Membrane potential changes little during the plateau and this is due to a balance between inward depolarising currents and outward repolarising currents.  $I_{Ca,L}$  is inward depolarising current and is conducted by  $Ca_v1.2$  channels in human cardiac myocytes (Catterall *et al.*, 2005).  $I_{Ca,L}$  activates by depolarisation, with a long lasting nature because L-type  $Ca^{2+}$  channels (LTCC) inactivates slowly. LTCC activation is slower than  $Na^+$  channel activation ( $\sim 10$ ms Vs  $\sim 1$ ms respectively in guinea-pig Purkinji cells at  $37^\circ C$ ) (Kay *et al.*, 1998). Following activation, LTCC subsequently undergo voltage-dependent and  $Ca^{2+}$ -dependent inactivation (Best and Kamp, 2012) with the latter process being most important in cardiac cells. The  $Ca^{2+}$ -dependent inactivation comprises a slow and a fast phase; the slow phase depends on  $Ca^{2+}$  flux through the channels while the fast phase depends on  $Ca^{2+}$  released from the sarcoplasmic reticulum (SR). Among these two phases; the fast phase which depends on the  $Ca^{2+}$  released from the SR, plays a major role in inhibition of  $Ca^{2+}$  entry through the LTCC (Sham *et al.*, 1995; Kubalova, 2003). Moreover,  $Ca^{2+}$ -dependent inactivation is mediated by calmodulin (CaM), a  $Ca^{2+}$ -sensing protein, by interacting with the carboxyl tail of the L-type  $Ca^{2+}$  channel  $\alpha 1$  subunit (Peterson *et al.*, 1999).  $Ca^{2+}$  (either entering myocytes via LTCC or released from SR) binds to CaM tethered to the channel COOH-terminus, thereby accelerating inactivation (Pitt *et al.*, 2001).

Voltage-gated calcium channels are formed of several different subunits:  $\alpha_1$ ,  $\alpha_2$ ,  $\delta$ ,  $\beta_{1-4}$ , and  $\gamma$ . The  $\alpha_1$  subunit forms the ion conducting pore while the associated subunits have several functions including modulation of gating. The structure of LTCC is shown in Figure 1.10. The structure of  $\text{Ca}_V$  and  $\text{Na}_V$  is the same as the structure of  $\text{K}_V$  channels, however,  $\text{Na}_V$  and  $\text{Ca}_V$  channels are a single peptide with four repeated domains joined by intracellular peptide linkers (Pitt *et al.*, 2001).

The other type of the  $\text{Ca}^{2+}$  channels in the cardiac myocytes is the T-type  $\text{Ca}^{2+}$  channel (which passes the T-Type  $\text{Ca}^{2+}$  current ( $I_{\text{Ca,T}}$ )), and are present principally in pacemaker, atrial and Purkinje cells and are not noticeable in most ventricular myocytes (Bers and Perez-Reyes, 1999). Both  $I_{\text{Ca,L}}$  and  $I_{\text{Ca,T}}$  activate rapidly upon depolarization, but  $I_{\text{Ca,T}}$  activates at more negative membrane potential than  $I_{\text{Ca,L}}$ .  $I_{\text{Ca,T}}$  activates around -50 mV while  $I_{\text{Ca,L}}$  activate at about -40 mV.  $I_{\text{Ca,T}}$  also inactivates more rapidly than  $I_{\text{Ca,L}}$ . Thus  $I_{\text{Ca,T}}$  contributes only to the early phase of the pacemaker AP while the  $I_{\text{Ca,L}}$  contributes to the slower rising AP upstroke in SAN and AVN cells. Moreover, LTCC have a large conductance, longer lasting openings and are sensitive to 1,4-dihydropyridines (DHPs) whereas T-type channels have a small conductance, brief openings and are insensitive to DHPs (Best and Kamp, 2012).

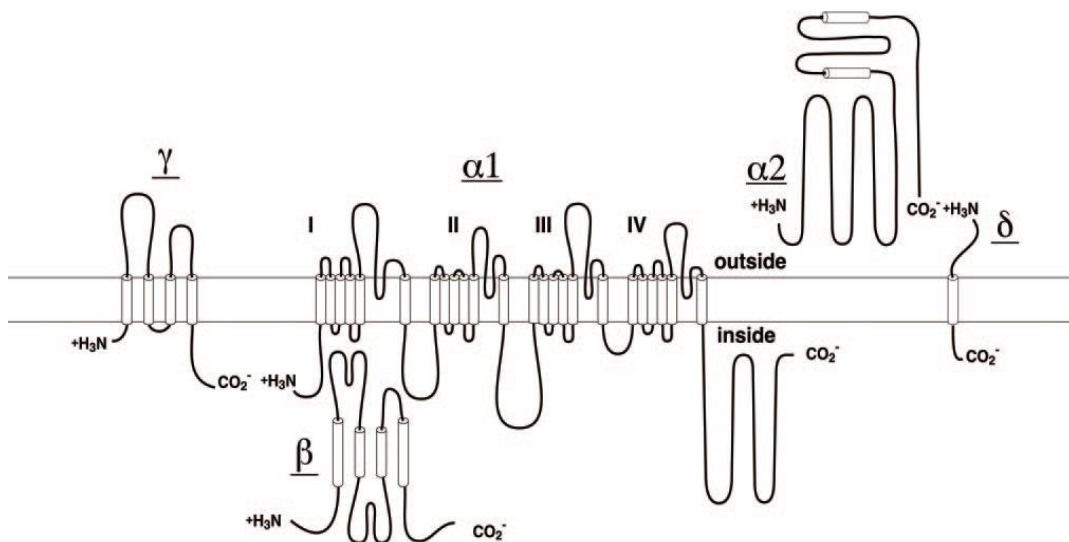


**Figure 1.10: Subunit structure of  $\text{Ca}^{2+}$  channels.** The pore forming and voltage sensing subunit is  $\alpha_1$ .  $\text{Ca}^{2+}$  channels have both transmembrane ( $\delta$ ,  $\gamma$ ), intracellular ( $\beta$ ) and extracellular ( $\alpha_2$ ) auxiliary subunits. Modified from Catterall, (2000).

### **Na<sup>+</sup>/Ca<sup>2+</sup> exchange current (NCX)**

The sodium calcium exchanger (Na<sup>+</sup>/Ca<sup>2+</sup> or NCX) is an important regulator of the cardiac AP and maintains Ca<sup>2+</sup> and Na<sup>+</sup> homeostasis and plays role in cardiac relaxation. At the resting membrane potential, three Na<sup>+</sup> ions enter the cell for each Ca<sup>2+</sup> ion that is extruded by the Na<sup>+</sup>/Ca<sup>2+</sup> exchanger (inward current); however, at more positive membrane potentials one Ca<sup>2+</sup> ion enters the cell in exchange for 3 Na<sup>+</sup> ions that leave the cell (outward current) .

Ca<sup>2+</sup> influx via Na<sup>+</sup>/Ca<sup>2+</sup> exchange produces outward I<sub>Na/ca</sub> ,and Ca<sup>2+</sup> extrusion causes inward I<sub>Na/ca</sub> and thus it is electrogenic, and generates membrane currents in the direction of Na<sup>+</sup> movement. Resting intracellular Ca<sup>2+</sup> [Ca<sup>2+</sup>]<sub>i</sub> is low so the amplitude of diastolic inward I<sub>Na/ca</sub> is small. Upon depolarization to the AP peak the membrane potential passes through E<sub>Na/ca</sub> which initially around -40mV and I<sub>Na/ca</sub> reverses and becomes outward. However, [Ca<sup>2+</sup>]<sub>i</sub> increases rapidly due to I<sub>Ca</sub> and SR Ca<sup>2+</sup> release and the E<sub>Na/ca</sub> shifts to much more positive potentials so more inward I<sub>Na/ca</sub> occurs and Ca<sup>2+</sup> is extruded. As repolarization proceeds and [Ca<sup>2+</sup>]<sub>i</sub> remains high so the I<sub>Na/ca</sub> becomes strongly inward. As [Ca<sup>2+</sup>]<sub>i</sub> decreases at diastolic E<sub>m</sub> so inward I<sub>Na/ca</sub> gradually declines (Sato *et al.*, 2012; Glitsch, 2001).

### **1.1.4 Cardiac excitation –contraction coupling**

Excitation contraction coupling (ECC) is a highly co-ordinated sequence of events that begins with electrical excitation of individual cardiac myocytes by the AP and ends with contraction of the whole heart. The AP propagates as a wave of depolarization along the cell surface and down the transverse tubules (T-Tubules), which are a network of deep invaginations of the cell membrane (sarcolemma). When the sarcolemmal potential is depolarized by the action potential; L-type Ca<sup>2+</sup> channels open and Ca<sup>2+</sup> ions will enter down their concentration gradient into the cytoplasm. Ca<sup>2+</sup> entry via the L-type Ca<sup>2+</sup> channels is involved in the activation of the SR to release Ca<sup>2+</sup> via the Ryanodine receptors (RyRs), which are ligand gated Ca<sup>2+</sup> channels. The SR is not continuous with the sarcolemma and its main function is sequestration and release of Ca<sup>2+</sup> into the cytoplasm. Its surface contains sarcoplasmic-endoplasmic reticulum-Ca<sup>2+</sup> ATP-ase (SERCA) which removes Ca<sup>2+</sup> from the cytoplasm back into the SR (Walker and Spinale, 1999).

The RyR specifically binds the plant alkaloid ryanodine that is why they are named Ryanodine receptors. Several isoforms of RyR have been identified by cloning; mammalian tissues have shown three isoforms, RyR1, RyR2, and RyR3 (Vega *et al.*, 2011; Zucchi and Ronica-Testoni, 1997). Each receptor is about 5000 amino acid residues. RyR1 and RyR2 are expressed mainly in skeletal muscle and cardiac muscle, respectively (Marks *et al.*, 1989; Takeshima *et al.*, 1989). RyR3 has a wide tissue distribution (Ledbetter *et al.*, 1994). Two mechanisms have been suggested to mediate excitation-contraction coupling. First, the direct-coupling model in skeletal muscle, in which SR  $\text{Ca}^{2+}$  release is produced by a direct interaction between the LTCC ( $\text{Ca}_v 1.1$ ) and the RyRs. Sarcolemmal depolarization is reported to produce a conformational change in  $\text{Ca}_v 1.1$  that is transmitted to the RyR and induces the release of  $\text{Ca}^{2+}$  from the SR (Ziolo *et al.*, 2008). The other mechanism of excitation-contraction coupling and the one relevant to cardiac myocytes is mediated by a process known as  $\text{Ca}^{2+}$ -induced  $\text{Ca}^{2+}$  release.  $\text{Ca}^{2+}$  ions which entered through LTCC in response to depolarization will induce a large  $\text{Ca}^{2+}$  release from the SR via  $\text{Ca}^{2+}$  gated opening of the RyRs (Fabiato, 1983) (Figure 1.11).

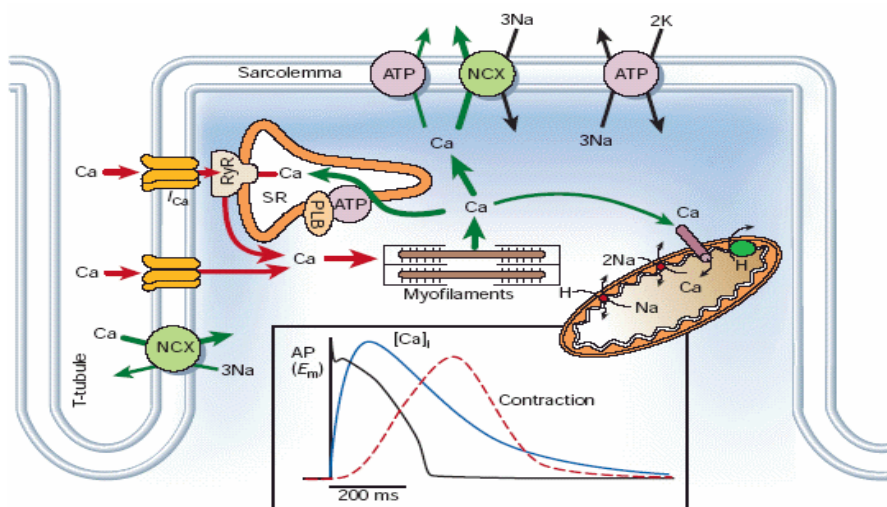


**Figure 1.11: Excitation contraction coupling in cardiac myocytes.** The electrical excitation at the sarcolemmal membrane activates  $\text{Ca}_v$  channels, and the resulting  $\text{Ca}^{2+}$  entry activates  $\text{Ca}^{2+}$  release from the sarcoplasmic reticulum (SR) via ryanodine receptors (RyRs), resulting in contractile element activation. The inset shows the relative time course of an AP,  $\text{Ca}^{2+}$  transient and contraction. Modified from Bers, (2002).

Once  $[Ca^{2+}]_i$  increases, it will be detected by the troponins, which have several  $Ca^{2+}$  binding sites, and together with other proteins in the troponin-tropomyosin complex cause conformational changes that exposes sites on the actin filaments for myosin binding and myosin cross bridge cycling, which develops force. When  $Ca^{2+}$  ions enter the cell they bind to  $NH_2$ - terminal of troponin C (TnC) and this terminal binds strongly to the  $COOH$ - terminal of Troponin I (TnI) which in turn comes off actin allowing the troponin T-Tropomyosin (TnT-Tm) complex to roll deeper into the actin filament and thus exposes sites on actin along the chain that can interact with the myosin head. When  $[Ca^{2+}]_i$  is low, the  $COOH$ - terminal of troponin I (TnI) is bound to actin, so anchoring the TnT-Tm complex complex, therefore preventing the myosin head from binding to actin (Klabunde, 2011).

#### **1.1.4.1 Cardiac relaxation**

For relaxation to occur  $Ca^{2+}$  ions must be removed from the cytoplasm via several transport processes:

- 1)  $Ca^{2+}$  can be transported into SR by SERCA.
- 2)  $Ca^{2+}$  can be pumped out of the cell by the sarcolemmal  $Ca^{2+}$ -ATPase pump.
- 3)  $Ca^{2+}$  can be transported out of the cell by the sarcolemmal  $Na^+/Ca^{2+}$  exchanger.
- 4)  $Ca^{2+}$  can be transported into mitochondria via the  $Ca^{2+}$  uniporter.

$Ca^{2+}$  that enters the cell must be extruded and primarily this is via  $Na^+/Ca^{2+}$  exchanger. Three  $Na^+$  ions enter the cell for each  $Ca^{2+}$  ion that is extruded.  $Na^+$  ions that enter the cell must in turn be extruded out via sarcolemmal  $Na^+/K^+$  ATP-ase ( $3Na^+$  out:  $2K^+$  in).  $Ca^{2+}$  released from the SR through RyR is predominantly pumped back into SR by SERCA. The other  $Ca^{2+}$  transport mechanisms play a much smaller role, although these can be important under certain pathological conditions, when  $[Ca^{2+}]_i$  become elevated (Sato *et al.*, 2012).

#### **1.2 Cardiac electrophysiology abnormalities**

Abnormalities in cardiac repolarisation are associated with an increased risk of arrhythmia and sudden cardiac death. In some cases, the risk of cardiovascular events can be predicted by the QT interval, which is a measure of ventricular

repolarisation (Post *et al.*, 2007). The QRS complex and the T wave are characteristic features of an electrocardiogram (ECG) during a cardiac cycle, which indicate ventricular depolarisation and repolarisation respectively (Sanguinetti and Tristani-Firouzi, 2006). The time between the start of the Q wave and the end of the T wave is used to determine the QT interval, as shown in Figure 1.12A. Abnormalities in the QT interval can be either short QT syndrome or long QT syndrome (LQTS), both be arrhythmogenic. LQTS is characterised by prolonged repolarisation and can be either congenital or drug-induced LQTS. Drug-induced LQTS can be caused by many drugs such as  $I_{Kr}$  blockers. Congenital LQTS is caused by inherited genetic mutations of ion channels underlying the cardiac AP (Kumar, 2012; Crotti *et al.*, 2008).

The main three common genetic subgroups of congenital LQTS are LQT1, 2 and 3 (Schwartz and Ackerman, 2013). LQT1 and 2 are caused by mutations in *KCNQ1* and *KCNH2* genes that encode  $K_v7.1$ ; which conducts  $I_{Ks}$ , and  $K_v11.1$  which conducts  $I_{Kr}$  channels respectively. Mutations lead to decrease in  $I_{Ks}$  or  $I_{Kr}$  and prolonged repolarisation (Wang *et al.*, 1996). On the other hand, LQT3 is due to mutations in the *SCN5A* gene that encodes  $Na_v1.5$  channels. Mutations lead to increase in  $I_{Na}$  usually due to reduced inactivation (Wang *et al.*, 1996).

LQTS increases the risk of arrhythmias, such as torsade de pointes (TdP) as shown in Figure 1.12B. Torsade de pointes can lead to ventricular fibrillation (VF) and sudden cardiac death (Crotti *et al.*, 2008). The electrophysiological mechanisms underlying TdP are not fully understood, but it has been suggested that it can occur when the repolarising capacity of the cardiac ventricles is reduced (Roden, 1998).

T-wave abnormalities on ECG include notched or biphasic T-waves and T-wave alternans, indicating electrical instability (Picht *et al.*, 2006). T-wave alternans on an ECG are caused by beat-to-beat alternation of repolarisation i.e. alternation of phases 2 and 3 (El-Sherif *et al.*, 1996). Several studies have hypothesised that this is caused by beat-to-beat alternans in release of  $Ca^{2+}$  from the SR (Walker *et al.*, 2003; Weiss *et al.*, 2006). Moreover, if AP repolarization alternate between long and short, this increases the repolarisation gradients that can result in a unidirectional block, leading to re-entrant arrhythmia (Laurita and and Rosenbaum, 2008). APD alternans has been shown in several studies to be a precursor to many arrhythmias

though the mechanisms underlying it are complex,  $\text{Ca}^{2+}$  cycling is the main suggested mechanism (Pruvot *et al.*, 2004; Walker *et al.*, 2003; Goldhaber *et al.*, 2005).

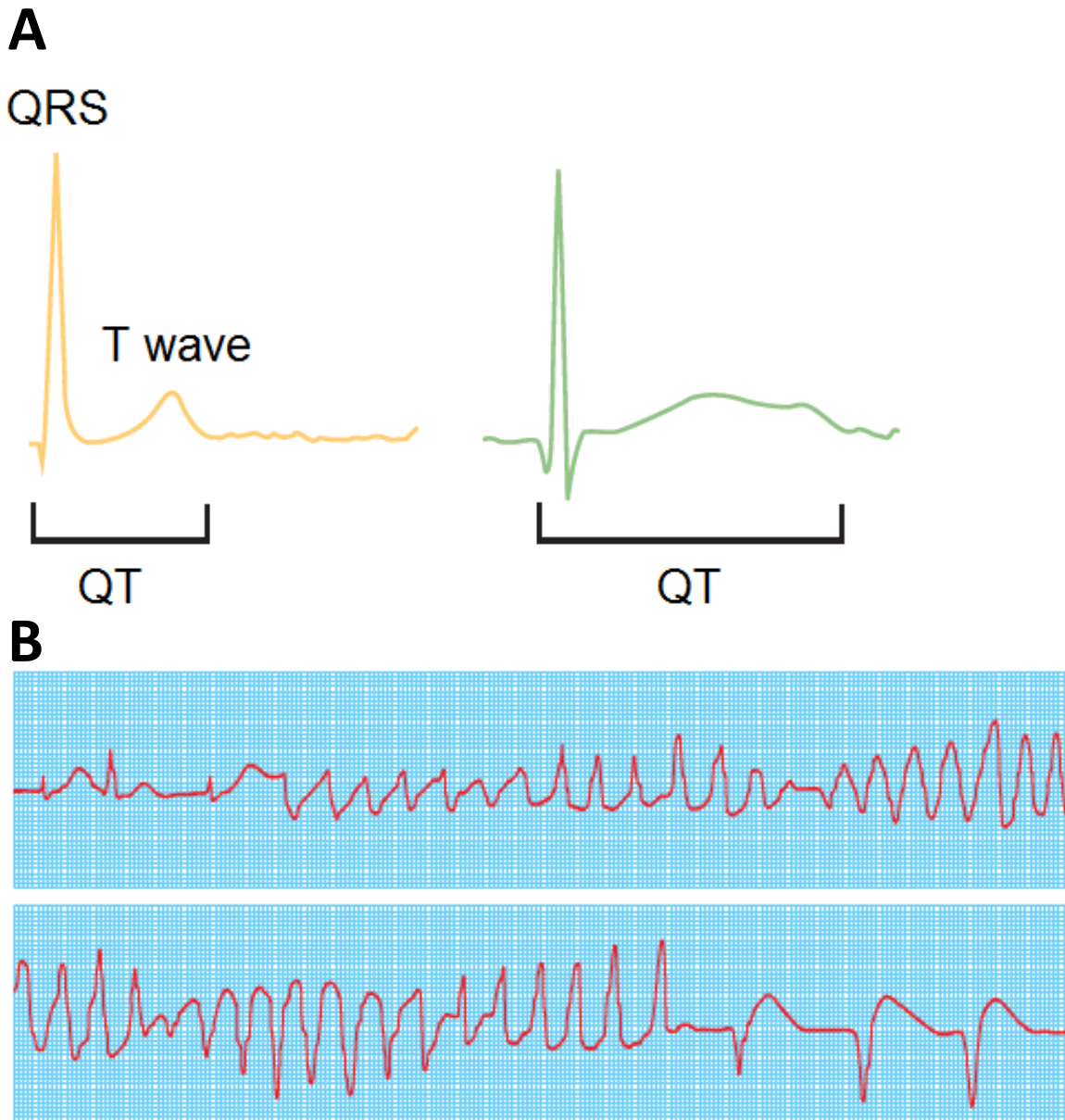


**Figure 1.12: The ECG-QT interval can predict the risk of torsade de pointes arrhythmias. A)** Representation of normal (orange) and abnormal (green) ECG traces for a single cardiac cycle. The abnormal trace displays a prolongation between the start of the Q wave and the end of the T wave, which is the QT interval. Modified from Sanguinetti and Tristani-Firouzi, (2006). **B)** An ECG demonstrating a supraventricular rhythm with a long QT (LQT) interval giving way to torsades de pointes. Modified from Kumar, (2012).

### **1.2.1 Background of cardiac arrhythmias and sudden cardiac death (SCD)**

An arrhythmia is a problem with the rate or rhythm of the heartbeat. During an arrhythmia, the heart can beat too fast, too slow, or with an irregular rhythm. A heartbeat that is too fast is called tachycardia. A heartbeat that is too slow is called bradycardia. Most arrhythmias are harmless, but some can be serious or even life threatening (Zipes *et al.*, 2006). During an arrhythmia, the heart may not be able to pump enough blood to support life.

Regardless of the specific arrhythmia, the pathogenesis of the arrhythmias falls into one of three basic mechanisms: enhanced or suppressed automaticity, triggered activity, or re-entry. Automaticity is a natural property of the SAN, the AVN, and Purkinji fibers, although rates in AVN and Purkinji fibers are too slow to pace the heart. Ischemia, scarring, electrolyte disturbances, medications, advancing age, and other factors may suppress or enhance automaticity in various areas (Sipido *et al.*, 1995). Suppression of automaticity of the SAN can result in sinus node dysfunction and in sick sinus syndrome (SSS). Enhanced automaticity can result in multiple arrhythmias, both atrial and ventricular. Triggered activity occurs when early after-depolarizations (EADs) and delayed after-depolarizations (DADs) initiate spontaneous depolarization (Figure 1.13). EADs are oscillations of phase 2 of the AP or later during phase 3 of repolarization. If it occurs during the plateau then it is likely due to reactivation of  $\text{Ca}^{2+}$  channels while those occurring during late repolarization ( $E_m$  below -40) are more likely to be due to  $\text{Ca}^{2+}$  activated currents likely by  $\text{Na}^+/\text{Ca}^{2+}$  exchanger and not due to reactivation of  $I_{\text{Ca,L}}$  because  $\text{Ca}^{2+}$  channels will not be activated at this negative  $E_m$ . EADs can trigger new APs that may appear as ectopic beats on the ECG (Volders *et al.*, 2000; Sipido *et al.*, 1995). On the other hand, DADs are oscillations in membrane potential that occur after repolarization of an AP has completed. It occurs due to an increase of  $[\text{Ca}^{2+}]_i$  and a high SR  $\text{Ca}^{2+}$  load which activates  $\text{Na}^+/\text{Ca}^{2+}$  exchanger, the resultant inward current generates DADs (Volders *et al.*, 2000; Weiss *et al.*, 2010; Nuss *et al.*, 1999). On the other hand, ventricular tachycardia and fibrillation are due to re-entrant mechanisms. Probably the most common mechanism of arrhythmogenesis results from re-entry. In re-entry a defect in the propagation of the cardiac impulse due to unidirectional conduction

block, a decrease in AP conduction velocity, and decreases in the refractory period which increases the probability of re-excitation (Weiss *et al.* 2002). For example, re-entry occurs with ventricular tachycardia from conduction around the scar of a myocardial infarction (MI). Ventricular fibrillation is the most life-threatening ventricular arrhythmia. Ventricular fibrillation is a heart rhythm problem that occurs when the heart beats with rapid, erratic electrical impulses (Jalife, 2000). This causes the ventricles to shake uselessly, instead of pumping blood. During ventricular fibrillation heart rate is so high (>500 beats/minute) that ventricular muscle contraction becomes severely uncoordinated and fails to effectively pump blood to the body vital organs (Weiss *et al.*, 2002). Emergency treatment for ventricular fibrillation includes cardiopulmonary resuscitation (CPR) and shocks to the heart with a defibrillator. VF is the leading cause for sudden cardiac death which is defined as unexpected natural death from a cardiac cause within a short time period, generally <1 hour from the onset of symptoms (Volders *et al.*, 2000). Ventricular tachyarrhythmias are considered life threatening conditions and knowing the underlying mechanisms behind their pathogenesis helps in treating them. One of the cardiac properties that determine arrhythmogenesis is electrical restitution which will be discussed in the coming section.

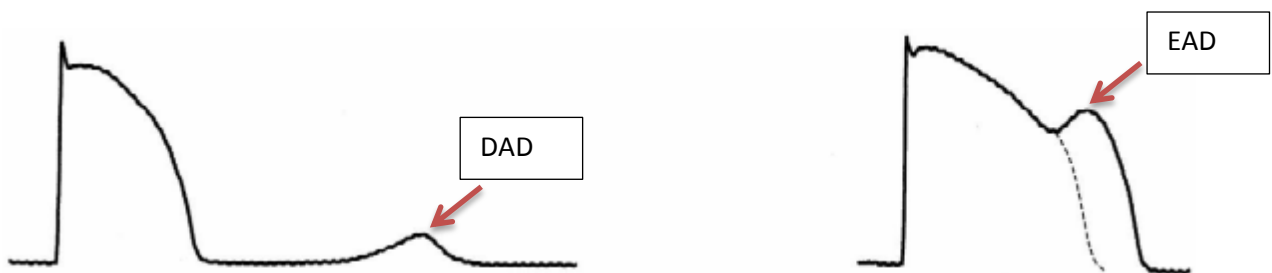


**Figure 1.13: Schematic representation of a DAD and an EAD.**

**Left panel:** Shows a completed AP followed by a delayed afterdepolarisation; DADs (indicated by red arrow). **Right panel:** Shows an AP with an early afterdepolarisation; EADs (indicated by red arrow) interrupting the repolarisation phase of the AP. Modified from Volders *et al.* (2000).

## **1.2.2 Electrical restitution**

### **1.2.2.1 Electrical restitution definition and link to arrhythmia**

Electrical restitution (RT) is an intrinsic property of the heart that modulates APD according to heart rate (HR). Therefore, the simplest definition for it is the relationship between APD and the preceding diastolic interval (DI), which is the interval between two action potentials, over a range of cycle lengths (CL) (Banville and Gray, 1998). The preceding DI is the time interval between full cardiac repolarisation and the upstroke of the next action potential. If APD did not adapt at high heart rate then heart block would occur. Restitution is thought to occur as some cardiac ion currents do not fully recover at short DI which leads to short APD at short DI<sub>s</sub>. Plotting APD against DI at different CL generates the APD electrical restitution curve. Rate dependent alterations of APD are known determinants of ventricular arrhythmias; stimulating cells at high rate will shorten DI and APD. So RT is known to be an adaptive mechanism to preserve diastole at high HR (Wilson and Rosenbaum, 2009). Many studies have concluded that the maximum slope of the electrical restitution curve provides information about arrhythmogenicity (Horner *et al.*, 1996; Brack *et al.*, 2007; Weiss *et al.* 2002). When the maximum slope of the curve is greater than 1, oscillations in the cardiomyocytes electrical activity are facilitated and thus arrhythmogenicity is higher because small changes in the DI can lead to larger changes in the APD, which makes the heart unstable. When the maximum slope of the electrical restitution curve is less than 1 that makes it less arrhythmogenic (Cao *et al.*, 1999). Moreover, there is supportive evidence that drugs which reduce restitution slope play a protective role against arrhythmias such as the antiarrhythmic drug procainamide (Riccio *et al.*, 1999). L-arginine which is the precursor of nitric oxide (NO) also prevented ventricular fibrillation by increasing the threshold for VF (Brack *et al.*, 2007).

RT can be measured experimentally using one of two types of protocol. The dynamic restitution (DYRT) and the standard restitution protocols (STRT). In DYRT (Figure 1.14) the preparation is paced at a constant rate until steady state has been

achieved, and subsequently at faster rates until a point at which APs fail to capture. At faster rates oscillations in APD would result, in which APs alternate between long and short durations (electrical alternans) (Banville *et al.*, 2002). As cycle length is equal to the sum of APD and DI, during alternans each long APD is followed by a short DI, which in turn is followed by a short APD and a long DI for a constant cycle length (Myles *et al.*, 2008).

In standard restitution protocols (STRT) (Figure 1.15) the preparation is paced at a constant cycle length using conditioning stimuli known as S1 until steady-state in APD and DI is reached; this is then followed by another stimulus (S2) at variable time intervals from the S1 stimulus. The preparation is then paced at S1 until steady-state has been reached again and is then perturbed by an S2 of shorter S1-S2 interval. Then the sequence will be repeated to the point of ERP, when no AP can be generated. The APD corresponding to the S2 stimulus and its preceding DI at a range of S1-S2 intervals are plotted to generate the restitution curve (Osadchii, 2012; Brack *et al.*, 2007).

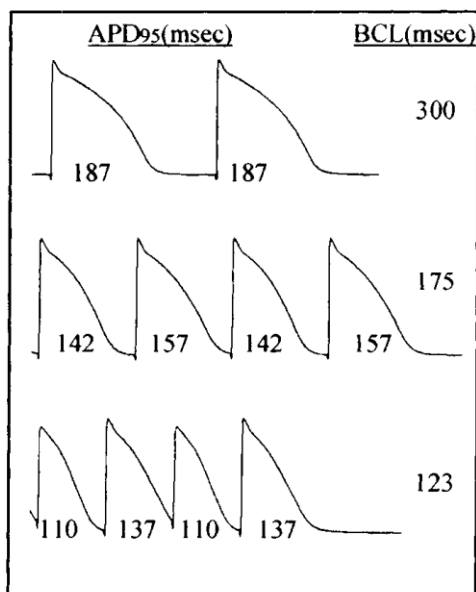


**Figure 1.14: Dynamic restitution protocol.** The APs in the Figure is from isolated, perfused canine left ventricles. The preparation is paced at faster rates (shorter CLs) until a point at which APs fail to capture. AP recordings corresponding CLs: 300, 175, and 123 ms. Numbers below APs indicate APD<sub>95</sub>, note alternans at CL of 175 ms and 123 ms. Modified from Koller *et al.* (1998).

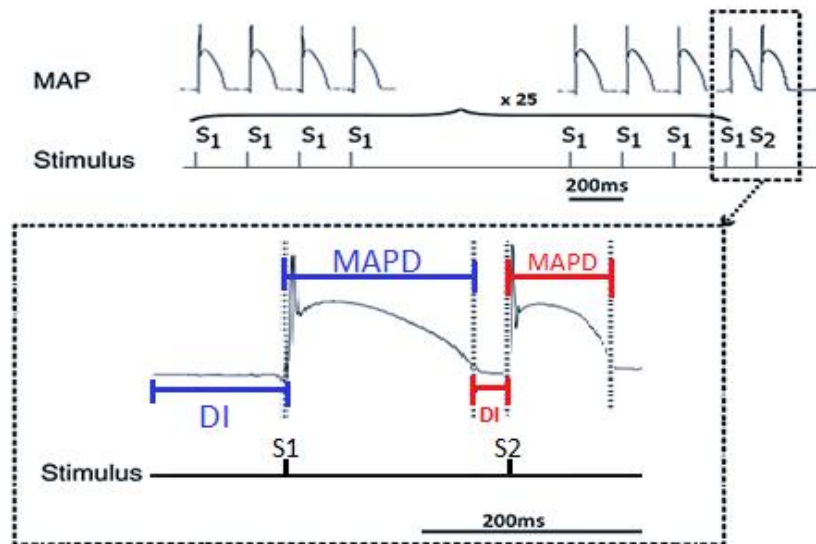


**Figure 1.15: Standard restitution protocol.** The upper panel shows Monophasic action potential (MAP) from whole rabbit heart used to determine the electrical restitution curve. The first four and the last four S1 MAPs and S2 MAPs are shown. The Lower panel illustrates an expanded section representing calculation of diastolic interval (DI) and measurement of MAP duration at 90% repolarisation (MAPD<sub>90</sub>). Modified from Ng, G.A *et al.* (2007).

### **1.2.3 Ionic mechanisms of electrical restitution**

Experimental studies exploring restitution in single cells are sparse. However, some studies have approached single cell restitution using computerised or simulated models (Cherry *et al.*, 2004; Fox *et al.*, 2002; Fenton *et al.*, 2002; Decker *et al.*, 2009). In 1987 the first study to characterise single cell electrical restitution was published (Robinson *et al.*, 1987). Before this study, it was widely accepted that ion accumulation and depletion in extracellular spaces were the major contributors to electrical restitution. Robinson *et al.* (1987), although did not conclusively explain the ionic mechanisms underlying RT, they anticipated that incomplete recovery of plateau currents could contribute to the restitution process in both single cells and intact tissue. It has been shown in computerised simulation studies that the ionic mechanisms of RT and APD dynamics have similarities between single cells and multicellular preparations (Decker *et al.*, 2009).

Pueyo *et al.*, (2010) studied right ventricle papillary muscles isolated from adult dogs' hearts and human ventricular tissue. Transmembrane APs were recorded at different stimulation frequencies and the ionic currents behind restitution were investigated. They measured the percentage of total change in peak value for each ionic current and during fast (with time constant  $< 30$  s) and slow (with time constant  $>2$  min) phases of APD adaptation for CL varying from 1,000 to 600 ms.  $I_{Ca,L}$  and  $I_{Ks}$  experienced the greatest percentage of total change during the initial phase of rate adaptation and are the key ionic currents driving that phase. The dynamics of the  $I_{Ca,L}$  slow voltage-dependent inactivation gate and the  $I_{Ks}$  activation gate play role in the initial phase of APD adaptation after sudden acceleration in heart rate (shorter CLs). Indeed, a sudden decrease in CL results in an insufficient time for  $I_{Ca,L}$  to fully recover whereas  $I_{Ks}$  is unable to completely deactivate at the end of each beat. This results in a reduction in the net inward current and an increase in the net outward current, thus shortening APD.

Long term adaptation ensues after 10-12 beats where  $[Ca^{2+}]_i$  accumulates as there is inadequate time for  $Na^+/Ca^{2+}$  exchanger to extrude it during phase 2 of the AP. High  $[Ca^{2+}]_i$  decreases further influx of  $Ca^{2+}$ , calcium dependent inactivation of  $I_{Ca,L}$ , whilst increasing  $Ca^{2+}$  extrusion through  $Na^+/Ca^{2+}$  exchanger, eventually decreasing the net entry of  $Ca^{2+}$  into the cell (Janvier *et al.*, 1997; Tseng *et al.*, 1988). Meanwhile, at short DIs, there is also insufficient time for the extrusion of  $Na^+$  (inward current from the previous AP). The increase in  $Na^+/Ca^{2+}$  exchanger activity leads to the accumulation of  $Na^+$ . Thus increases the  $Na^+/K^+$  pump (3 $Na^+$  out: 2 $K^+$  in). Therefore  $Na^+$  influx and efflux goes to equilibrium. Additionally, stimulation at shorter CLs leads to accumulation of  $K^+$  in extracellular clefts, effectively shortening the APD by greater outward  $K^+$  currents (Eisner *et al.*, 2009; Carmeliet, 2004) due to stabilization of the opening conductance of the channels by the high extracellular  $K^+$ . Research on currents other than  $Ca^{2+}$  in underlying electrical restitution is scant. Most research studies have been studying  $Ca^{2+}$  cycling role in mediating APD adaptation to stimulation frequencies.

Goldhaber *et al.* (2005) investigated the role of  $[Ca^{2+}]_i$  cycling in regulating APD restitution slope and APD alternans in rabbit ventricular myocytes at 35-37°C, using perforated patch clamp techniques with Fura-2-AM to measure  $[Ca^{2+}]_i$ . APD

restitution was measured by either the STRT or the DYRT protocols. To test the importance of SR  $[Ca^{2+}]_i$  cycling on APD restitution and alternans; Thapsigargin and Ryanodine have been used to suppress SR- $Ca^{2+}$  cycling. Thapsigargin and Ryanodine treatment markedly suppressed the  $[Ca^{2+}]_i$  transient (Figure 1.16B, inset). In addition, Thapsigargin and Ryanodine significantly flattened the maximum slope of APD restitution by both the STRT and DYRT pacing methods. In DYRT, APD restitution slope became  $<1$  for all DIs, consistent with the abolition of APD alternans (Figures 1.16D). In STRT, the slope was reduced but remained  $>1$  over a similar range of DIs. Moreover, APD alternans was abolished with Thapsigargin and Ryanodine (Figure 1.16F). Which means that eliminating the SR  $Ca^{2+}$  release decreases the slope of the AP restitution curve and alternans which confirms the role of  $[Ca^{2+}]_i$  level in APD adaptation.

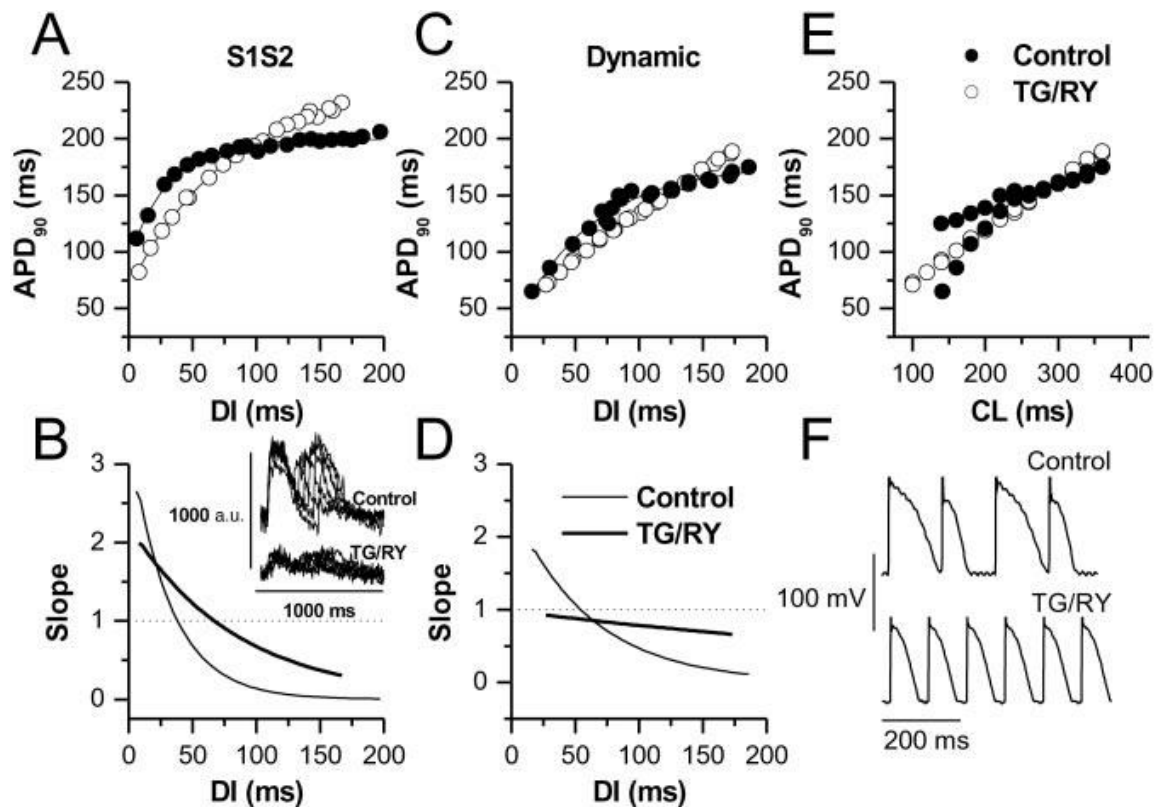


**Figure 1.16: Effect of eliminating SR  $Ca^{2+}$  release on APD restitution during STRT pacing (A and B) and DYRT (C and D).** Solid symbols are before, and open symbols are with thapsigargin and ryanodine (TG/Ry). Inset in **B** shows that TG/Ry markedly suppressed the  $[Ca^{2+}]_i$  transient. **E**) Illustrates that APD alternans during DYRT was abolished by TG/Ry. **F**) shows representative APs control and TG/Ry. Modified from Goldhaber *et al.* (2005).

In addition to the previous evidence, 100% blockade of  $I_{Ca,L}$  using Nisoldipine (LTCC blocker) has been shown to inhibit APD adaptation/shortening during single cell electrical restitution protocols in isolated rabbit cardiac ventricular myocytes. Moreover, the use of Thapsigargin and Ryanodine partially flattened APD restitution curve (Tolkacheva *et al.*, 2006) (Figure 1.17).

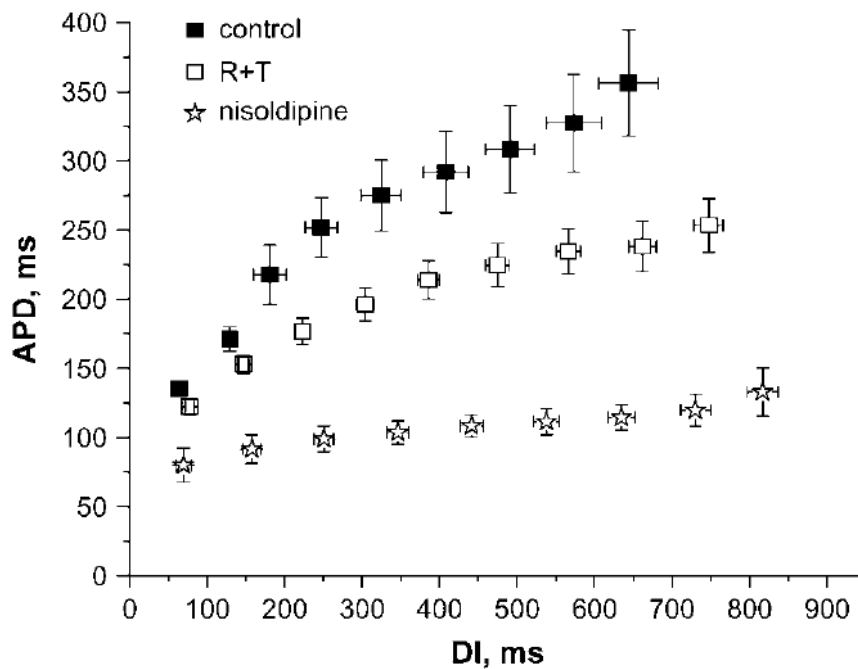


**Figure 1.17: Effect of Ryanodine plus Thapsigargin (R+T) and Nisoldipine on electrical restitution curve in isolated rabbit ventricular myocytes.** Use of ryanodine and thapsigargin partially flattens APD restitution. Nisoldipine completely inhibits APD restitution over the entire range of DI. Modified from Tolkacheva *et al.*, (2006).

Because intracellular calcium cycling is a dynamic process; alternans in  $Ca^{2+}$  transient amplitude ( $[Ca^{2+}]_i$  Alternans) may drive APD to also alternate because  $I_{Ca,L}$  and the  $Na^+/Ca^{2+}$  exchanger are sensitive to  $[Ca^{2+}]_i$  (Tusscher and Panfilov, 2006). Goldhaber *et al.*, (2005) studied the effect of BAPTA-AM, a buffer of the global  $[Ca^{2+}]_i$  transient, on electrical restitution curve. Interestingly, APD alternans was completely abolished, thus suggesting that  $[Ca^{2+}]_i$  cycling is required for APD alternans. They used BAPTA-AM at frequencies where they normally see alternans.

Using genetic approaches to upregulate the cardiac isoform of SERCA (SERCA2a) resulted in suppression of alternans in isolated guinea-pig myocytes (Cutler *et al.*,

2009). That makes sense as at higher pacing frequencies, limitations of SR  $\text{Ca}^{2+}$  uptake kinetics preclude adequate refilling of  $\text{Ca}^{2+}$  stores. Moreover, the RyR is the main SR  $\text{Ca}^{2+}$  release channel and the primary activator of the RyR is a cytosolic elevation of  $\text{Ca}^{2+}$ .  $\text{Ca}^{2+}$  release from RyR is unavailable immediately after release due to RyR inactivation. Recovery of RyR requires several hundred milliseconds to reach full availability (Brochet *et al.*, 2005; Ramay *et al.*, 2011). Incomplete RyR recovery from inactivation may contribute to instabilities of  $\text{Ca}^{2+}$  release and vulnerability to alternans and arrhythmias which means factors other than  $I_{\text{Ca,L}}$  might play a role in the mechanism of APD alternans (Edwards and Blatter, 2014).

Literature on other ionic currents role in alternans, other than  $\text{Ca}^{2+}$ , is sparse. In one study, APD alternans was suppressed by increasing the magnitude of  $I_{\text{K1}}$ ,  $I_{\text{Kr}}$ , or  $I_{\text{Ks}}$  in canine ventricle. These results suggest a role of other ionic basis for APD alternans, which should facilitate the development of pharmacological approaches to eliminating alternans and need further investigation (Fox *et al.*, 2002).

### **1.3 Autonomic control of the heart**

The heart is continually innervated by both sympathetic and parasympathetic nerves so that at any one time, either division may dominate. The degree of imbalance between the two divisions is termed autonomic tone. In humans at rest, the parasympathetic tone predominates, which causes the resting heart rate of humans to be approximately  $60 \text{ beats}\cdot\text{min}^{-1}$  (Levick *et al.*, 2000).

Autonomic influence on heart physiology has been extensively characterised but traditionally, it is known to have an effect on 3 main parameters of heart function: chronotropy (heart rate), inotropy (force of contraction) and dromotropy (impulse conduction). Sympathetic nerves up-regulate all three parameters whereas parasympathetic nerves generally have the opposite effect.

#### **1.3.1 The effects of autonomic nervous system on electrical restitution curve and ventricular fibrillation risk**

The autonomic nervous system (ANS) plays an important role in the modulation of cardiac electrophysiology and arrhythmogenesis. Decades of research has contributed to a better understanding of the anatomy and physiology of cardiac ANS and provided evidence supporting the relationship of autonomic tone to clinically

significant arrhythmias (Shen and Zipes, 2014). The first study of the effect of the vagus nerve stimulation (VS) on the susceptibility of the ventricle to experimental arrhythmia was undertaken by Einbrodt (1859), who confirmed that ventricular fibrillation was harder to induce in dogs during stimulation of the parasympathetic division of the autonomic system (vagus nerve). Sympathetic stimulation with epinephrine in porcine models increases the slope of ventricular APD restitution curves (Taggart *et al.*, 1990). This was confirmed in humans, in whom stimulation with adrenalin increased the steepness of the slope of APD restitution curves, further demonstrating the known effects of adrenergic stimulation in facilitating ventricular fibrillation (Taggart *et al.*, 2003). The effect of the ANS system on the electrical restitution curve is important clinically as  $\beta$ -blockers have been shown to reduce the risk of sudden death in heart failure patients further, highlighting the important association between the ANS and sudden death (Trujillo and Nolan, 2000).

Moreover, VS in innervated, isolated rabbit hearts during STRT flattened maximum RT slope, which means a protective effect has been encountered by VS. Sympathetic stimulation (SS) has shown to have opposite effect (Ng, G.A *et al.*, 2007). As demonstrated in Figure 1.18; the slope of the electrical restitution curve under SS was higher than the slope under VS. In the same study, the VF threshold, which is the minimum current which can induce VF, was higher during VS while lower during SS, which means inducing VF during SS is easier than during VS which approve the protective role of the vagus stimulation. Interestingly, this protective role of the vagus nerve is recently attributed to NO production from the nerve terminals; that's what make it really important to understand the NO signalling pathways and how does it work in protecting from arrhythmias in the single cell level.

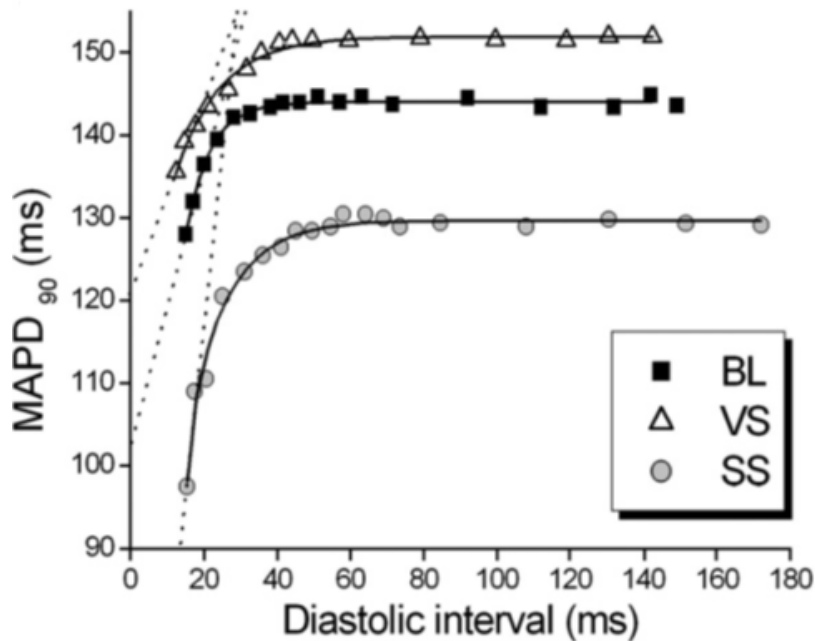


**Figure 1.18: The effects of VS and SS on STRT and VF risk.** Representative composite STRT curves during baseline, SS and VS. BL: Baseline; VS: Vagal stimulation; SS: Sympathetic stimulation. Modified from Ng, G.A, *et al.*, (2007).

### **1.3.2 Role of Nitric oxide in electrical restitution and VF risk**

Modification in function of the cardiac ANS has proved to be a powerful predictor of cardiac death and cardiac arrhythmia. However, little is known about the mechanisms by which this system is regulated. Recent studies suggested that NO may act as an important mediator in this pathway (Herring and Paterson, 2001; Chowdhary *et al.*, 2000). NO derived from nNOS can mediate a number of the effects of vagal nerve in the heart including heart rate control (Jumrussirikul *et al.*, 1998), atrio-ventricular conduction (Conlon and Kidd, 1999), and enhances the bradycardic effects of vagal activity on the sinus node (Paterson, 2001). Histochemical staining techniques have identified neuronal populations that contain the neuronal isoform of nitric oxide synthase (nNOS) within medullary cardio-regulatory sites and their peripheral autonomic pathways (Chowdhary and Townend 1999).

As previously mentioned the VS reduces the electrical restitution slope thus protecting the heart against VF. It has been concluded that NO is responsible for a great part of this protective effect of VNS. Brack *et al.*, (2007) studied Langendorff perfused isolated rabbits hearts with intact vagal nerve innervation and presented evidence that NO mediates the protective effect of vagus nerve on ventricular fibrillation via effects on electrical restitution. VS increased ventricular fibrillation threshold (VFT) and decreased the maximum slope of APD restitution, these effects were blocked using the nonspecific nitric oxide synthase inhibitor, N-Nitro-L-arginine (L-NNA) and reversed by adding the nitric oxide synthase substrate (L-Arginine) (Figure 1.19). Moreover, Brack *et al.*, (2009) have provided direct evidence that VS leads to the release of NO in the ventricle via nNOS activation in isolated innervated rabbit heart using the NO fluorescent indicator 4, 5-diaminofluorescein diacetate (DAF-2 DA) during stimulation of the cervical vagus nerves. The vagally mediated increase in fluorescence was abolished during L-NNA perfusion and returns on washout of L-NNA. Compared to control, L-NNA significantly decreased the basal fluorescence signal. The selective neuronal nitric oxide synthase inhibitor, 1-(2-trifluoromethylphenyl)-imidazole (TRIM), also abolished the vagally mediated increase in fluorescence. Unlike perfusion with L-NNA, TRIM did not alter the basal fluorescence signal. Therefore, activation of cardiac parasympathetic efferent nerve fibres by stimulation of the cervical vagus is associated with NO production and release in the ventricle of the rabbit, via the neuronal isoform of nitric oxide synthase. What is not known is whether NO affects single cell electrical restitution and AP repolarization.

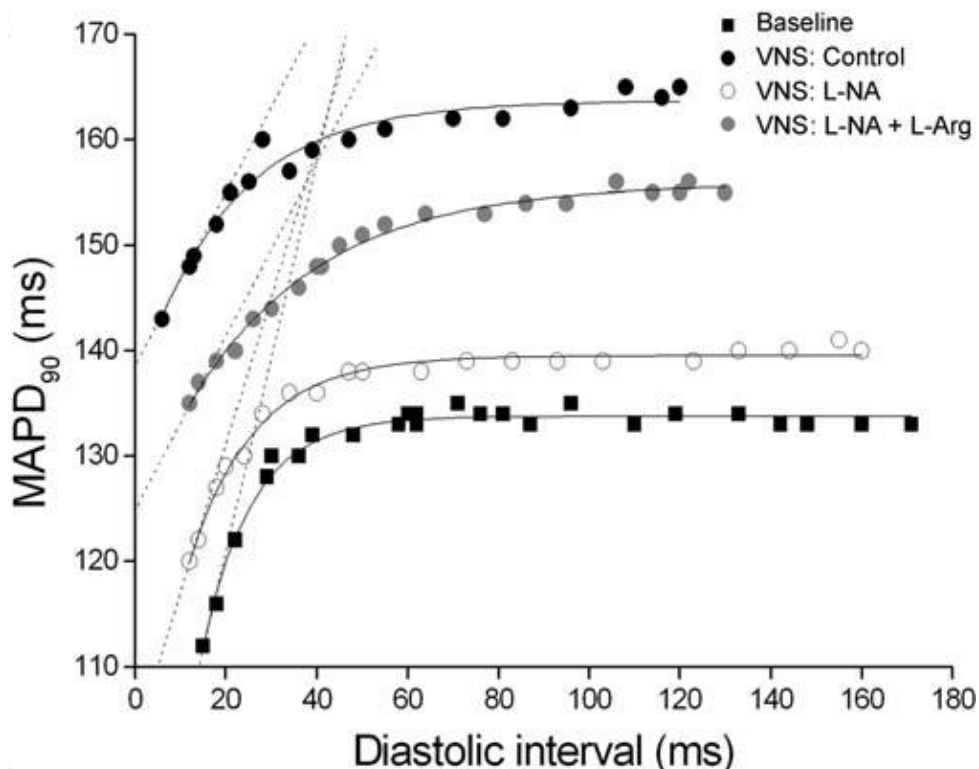


**Figure 1.19: Effect of L-Arginine and L-NNA under VNS on STRT in the whole heart.** STRT curves demonstrating that the protective effect of VNS on electrical restitution is lost when NOSs were blocked by L-NNA. That was reversed by introducing L-Arginine, a substrate required for NO synthesis. VNS: Vagal nerve stimulation; L-NNA: NOS inhibitor; L-Arg: L-Argenine. Modified from Brack *et al.*, (2007).

## **1.4 Nitric oxide:**

### **1.4.1 Nitric oxide synthesis:**

Our understanding of the biological function of Nitric oxide (NO) has come from discovering that it is a vital second messenger molecule mediating intracellular and intercellular signals. In 1998 Robert Furchgott, Louis Ignarro and Ferid Murad were awarded the Nobel Prize in physiology because they concluded that NO functions as a signalling molecule in the cardiovascular system. Obviously NO is composed of one nitrogen atom and one oxygen atom. Its half-life is only a few seconds (Ignarro and Napoli, 2005). NO functions as endothelial derived relaxation factor (EDRF) in the vasculature, and it participates in a number of physiological processes, such as

smooth muscle relaxation, inhibition of platelets and leukocyte aggregation, attenuation of vascular smooth muscle cell proliferation, neurotransmission, and immune defence. Also it is involved in the pathology of many inflammatory diseases, including myocarditis, colitis (Iwashita *et al.*,1995), nephritis (Kelly and Gold, 1999), cancer (Wink *et al.*,1998), diabetes (Chan *et al.*, 2000), and neurodegenerative disease (Bolanos *et al.*,1997). Recently, it has also become clear that NO has important roles in cardiac muscle physiology.

NO is synthesized by nitric oxide synthases (NOS), which are specialized enzymes that catalyze the O<sub>2</sub> dependent oxidation of the guanidino nitrogen of L -arginine to give NO and L-citrulline . Three isoforms of NOS have been identified; NOS1 which is the neuronal NOS (nNOS), was first identified in neuronal tissue. NOS2 which is the inducible NOS (iNOS) is upregulated in response to a variety of stimuli and was first detected in macrophages. NOS3 which is the endothelial NOS (eNOS), was first detected in the endothelium and is considered the major source of plasma NO (Walter and Gambaryan, 2009). All three isoforms of NOSs are present in the heart. The activity and expression of nNOS and eNOS differs from that of iNOS. All three isoforms can bind calmodulin (CaM) which in turn binds Ca<sup>2+</sup>. However, the activities of nNOS and eNOS are Ca<sup>2+</sup>-dependent, in contrast to the Ca<sup>2+</sup>-independent activity of iNOS. In the healthy heart, nNOS and eNOS are constitutively expressed (Brahmajothi and Campbell, 1999), whereas iNOS expression is induced by an increase in cytokines under pathophysiological conditions (Gidday *et al.*, 1999).

A NOS monomer consists of an oxygenase domain on the N-terminus, which binds to tetrahydrobiopterin (BH<sub>4</sub>) and Zn<sup>2+</sup>, and a reductase domain on the C-terminus which binds nicotinamide adenine dinucleotide phosphate (NADPH), flavine mononucleotide (FMN), and flavine adenine dinucleotide (FAD). The reductase domain transfers electrons from the reduced form of NADPH to FAD and FMN (Matsuda *et al.*, 1999). These electrons are transferred to the heme group on the oxygenase domain and used to convert L-arginine and O<sub>2</sub> to L-citrulline and NO. BH<sub>4</sub> and Zn<sup>2+</sup> are cofactors important for the dimerization of NOS. Electron flow appears to be from the reductase domain of one monomer to the heme/oxygenase domain of the other monomer which makes monomers inactive and dimerization necessary for NOS activation (Sagami *et al.*, 2001). Each NOS monomer has the

post-synaptic density-protein, discs-large, ZO-1 (PDZ) domain which can bind to regulatory proteins such as CAPON (carboxy-terminal PDZ ligand of nNOS) (Zhang *et al.*, 2014).

Electron transfer from the reductase domain to the oxygenase is facilitated by  $\text{Ca}^{2+}$ /calmodulin binding (Roman and Masters, 2006) to a calmodulin binding motif which is in between the oxygenase and the reductase domains (Figure 1.20). Calmodulin is  $\text{Ca}^{2+}$  binding messenger protein. When calmodulin and  $\text{Ca}^{2+}$  are absent; electron flow from FAD to FMN decreases (Matsuda *et al.*, 1999), so calmodulin is considered as an allosteric activator of NOS. When  $[\text{Ca}^{2+}]_i$  decreases to basal levels, calmodulin disassociates from NOS, and it becomes inactive. nNOS and eNOS bind calmodulin with an increase in  $[\text{Ca}^{2+}]_i$  of more than 500 nM. However the interaction of calmodulin and iNOS occurs at resting  $[\text{Ca}^{2+}]_i$  which makes iNOS independent of changes in  $[\text{Ca}^{2+}]_i$  (Nathan *et al.*, 1994, Yamamoto *et al.*, 2004). The  $\beta$ -AR signalling pathway and NO signalling are linked through the  $\text{Ca}^{2+}$ -CaM dependent regulation of NOS isoforms. NOS is activated by  $\text{Ca}^{2+}$ -CaM, so increases in intracellular  $\text{Ca}^{2+}$  with the nonspecific  $\beta$ -agonist Isoprenaline (ISO) could also activate NOS (Barouch *et al.*, 2002).

L-Arginine analogues, such as NG-monomethyl-L-arginine (L-NMMA), NG-nitro-L-arginine (L-NNA) and its methyl ester (L-NAME), are non-isoform-specific inhibitors of NOS which have proved to be valuable tools in the investigation of the physiological roles of NO (Chowdhary and Townend, 1999). The non-selective NOS inhibitor L-NNA antagonises the electron transfer to L-arginine or  $\text{O}_2$  and therefore inhibits NO synthesis (Munzel *et al.*, 2005). L-NNA is a commonly used inhibitor of NOS and was used in many of my experiments.

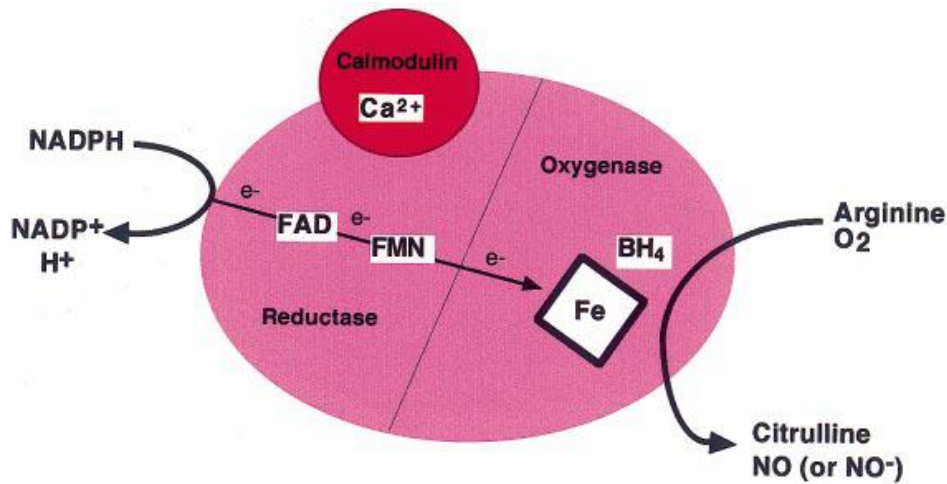


**Figure 1.20: Representation of a NOS monomer and the pathway involved in NO synthesis.** Nicotinamide adenine dinucleotide phosphate (NADPH), flavine mononucleotide (FMN), and flavine adenine dinucleotide (FAD), tetrahydrobiopterin (BH<sub>4</sub>). Modified from Alderton *et al.*, (2001).

### 1.4.1.1 Nitric oxide synthase isoforms

#### 1.4.1.1.1 Neuronal Nitric Oxide Synthase (nNOS)

nNOS is expressed in the cardiomyocytes and the cardiac autonomic nerves. nNOS localization in the cardiac myocytes has been studied by many research groups. nNOS has been found to be localized near to the SR with the Ca<sup>2+</sup>-ATPase (SERCA), RyR, on the sarcolemma with Na<sup>+</sup>-K<sup>+</sup>-ATPase (Na<sup>+</sup>/K<sup>+</sup> Pump), Ca<sup>2+</sup>/calmodulin-dependent Ca<sup>2+</sup>-ATPase, and with mitochondria (Kelly *et al.*, 1996; Massion *et al.*, 2003; Schulz *et al.*, 2005; Gonzalez *et al.*, 2007; Barouch *et al.*, 2002).

Not too much literature is known about nNOS effect on APs while most studies have concentrated on its effect on I<sub>Ca,L</sub> and contractility. Myocytes from nNOS knock-out mice (nNOS<sup>-/-</sup>) blunted contractility and decreased Ca<sup>2+</sup> transient amplitudes (Gonzalez *et al.*, 2007). Another target for nNOS signalling is phospholamban (PLB), which regulates the activity of SERCA. SERCA is inhibited by unphosphorylated PLB, while phosphorylation relieves this inhibition. It has been concluded by Wang *et al.* (2008) that inhibition of nNOS in wild-type mice reduced PLB phosphorylation and decreased contraction in both unstimulated and β-AR stimulated myocytes. In contrast, contraction was unaffected by nNOS inhibition in myocytes from PLB knock-out mice. This suggests that nNOS is important for

phosphorylation of PLB due to activating adenylyl cyclase and protein kinase A (Wang *et al.*, 2008, Zhang *et al.*, 2008; Hammond and Balligand, 2012).

#### **1.4.1.1.2 Endothelial Nitric oxide synthase (eNOS)**

eNOS is found in the coronary artery endothelial cells, and cardiomyocytes (Feron *et al.*, 1996). In cardiomyocytes, eNOS is preferentially localized in the caveolae and co-immunoprecipitates with caveolin-3 (Massion *et al.*, 2003, Ziolo *et al.*, 2008). Caveolins are a family of integral membrane proteins that are the principal components of caveolae membranes in the sarcolemma and involved in receptor-independent endocytosis and act as scaffolding proteins within caveolar membranes by compartmentalizing and concentrating signaling molecules such as non-receptor tyrosine kinases and eNOS.

Activation of eNOS causes depression of  $I_{Ca,L}$ , enhancement of  $I_{Ks}$ , and shortening of AP duration in guinea-pig ventricular myocytes (Bai *et al.*, 2005). eNOS has been found to affect rat ventricular cardiomyocytes contraction directly by targeting myofilament proteins such as troponin I (TnI) and decreases myofilament  $Ca^{2+}$  sensitivity (Kaye *et al.*, 1999) but the exact mechanism behind this interaction is not fully understood but maybe by activating guanylyl cyclase and a protein kinase G with subsequent phosphorylation of (TnI).

A number of studies have been conducted using knock-out eNOS (eNOS<sup>-/-</sup>) to demonstrate the effect on cardiac muscle physiology. Barouch *et al.*, (2002) demonstrated that eNOS<sup>-/-</sup> mice have enhanced inotropy and they next went on to determine the  $\beta$ -AR-stimulated cardiac reserve using ISO. eNOS<sup>-/-</sup> animals had augmented responses to ISO.

#### **1.4.1.1.3 Inducible Nitric oxide synthase (iNOS)**

iNOS is only expressed during immune responses such as ischemic reperfusion injury (Wildhirt *et al.*, 1999; Balligand *et al.*, 1994), septicaemia (Ichinose *et al.*, 2003), aging (Yang *et al.*, 2004), and heart failure (Ziolo *et al.*, 2004). iNOS is expressed in cardiomyocytes, endothelial and vascular smooth muscle cells, fibroblasts, and inflammatory cells (macrophages) and is stimulated by pro-inflammatory mediators such as cytokines and endotoxin. Interestingly, iNOS produces high levels of NO; these large fluxes determine the antimicrobial and antiparasitic function of the iNOS

(MacMicking, 1997). Such high output of NO results in a drop of blood pressure in septic shock (Ziolo and Bers, 2003).

### 1.4.2 Nitric oxide signalling pathways

Nitric Oxide conducts its effects on many physiological processes by different signalling pathways as shown in figure 1.21. NO can exert its effects either through cGMP dependent pathways or cGMP independent pathways. I will explain briefly these signalling pathways in the next sections.

## Nitric Oxide signalling pathways

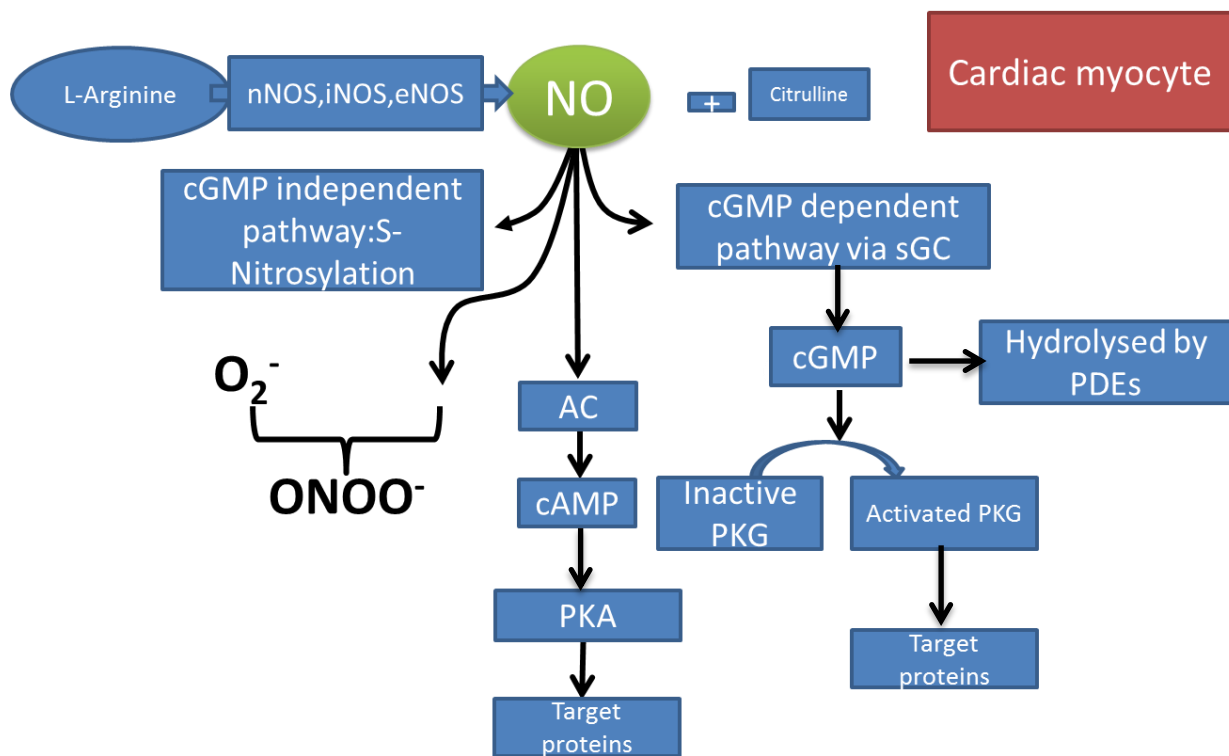


**Figure 1.21: Nitric oxide signalling pathways.** Nitric oxide synthase (NOS) isoforms catalyse the synthesis of NO. NO signalling pathways can be mediated via cGMP-dependent or cGMP-independent pathways. cGMP-dependent NO signalling activates soluble guanylyl cyclase (sGC), increases cGMP and directly activates protein kinase G (PKG). cGMP-independent NO signalling occurs mainly by S-nitrosylation or by reaction with superoxide to generate peroxynitrite (ONOO<sup>-</sup>). Protein kinase A (PKA) activity can also be indirectly regulated via cAMP. PDEs: phosphodiesterases.

### **1.4.2.1 Cyclic Guanosine Monophosphate (cGMP) dependent Nitric oxide signalling pathway**

Two types of NO signalling pathways have been described, one is the cyclic guanosine monophosphate (cGMP)-dependent and the other is cGMP-independent (Wedel and Garbers, 1998). In cGMP-dependent NO signalling, NO binds to the haem group of soluble guanylyl cyclase (sGC) resulting in its activation. Activation of sGC by NO catalyses the conversion of guanosine triphosphate (GTP) into cGMP. cGMP is an important second messenger that activates protein kinase G (PKG) directly and can regulate protein kinase A (PKA) indirectly. It does this by modulating the activity of cyclic nucleotide phosphodiesterases (PDEs) and the hydrolysis of cyclic adenosine monophosphate (cAMP). cGMP can stimulate PDE2 to increase degradation of cAMP which consequently decreases PKA activity or conversely cGMP inhibition of PDE3 can lead to increases of cAMP and consequently increased PKA activity (Fischmeister *et al.*, 2006). Protein kinases mediate the effects of cyclic nucleotides by phosphorylating protein targets, such as ion channels and proteins involved in excitation-contraction coupling (Draijer *et al.*, 1995).

#### **1.4.2.1.1 Soluble guanylyl cyclase**

sGC is a heterodimer that consists of one  $\alpha$  and one  $\beta$  subunit. In mammals two isoforms for each subunit have been identified  $\alpha 1$ ,  $\alpha 2$ ,  $\beta 1$  and  $\beta 2$  (Harteneck *et al.*, 1991) (Figure 1.22). The most common sGC isoform is  $\alpha 1\beta 1$ , which is found all over the body, but highest levels are found in lungs, nervous system and liver. sGC heterodimers are considered the active forms of sGC rather than homodimers (Andreopoulos and Papapetropoulos, 2000). The subunits of sGC consist of three different domains, a C-terminal regulatory domain, a central dimerisation domain and N-terminal catalytic domain. The C-terminal portions of  $\alpha$  and  $\beta$  subunits contain the cyclase homology domain which is responsible for the catalytic function and is responsible for binding GTP and converting it into cGMP (Koesling, 1999). NO dependent activation of sGC and the synthesis of cGMP is a key step in the NO/cGMP pathway.

sGC contains one protoporphyrin type IX haeme moiety in each heterodimer. This haem moiety is the target for NO. Upon binding to the haem moiety; NO forms a

hexacoordinated intermediate, which is transient and rapidly transformed to the stable pentacoordinated NO-haem complex (Hammond and Balligand, 2012). Formation of the pentacoordinated NO-haem complex is responsible for the high output activity of sGC. The N-terminal portion binds to haem which contains a central iron (Fe) atom which binds to NO (Wedel *et al.*, 1995).

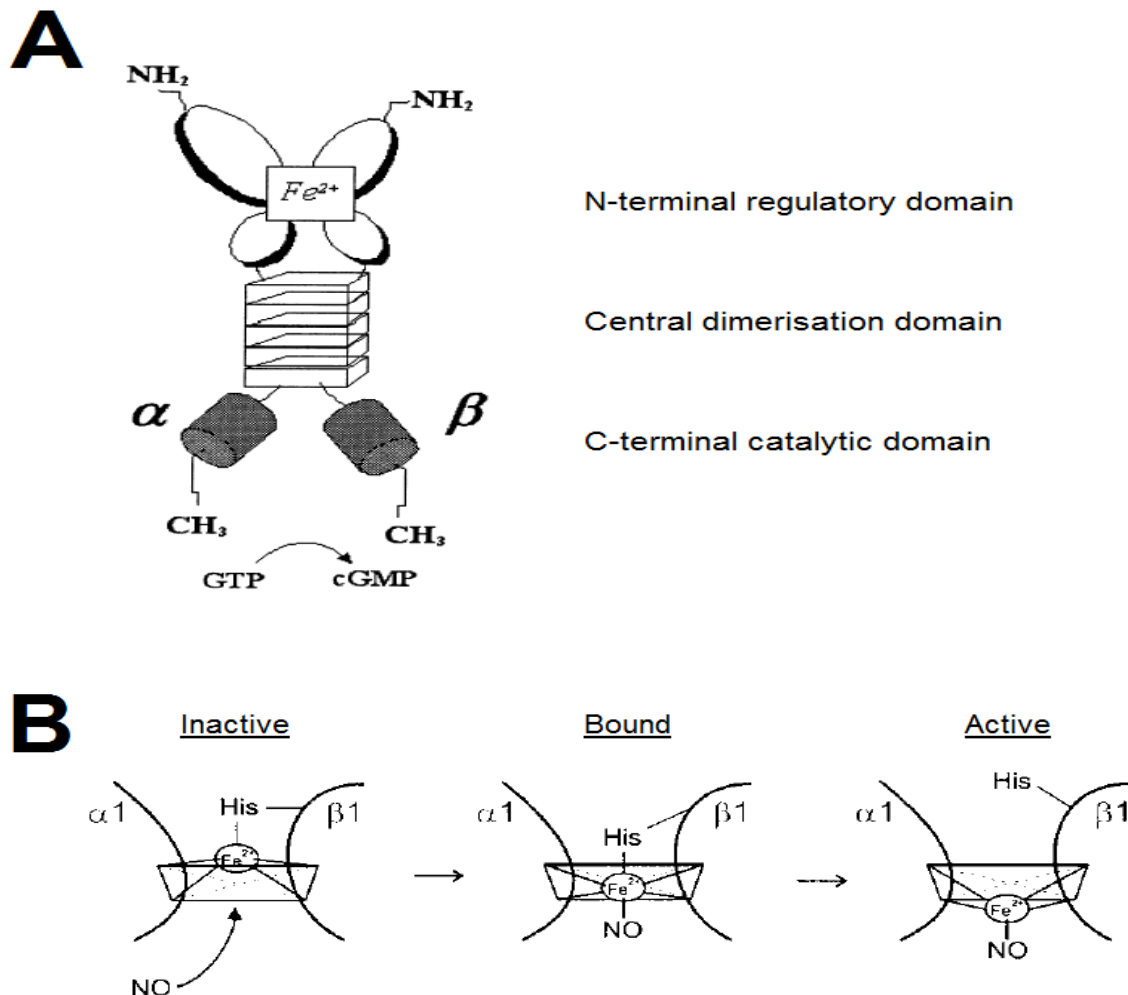


**Figure 1.22: sGC structure and activation by nitric oxide. A)** Structure of sGC. A heterodimer consisting of  $\alpha$  and  $\beta$  subunits each comprised of an N-terminal regulatory domain containing a haem group with a central  $\text{Fe}^{2+}$  that binds NO, a central dimerisation domain and a C-terminal catalytic domain that catalyses the conversion of GTP into cGMP. Modified from Andreopoulos and Papapetropoulos, (2000). **B)** The activation of sGC by NO. In its inactive state sGC exists as a five membered ring structure and  $\text{Fe}^{2+}$  is bound to histidine (His) a residue found on the  $\beta 1$  subunit. Upon NO binding to  $\text{Fe}^{2+}$  a six membered structure is formed. In its active form the bond between histidine and  $\text{Fe}^{2+}$  is broken forming a five membered nitrosyl haem complex. Modified from Bellamy and Garthwaite, (2002).

#### **1.4.2.1.1 Soluble guanylyl cyclase inhibition and activation**

Selective inhibitors of sGC have been identified that enabled discrimination of the sGC-mediated signalling from other signalling pathways. One of the most widely used selective inhibitors is 1H-[1,2,4] oxadiazolo-[4,3-a]quinoxalin-1-one (ODQ) which binds to the haem group of sGC, in competition with NO, and inhibits sGC by oxidising the haem group and making sGC inactive (Lies *et al.*, 2013). NO can bind to both ferrous/Fe<sup>+2</sup> and ferric/Fe<sup>3+</sup> Haem, however NO has higher affinity to the ferrous haem. Zhao *et al.* (2000) studied the mechanism of action of ODQ using electronic absorption spectroscopy and by measuring sGC activity. When ODQ was applied to the recombinant sGC, the electronic absorption spectra showed that the Soret peak shifted from 431 nm to 392 nm which indicates oxidation of the ferrous haem to ferric haem. In the absence of NO, ferrous sGC had a specific activity of  $68 \pm 12 \text{ nmol min}^{-1} \text{ mg}^{-1}$ . When sGC was treated with ODQ, sGC maintained a specific activity that was not too different of the untreated enzyme ( $88 \pm 11 \text{ nmol min}^{-1} \text{ mg}^{-1}$ ), suggesting that even though ODQ oxidized the haem, it had very little effect on the basal catalytic activity. But, ODQ inhibited NO-stimulated sGC activity ( $3804 \pm 593 \text{ nmol min}^{-1} \text{ mg}^{-1}$ ) (Zhao *et al.*, 2000). Inhibition of the NO-stimulated sGC activity by ODQ is due to oxidation of the sGC haem and not to perturbation of the catalytic site, since the ODQ-treated sGC has the same basal activity as untreated sGC.

Two different types of drugs have been developed to activate sGC; the haem-dependent sGC stimulators that enhance the NO sensitivity of sGC in its reduced ferrous state and haem-independent sGC activators that activate oxidised/haem-free NO-insensitive sGC. An example of the haem-independent sGC activator is BAY 58-2667, which binds to the haem binding pocket of sGC. Histidine 105, tyrosine 135 and arginine 139 located in the haem binding pocket have been identified as essential residues involved in sGC activation by BAY 58-2667 (Schmidt *et al.*, 2004). Stasch *et al.*, (2002) provides evidence that BAY 58-2667 activates sGC in a haem-independent manner. Ultra violet spectroscopy found that when NO was applied; the Soret peak shifted to a lower wavelength which is indicative of NO binding to haem. However, there was no change with the application of BAY 58-2667, suggesting it does not bind to haem. Furthermore, BAY 58-2667 activated sGC after removal of haem by detergents and oxidation of haem by ODQ. Amusingly, BAY 58-2667-

induced sGC activity was higher in the presence of ODQ. BAY 58-2667 and ODQ in combination, resulted in a potent concentration-dependent increase in sGC activity. Receptor binding studies indicated that sub-micromolar concentrations of BAY 58-2667 were sufficient for saturation of binding to sGC, in the presence of ODQ. The maximum saturation decreased by half in the absence of ODQ (Stasch *et al.*, 2002). As BAY 58-2667 is a weaker activator of sGC compared to NO, a higher concentration of BAY 58-2667 is required to exert similar effects to organic nitrates. However, concentrations as low as 1 nM produced physiologically relevant increases in cGMP and the effects are longer lasting due to a low clearance and long half-life which is therapeutically promising. Animal models and clinical trials have demonstrated that BAY 58-2667 increases cardiac output, decreases blood pressure by potent vasodilation, is cardioprotective similar to ischaemic preconditioning and inhibits platelet aggregation (Lapp *et al.*, 2009; Krieg *et al.*, 2009; Stasch *et al.*, 2002).

As an alternative to BAY 58-2667, Bayer AG kindly provided a closely related chemical analogue BAY 60-2770. An in-vitro study on purified sGC by Knorr *et al.* (2007) demonstrated that BAY 60-2770 shared similar characteristics with BAY 58-2667. The application of 0.0001 to 10  $\mu$ M concentrations of BAY 60-2770 increased sGC activity between 2 and 53 fold over basal activity, in a concentration-dependent manner. BAY 60-2770-induced increases in sGC activity were potentiated at all concentrations in the presence of 10  $\mu$ M ODQ. The activity of sGC increased substantially by 176 fold with 10  $\mu$ M BAY 60-2770, in combination with ODQ. Furthermore, haem-free sGC was also activated by BAY 60-2770 in the absence and presence of ODQ. In the presence of ODQ, 10  $\mu$ M BAY 60-2770 increased sGC activity dramatically by 242 folds. BAY 60-2770 was used in this project as a novel NO/haem-independent sGC activator in subsequent experiments to investigate the role of cGMP-dependent signalling pathways in cardiac repolarisation.

#### **1.4.2.1.2 Phosphodiesterases (PDEs)**

Cyclic nucleotide phosphodiesterases (PDEs) are responsible for hydrolysis of cyclic nucleotides; cGMP and cAMP. Therefore, they play a major role in NO/cGMP signaling pathways. The catalytic domains of all PDEs contain two Zn<sup>2+</sup> binding

sequences arranged in tandem (Fischmeister *et al.*, 2006; Francis *et al.*, 1994). More than 50 different mammalian PDEs exist which are divided into 11 families (PDE 1-11) according to coding sequence, domain structure and regulation (Maurice *et al.*, 2003).

Different PDEs have different mechanisms of regulation. For example, some PDEs are regulated by the change in concentration of cyclic nucleotide or by competition between cAMP and cGMP as in the case of dual specificity for PDE 1, 2, 3, 10, and 11. PDEs 5, 6, and 9 are considered to be “cGMP specific PDEs” while PDE 4, 7, and 8 are cAMP specific (Figure 1.23). PDEs are also differentially regulated. PDE1 is stimulated by  $\text{Ca}^{2+}$ -CaM and PDEs 2 and 5 are stimulated by cGMP (Zhang and Kass, 2011). In contrast, PDE3 is inhibited by cGMP (Miller and Yan, 2010).

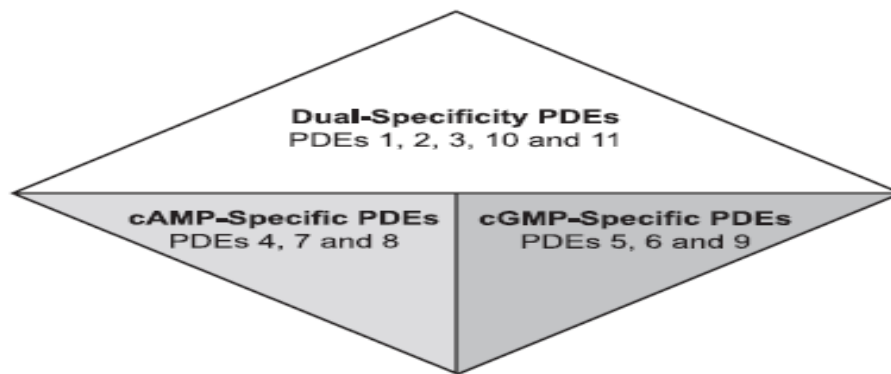


**Figure 1.23: Representation of mammalian families of phosphodiesterases (PDEs) according to preferences for either cAMP or cGMP.** Modified from Francis *et al.*, (2010).

#### **1.4.2.1.3 cGMP dependent protein kinase**

Protein kinase G (PKG) is selectively activated by cGMP. PKG is a homodimeric serine/threonine cGMP dependent protein kinase and considered the main effector molecule in the NO/cGMP pathway. Three different isoforms of mammalian PKG termed PKGI $\alpha$ , PKGI $\beta$  and PKGII have been identified (Francis *et al.*, 1999). PKG-I ( $\alpha$  and  $\beta$ ) is highly expressed in vascular smooth muscle cells and endothelial cells (Draijer *et al.*, 1995; Mery *et al.*, 1991). PKG-I ( $\alpha$  and  $\beta$ ) is the predominant isoform in the cardiac cells, whereas PKG-II expression is found largely in the brain, kidney and intestine (Feil *et al.*, 2003; Uhler, 1993; Jarchau *et al.*, 1994).

PKG-I and PKG-II have a homodimeric structure, with two identical monomer subunits. On each subunit, three different functional domains can be found, an N-terminal domain, a regulatory domain and a C-terminal catalytic domain (Takimoto, 2012). The N-terminal domain is involved in high affinity dimerization and also inhibits the catalytic domain in the absence of cGMP (Richie-Jannetta *et al.*, 2003; Monken and Gill, 1980). The structural features of the regulatory domain include two allosteric binding sites for cGMP (Lincoln *et al.*, 1977) and the C-terminal catalytic domain contains an adenosine triphosphate (ATP) binding site that is essential for phosphotransferase activity. cGMP binding induces a change in conformation and auto-phosphorylation, which in turn increases the affinity for further cGMP binding and relieves the inhibition on the catalytic domain, resulting in PKG activation (Francis *et al.*, 2010). PKG is then able to phosphorylate target proteins such as PDE5. Phosphorylation of PDE5 leads to an increase in cGMP hydrolysis and a subsequent decrease in cGMP levels. PKG-mediated phosphorylation of PDE5 is an important negative feedback mechanism in cGMP-dependent signalling (Corbin *et al.*, 2000).

#### **1.4.2.2 cGMP-independent Nitric oxide signalling pathways**

NO can also show effects via cGMP-independent signalling pathways. The primary mechanism of the cGMP-independent NO signalling pathway is the S-nitrosylation. S-nitrosylation is a reversible protein modification in which the thiol group (RSH) in the amino acid cysteine/ or tyrosine is converted into S-nitrosothiol (SNO). The RSH group has a sulphur-hydrogen bond. During S-nitrosylation; NO replaces the hydrogen atom (Sun and Murphy, 2010). S-nitrosylation of proteins leads to changes in protein structure and function which also prevents thiol group from going through irreversible oxidative (Gonzales *et al.*, 2009). The cGMP-dependent pathway and S-nitrosylation pathway in NO signalling and enzymatic protein denitrosylation are illustrated in Figure 1.24.

Many effects of NO are mediated by S-nitrosylation because cysteine is involved in the composition of many proteins such as ion channels. S-nitrosylation also affects RyR by increasing open probability which increases  $Ca^{2+}$  efflux (Xu *et al.*, 1998). Moreover, protein S-nitrosylation has been found to play an important role in NO-

mediated cardiovascular effects, including mitochondrial metabolic regulation, intracellular Ca<sup>2+</sup> handling, protein trafficking, and regulation of cellular defence against apoptosis, and oxidative stress as NO might provide protection to cells by S-nitrosylation of some critical protein thiols, preventing them from further oxidative modification by the reactive oxygen species (Sun *et al.*, 2006).

S-nitrosylation can be reversed by a number of denitrosylase enzymes; S-nitrosogluthathione reductase (GSNOR) and thioredoxin reductase (Trx) (Benhar *et al.*, 2009). The primarily denitrosylation enzyme in the cardiac myocytes is GSNOR although recently a role of Trx has been implicated (Shao *et al.*, 2012; Lima *et al.*, 2010). Protein denitrosylation has been shown to play a major role in controlling cellular S-nitrosylation with a lot of experimental studies have been conducted to investigate the evidence of denitrosylation in many target proteins (Benhar *et al.*, 2009).

A study conducted by Beigi *et al.*, (2012) demonstrated that GSNOR knock-out (GSNOR<sup>-/-</sup>) mice exhibit cardiovascular changes characterized by decreased vascular tone and impaired cardiac inotropic response to β-AR stimulation in comparison to wild type mice. Which indicates that protein denitrosylation by GSNOR is essential for cardiovascular regulation. Moreover, GSNOR<sup>-/-</sup> mice have increased mortality following endotoxic challenge and manifest hypotension under anesthesia (Schulman and Hare, 2012). These findings support the notion that hypo- and hyper-nitrosylation of specific protein targets correlate with pathophysiology.

In denitrosylation mediated by GSNOR; transnitrosylation of glutathione (GSH) by S-nitrosylated proteins generates S-nitrosogluthathione (GSNO). GSNO undergoes NADH dependent reduction by GSNOR to generate glutathione S-hydroxysulfenamide (GSNHOH), which then further reacts with GSH to form oxidized glutathione (GSSG). The redox cycle is completed by reduction of GSSG to GSH via GSSG reductase. GSNOR is a homodimeric enzyme with no cooperativity between the subunits. Each subunit consists of a large catalytic domain comprised of the N-terminal half of the protein and a C-terminal cofactor binding domain. GSNOR is a zinc-dependent, NAD<sup>+</sup> and NADH-dependent enzyme. The active binding pocket of GSNOR lies in a large cleft between the cofactor and catalytic domains (Green *et al.*, 2012). N6022 is a useful compound for investigating the effect of S-nitrosylation and has been used in this project. N6022 inhibits GSNOR by binding to the active binding

pocket of the GSNOR in a tight-binding, specific, and fully reversible way. N6022 has shown safety and efficacy in animal models of asthma, chronic obstructive pulmonary disease, and inflammatory bowel disease (Blonder *et al.*, 2014). In asthmatics; inhibiting GSNOR will increase pulmonary GSNO and induce bronchodilation and that was achieved in asthmatics rats using N6022 which is evidence that N6022 inhibits denitrosylation (Colagiovanni *et al.*, 2011). Moreover, recombinant human GSNOR, and ADH were produced in *Escherichia coli* and the GSNOR functional activity assay was measured in the absence and presence of N6022. Inhibition by N6022 is roughly 1000- fold more potent for GSNOR than for ADH (Green *et al.*, 2012). ADH assay was used as control.

In denitrosylation mediated by the Trx system; the active site dithiol motif of Trx1 (cytoplasmic) or Trx2 (mitochondrial) undergoes oxidation coupled to denitrosylation of SNO substrate. Oxidized Trx is reduced by the Trx reductase (TrxR), which employs the reducing power of NADPH to regenerate active Trx (Schulman and Hare, 2012). The cytoplasmic and mitochondrial thioredoxins mediate the denitrosylation of multiple s-nitrosylated proteins in a stimulus coupled, substrate specific, and spatially restricted manner. Following denitrosylation, the thioredoxin system uses thioredoxin reductase and NADPH to regenerate reduced thioredoxin (Haendeler *et al.*, 2002).

NO exert its effect by another cGMP-independent pathway when it combines with reactive oxygen species (ROS) to form peroxynitrite ( $\text{ONOO}^-$ ) (Ferdinandy, 2006; Zweier and Talukder, 2006). The reactive intermediates produced from reduction of molecular oxygen ( $\text{O}_2$ ), such as superoxide ( $\text{O}_2^-$ ) and hydrogen peroxide ( $\text{H}_2\text{O}_2$ ), are known collectively as (ROS) (Paolucci *et al.*, 2000). Recently, studies have demonstrated that peroxynitrite behaves as a nitrosylating agent; donor of nitrosonium ion ( $\text{NO}^+$ ) (Choi *et al.*, 2011; Vandelle and Delledonne, 2011; Dutka *et al.*, 2011; Hlaing and Clement, 2014).

Alterations in the regulation of NO and ROS generating enzymes, or the levels of antioxidants such as superoxide dismutase (SOD) will alter NO and ROS signalling and thus the protein modification process. Superoxide dismutase is antioxidant enzyme in which it dismutase the superoxide ion ( $\text{O}_2^-$ ), which is known to be

required to form some of the intermediaries of  $N_2O_3$ , the chemical species that is a donor of  $NO^+$  (nitrosylation agent) (Ziolo *et al.*, 2008).

4-hydroxy-[2, 2, 4, 4-tetramethyl-piperidine-1-oxyl] (Tempol) is a superoxide dismutase mimetic, which promotes the metabolism of many reactive oxygen species and improves nitric oxide bioavailability (Wilcox, 2010). In 2003; Schrammel *et al.* studied the link between Tempol and S-nitrosylation using quantitative spin trapping experiments. GSNO formation was stimulated by 2-folds in the presence of Tempol which suggested more substrate for GSNOR to denitrosylase, thus decrease nitrosylation. Tempol has been used in this project as an agent which decreases S-nitrosylation. Tempol has been used clinically in preventing several of the adverse consequences of oxidative stress and inflammation that underlie radiation damage such as radiation induced alopecia and many of the diseases associated with aging (Fleenor *et al.*, 2012).

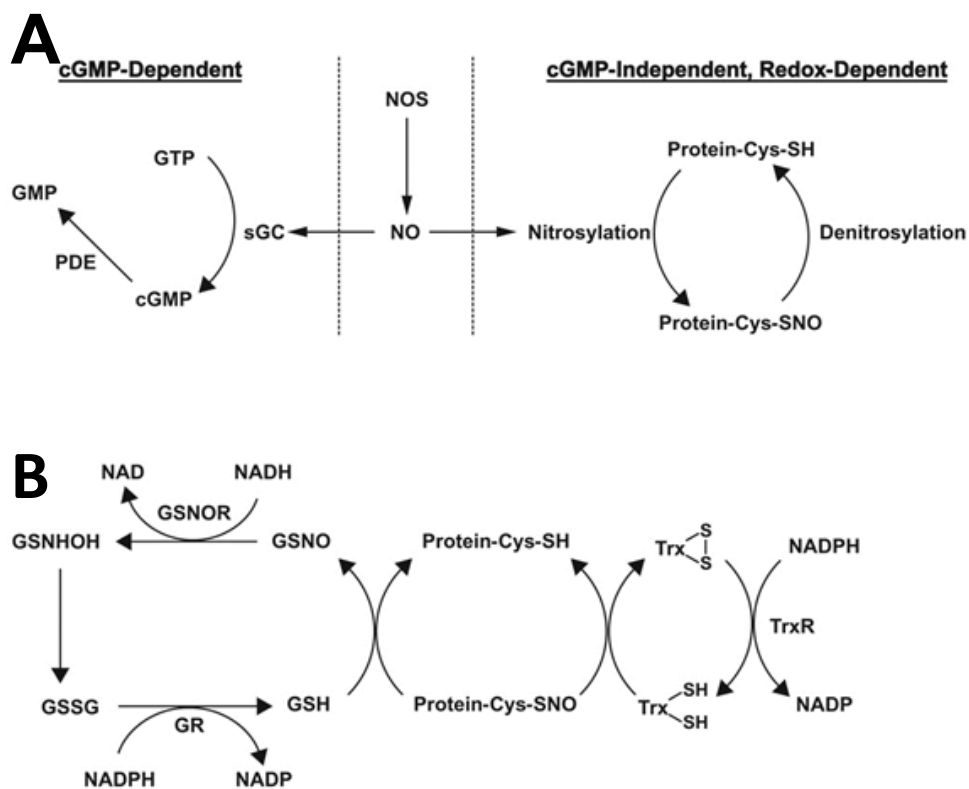


**Figure 1.24: The cGMP and S-nitrosylation pathway in NO signalling. A)** The role of cGMP and S-nitrosylation in NO signalling. **B)** Enzymatic protein denitrosylation mediated by GSNOR and Trx systems. Glutathione (GSH); s-nitrosoglutathione (GSNO); glutathione S-hydroxysulfenamide (GSNHOH); oxidized glutathione (GSSG); Nicotinamide adenine dinucleotide phosphate (NADPH). thioredoxin (Trx); thioredoxin reductase (TrxR). Modified from Lima *et al.*, (2010).

### **1.4.3 Nitric oxide effects on heart**

#### **1.4.3.1 Effect of nitric oxide on the QT interval**

NO signalling has only recently been linked with the QT interval (Aarnoudse *et al.*, 2007; Eijgelsheim *et al.*, 2009; Kao *et al.*, 2009). The link between the QT interval and NO was discovered by genome-wide association studies. Arking *et al.* (2006) identified in the general population, that extremely long or short QT intervals were associated with a common genetic variant in the *NOS1AP* gene that encodes carboxy-terminal PDZ ligand of nNOS (CAPON). CAPON is an adaptor protein that binds to the post-synaptic density-protein, discs-large, ZO-1 (PDZ) domain located in the oxygenase domain of nNOS (Zhou and Zhu, 2009). A study by Crotti *et al.*, (2009) reported that in a LQTS population, the occurrence of symptoms and a greater probability of sudden cardiac death were also linked with *NOS1AP* variants. These studies suggested that NO signalling might play an important role in the regulation of the QT interval and cardiac AP repolarisation. Furthermore, Chang *et al.* (2008) found that adenoviral-mediated overexpression of CAPON in guinea-pig ventricular myocytes resulted in a shortening of APD by inhibiting  $I_{Ca,L}$  and enhancement of  $I_{Kr}$ . Pre-treatment with the NOS inhibitor L-NAME reversed these effects. In addition, CAPON overexpression was also associated with an up-regulation of nNOS protein levels, an enhancement of nNOS activity and a modest increase in NO generation. Therefore, it is likely that the effects of CAPON overexpression were mediated by a nNOS signalling pathway. CAPON protein is expressed in the heart and interacts with nNOS to accelerate cardiac repolarization by inhibition of LTCC with regard to the link recently established between LQTS and a common generic variant in the *NOS1AP* gene that encodes CAPON, modulation of NO signalling may have the potential to treat LQTS (Arking *et al.*, 2006; Crotti *et al.*, 2009; Chang *et al.*, 2008).  $\beta$ -AR blockade is the most widely used therapy for LQTS. The use of  $\beta$ -blockers is a highly effective therapy for LQT1 patients, and has been reported to reduce the risk of cardiac events considerably (Vincent *et al.*, 2009). In contrast,  $\beta$ -blockers appear to be less effective at decreasing the number or severity of cardiac events for LQT2 and 3 patients (Schwartz and Ackerman, 2013). NO signalling is known to modulate  $\beta$ -AR signalling and may therefore be a target for therapeutic agents aimed at treating LQTS.

#### **1.4.3.2 Effect of Nitric oxide on cardiac ion currents**

There is evidence in animal models and humans that NO can play a physiological role in the regulation of some cardiac ionic channels; although the effect can be variable and there are many examples of contradictory findings.

The effect of NO on  $I_{Na}$  is controversial. The NO donor S-Nitroso-N-acetyl-DL-penicillamine (SNAP) may either inhibit or increase  $I_{Na}$  in mice and guinea pig ventricular cardiomyocytes using whole cell patch clamp technique. The inhibition effect of SNAP was reproduced by application of cGMP and cAMP analogues (Ahmed *et al.*, 2001). Therefore, inhibition of  $I_{Na}$  was mediated by a cGMP-dependent pathway. On the other hand, it has been concluded by Ahern *et al.*, (2000) that application of NO donors enhanced  $I_{Na}$  and resulted in a late persistent  $Na^+$  current in rat ventricular myocytes and this increase in  $I_{Na}$  was inhibited by using thiol-alkylating agent to prevent s-nitrosylation. As a result,  $I_{Na}$  appears to be inhibited by cGMP-dependent signalling pathway and enhanced by cGMP-independent signalling pathway.

A variety of different effects of NO on  $I_{Ca,L}$  have also been reported. NO has been reported to inhibit, enhance, or not affect  $I_{Ca,L}$  in studies conducted on atrial and ventricular myocytes. Applying the NO donor SIN decreased ferret ventricular  $I_{Ca,L}$  by a cGMP-dependent pathway as this inhibition was blocked in the presence of the sGC inhibitor ODQ and the PKG inhibitor KT5823 (Grushin *et al.*, 2008). Moreover, applying SIN with superoxide dismutase mimetic (Tempol) decreased  $I_{Ca,L}$ ; because Tempol will degrade superoxide thus decrease the level of peroxynitrite production which will favour cGMP-dependent signalling pathway as peroxynitrite will not be available to help in nitrosylation (Ziolo *et al.*, 2008). Moreover, Gallo *et al.*, (2001) used ODQ and an enhancement of  $I_{Ca,L}$  has been also noticed in guinea-pig ventricular myocytes. Also, applying S-nitrosothiol NO donors increased  $I_{Ca,L}$  which also emphasizes the effect of cGMP independent pathway on  $I_{Ca,L}$ . The NO donor SNAP reported no effect on  $I_{Ca,L}$  in rat ventricular myocytes (Abi-Gerges *et al.*, 1997), while it decreases  $I_{Ca,L}$  in frog ventricular myocytes by SNAP (Gomez *et al.*, 2009) which might be due to species differences. In summary, ventricular  $I_{Ca,L}$  appears to be inhibited by cGMP-dependent NO signalling and enhanced by cGMP-independent NO signalling.

Not too many studies have been conducted of the effect of NO on other ionic currents. However, research indicates that NO donors inhibited  $I_{to}$  and  $I_{Kr}$  in hamster ovarian cells (Gomez *et al.*, 2008); the mechanism of inhibition of  $I_{to}$  is not well known, while inhibiting  $I_{Kr}$  was not mediated by cGMP-dependent pathway as neither ODQ nor cGMP analogues modified this effect (Taglialatela *et al.*, 1999).  $I_{K1}$  may also be enhanced by NO signalling. Gomez *et al.*, (2009) demonstrated that  $K_{ir2.1}$  current expressed in Chinese hamster ovary cells was enhanced by the application of the NO donor SNAP.  $K_{ir2.1}$  channels are proposed to be the major isoform that mediate  $I_{K1}$  in ventricular myocytes. Moreover, the enhancement of the  $K_{ir2.1}$  current was unaffected by ODQ but was prevented in the presence of the reducing agent dithiothreitol.  $K_{ir2.1}$  current enhancement was found to be due to an increase in the opening probability of the channels as a result of S-nitrosylation using the site-directed mutagenesis analysis demonstrated that NO effects were mediated by the selective S-nitrosylation of Kir2.1 Cys-76 residue.

There is not too much known about the regulation of  $I_{Ks}$  by NO. However, Bai *et al.*, (2004) found that Ginsenoside Re which protect the heart from ischemia enhances  $I_{Ks}$  and suppresses  $I_{Ca,L}$ , in guinea-pig ventricular myocytes which may account for APD shortening and both effects are through NO signalling pathways as these effects were abolished by adding NOS inhibitor. Moreover, Asada *et al.*, (2009) reported that NO regulates  $I_{Ks}$  irrespective of sGC activation. They investigated S-nitrosylation using biotin switch assay and found that NO induced S-nitrosylation of the  $\alpha$ -subunit of the  $I_{Ks}$  channel, KCNQ1, at Cys-445 residue and increases  $I_{Ks}$ . Therefore, S-nitrosylation enhances  $I_{Ks}$  which might be a preliminary evidence for the effect of S-nitrosylation on  $I_{Ks}$ .

#### **1.4.4 Nitric Oxide role in the accentuated antagonism effect of the vagus nerve on the sympathetic system**

In addition to acetylcholine (ACh) release, pre-synaptic vagus nerve terminals synthesise and release NO via nNOS (Brack *et al.*, 2007). NO is also synthesised following binding of ACh to muscarinic acetylcholine receptor (mAChR) on the post synaptic membrane. NO via these mechanisms of synthesis can co-ordinate downstream events in post-synaptic terminals (Herring and Paterson, 2001) (Figure

1.25). Moreover, NO appears to modulate both the effects of muscarinic activation ('direct' vagal effect) and the muscarinic antagonism of sympathetic cardiac control ('indirect' vagal) effect by augmenting the rate of decrease of the heart rate in response to vagal stimulation during adrenergic drive (Sears *et al.*, 1998). This indirect interaction of sympathetic and parasympathetic pathways is termed accentuated antagonism and now thought to be due to NO/cGMP pathway. In adult rat ventricular myocytes, inhibition of the NO/cGMP pathway using L-NMMA abolished the muscarinic attenuation of ISO-induced increases in contractility (Balligand *et al.*, 1995). Therefore, NO is reported to attenuate the effect of ISO and play a protective role. The mechanism by which NO mediates the indirect cardiac vagal activity is not fully understood, but in pacemaker cells may be due to cGMP-mediated inhibition of  $I_{Ca,L}$ . This is supported by a study on isolated rabbit SAN cells showing that NOS inhibitors prevented cholinergic inhibition of the sympathetically augmented  $I_{Ca,L}$  (Han *et al.*, 1996). Further evidence for a role of NO in the modulation of  $I_{Ca,L}$  with indirect vagal control of heart rate was provided in studies on isolated guinea-pig atria in which L-NMMA slowed the rate of heart-rate decrease with vagal stimulation, an effect duplicated by Nifedipine, an inhibitor of LTCC (Sears *et al.*, 1998).

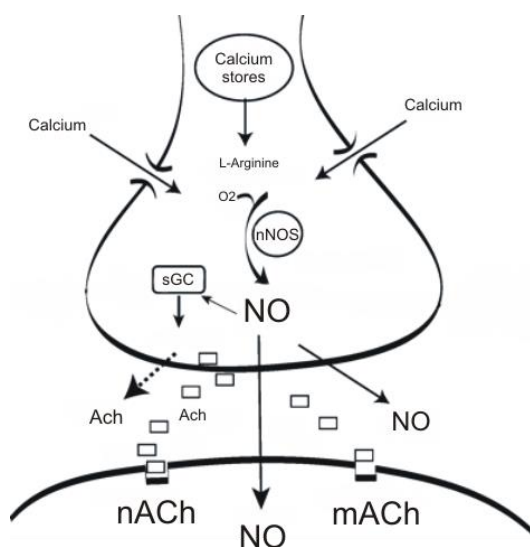


**Figure 1.25: VS-NO Pathway.** NO is synthesised in pre-synaptic terminals via nNOS and is also synthesised as a secondary product post synaptically after ACh binds to mACHR. ACh release from pre-synaptic terminals increases under the influence of NO derived from nNOS. Modified from Herring and Paterson, (2001).

### **1.4.5 Role of Nitric oxide in sympathetic regulation of cardiac function:**

#### **1.4.5.1 Regulation of the adrenergic pathway by nNOS:**

Several lines of research indicate that NO produced endogenously by nerve terminals plays a role in the regulation of catecholamine release during electrical sympathetic stimulation. This was studied first in isolated perfused rat hearts (Schwarz *et al.*, 1995) and in co-cultures between adult peripheral cardiac neurons and cardiomyocytes (Horackova *et al.*, 1995). The results suggested that NO inhibits the reuptake of neuron-derived catecholamines. This interpretation was supported by experiments showing that S-nitrosothiols inhibit neuronal norepinephrine transport in rat cervical ganglia (Kaye *et al.*, 1997).

Choate and Paterson, (1999) designed a study to determine whether NO modulates the positive chronotropic and inotropic responses to cardiac sympathetic nerve stimulation (SS) in the isolated guinea-pig double atrial right stellate ganglion preparation. The ganglion was stimulated at 1, 2, 3 and 5 Hz and the changes in heart rate or force of contraction were measured. The selective nNOS inhibitors TRIM and 7-NiNa significantly enhanced the positive chronotropic and inotropic responses to SS. Similar results for heart rate were seen with the non-selective NOS inhibitor L-NNA. All effects were reversed with L-Arginine. The NO donor sodium nitroprusside (SNP) attenuated the positive chronotropic and inotropic responses to SNS. SNP also decreased the positive chronotropic response to bath-applied noradrenaline. ODQ enhanced and the cGMP analogue (8-Br-cGMP) attenuated the positive inotropic response to sympathetic nerve stimulation. Taken together, these results are consistent with endogenous NO, synthesized from nNOS, inhibiting the positive chronotropic and inotropic responses evoked by cardiac SS via cGMP-dependent pathway.

#### **1.4.5.2 $\beta$ 3- ARs are coupled to eNOS**

The role of NO signalling within cardiac muscle is important in the regulation of excitation-contraction coupling by  $\beta$ -AR signalling (Ziolo *et al.*, 2008). Interestingly, contractility is differentially influenced by nNOS and eNOS due to differences in localisation and signalling targets (Ziolo, 2008) as mentioned previously. Classic  $\beta$ -

adrenergic signalling is mediated by  $\beta 1$  and  $\beta 2$ -adrenergic G-protein coupled receptors.  $\beta 1$  and  $\beta 2$ -AR couple to G protein which stimulates adenylyl cyclase (AC), an enzyme which produces cAMP which in turn activates PKA resulting in an increase in contractility by increasing  $I_{Ca,L}$ , SERCA activity and SR  $Ca^{2+}$  load. However, the discovery and characterisation of the  $\beta 3$ -AR in the human heart has been shown to have negative inotropic effect and decrease contractility (Gauthier *et al.*, 1996).  $\beta 3$ -AR belongs to the superfamily of G protein-coupled receptors like the  $\beta 1$  and  $\beta 2$ -ARs.  $\beta 3$ -AR activation is proposed to play an important protective role during sympathetic overstimulation by antagonising  $\beta 1$  and  $\beta 2$ -ARs activity (Moens *et al.*, 2010).

Interestingly, the  $\beta 3$ -AR couples with and activates eNOS, thus its effects are mediated by NO (Saraiva and Hare, 2006). Cawley *et al.*, (2011) demonstrated that application of a  $\beta 3$ -selective adrenergic receptor agonist (BRL37344) provoked a negative inotropic effect in wild-type mice but had no effect in sGC- $\alpha 1$  subunit deficient mice, establishing a role for  $\beta 3$ -AR coupling to the cGMP-dependent signalling pathway. The non-specific  $\beta$ -agonist Isoprenaline has been used widely in this project.

#### **1.4.5.2.1 eNOS stimulation reduces cardiac response to $\beta$ -ARs**

Signalling via eNOS limits the heart's response to  $\beta$ -adrenergic stimulation, which may be protective against arrhythmias via inhibition of the L-type  $Ca^{2+}$  current. A study has been conducted by Wang *et al.*, (2008) to measure the L-type  $Ca^{2+}$  current from myocytes isolated from wild-type (WT) and eNOS knockout (eNOS<sup>-/-</sup>) mice. eNOS<sup>-/-</sup> myocytes had a significantly larger  $\beta$ -AR stimulated increase in  $I_{Ca,L}$  compared with WT myocytes. In addition, eNOS<sup>-/-</sup> myocytes had a larger response to  $\beta$ -AR stimulation compared with wild type myocytes in terms of  $Ca^{2+}$  transient amplitude, cell shortening amplitude, and APD. Moreover eNOS<sup>-/-</sup> myocytes exhibited a larger incidence of  $\beta$ -adrenergic induced EADs in response to ISO. Similar effects have been shown using the specific eNOS inhibitor [L-N5-(1-iminoethyl)-ornithine (I-NIO) in wild type myocytes as with eNOS<sup>-/-</sup>. Therefore results indicate that eNOS signalling inhibits the  $\beta$ -AR stimulation response by reducing  $I_{Ca,L}$  and protects against arrhythmias.

As mentioned earlier it is well known that  $\beta$ -AR signalling via cAMP generation and PKA activation mediates the positive inotropic effect of catecholamines on heart cells. PDEs degrade cAMP and thus regulate intracellular cAMP gradients. Their confinement to discrete compartments and functional coupling to individual receptors provides an efficient way to control local cAMP. By performing real-time imaging of cyclic nucleotides in living rat ventricular myocytes it has been identified that there is a prominent role of PDE2 in selectively shaping the cAMP response to catecholamines via a pathway involving  $\beta$ 3-AR, NO generation via eNOS phosphorylation, and cGMP production, as cGMP can stimulate PDE2 to increase degradation of cAMP (Mongillo *et al.*, 2006). PDE2 has been shown to be compartmentalized to the pool of adenylyl cyclases activated by  $\beta$ -AR stimulation. Activation of  $\beta$ 3-AR counteracts cAMP generation obtained via stimulation of  $\beta$ 1 and  $\beta$ 2-ARs. Selective inhibition of PDE2 attenuates the negative inotropic effect of  $\beta$ 3-adrenergic signalling and positively influence cardiac performance in rat ventricular cardiac myocytes (Mongillo *et al.*, 2006) (Figure 1.26). Moreover, the effect of PDE2 inhibition on contractility was dramatically reduced in myocytes obtained from mice with eNOS<sup>-/-</sup> (Shesely *et al.*, 1996). So it has been concluded that the stimulating  $\beta$ 3-AR by sympathetic stimulation mediate a negative inotropic effect due to NO generation, then to sGC activation, synthesis of cGMP, activation of PDE2, and reduction of cAMP level. However, this research area needs more illustration of the exact mechanism by which  $\beta$ 3-AR stimulates eNOS.

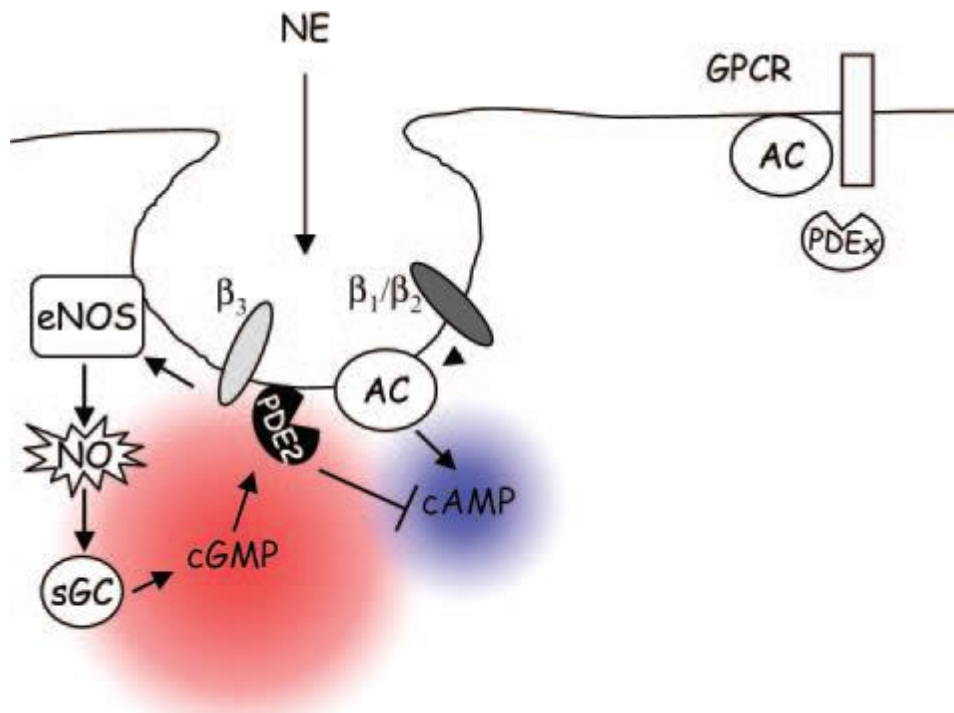


**Figure 1.26: Schematic representation of the proposed  $\beta_3$ -adrenergic feedback control loop.** A spatially defined signalling domain includes  $\beta_3$ -adrenergic receptor, AC, eNOS, and PDE2. G protein-coupled receptors (GPCR) other than  $\beta$ -adrenergic receptors are localized outside such signaling domain and activate a separate pool of AC. PDE isozymes different from PDE2, and here denoted as PDE<sub>x</sub>, are responsible for modulating the cAMP response in such separate domains. Modified from Mongillo *et al.* (2006).

### **1.5 Diurnal variation of cardiac electrophysiology**

The oscillation of biological processes with a 24 hour cycle is referred to as a circadian rhythm (Jeyaraj *et al.*, 2012). The cardiovascular system is prone to biological circadian rhythm. For example, in the morning there is a peak in stroke volume, heart rate and blood pressure in humans and a corresponding to peak of these variables in the night in nocturnal animals (Degaute *et al.*, 1991; Scheer *et al.*, 2004). Interestingly, the incidence of sudden cardiac death resulting from ventricular arrhythmias, exhibits a similar circadian variability, with a low incidence of sudden cardiac death during the night and a prominent increase in the number of cases from 7 to 11 AM. The pattern in circadian variation resembles that reported for myocardial infarction (Maron *et al.*, 1994). As mentioned earlier many key variables of the cardiovascular system exhibit diurnal patterns, some of these variables reflect

changes in excitation contraction coupling of the individual ventricular myocytes. It has been proposed that much of the diurnal variation in ventricular function is related to variation at the genes level regulated by a complex interaction of extracellular neurohumoral influences and the central and peripheral circadian clock (Young, 2003; Durgan *et al.*, 2005).

Hohnloser *et al.*, (1993) investigated diurnal variation of ventricular repolarisation in response to changes in heart rate in patients with ventricular arrhythmia. Heart rate and QT interval exhibited distinct circadian patterns. Heart rate exhibited a circadian pattern, with the lowest measurements at 5 AM, which increased at 6 AM, peaked at noon and decreased throughout the remainder of the day. However, heart rate remained relatively high during the morning with a substantial decrease in the evening. On the other hand, the QT interval peaked a few hours prior to 6 AM, decreased thereafter and started to increase at 6 PM. Therefore, QT intervals are longer during sleep. The ANS also displays diurnal variation and has long been proposed to affect the QT interval. Bexton *et al.*, (1986) showed that the circadian pattern of the QT interval varied between innervated and denervated hearts. Pacemaker patients with normally innervated hearts displayed distinct diurnal changes in the QT interval, with a profound shortening between 6 and 9 AM. However, in transplant patients with denervated hearts, the circadian pattern was abolished and the pronounced change in the morning was absent. This study suggests that the ANS plays an essential role in the diurnal changes of the QT interval. Moreover, Honda *et al.*, (2013) investigated the influence of parasympathetic and sympathetic nervous activity on diurnal variation of the QT interval in marmosets. QT interval prolongation during the dark period was blocked by atropine, a muscarinic receptor antagonist which suppresses parasympathetic activity. In opposition, QT interval shortening during the light period was blocked by  $\beta$ - blocker. This suggests that the parasympathetic nervous system prolongs and the sympathetic nervous system shortens the QT interval, during the dark and light periods respectively. Therefore, an increase in the activity of the sympathetic nervous system during the transition from resting to active may increase the susceptibility to arrhythmias by modifying repolarisation.

Furthermore, diurnal variations have been detected in the expression of genes and proteins associated with the  $K^+$  channels that underlie repolarisation. Yamashita *et*

*al.*, (2003) investigated cardiac K<sup>+</sup> channel gene expression in rat hearts at periodic intervals during the day. Circadian variation in the expression of Kv4.2 and Kv1.5 genes which mediate I<sub>to</sub> and I<sub>Kur</sub> respectively, were discovered. Expression levels increased for both genes by almost two fold throughout the course of the day. The expression and current density of Kv4.2 peaked during the light period (when rats are resting) whereas Kv1.5 decreased. These diurnal patterns were partially inverted by reversal of light conditions. Therefore, this suggests that light is a fundamental parameter governing diurnal variation of the repolarising K<sup>+</sup> currents I<sub>to</sub> and I<sub>Kur</sub>.

Diurnal variation of excitation contraction through regulation of NO signalling has also been investigated. Collins and Rodrigo, (2010) investigated whether multiple excitation contraction parameters including Ca<sup>2+</sup> transients, cell shortening and I<sub>Ca,L</sub> density demonstrate diurnal variation in rat left ventricular myocytes. Paradoxically, cell shortening was greater in resting period myocytes, whereas I<sub>Ca,L</sub> density was greater in active period myocytes, under basal conditions. However, both Ca<sup>2+</sup> transients and I<sub>Ca,L</sub> density responded more strongly to β-AR stimulation with ISO, in resting than active period myocytes. To investigate if NO signalling played a role in the response to ISO, NOS was inhibited with L-NNA. L-NNA increased I<sub>Ca,L</sub> density in response to ISO in active period myocytes, but had little effect in resting period myocytes. Furthermore, arrhythmic activity in response to ISO was greater in resting period myocytes and inhibition of nNOS increased arrhythmic activity in response to ISO in active period myocytes but had no effect in resting period myocytes. In addition, active period myocytes had a higher expression of nNOS than resting period myocytes. Therefore, NOS-dependent signalling exhibited diurnal variation, and suppressed excitation contraction and arrhythmic activity in active but not resting period myocytes.

The study of diurnal variation of the ionic currents underlying the ventricular AP is in its beginning. Studies have been conducted mainly on mice and rats, in which ventricular APD is short and repolarisation. What happens in larger mammals with the longer ventricular APD is not known yet.

## **1.6 Ivabradine may influence ventricular repolariation**

Ivabradine is an anti-anginal agent that lowers heart rate through inhibition of sinoatrial nodal HCN (hyperpolarization activated cyclic nucleotide gated non-selective cation) channels, and thus inhibits the pacemaker current  $I_f$ . Ivabradine treatment has been used to treat patients with coronary artery disease and heart failure by lowering heart rate and thus reducing oxygen demand and wall stress (Scicchitano *et al.*, 2014). Studies on whole heart have suggested that ivabradine prolongs ventricular repolarization and alters electrical restitution properties (Hancox *et al.*, 2008; Melgari *et al.*, 2015).

Melgari *et al.* (2015) investigated the effect of 0.1 - 0.5  $\mu\text{M}$  ivabradine (a therapeutically relevant concentration) on monophasic action potentials (MAP) recorded from guinea-pig Langendorff-perfused hearts during constant ventricular pacing at 200-ms cycle length. Ivabradine prolonged ventricular repolarization and altered electrical restitution properties at concentrations relevant to the upper therapeutic range. The ability of ivabradine to inhibit hERG1 potassium channels, which strongly influence ventricular repolarization and susceptibility to TdP arrhythmia was also investigated. They demonstrated that ivabradine can inhibit  $I_{\text{hERG}}$ , with an  $\text{IC}_{50}$  of  $\sim 2$  to  $3 \mu\text{mol/L}$ . So, ivabradine does not discriminate between hERG and HCN channels. These are surprising findings and may have important implications both clinically and for the future design of HCN-selective bradycardic agents based on ivabradine structure (Miller *et al.*, 2015; Melgari *et al.*, 2015).

Colleagues at Glenfield hospital (Leicester) and collaborators at the University of Bristol had results indicating that the bradycardiogenic drug ivabradine might influence cardiac repolarisation. In this study we aimed to bridge the gap between the whole heart and the recombinant channel studies by investigating the effect of ivabradine on APs recorded using the perforated patch clamp technique at physiologically relevant temperature, in acutely isolated guinea-pig left ventricular myocytes. Electrical restitution experiments using the dynamic protocol, and constant pacing experiments were performed to determine if ivabradine had unexpected effects on ventricular repolarization. Ivabradine studies served as another tool with which to investigate restitution slope in isolated cells.

## **1.7 Aims**

The overall aim of this PhD was to explore the effect of NO signalling on cardiac action potential repolarisation in acutely isolated guinea-pig left ventricular myocytes. Many cardiovascular variables exhibit diurnal variation and a role of NO signalling has been implicated in the diurnal variation of excitation contraction coupling. In addition, the autonomic nervous system has been proposed to influence the diurnal variation of ventricular repolarisation and is also known to regulate the activity of NOSs. Literature on the modulation of the ventricular AP by NO and its underlying signalling pathway is sparse and inconsistent. Therefore, the main aims were as follows:

1) To investigate the diurnal variation in electrical restitution parameters, particularly the maximum slope which is an indicator of arrhythmogenicity of the cells. Electrical restitution curves were compared using DYRT under baseline conditions, in response to  $\beta$ -AR stimulation with ISO, and in the presence of ISO and the NOS inhibitor L-NNA.

2) To investigate the diurnal variation in AP repolarization by measuring APD<sub>90</sub> under baseline conditions, in response to  $\beta$ -AR stimulation, and in the presence of the NOS inhibitor L-NNA using the DYRT protocol.

3) To investigate the cellular mechanisms of NO on APD restitution parameters mainly the maximum slope as an indicator of susceptibility to VF using the DYRT protocol.

4) To investigate the NO signaling pathway modulators effect on AP repolarization using constant pacing. The sGC activator BAY, the sGC inhibitor ODQ, the denitrosylation inhibitor have been investigated in the presence of  $\beta$ -AR stimulation.

In all experiments I chose to use the perforated patch-clamp technique to minimise changes to the intracellular signalling environment of cardiac myocytes and to record at the physiologically relevant temperature of 37 °C.

## **Chapter 2. Materials and Methods**

### **2.1 Guinea pig housing**

Adult male Dunkin Hartley guinea pigs (Harlan Laboratories) were housed in environmentally controlled rooms prior to experiments. Guinea pig ventricular APs share many properties with human ventricular APs, especially a relatively long duration and the dependence on delayed rectifier K<sup>+</sup> currents for repolarisation (Rosati *et al.*, 2008). Therefore, guinea pigs were used as a model animal in preference to rat or mouse animal models.

Guinea pigs are active during daylight hours and are therefore diurnal as opposed to nocturnal. The majority of animals were housed in light controlled rooms with lights on at 6 AM and off at 6 PM. Culling was carried out at 9:00 AM, therefore these animals were in an active period. An exception was one group of guinea pigs used in experiments presented in chapter 3 investigating diurnal variation (Figure 2.1), in which guinea pigs were housed in a reverse 12 hour light cycle, with lights on at 6 PM and off at 6 AM, for a minimum of three weeks prior to experiments and throughout the course of experiments. Therefore, these experimental animals were in a resting period when culled. Light controlled conditions were used because light is the main parameter responsible for setting the circadian clock. Culling of the animal stops the cycling of the circadian clock at its current state (Collins and Rodrigo, 2010).

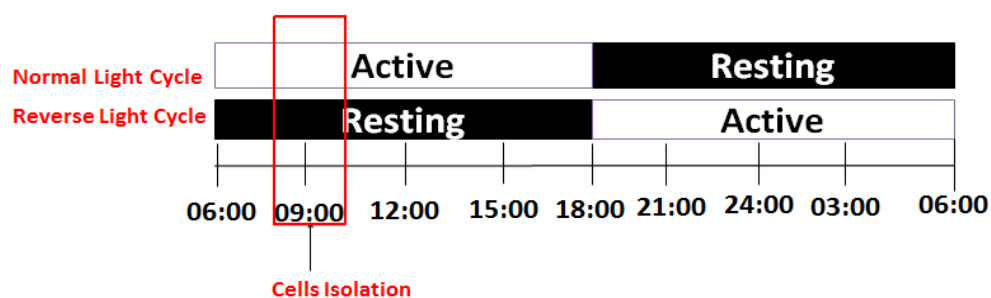


**Figure 2.1: Diurnal variation experimental protocol.** Left ventricular myocytes were isolated from two populations of adult male guinea pigs (550-700g), housed in either normal (Light on 06:00-18:00) or reverse (Light on 18:00-06:00) light cycle. Myocytes were isolated at 09:00 corresponding to active or resting period of normal or reverse light cycle animals respectively.

## **2.2 Isolation of guinea pig ventricular myocytes**

Animals were humanely culled by cervical dislocation without sedative or anaesthetics under the authority of Home Office project licences (PPL 70/8501 and PPL 40 2414). Most guinea pigs were 550-700 g, as animals over 550 g are reported to have fully developed vagal innervation and NO signalling (Herring *et al.*, 2000). However some large guinea pigs (> 700g) have been used in some experiments. The heart was immediately excised and submerged in a petri dish of cold 0 mM Ca<sup>2+</sup> Tyrode. The perfusion system was switched on, and the heart then attached by the aorta to the cannula of a Langendorff set up using a clip and suture. The aorta was retrogradely perfused with 0 mM Ca<sup>2+</sup>-Tyrode for 4-6 minutes via Langendorff apparatus (Figure 2.2) while excess tissue surrounding the heart was removed. The 0 mM Ca<sup>2+</sup> Tyrode solution contained (in mM); 135 NaCl, 4 KCl , 10 Glucose , 10 HEPES , 5 Na<sup>+</sup> Pyruvate, 0.33 NaH<sub>2</sub>PO<sub>4</sub> , 1 MgCl<sub>2</sub> , adjusted to pH 7.4 with NaOH. For most experiments, 0.5 mM ethylene glycol tetraacetic acid (EGTA) was added to the 0 mM Ca<sup>2+</sup>- Tyrode which improved the yield and viability of the myocytes. Then the heart was perfused with an enzyme solution of 0 mM Ca<sup>2+</sup>-Tyrode that contained 1.04 mg ml<sup>-1</sup> collagenase (type I), 0.62 mg ml<sup>-1</sup> protease (type XIV) and 1.67 mg ml<sup>-1</sup> bovine serum albumin (BSA) for 8-11 minutes. After 1-2 minutes of perfusion, the enzyme solution was collected and recirculated. Finally the heart was perfused with 0 mM Ca<sup>2+</sup> -Tyrode for 1-2 minutes to washout the enzyme solution. All solutions were bubbled with 100% oxygen and maintained at 37°C. The perfusion rate of all solutions was 18 ml min<sup>-1</sup>.

The left ventricle was removed from the heart, dissected into smaller pieces and added to a flask that contained 5 - 10 ml of 2 mM Ca<sup>2+</sup>-Tyrode (normal Tyrode) that contained the same components and concentration of 0 mM Ca<sup>2+</sup>-Tyrode but with 2 mM CaCl<sub>2</sub> and no EGTA was added. The flask was bubbled with oxygen and placed into a water bath set at 37°C and shaken mechanically to aid the dispersion of cells from the tissue into suspension. At periodic intervals the tissue was separated from the cell suspension, re-suspended in fresh normal Tyrode and returned to the water bath. This process was repeated until a decrease in the yield of rod shaped quiescent myocytes was observed, or until the cardiac tissue had fully dissociated. The cell suspensions were filtered using a sieve and left to sediment. Following

formation of a loose pellet, the supernatant was discarded and the cell pellet was re-suspended in normal Tyrode. The cell suspensions were left to sediment for a second time, the supernatant discarded and the cell pellets were re-suspended in normal Tyrode and transferred to labelled petri dishes and kept at room temperature for use in patch-clamp experiments. Figure 2.3 shows a fraction of the isolated myocytes.

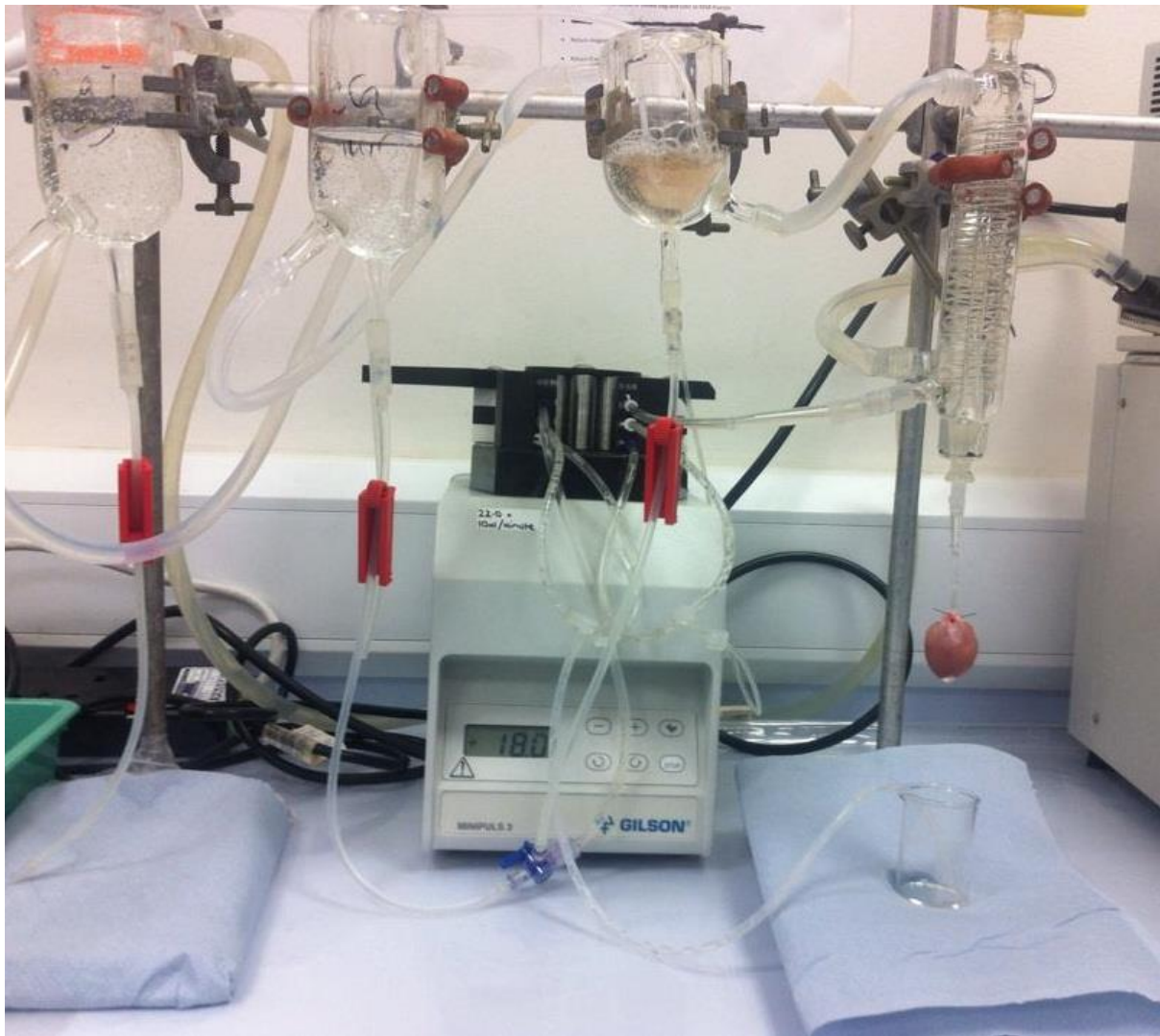


**Figure 2.2: Photograph of the Langendorff perfusion apparatus used to isolate guinea pig ventricular myocytes.** Solutions were maintained at 37°C by heated water jackets and pumped through a heat exchange coil to the cannulated heart by a peristaltic pump. 0 mM Ca<sup>2+</sup>-Tyrode solution is in the middle chamber, normal Tyrode in the left chamber, and the enzymes in the small right chamber. Enzyme solution was collected and recirculated to the reservoir via a different line by the peristaltic pump.

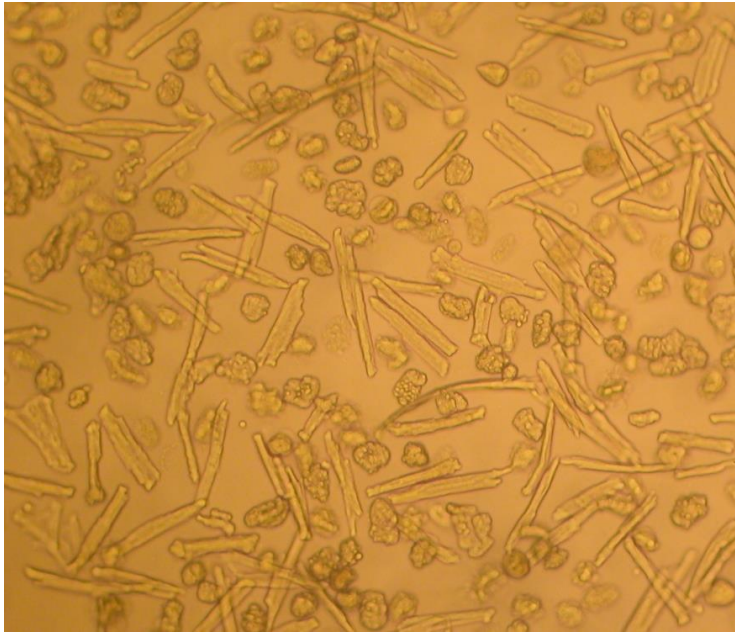


**Figure 2.3: Myocyte Isolation.** A fraction of guinea-pig cardiac myocytes isolated from the left ventricle.

## **2.3 Electrophysiology**

### **2.3.1 Electrophysiology apparatus**

Myocytes were placed in a recording chamber and superfused with normal Tyrode using a peristaltic pump (Gilson). The perfusion line contained a bubble trap to prevent air flow caused by switching solutions. Solutions were warmed by a Cornerstone heat controller device (HW30-controller model) before flow into the recording chamber so that recording chamber temperature was 35-37°C. A suction tube connected to the pump, removed solution and air from the recording chamber and was positioned to maintain the level of solution. The myocytes and electrode in the recording chamber were viewed using phase contrast microscopy. The microscope (Nikon-808228) was supported on an anti-vibration table, to prevent external vibrations from disrupting electrical access between the electrode and myocyte. The electrode was secured to a headstage (Axon CV203BU, Molecular Devices) and moved around the recording chamber in three planes by a micromanipulator (MC1000c-Controller GEARHEAD Model, Siskiyou). The solution in the recording chamber was connected to the ground input of the headstage via an agar bridge in KCl and silver chloride (AgCl) pellet assembly. The agar bridge minimised the transfer of potentially toxic Ag/AgCl to the recording chamber.

### **2.3.2 Patch-clamp recording techniques**

Patch clamp techniques can be used to measure membrane currents by a technique known as voltage clamp (V-clamp) and action potentials by a technique known as current clamp (I-clamp). In V-clamp mode the membrane potential is controlled, and the current required maintaining the membrane potential at the chosen potential is recorded. In a I-clamp experiment, current through the micropipette is clamped at a constant level and then a short injection of current is used to stimulate the cell and the change in membrane potential caused by the applied current is measured. In this project, electrical access to the cell was initially made and monitored in voltage clamp mode and then once whole cell access was established, the recording mode was changed to current clamp so that APs could be recorded.

In simple terms, the V-clamp technique uses a feedback circuit which allows the user to control the membrane potential of an excitable cell such as a neuron or myocyte independently of the current produced by ionic movement across the cell membrane. This therefore allows the voltage and time-dependence of membrane currents in a cell to be explored. For membrane currents recording, a command potential is set and the membrane potential of the myocyte is clamped at this voltage. Any difference between the membrane potential and the command potential is detected by the feedback amplifier and current is injected to maintain the voltage at the command potential.

In this project, I-clamp was used to measure APs from acutely isolated guinea pig left ventricular myocytes. I-clamp controls the amplitude of the injected current and allows the voltage to vary. Injection of a depolarizing current across an excitable membrane may be sufficient to generate AP. Membrane voltage changes cause membrane conductance changes that generate APs. The Axoclamp 200B amplifier (Molecular Devices) has two I-clamp modes, I-clamp normal and I-clamp fast. I-clamp normal is used when series resistance (electrode resistance) is greater than 1 M $\Omega$  while I-clamp fast is recommended when the series resistance is greater than 10 M $\Omega$ . Recordings were made using I-clamp fast.

Perforated and ruptured patch-clamp are the two commonly used techniques to record from cells. In both techniques, a glass microelectrode is touched onto the cell

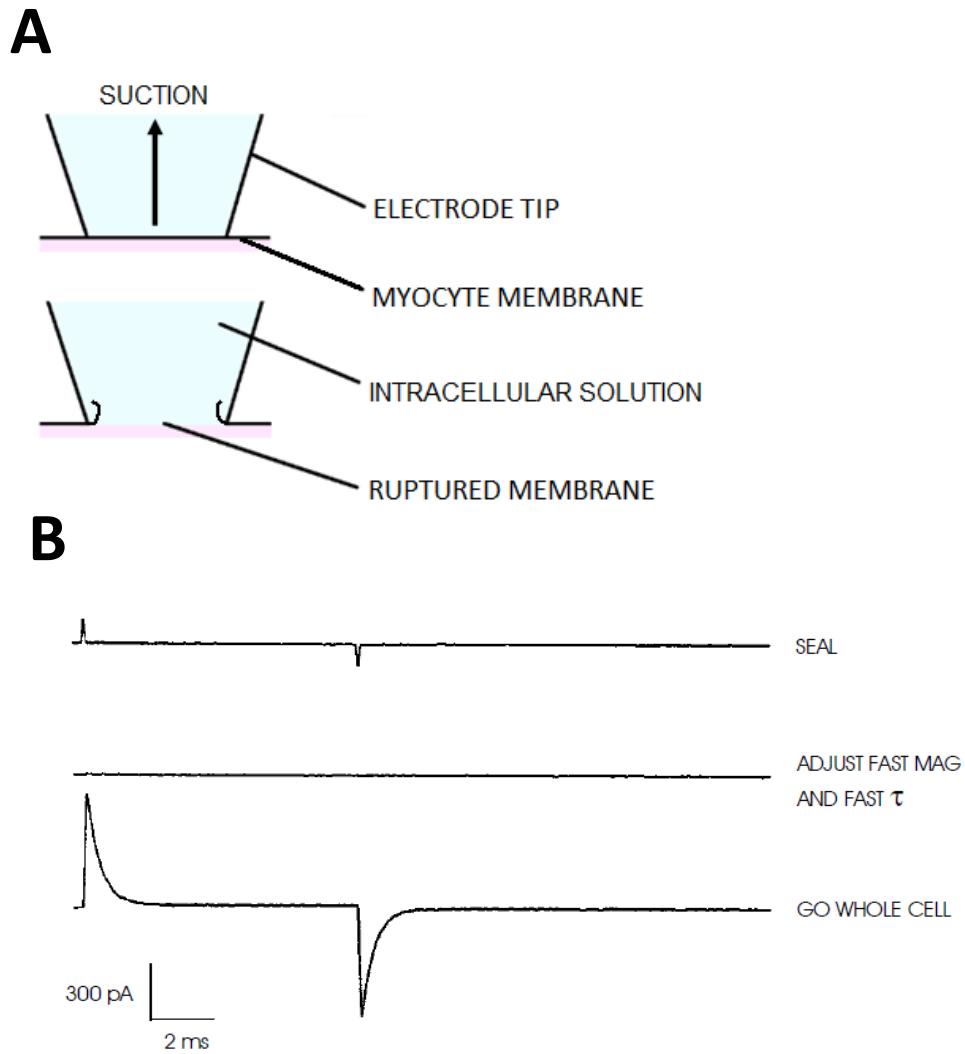
membrane and a high resistance gigaohm seal is formed. The perforated patch-clamp technique uses pore-forming ionophores such as amphotericin B (an antifungal drug) to make pores in the cell membrane and thus enables electrical access to the cell. The ruptured patch-clamp technique uses suction to rupture the patch of membrane beneath the electrode tip to gain electrical access inside the cell (Figure 2.4). An advantage of the perforated patch-clamp technique is the maintenance of the cytosolic components, as the amphotericin B pores are small and thus cyclic nucleotides, and rapidly diffusible solutes are not dialysed from the cytoplasm. The ruptured-patch-clamp technique can dialyse the contents of the cell, and thus the cell might lose some of the important components of signalling pathways. To avoid this phenomenon, all recordings in this project were obtained using the perforated patch-clamp technique. However, disadvantages with the perforate patch technique are less electrical access to the cell and a longer time required to gain sufficient access.

### **2.3.3 Perforated patch-clamp of guinea pig ventricular myocytes**

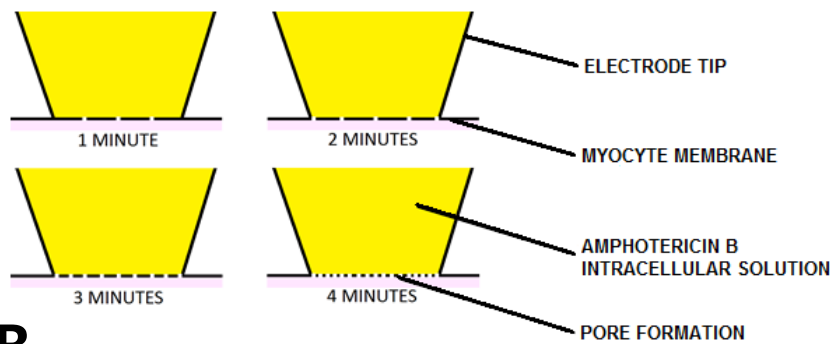
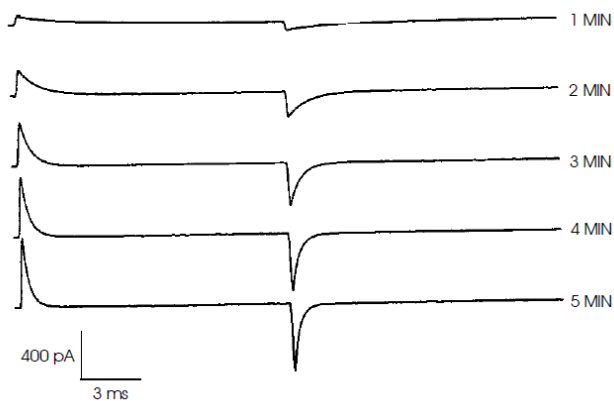
Electrodes were made using borosilicate standard wall unfilamented glass (Harvard Apparatus, UK) pulled by a micropipette puller (P-97 Flaming/Brown, Sutter Instrument Company) to a resistance of 2-3 M $\Omega$ . Electrodes were tip-filled by 2-3 mm of amphotericin B-free intracellular solution and back filled with intracellular solution that contained 0.48 mg ml<sup>-1</sup> amphotericin B. The intracellular solution used to record action potentials contained (in mM): 10 NaCl, 20 KCl, 110 L-aspartic acid K<sup>+</sup> salt, 5 MgCl<sub>2</sub>, 10 HEPES, pH 7.2 (adjusted with KOH). All solutions containing amphotericin B were prepared from stock solutions on each experimental day, protected from light and kept on ice. Amphotericin B stock solution (60 mg ml<sup>-1</sup>) was prepared in dimethyl sulfoxide (DMSO, stored in glass ampules), sonicated and stored at -20°C for use within one week. Amphotericin B could diffuse quickly to the electrode tip and prevented seal formation. Amphotericin B could also potentially be ejected over cells before seal formation, which could make them 'leaky' and depolarised. Therefore, as a preventative measure, minimal positive pressure was applied to the patch pipette before seal formation. Positive pressure in the line had two main functions; the first was to keep the sharp end of the micropipette free of debris and the second was to

aid in seal formation after pushing onto the membrane and releasing the positive pressure. Following formation of a Gigaohm seal, the pipette capacitance compensation was finely adjusted. Electrical access to the myocyte was gained by increased pore formation in the membrane over time, as observed by the increased amplitude and faster decay rate of capacitance transients (Figure 2.5). Usually, transients formed within a few minutes and took 5-10 minutes to reach an acceptable access resistance (considered as less than 15 M $\Omega$ ), which was monitored using whole cell capacitance and series resistance compensation parameters on the amplifier.

Once the series resistance was <15 M $\Omega$  the electrical access was sufficient to start to make recordings and the experiment commenced. However, APs can still be recorded at a series resistance higher than 15 M $\Omega$ . Series resistance was monitored at periodic intervals during the experiments. In the majority of recordings, series resistance was 10-15 M $\Omega$ . After getting access to the cell by the perforated patch clamp technique in V-clamp mode, the amplifier was first set to I=0 mode and resting membrane potential noted. The holding command (holding current in I-clamp) was set to 0, and the mode was then switched to I-clamp fast for action potential recording. The current signal was also recorded so that the quality and speed of the I-clamp could be verified.



**Figure 2.4: Representation of the ruptured patch-clamp technique. A)** Diagram showing application of suction to rupture the myocyte membrane and go whole-cell. **B)** Current traces at indicated stages of the procedure. Taken from Axopatch 200B Patch Clamp Theory and Operation.

**A****B**

**Figure 2.5: Representation of the perforated patch-clamp technique. A)** Diagram showing increased amphotericin B pore formation in the myocyte membrane with time. **B)** Increased capacitance transient amplitude and faster decay rate with time as the number of amphotericin B pores in the membrane increased. Modified from Axopatch 200B Patch Clamp Theory and Operation.

### **2.3.4 Recording solutions**

Guinea pig ventricular myocytes were superfused with normal Tyrode. Intracellular solutions were stored at  $-20^{\circ}\text{C}$  and kept on ice during experimental days. Reagents were made up as stock solutions, typically in DMSO or water, stored at  $-20^{\circ}\text{C}$  and diluted to the required concentration in normal Tyrode on the day of the experiment. However, care was taken to ensure DMSO concentration in the recording solution did not exceed 0.1%.

### **2.3.5 Data acquisition**

Electrophysiological recordings were acquired using an amplifier (Axopatch 200B, Molecular Devices), an analogue to digital converter (1440A Digidata, Molecular

Devices) and Clampex software (version 10.2, Molecular Devices). The low pass filter frequency was 5 kHz and the sampling frequency 5 kHz. A pipette voltage offset of -13 mV was applied for perforated patch-clamp recordings to counteract a junction potential of 13 mV at the electrode tip, due to a difference in the concentrations and the movement of anions and cations between the intracellular electrode solution and the extracellular Tyrode solution. The junction potential was calculated within the Clampex software using the ion concentrations and experimental conditions and was measured experimentally by a previous PhD student.

The gap-free acquisition mode in Clampex software was used to continuously record action potentials from guinea pigs left ventricular myocytes. The gap-free data acquisition mode allows large amounts of data to be continuously digitized, displayed, and saved without any interruptions to the data record.

#### **2.4 Action Potential Recording**

APs in guinea pig left ventricular myocytes were electrically stimulated using a pulse generator (TG-315 Function Generator, Aim-TTI Instruments, Huntingdon UK) that triggered an electrically isolated constant voltage stimulator (DS2A.MK II Model, Digitimer Ltd) connected to the external command input of the patch-clamp amplifier (Axopatch 200B, Molecular Devices). This configuration enabled fine control of the duration and the amplitude of current stimulus through the controls on the stimulator, as well as user defined real-time control of stimulation frequency through adjustments of the pulse generator. The current pulse duration applied from the stimulator via the recording electrode was 2 ms and the initial stimulation frequency was 1 Hz. Current pulse amplitude was increased incrementally using the stimulator until the threshold potential for triggering an AP was reached (Figure 2.6). APs were monitored on a digital oscilloscope (DL1520, YOKOGAWA) to ensure the AP upstroke was separate from the stimulus artefact. Cells were regularly visualised for evidence of contraction and to monitor signs of ill health as determined by cell membrane blebbing and cell depolarization by monitoring resting membrane potential.

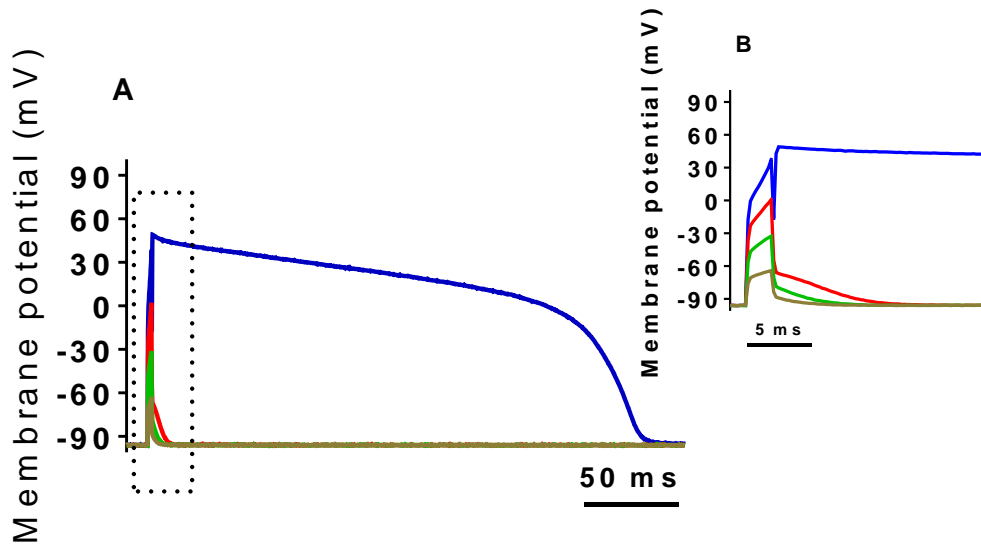


**Figure 2.6: Stimulation of guinea pig ventricular action potentials.** The amplitude of current pulses was increased incrementally until an AP was triggered. **A)** An AP was triggered in the blue trace but not in the preceding dark green, light green and red traces. **B)** Expansion of dashed box in A, to show membrane potential responses to current stimuli.

## 2.5 Electrical Restitution Protocols

Electrical restitution data were obtained using the dynamic restitution protocol (DYRT) in which APs were repetitively stimulated at a particular cycle length (CL) until APD had stabilized using the oscilloscope to monitor stabilization of APD. CL was decreased to a new length systematically using the pulse generator. APs were stimulated starting at CL 1000 ms (1 Hz) then going to 500 ms (2 Hz), then 333 ms (3 Hz), decreasing CL incrementally until APs failed, which means ERP had been reached. CL was then returned to 1000 ms, and the protocol repeated. It was decided that the AP had failed and the cell had reached ERP when the stimulus supplied fails to generate the normal upstroke of the action potential, and when the amplitude of the AP decreased by 10%.

An example of APD shortening at two different frequencies of stimulation (1 Hz and 5 Hz) is shown in Figure 2.7. The same protocol was repeated under different experimental conditions. The cell was allowed to recover at 1Hz between different experimental conditions.

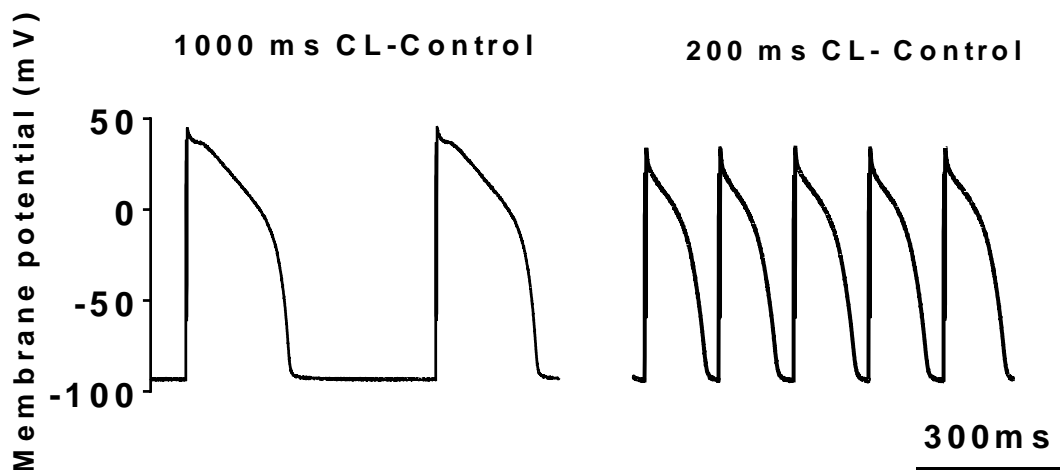


**Figure 2.7: The dynamic restitution protocol.** The figure illustrates representative APs from an acutely isolated left ventricular guinea pig myocytes at cycle lengths (CLs) of 1000 ms and 200 ms. APs were recorded at 35-37 °C, using the amphotericin-perforated patch-clamp technique. Note the decrease in APD and the time between APs (Diastolic interval, DI) at 200 ms CL compared to 1000 ms CL.

The standard restitution protocol (STRT) was used in some experiments (Refer to Appendix) in which the cells were paced initially with 20 S1 stimuli at CL of 500 ms. These S1 stimuli generate a conditioning train of APs before a single S2 stimuli is applied. S1-S2 interval was shortened until AP failure occurs (Figure 2.8).

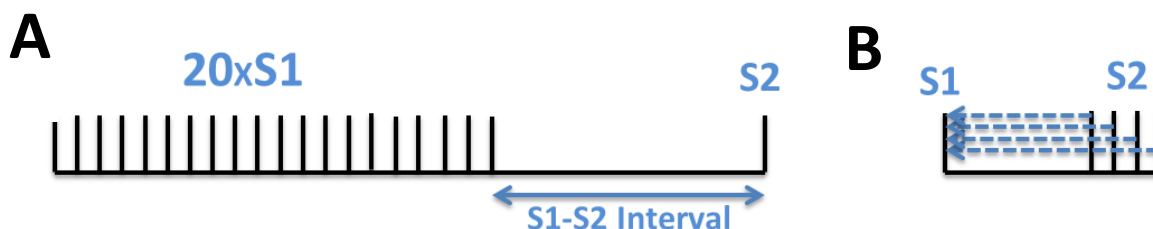


**Figure 2.8: Standard restitution protocol.** **A)** The cells are paced at a CL of 500 ms initially with a train of 20X S1 stimuli before a single S2 stimuli is. **B)** S1-S2 interval was shortened until AP failure occurs. The dashed arrows represent the S1-S2 interval at each S2 pulse.

### 2.5.1 Electrical Restitution Data Analysis and APD<sub>90</sub> repolarization measurement

APs were analysed using Tracan software by Microsoft Visual Studio and National Instruments Measurement Studio Library. Tracan was developed locally by Dr Noel

Davies at university of Leicester. Tracan was used to measure the AP duration until 90% repolarization ( $APD_{90}$ ). Tracan automatically distinguish between the stimulus artefact and AP upstroke and measures the time from AP upstroke threshold to AP peak and adds this onto the time from AP peak to 90% repolarisation. Clampfit files were imported into Tracan, a cursor was placed after the stimulus artefact and the AP upstroke threshold was typically set at -20 mV. To test the accuracy of the Tracan analysis,  $APD_{90}$  in a number of cells were analysed using this method and manual analysis; both produced similar results. Mean  $APD_{90}$  at each frequency and under each experimental condition was obtained by averaging 20 consecutive steady-state APs. Tracan also measures diastolic interval, cycle length, and resting membrane potential of all action potentials in the exported file. APs and analysis points can be viewed for individual APs to confirm the APs are being detected and analysed correctly. The diastolic interval was measured between  $APD_{90}$  of the AP and the upstroke of the next AP (Figure 2.9). For analysis of DYRT data, Mean  $APD_{90}$  and DI at each frequency and under each experimental condition was obtained by averaging 20 consecutive APs once  $APD_{90}$  had declined to a new steady-state level and these were then plotted against mean corresponding DI to obtain the electrical restitution curve for each experimental condition (Figure 2.10).

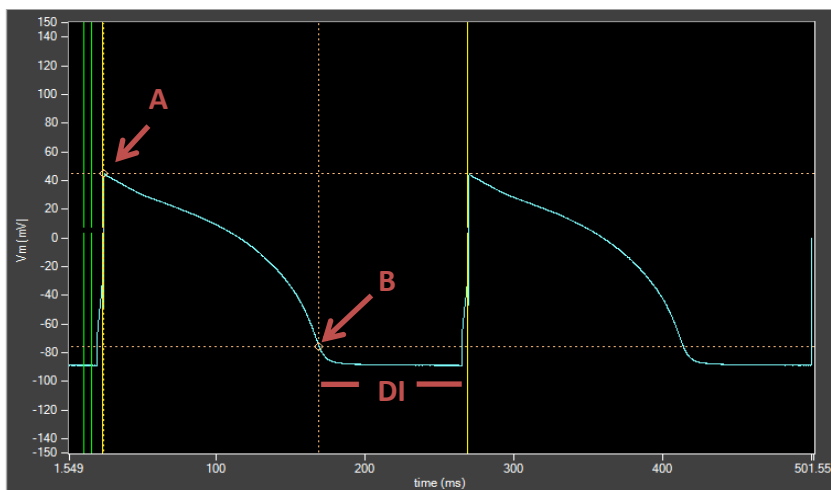


**Figure 2.9: Measuring  $APD_{90}$  and DI using Tracan software.** Tracan was used to measure the  $APD_{90}$  and the diastolic interval between APs. The analysis panel is shown, illustrating two consecutive APs. The green lines measure the resting membrane potential, cursor at point A measures the AP peak, point B is a measure of  $APD_{90}$ , and the yellow line measures the upstroke of the AP.

Prism graphics software (version 6.0, GraphPad) was used to plot data and perform statistical analysis. All data are presented as mean  $\pm$  standard error of the mean (SEM). Significance was tested using one-way analysis of variance (ANOVA) in most of the experiments or two-way analysis of variance (ANOVA) in the diurnal variation experiments as we compared between different experimental conditions in two time period myocytes. P values are presented as \* for  $p \leq 0.05$ , \*\* for  $p \leq 0.01$ , \*\*\* for  $p \leq 0.001$  and no significance (ns) for  $p > 0.05$ . One-way ANOVA and two-way ANOVA were used to check statistical significance. Paired t-test was used sometimes to double check results of One-way ANOVA.

### **2.5.2 Fitting the electrical restitution curve**

Nonlinear regression and one phase decay functions were used to fit electrical restitution data points (Figure 2.10). After fitting the data on the curve;  $APD_{90Max}$  which is  $APD_{90}$  at infinite times, and the time constant ( $\tau$ ) of the curve, were obtained.

As mentioned in Chapter 1 the slope of the electrical restitution curve at maximum stimulation frequency -maximum slope- provides information about the risk of arrhythmogenicity. Electrical restitution curves were analysed using methods similar to those used previously by Ng, G.A *et al.* (2007); Goldhaber *et al.* (2005); Miyauchi *et al.* (2003); and many other groups. In our experiments in acutely isolated single left ventricular myocytes the slope at maximum stimulation frequency was calculated and provided an index of APD variability at short  $DI_{(s)}$ . Maximum slopes were calculated using the following equation:

$$\text{Slope} = ((APD_{90Max} - Y_0) / \tau) * e^{(-DI/\tau)}$$

**$APD_{90Max}$**  is the maximum  $APD_{90}$  at long DI values,

**$Y_0$**  is the  $APD_{90}$  when time is 0,

**Tau ( $\tau$ )** is the time constant of the exponential change of the restitution curve, which is the time taken for the change of  $APD_{90}$  to be 63% of the maximum change of  $APD_{90}$  and

**DI** is the diastolic interval. When calculating slope at maximum stimulation frequency then DI at the maximum stimulation frequency was used.

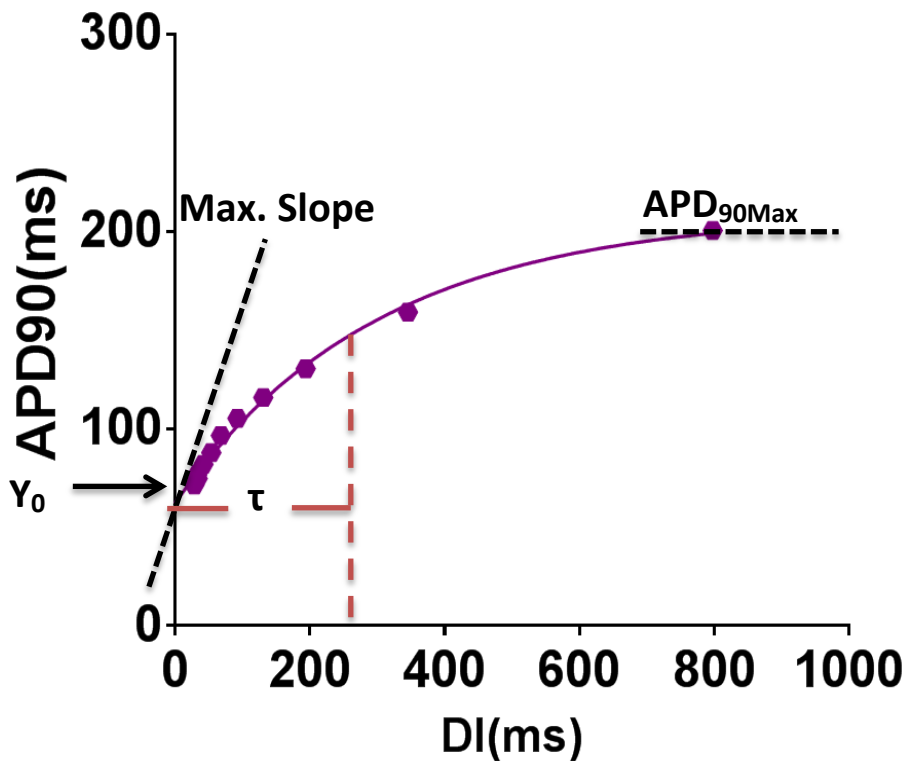
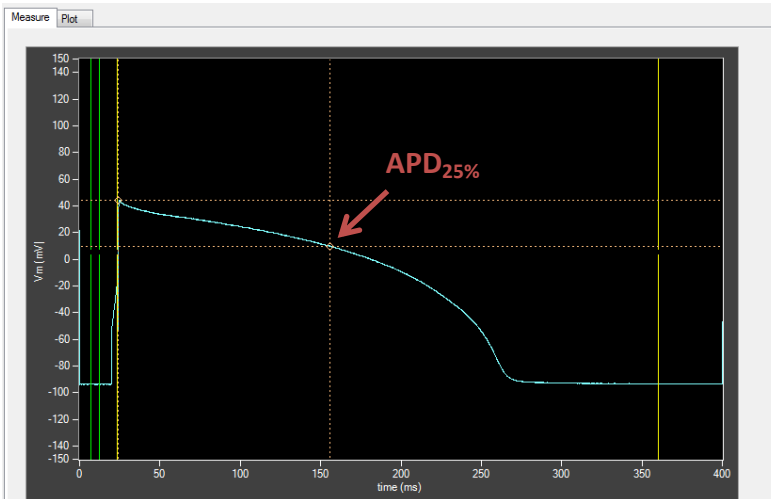


**Figure 2.10: Electrical restitution curve and slope of restitution.** An example of Plot of dynamic restitution curve ( $APD_{90}$  versus preceding DI) in a typical experiment at baseline conditions. The curve was fitted with an exponential function (solid line) to determine time constant ( $\tau$ ), and maximum  $APD_{90}$ . The maximum slope was calculated as described in the methods text. Red dash line represent the point were 63% of  $APD_{90}$  has changed.

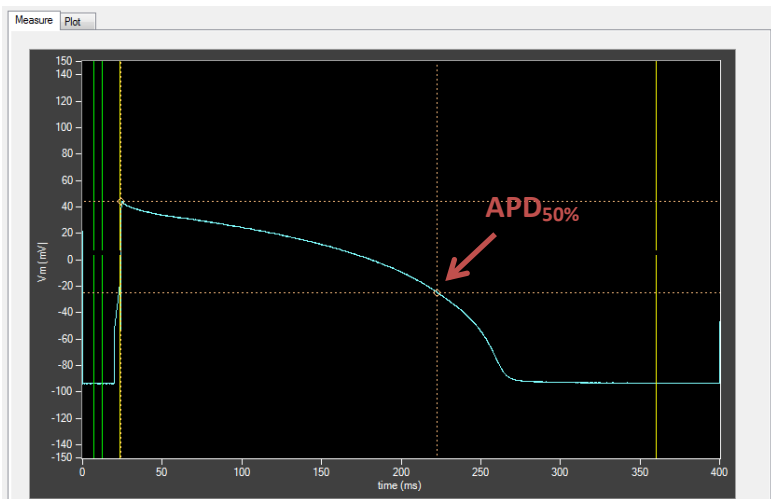
## **2.6 Constant pacing data analysis and $APD_{25, 50, 90}$ measurement**

The stimulation process is similar to what was mentioned in section 2.X but the CL of stimulation was constant and is 500 ms (2Hz). Tracan was used to measure APD until 25% repolarization ( $APD_{25}$ ), 50% repolarization ( $APD_{50}$ ), and 90% repolarization ( $APD_{90}$ ) to figure out the effect of the agents used on the shape and duration of the APs (Figure 2.11). Mean  $APD_{25, 50, 90}$  at each experimental condition was obtained by averaging 20 consecutive steady-state APs.

**A**



**B**



**C**

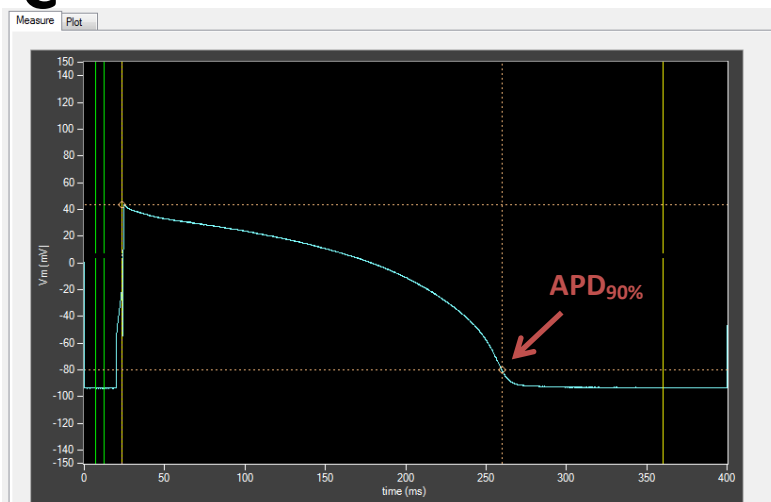


**Figure 2.11: Measuring  $APD_{25}$ ,  $APD_{50}$ , and  $APD_{90}$  using Tracan. Red arrow indicates time points to 25%, 50%, and 90% repolarization.**

## **Chapter 3. Diurnal variation of the electrical restitution properties of acutely isolated guinea-pig left ventricular cardiac myocytes**

### **3.1 Introduction**

Many of the cardiovascular system hemodynamic parameters are prone to diurnal variations, with a morning peak in stroke volume, heart rate and blood pressure in man (Degaute *et al.*, 1991). It was known that this diurnal variation is originally driven by external influences, such as an increase in circulating adrenaline and noradrenaline in the morning, reflecting diurnal patterns of sympathetic activity that also peak early in the morning (Morris *et al.*, 2012). However, recently, the myocardial cells have been shown to possess the key molecular elements that establish the circadian clock and it has been proposed that much of the diurnal variation in ventricular function reflects variation in gene transcription regulated by a complex interaction of extracellular neurohumoral influences and the central and peripheral circadian clock (Young *et al.*, 2001).

Furthermore, the occurrence of arrhythmias and sudden cardiac death is higher in the morning, mainly upon awakening (Honda *et al.*, 2013). Therefore, an increase in the activity of the sympathetic nervous system during the transition from resting to active periods may increase the susceptibility to arrhythmias by modulating repolarisation (Mahmoud *et al.*, 2011). Diurnal variation of repolarisation may also be due to alterations in the expression of genes and proteins associated with  $K^+$  channels. Recently, diurnal variation in the expression of a wide variety of genes in the heart has been detected, including those regulating  $I_{to}$  and  $I_{Kur}$  (Jeyaraj *et al.*, 2012; Yamashita *et al.*, 2003). Diurnal variation of excitation contraction coupling (ECC) through regulation of NO signalling has also been demonstrated. Collins and Rodrigo (2010) showed that in rat left ventricular myocytes, paradoxically,  $Ca^{2+}$  transients and cell shortening were larger in resting than active period myocytes and that resting period myocytes also responded more strongly to  $\beta$ -AR stimulation, with more arrhythmic episodes. These effects were largely mediated by a diurnal variation in NO signalling pathways, with a higher expression of nNOS and greater suppression of ECC in active than resting period myocytes.

The objective of the current study was to investigate whether there is diurnal variation of repolarization at different stimulation frequencies and electrical restitution

properties of acutely isolated guinea-pig left ventricular cardiac myocytes under basal conditions and in response to ISO. The main three questions in this study were the following. 1) Is there diurnal variation in guinea-pig APs under basal conditions? 2) Is there diurnal variation in response of APs to ISO? 3) Is there a role of NO signalling in responses to ISO and does that vary with time of the day?

### **3.2 Electrical restitution experimental design**

As mentioned earlier electrical restitution data were obtained using the DYRT in which pacing cycle lengths were shortened until APs failed. The first experiments performed tested if  $APD_{90}$  remained stable with repetitive stimulation under our recording conditions. Figure 3.1 shows  $APD_{90}$  plotted against time through an experiment in a representative electrical restitution data which has been obtained using pacing cycle lengths that were shortened until AP capture failure.  $APD_{90}$  starts at close to 500 ms and then declines exponentially to a new 'steady state' duration due to APD restitution as the AP adapts to the changing diastolic interval. When the frequency is changed there is an exponential decline to the new steady state duration. The APD was given time to stabilize at each cycle length. At 6 Hz, the AP failed to capture. The myocyte was then allowed to recover at 1 Hz stimulation frequency and the  $APD_{90}$  starts to increase exponentially with time. It took time for  $APD_{90}$  to increase when stimulation frequency went from fast to slow.

Figure 3.2 shows AP traces at different stimulation frequencies (1 Hz – 5 Hz) and at different time points, during protocol 1 and protocol 2 in the experiment under basal conditions. APs were chosen when the cell stabilized at each stimulation frequency from protocol 1 and protocol 2. The last panel in the Figure shows when the myocyte reached the maximum stimulation frequency (MSF) and failed to capture an AP. Figure 3.1 and Figure 3.2 confirm that there was no significant change of  $APD_{90}$  during protocol 1 and 2, at each frequency, under our recording conditions and while perfusing the myocyte with normal Tyrode at 37°C.

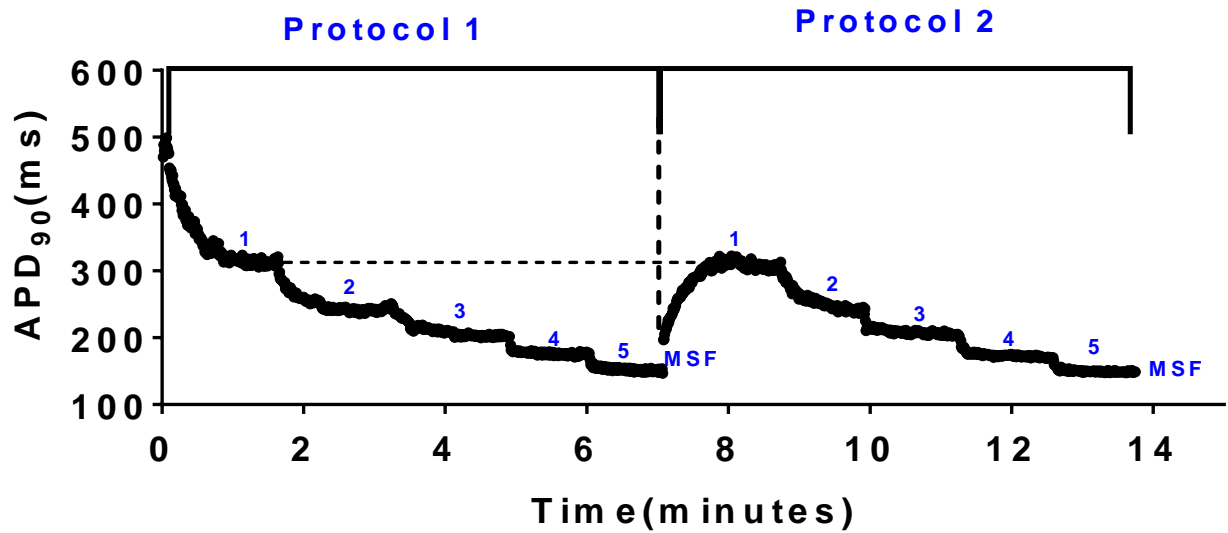


**Figure 3.1: Dynamic restitution protocol.** Representative plot of APD<sub>90</sub> against time throughout the experiment. The myocyte was stimulated at a given frequency until APD<sub>90</sub> had stabilized and then the stimulated frequency was increased (Protocol 1). The cell was allowed to recover after AP failure (in this case at 6 Hz) at 1 Hz stimulation frequency before starting the restitution protocol again as a subsequent run (Protocol 2). The horizontal dashed line shows that APD<sub>90</sub> recovered to the same level of APD<sub>90</sub> of the previous 1 Hz stimulation frequency. In this recording, the myocyte was perfused with control normal Tyrode throughout the recording to establish how stable APs were under our recording conditions. Numbers on the Figure represent stimulation frequency (Hz). MSF: Maximum stimulation frequency.

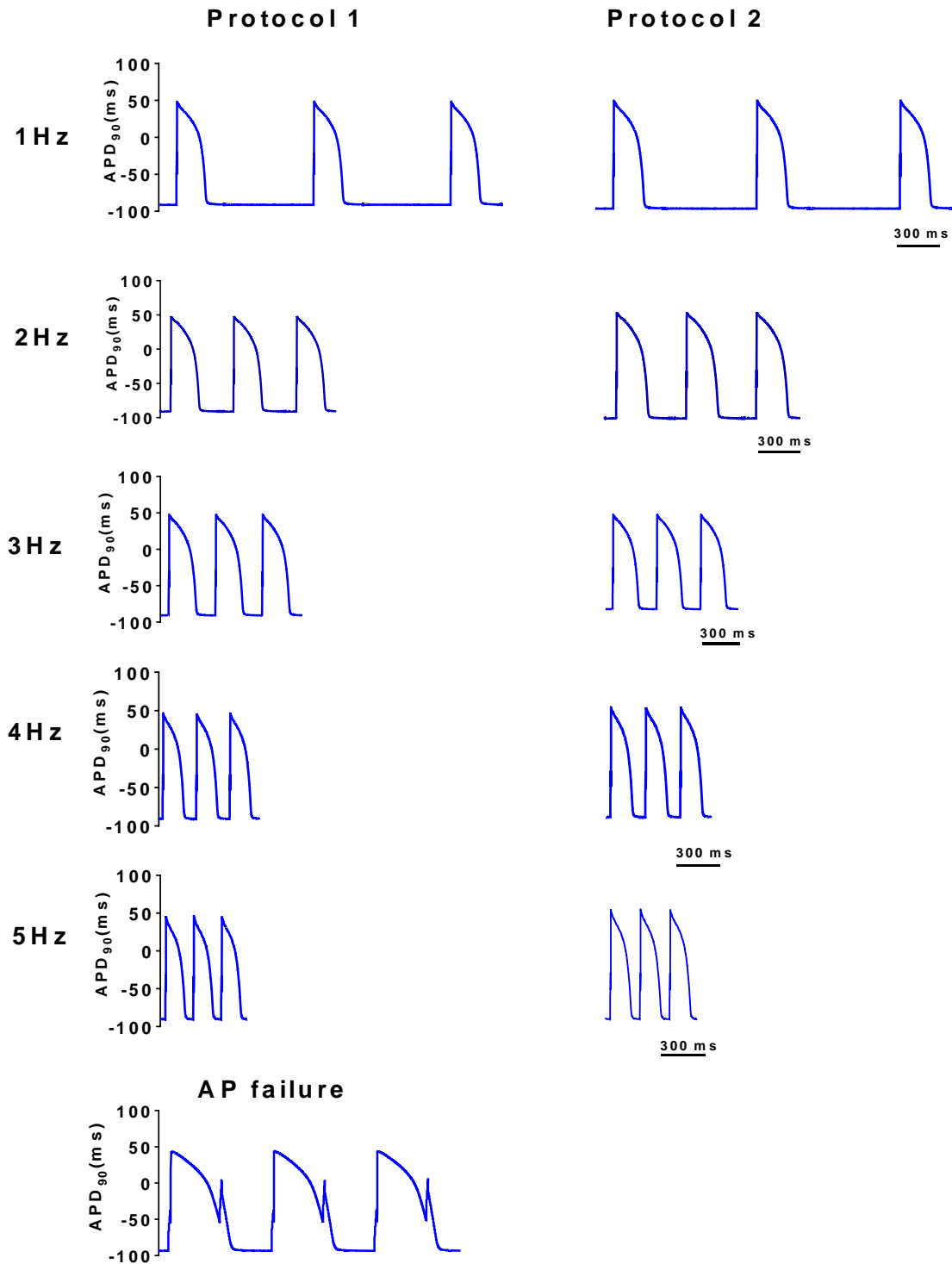


**Figure 3.2: Representative action potentials at different stimulation frequencies and time points in the experiment under basal conditions.** Three action potentials have been chosen as representative APs at each stimulation frequency and at two different time points (Protocol 1 and protocol 2) when the cell stabilized at each stimulation frequency. The last panel in the Figure shows when the myocyte failed to capture an AP.

The effect of repeated stimulation on mean APD<sub>90</sub> at each stimulation frequency (1 Hz – 5 Hz) during protocol 1 and protocol 2 under basal conditions is illustrated in Figure 3.3. Using paired t-test statistical analysis; there was no significant change in mean APD<sub>90</sub> at each stimulation frequency, or the maximum attainable stimulation frequency (data not shown) which confirm the stability of APs under our recording conditions. N-number shown in the Figure is from different hearts isolation experiments.

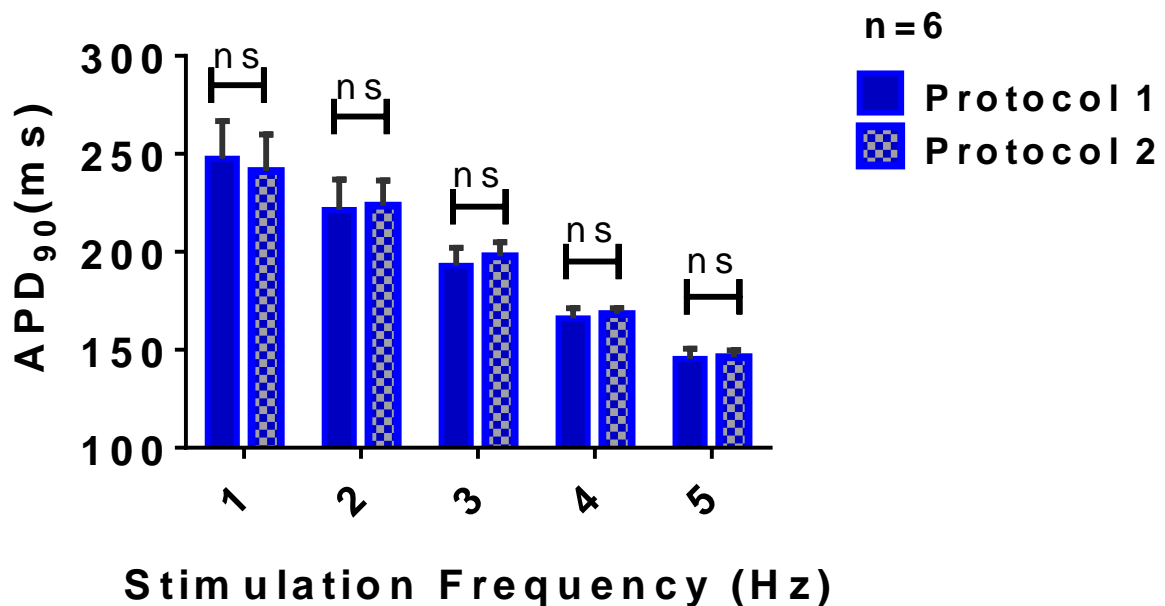


**Figure 3.3: The effect of repeated stimulation on mean APD<sub>90</sub> under basal conditions.** Mean APD<sub>90</sub> at each stimulation frequency from protocol 1 and protocol 2. Data are presented as mean ± SEM (n=6 cells from 4 guinea pigs). Data with P-value >0.05 are considered non-significant. ns =non-significant.

### 3.3 Results

To study diurnal variation of AP repolarization, guinea-pigs were divided into two groups and housed in opposing 12 hour light cycles prior to use in experiments (Figure 2.1). Therefore, experimental animals were either in an active or resting period when culled at 9:00 AM. APs were recorded from single acutely isolated guinea-pig left ventricular myocytes using the DYRT protocol. Data was taken from 30 active myocytes from 15 active guinea pigs and 22 resting myocytes from 10 guinea pigs. Figure 3.4 illustrates plots of APD<sub>90</sub> against time throughout the

experiment from active and resting period myocytes.  $APD_{90}$  started at around 300 ms and then declines exponentially. When the frequency is changed there was an exponential decline to the new steady state level. The APD was given time to stabilize at each cycle length. In the representative myocytes in the Figure, the myocytes reached the maximum stimulation frequency at 6 Hz under basal conditions in both active and resting period myocytes. Then the myocyte was allowed to recover at 1 Hz stimulation frequency and  $APD_{90}$  started to increase exponentially with time. When  $APD_{90}$  stabilized at 1 Hz, the myocyte was perfused with 10 nM ISO and a note was added at that time point to the gap-free recording file. It takes ~ 1 minute for ISO to reach the bath from the perfusion pump. The DYRT protocol was started again until the cell reached the maximum stimulation frequency with the  $\beta$ -AR agonist ISO and failed to capture an AP; which was at 7 Hz in the representative myocytes. Then the myocyte was allowed to recover again at 1 Hz and when  $APD_{90}$  stabilized the non-specific NOS inhibitor L-NNA (500  $\mu$ M) was added in the continued presence of ISO and the same experimental protocol was repeated again until the myocyte reach the maximum stimulation frequency, which was 9 Hz in the examples shown. The duration of the experiments varied according to maximum stimulation frequency of each cell in response to each experimental condition and according to how long it took for APD to stabilise at each stimulation frequency; as going to the next stimulation frequency only occurred when APD had stabilized at the previous stimulation frequency.

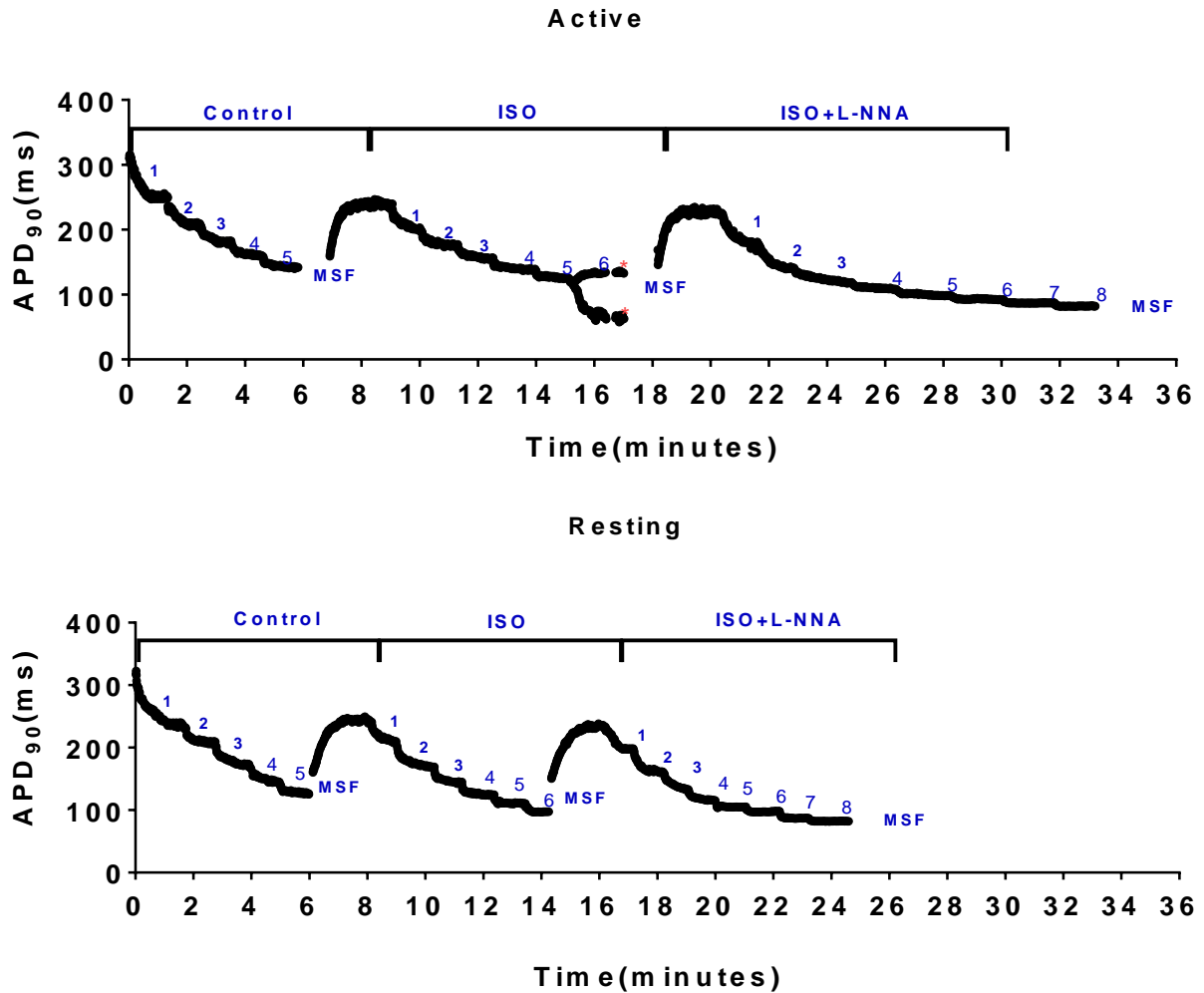


**Figure 3.4: Representative plots of APD<sub>90</sub> against time throughout the experiment from active (upper panel) and resting (lower panel) period myocytes.** The myocyte was stimulated under basal conditions at a given frequency until APD<sub>90</sub> had stabilized and then the stimulated frequency was increased. The cell was allowed to recover after AP failure at 1 Hz stimulation frequency before starting the restitution protocol again under  $\beta$ -AR stimulation (10 nM ISO) until the myocyte reached the MSF then the myocyte was allowed again to recover at 1 Hz before adding the NOS inhibitor (500  $\mu$ M L-NNA) in the continued presence of ISO. Numbers on the Figure represent stimulation frequency (Hz). The red stars in the upper panel demonstrate alternans in APD<sub>90</sub> in the active period myocyte at 6 Hz stimulation frequency. MSF: Maximum stimulation frequency.

### **3.3.1 Is there diurnal variation in APD<sub>90</sub> under basal conditions at each stimulation frequency?**

After establishing that the AP recordings are stable over time the next question was to figure out if there is a diurnal variation in APD<sub>90</sub> under basal conditions at each stimulation frequency. Figure 3.5A illustrates representative AP traces at different stimulation frequencies under basal conditions in an active and a resting myocyte. The traces have been overlaid so that the AP adaptations at different stimulation frequencies can be compared. In these examples it can be seen that the AP morphologies and durations were similar. Mean APD<sub>90</sub> from the two time periods myocytes at stimulation frequencies 1 Hz – 5 Hz is shown in Figure 3.5B. There was no significant diurnal variation in APD between active and resting period myocytes under basal conditions at 1 Hz – 5 Hz. We chose to show mean APD<sub>90</sub> data at each frequency up until 5 Hz as almost all the cells passed through 5 Hz and their maximum stimulation frequency was > 5 Hz. However, the maximum stimulation frequency for cells was variable.

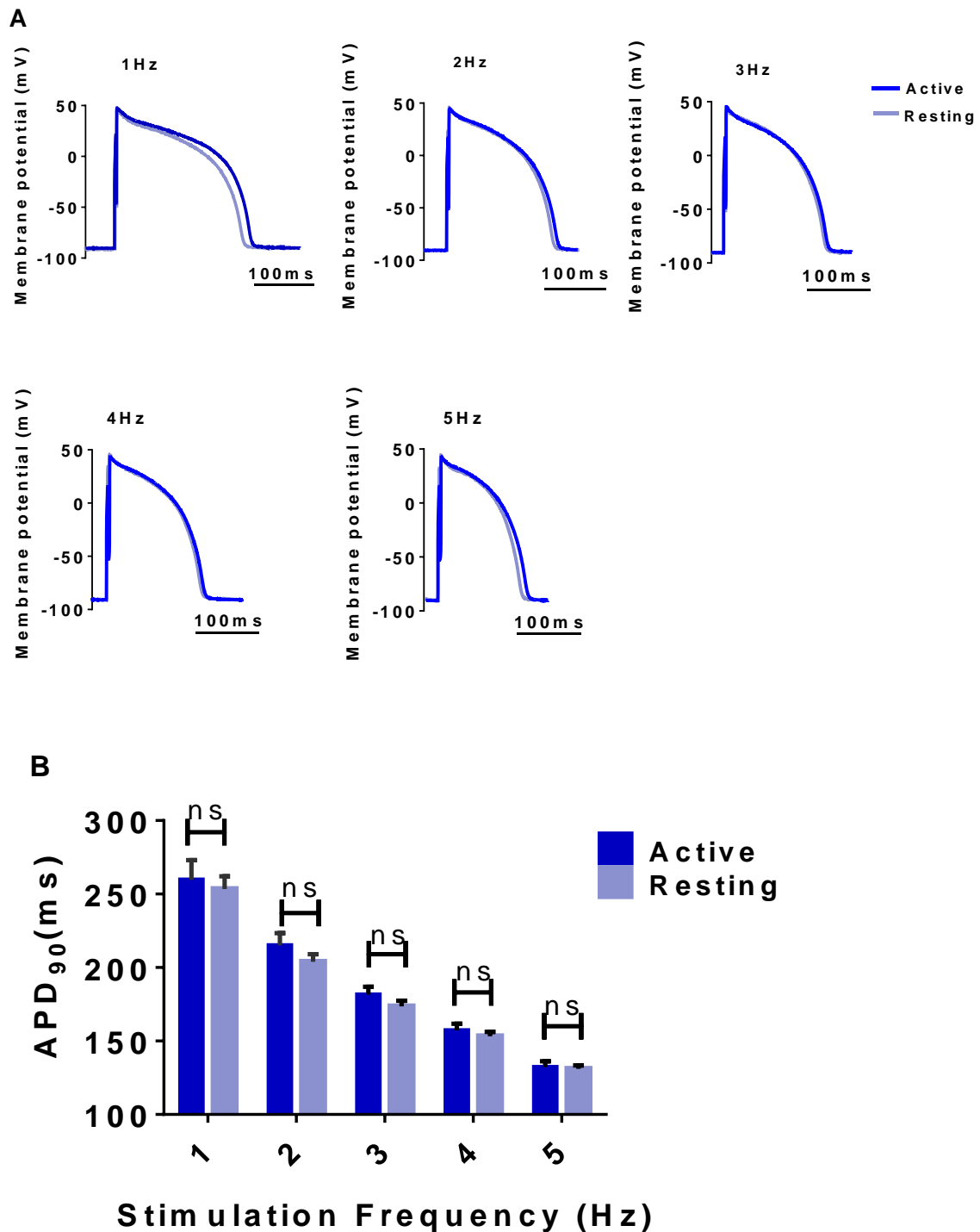


**Figure 3.5: Diurnal variation in APD<sub>90</sub> under basal conditions. A)** Representative AP traces under basal conditions, at the indicated stimulation frequencies, in an active and a resting myocyte. **B)** Mean APD<sub>90</sub> data at different stimulation frequencies under basal conditions in active versus resting myocytes. Active myocytes (n=30 cells from 15 active guinea pigs), resting myocytes (n=22 cells from 10 resting guinea pigs).

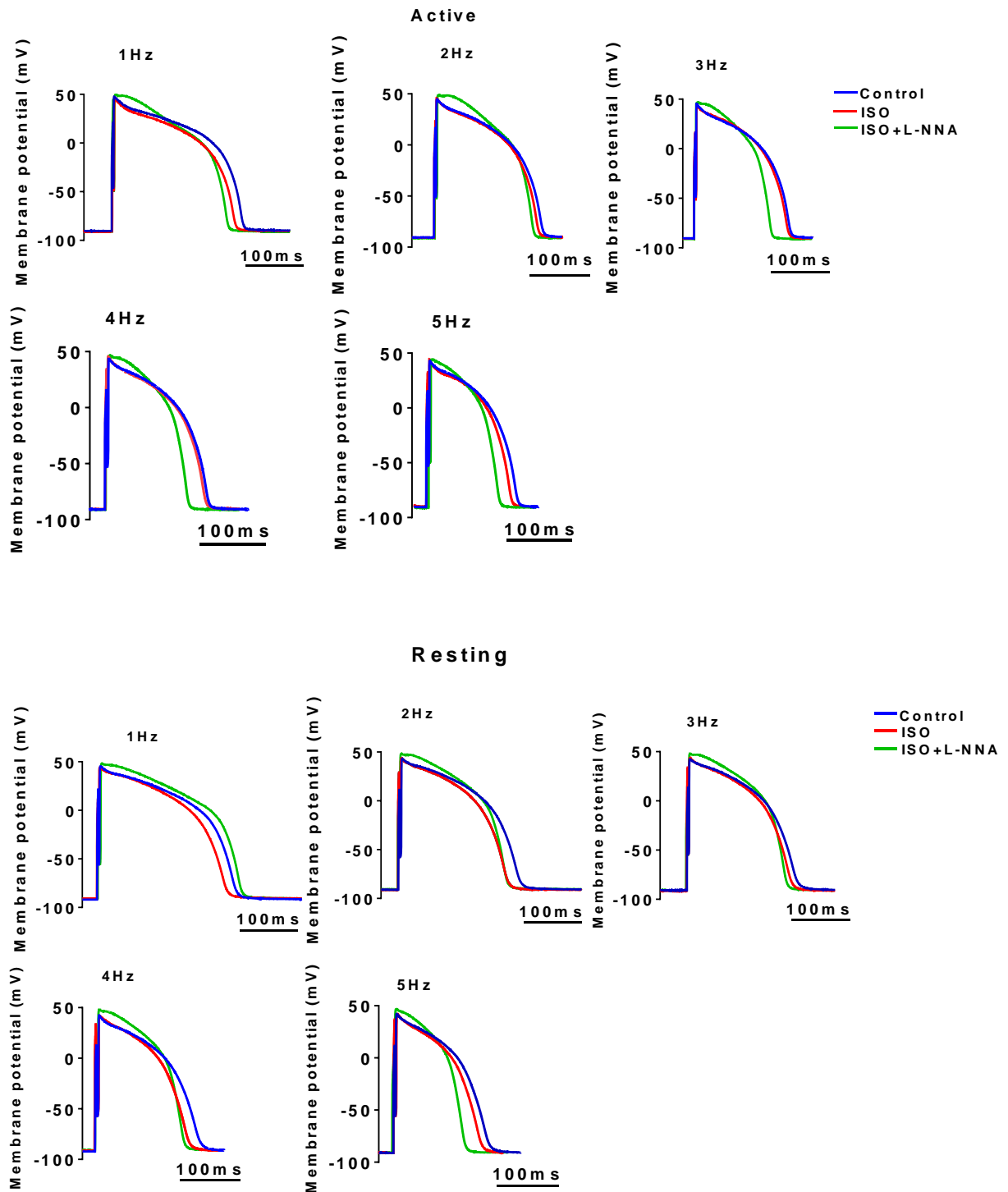
### **3.3.2 Are there differences in how active and resting period myocytes respond to $\beta$ -AR stimulation (ISO) and the role of NO in regulating the ISO response?**

Diurnal variation of  $I_{Ca,L}$  responses to  $\beta$ -AR stimulation in rat left ventricular myocytes have been reported (Collins and Rodrigo, 2010). Our objective was to establish whether there is diurnal variation in guinea-pig left ventricular myocyte APs in response to  $\beta$ -AR stimulation by using the non-selective  $\beta$ -AR agonist Isoprenaline (ISO) at different stimulation frequencies. As a follow up question, we then wanted to investigate if there is a role of NO signalling in the response to ISO and whether that varies with time of day.

As mentioned earlier ISO is a nonselective  $\beta$ -AR agonist that stimulates  $\beta_1$ ,  $\beta_2$ , and  $\beta_3$  receptors. Whereas activation of both  $\beta_1$  and  $\beta_2$  receptors results in positive inotropy, in part because of an increase in the L-type  $Ca^{2+}$  current and SR  $Ca^{2+}$  loading, activation of  $\beta_3$ -AR is known to have a negative inotropic effect through the action of NO (Gauthier *et al.*, 2000).

Cells were stimulated under basal (control) conditions at progressively higher frequencies until AP capture failure then the solution was switched to 10 nM ISO and the DYRT protocol repeated and then finally in (some cells) the solution was switched to 10 nM ISO plus 500  $\mu$ M L-NNA. The L-NNA concentration used should maximally inhibit nNOS and eNOS (Chowdhary and Townend, 1999). L-NNA was not applied in all the resting period myocytes as we decided to add the L-NNA to our experiments in the middle of the diurnal variation project when most of the resting period animals had been used. To allow parametrical statistical tests to be used, when investigating effects of L-NNA, data is only included from cells exposed to control, ISO, and ISO plus L-NNA.

Figure 3.6 illustrates AP traces from representative active and resting period myocytes under basal conditions, in response to ISO, and in response to L-NNA in the continued presence of ISO at different stimulation frequencies from 1 Hz - 5 Hz. ISO caused a small amount of shortening in both myocytes, which was most noticeable at the slower stimulation frequencies. ISO alone did not change the AP plateau. In contrast, L-NNA (in the presence of ISO) caused a pronounced depolarisation of the AP plateau as well as a further shortening of APD.



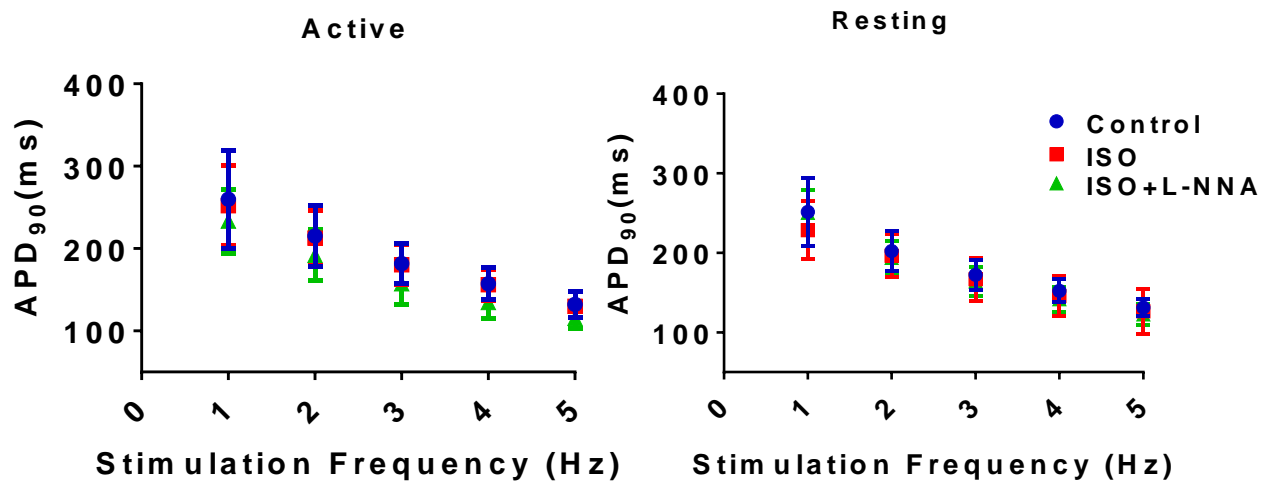
**Figure 3.6: Representative AP traces from active and resting period myocytes at different stimulation frequencies under basal conditions, in response to 10 nM ISO, and in response to 500  $\mu$ M L-NNA in the continued presence of ISO. The upper panel shows AP traces from active period myocytes. The Lower panel shows representative AP traces from resting period myocytes. Each panel has been taken from one cell.**

Figure 3.7 shows the mean APD<sub>90</sub> under basal conditions, in response to 10 nM ISO, and when 500 μM L-NNA was applied in the continued presence of ISO at different stimulation frequencies (1 Hz – 5 Hz) in the two time period myocytes. Simply comparing mean values did not enable a clear effect of reagents to be observed, probably because cell to cell differences in APD introduced too much variability. As an alternative form of analysis the change of APD<sub>90</sub> in response to reagents was measured in individual cells and the mean results are shown in Figure 3.8.

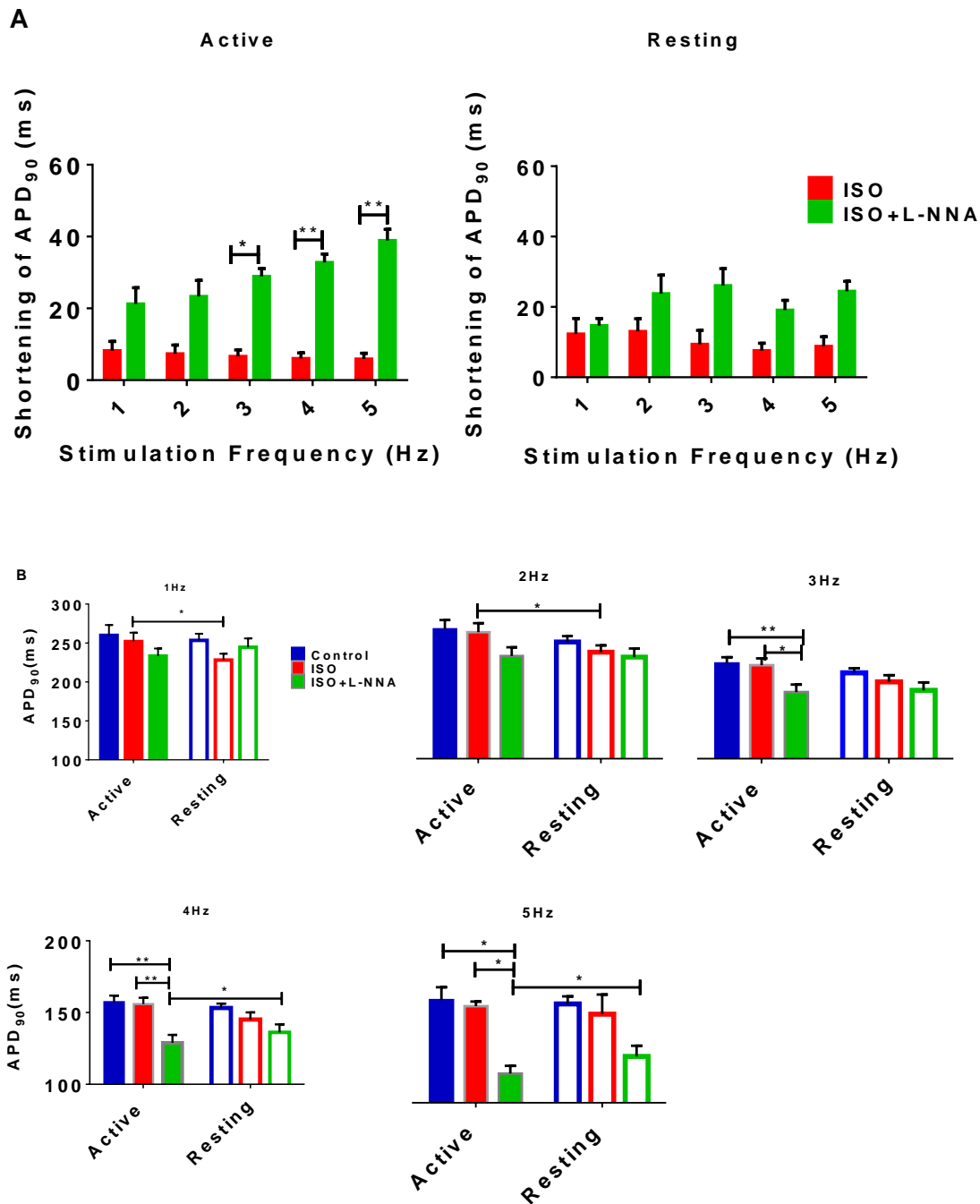
Figure 3.8A illustrates the shortening of APD<sub>90</sub> in response to L-NNA (in the continued presence of ISO) relative to control at each stimulation frequency. This has been done for individual myocytes and then mean ± SEM has been calculated. Interestingly active and resting period myocytes showed differences. In active period myocytes, the mean response to ISO alone was absent and didn't change much with frequency in comparison to control. However, when L-NNA was also applied the total change in APD was much larger and increased progressively with stimulation frequency. In contrast, in resting period myocytes, the response to ISO appeared larger than in active period cells, but the additional response to L-NNA was not as large. Stars of significance are shown in the Figure just to illustrate that the change in APD<sub>90</sub> in response to L-NNA in comparison to control is more significant than the change in APD<sub>90</sub> in response to ISO compared to control in the active period myocytes at higher frequencies.

Figure 3.8B shows mean APD<sub>90</sub> at different stimulation frequencies (1 Hz - 5 Hz) in active and resting period myocyte under baseline conditions, in response to ISO, and in response to ISO plus L-NNA. To determine if there was a difference in how active and resting period cells respond to both experimental conditions, the responses were compared at each frequency using a paired t-test. In other words, the question addressed was if effect of ISO on APD<sub>90</sub> at 1, 2, 3, 4, 5 Hz was different in the resting period myocytes to its effect on the active period myocytes. Similarly, was the effect of ISO plus L-NNA on APD<sub>90</sub> at 1, 2, 3, 4, 5 Hz different in the resting and active period myocytes. Comparing the response to ISO of the active versus resting period myocytes at each stimulation frequency, showed that there was a statistically significant difference at 1 Hz ( $p \leq 0.05$ ) and 2 Hz ( $p \leq 0.05$ ); with the resting period myocytes being more responsive. Comparing the response when L-NNA was applied

showed that there was a statistically significant different response at 4 Hz ( $p \leq 0.05$ ) and 5 Hz ( $p \leq 0.05$ ); with the active period myocytes being more responsive.



**Figure 3.7: Mean APD<sub>90</sub> at different stimulation frequencies (1 Hz – 5 Hz) in active and resting period myocyte under basal conditions, 10 nM ISO, and ISO plus 500  $\mu$ M L-NNA.** Data are presented as mean  $\pm$  SEM. Active myocytes (n=15 cells from 8 guinea pigs), resting myocytes (n=10 cells from 5 guinea pigs).



**Figure 3.8: A) Shortening of APD<sub>90</sub> at different stimulation frequencies (1 Hz - 5 Hz) in active and resting period myocyte in response to 10 nM ISO, and 500  $\mu$ M L-NNA in the continued presence of ISO relative to control. B) Mean APD<sub>90</sub> at different stimulation frequencies (1 Hz - 5 Hz) in active and resting period myocyte under baseline conditions, in response to ISO, and in response to ISO plus L-NNA. Data are presented as mean  $\pm$  SEM. Active myocytes (n=15 cells from 8 guinea pigs), resting myocytes (n=10 cells from 5 guinea pigs). \* P  $\leq$ 0.05, \*\* P $\leq$ 0.01, \*\*\* P $\leq$ 0.001.**

The representative APs in Figure 3.6 shows that the membrane potential of the early plateau phase changed modestly and more positive when L-NNA was applied in the continued presence of ISO and this change in the AP shape was noticed in the two time period myocytes. This change in the AP plateau suggests augmentation of  $I_{Ca,L}$ . Mean APD from AP upstroke to 10% repolarization ( $APD_{10}$ ) was measured for the two time periods to quantify the change in the plateau noticed (Figure 3.9).  $APD_{10}$  was chosen as this is the percentage which should indicate the alteration of the plateau. There was a clear trend for mean  $APD_{10}$  to be higher at all stimulation frequencies in active period myocytes in comparison to resting period myocytes, but this was most obvious and significant) when L-NNA was added to ISO. A diurnal variation in  $APD_{10}$  at 1, 3, 4, and 5 Hz was significant ( $p \leq 0.05$ ), which means that the active period myocytes were more responsive to L-NNA and showed a more depolarized plateau in comparison to the resting period myocytes. ISO showed higher plateau at 4 and 5 Hz in active period myocytes compared to resting ones and that was obvious with diurnal variation in  $APD_{10}$  at 4 and 5 Hz.

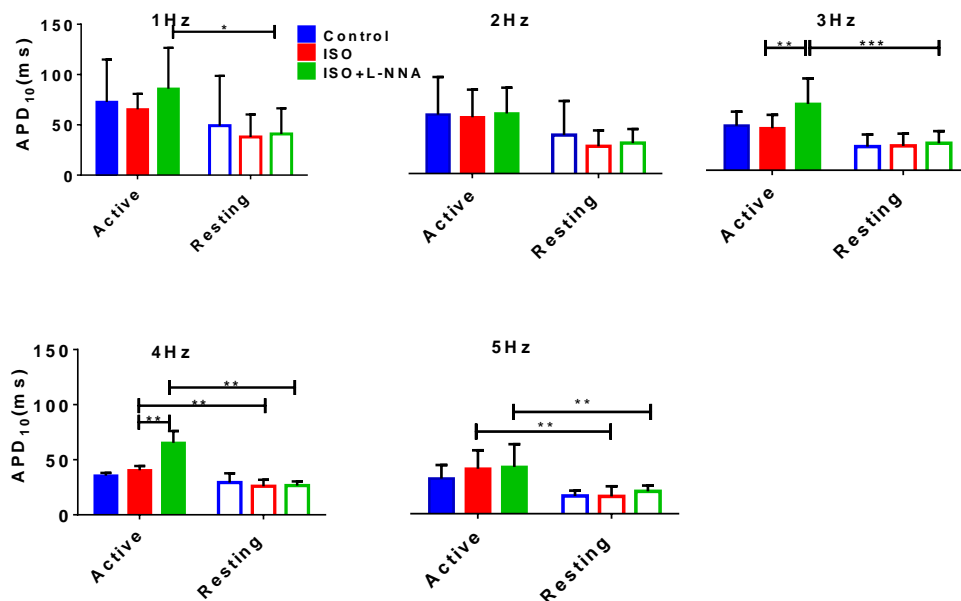


**Figure 3.9: Mean  $APD_{10}$  at stimulation frequencies 1 Hz – 5 Hz in active and resting period myocytes.** Diurnal variation in  $APD_{10}$  in basal conditions, in response to 10 nM ISO, and in response 500  $\mu$ M L-NNA in the continued presence of ISO. Data are presented as mean  $\pm$  SEM. Active myocytes ( $n=15$  cells from 8 guinea pigs), resting myocytes ( $n=10$  cells from 5 guinea pigs). Two- Way ANOVA was used to obtain this data. Data with  $p$ -value  $\leq 0.05$  are considered significant.

### 3.3.3 Is there diurnal variation in the electrical restitution curve?

Electrical restitution curve parameters have been used to compare the electrical restitution curves plotted under basal conditions with those plotted under different experimental conditions. These parameters are: time constant ( $\tau$ ), maximum  $APD_{90}$  ( $APD_{90Max}$ ), and the maximum slope (Slope =  $((APD_{90Max} - Y_0) / \tau)^{Exp(-DI/\tau)}$ ). The data below explains in details if there was diurnal variation in each parameter and under which experimental condition. Figure 3.10 shows representative electrical restitution curves from two time period myocytes in basal conditions, in response to 10 nM ISO, and in response to ISO plus 500  $\mu$ M L-NNA. Tracan software was used to measure  $APD_{90}$  and DI.  $APD_{90}$  values and DI values were copied to excel to calculate mean  $APD_{90}$  at each frequency and under each experimental condition by averaging 20 consecutive steady-state APs. For analysis of DYRT data, mean  $APD_{90}$  values for each stimulation frequency were then plotted against mean corresponding DI to obtain the electrical restitution curve for each experimental condition. Prism graphics software was used to plot the mean  $APD_{90}$  values against the corresponding mean DI values and to perform statistical analysis. Nonlinear regression and one phase decay functions were used to fit electrical restitution data points and obtain  $APD_{90Max}$ , and  $\tau$  of the curve and then maximum slope was calculated.

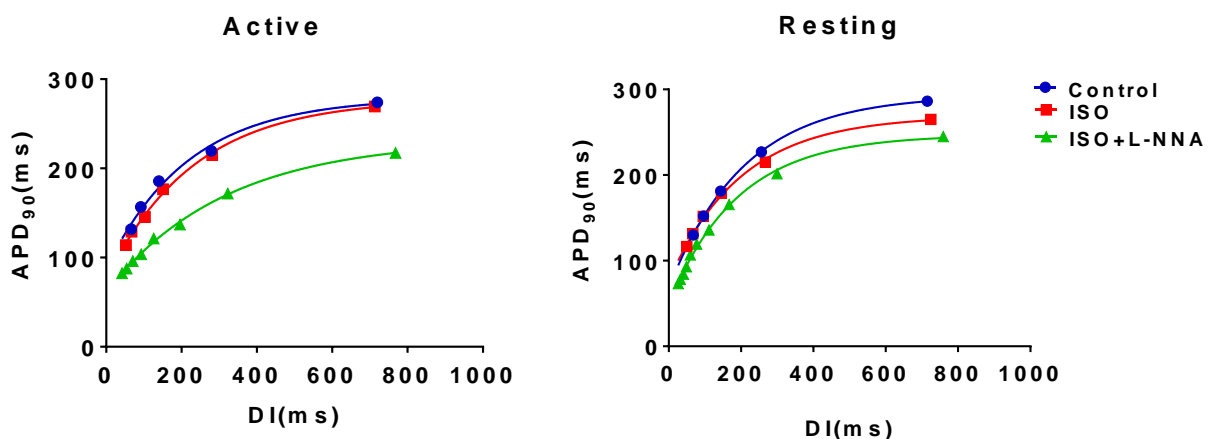


**Figure 3.10: Representative electrical restitution curves from active and resting period myocytes.** Points are fitted with exponential function (solid line in each curve) to determine  $APD_{90Max}$ , slope, and  $\tau$ .

### 3.3.3.1 APD<sub>90Max</sub>:

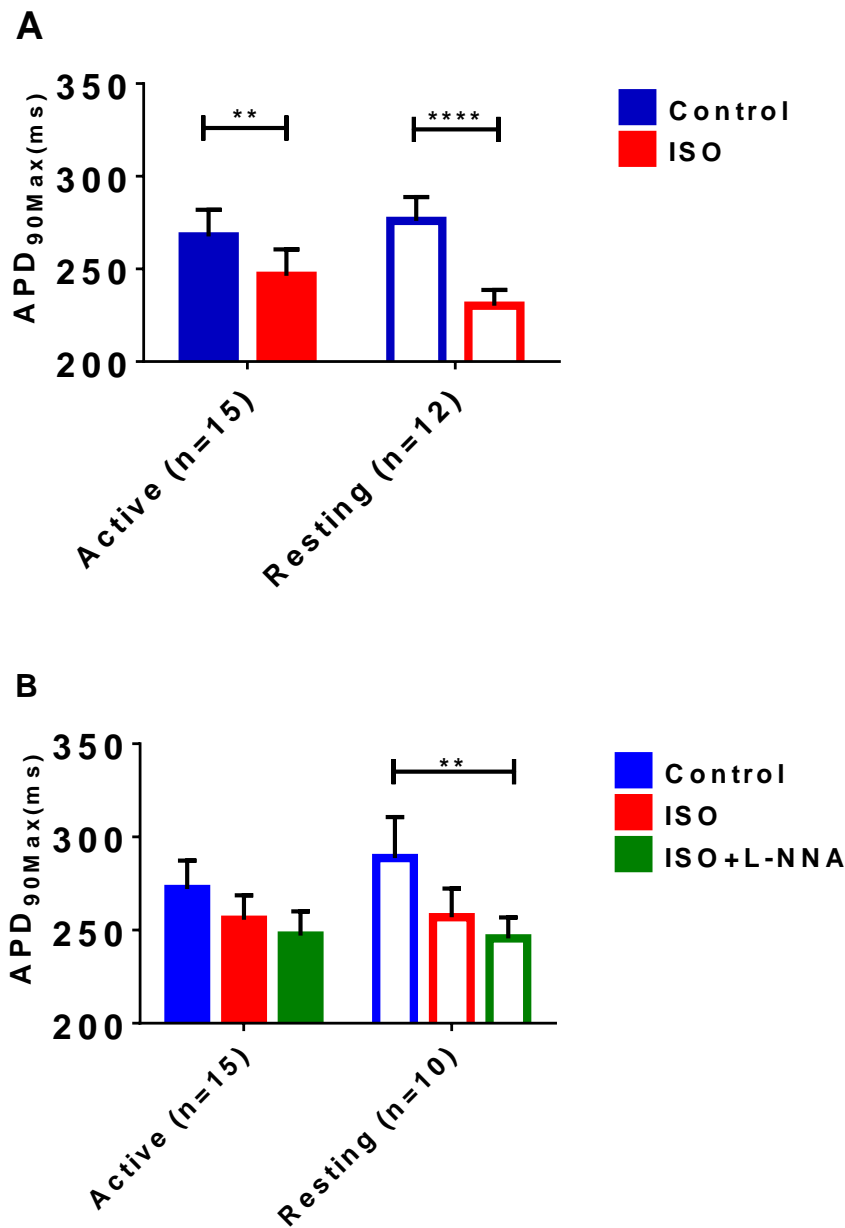


**Figure 3.11: Diurnal variation in APD<sub>90Max</sub>.** **A)** Diurnal variation in APD<sub>90Max</sub> under basal conditions and in response to 10 nM ISO. Active myocytes (n=15 cells from 7 guinea pigs), resting myocytes (n=12 cells from 5 guinea pigs). **B)** Diurnal variation in APD<sub>90Max</sub> from the cells which were exposed to 500  $\mu$ M L-NNA in the continued presence of ISO. Active myocytes (n=15 cells from 8 guinea pigs), resting myocytes (n=10 cells from 5 guinea pigs). Two-Way ANOVA was used to check for diurnal variation while paired t-test was used to check for significant difference between each two conditions in the same time period.

Mean  $APD_{90Max}$  results are shown in Figure 3.11. The top panel shows results for control and ISO data only, whereas the bottom panel is from myocytes where L-NNA was also applied. The mean  $APD_{90Max}$  in the active period myocytes was decreased by 10 nM ISO by 21.24 ms in comparison to control ( $p \leq 0.01$ ), while a more significant decrease of 45.74 ms was observed in resting period myocytes ( $p \leq 0.0001$ ). As discussed earlier, ISO showed that there was a statistically significant shortening in  $APD_{90}$  at 1 Hz ( $p \leq 0.001$ ) and 2 Hz ( $p \leq 0.05$ ); with the resting period myocytes being more responsive. Therefore, the different effect of ISO on  $APD_{90Max}$  indicates an important stimulation rate-dependent effect of ISO. The trends in how the resting and active period myocytes responses to ISO were similar, with a larger response in the resting period myocytes. L-NNA resulted in a small further reduction of  $APD_{90Max}$  in both active and resting period myocytes which was statistically significant in the resting period myocytes ( $p \leq 0.01$ ). In conclusion, there was no diurnal variation between the two time period myocytes in  $APD_{90Max}$  under basal conditions, with ISO, or when L-NNA was applied in the continued presence of ISO. However, resting period myocytes showed more shortening in  $APD_{90Max}$  in response to ISO, and when L-NNA was applied in continued presence of ISO

### 3.3.3.2 Slope:

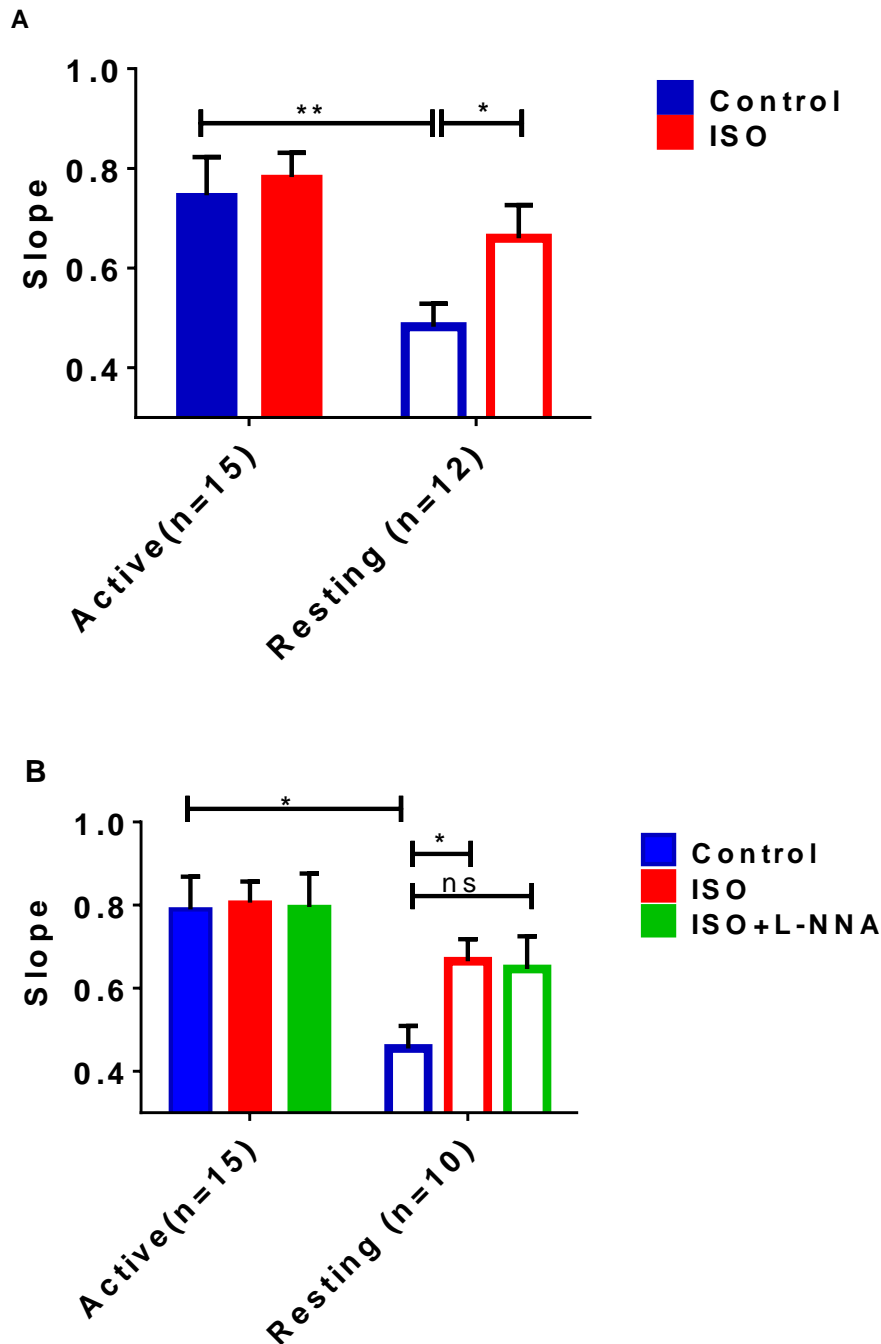


**Figure 3.12: Diurnal variation in maximum slope of restitution values. A)** Diurnal variation in maximum slope in basal conditions and in response to 10 nM ISO. Active myocytes (n=15 cells from 7 guinea pigs), resting myocytes (n=12 cells from 5 guinea pigs). **B)** Diurnal variation in maximum slope from the cells which were exposed to 500 μM L-NNA in the continued presence of ISO. Active myocytes (n=15 cells from 8 guinea pigs), resting myocytes (n=10 cells from 5 guinea pigs).

The slope of the electrical restitution curve is a strong indicator of the electrical stability. The higher the slope of the electrical restitution curve the greater the likelihood of arrhythmias and VF due to break up of wave-form in the intact heart. We were interested in studying single cell restitution to compare it to responses in the whole heart. The slope of the single cell electrical restitution curves was calculated for each experimental condition using the equation described in chapter 2. The mean slope of the curve at the maximum frequency of stimulation is plotted in Figure 3.12. Figure 3.12A represents cells from the two time period myocytes which have been exposed to control conditions and ISO. The mean control slope values of the active period myocytes was significantly higher than the resting period myocytes ( $p \leq 0.01$ ). In the presence of ISO, the mean slope value was increased compared to control in both cell groups but the increases were larger in the resting period myocytes ( $p \leq 0.05$ ). This behaviour was preserved in the group of cells to which L-NNA was also added (Figure 3.12B). These results suggest that there is diurnal variation in the electrical restitution curves under control conditions as mean slope values in the active period myocytes restitution curves were higher in comparison to resting period myocytes. Moreover, diurnal variation in response to  $\beta$ -AR stimulation has been noticed as resting period myocytes were more responsive to ISO than active period myocytes.

### 3.3.3.3 Time constant ( $\tau$ ):

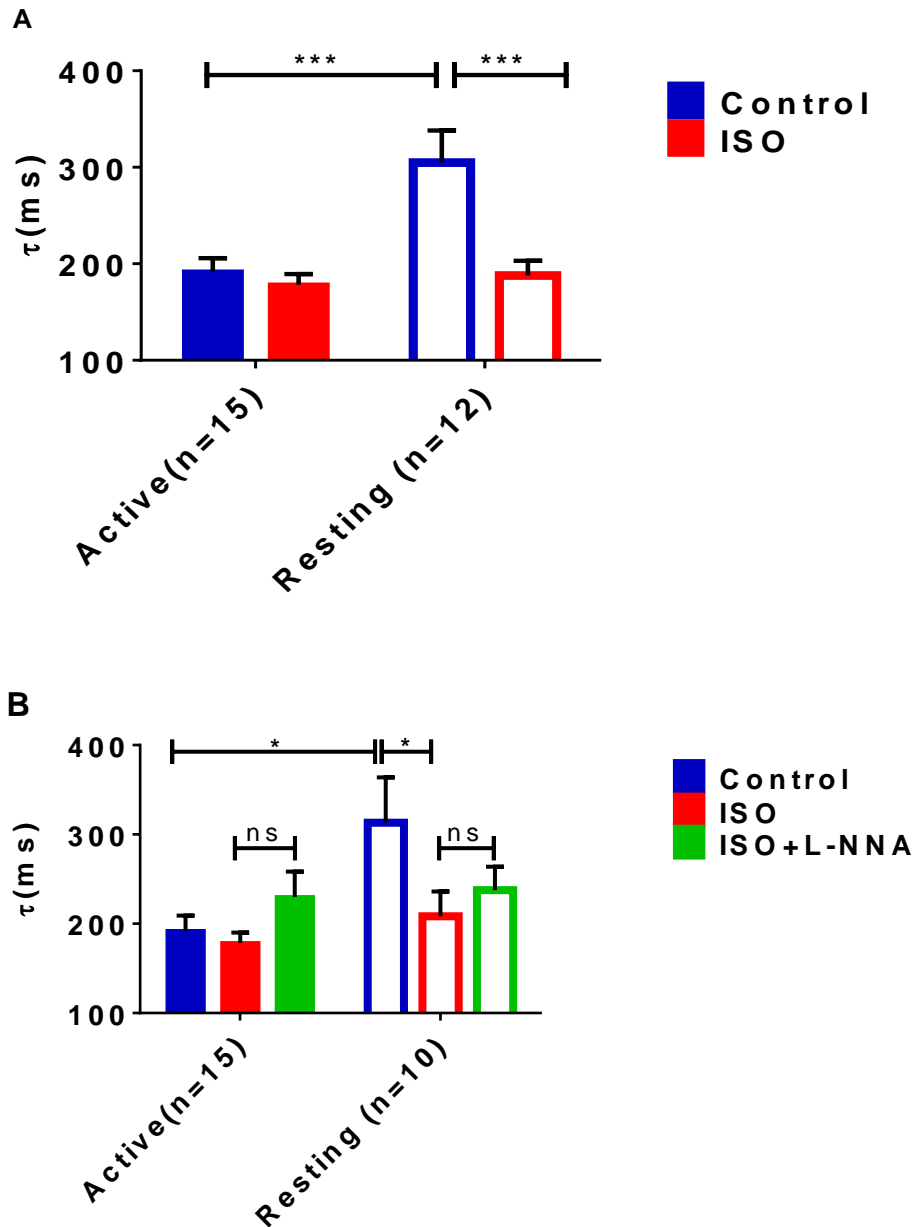


**Figure 3.13: Diurnal variation in time constant values  $\tau$  values.** **A)** Diurnal variation in  $\tau$  under basal conditions and in response to 10 nM ISO. Active myocytes (n=15 cells from 7 guinea pigs), resting myocytes (n=12 cells from 5 guinea pigs). **B)** Diurnal variation in  $\tau$  from the cells which were exposed to 500  $\mu$ M L-NNA in the continued presence of ISO. Active myocytes (n=15 cells from 8 guinea pigs), resting myocytes (n=10 cells from 5 guinea pigs).

The time constant ( $\tau$ ) of the curve is the taken for the change of  $APD_{90}$  to be 63% of the maximum change of  $APD_{90}$ . The  $\tau$  value defines the electrical restitution curve shape. The shorter the time constant; the higher the slope and thus the more instability of the cell.

Figure 3.13A represents cells from the two time periods which have been exposed to control conditions and ISO. The mean  $\tau$  value in the active period myocytes under control conditions was 112.9 ms shorter in comparison to the resting period myocytes under the same conditions ( $p \leq 0.001$ ). However, the resting period myocytes showed a pronounced and significant decrease in the mean value of  $\tau$  in response to ISO ( $p \leq 0.001$ ) while no significant difference has been seen between the two conditions in the active period myocytes ( $p > 0.05$ ). This is consistent with the maximum slope values described earlier. There was a trend for application of L-NNA in the continued presence of ISO to increase  $\tau$  (Figure 3.13B) in both active and resting myocytes, but the effect was not statistically significant. These results suggest that there is diurnal variation in mean  $\tau$  values and the resting period myocytes were more respondent to ISO.

### 3.3.3.4 Maximum stimulation frequency:

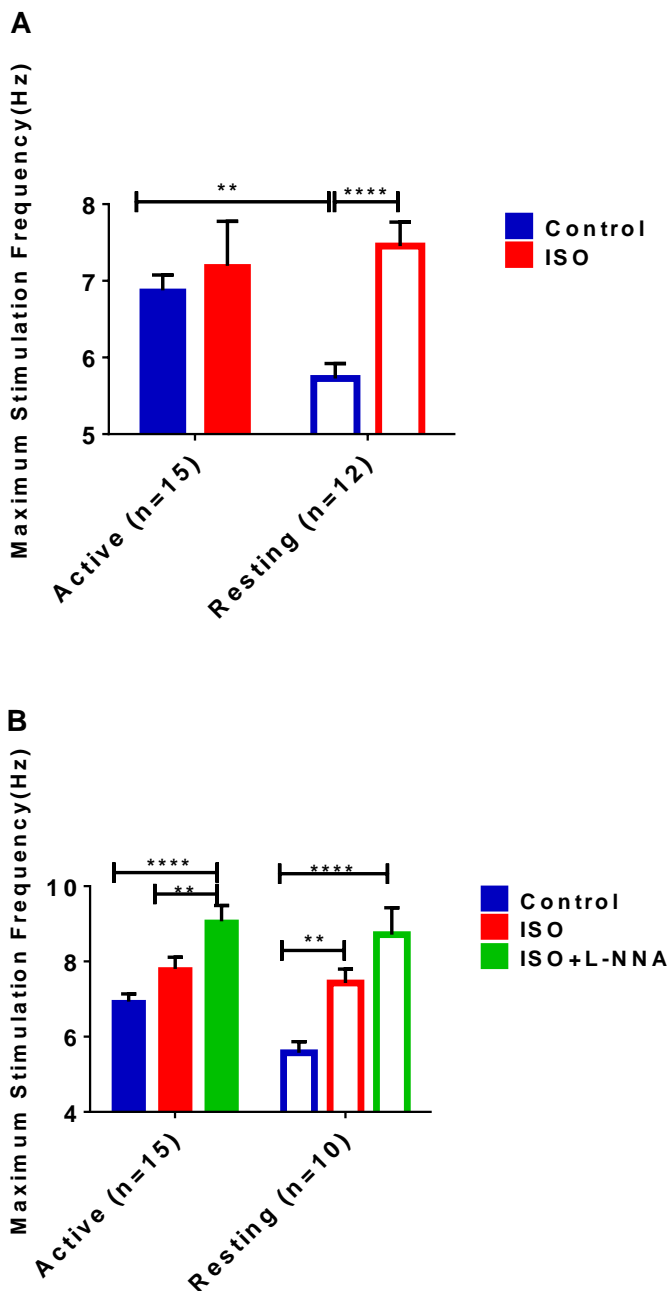


**Figure 3.14: Diurnal variation in maximum stimulation frequency (Hz). A)** Diurnal variation in maximum stimulation frequency under baseline conditions and in response to 10 nM ISO. Active myocytes (n=15 cells from 7 guinea pigs), resting myocytes (n=12 cells from 5 guinea pigs). **B)** Diurnal variation in maximum stimulation frequency from cells which were exposed to 500  $\mu$ M L-NNA in the continued presence of ISO. Active myocytes (n=15 cells from 8 guinea pigs), resting myocytes (n=10 cells from 5 guinea pigs).

In the DYRT protocol, the maximum stimulation frequency is increased until AP capture failure. AP failure is due to stimuli being applied during the ERP and therefore changes to the maximum stimulation frequency reflect potential alteration to ERP. Nevertheless, the DYRT protocol only gives limited insight because stimulation frequency is changed on 1 Hz intervals and a precise quantitative determination of ERP is not made. Despite these limitations, maximum stimulation frequency provides interesting qualitative insights on changes in refractoriness. Figure 3.14A shows maximum stimulation frequency for active and resting period myocytes period which have been exposed to control conditions and ISO. The maximum stimulation frequency was higher under control conditions in active period myocytes, suggesting shorter effective refractory period compared to resting period myocytes ( $p \leq 0.01$ ).  $\beta$ -AR stimulation increased the maximum stimulation frequency of resting period myocytes so it was similar level in both cell populations. However, ISO showed more effect in comparison to control in the resting period myocytes ( $p \leq 0.0001$ ). Figure 3.14B shows that there was a further significant increase of maximum stimulation frequency when L-NNA was applied in the continued presence of ISO, with maximum stimulation frequency being similar in active and resting period myocytes. These results suggest that the maximum frequency at which cells could be stimulated was significantly higher in active than resting cells under control conditions. Applying ISO alone or L-NNA in the continued presence of ISO increased the maximum stimulation frequency in both time period myocytes to a similar level, so no diurnal variation when the drugs have been applied has been noticed.

#### **3.3.4 Is there a diurnal variation between the two time period myocytes in developing arrhythmic activity such as alternans, EADs, or DADs?**

In addition to quantifying change in electrical restitution, we also quantified abnormalities of electrical activity that could indicate an altered substrate or trigger for arrhythmias. APD alternans was quantified as a consistent oscillation between long and short action potentials; with an amplitude  $\geq 5$  ms. EADs are voltage oscillations at the plateau level of membrane potential or later during phase 3 of repolarization. DADs are depolarizations that begin after repolarization is completed but before another action. EADs and DADs have been recognized and diagnosed

according to the definitions provided in many old and recent studies (Rolls *et al.*, 2007; Volders *et al.*, 2000; Yan *et al.*, 2001; Liu *et al.*, 2012). Figure 3.15 shows representative APs illustrating alternans, EADs, or DADs. Potential arrhythmogenic activity measured under each experimental condition is shown in Table 3.1. The incidence of abnormal electrical activity was higher in the active period myocytes than the resting period myocytes. Arrhythmic events (alternans, early after-depolarizations) were detected in 12 active myocytes out of total 30 active myocytes (15 total active guinea pigs) and only 3 resting period myocytes out of 22 total resting myocytes (10 total resting guinea pigs). Almost all episodes were alternans. 5 Hz was the minimum stimulation frequency at which alternans occurred in each condition. While the occurrence of DADs was variable; happened at 2 Hz, 3 Hz, 4 Hz, and 5 Hz. EADs occurred only once at 2 Hz. Cells which showed abnormal electrical activity in response to one experimental condition not necessary show it with other experimental conditions. However, some cells showed alternans at all the experimental conditions. Almost all cells reached maximum stimulation frequency after showing alternans.

	<b><i>Alternans</i></b>	<b><i>DADs</i></b>	<b><i>EADs</i></b>
<b><i>Control</i></b>	<b><i>1 Resting cell</i></b> <b><i>7 Active cells</i></b>		
<b><i>ISO</i></b>	<b><i>1 Resting cell</i></b> <b><i>6 Active cells</i></b>	<b><i>1 Resting cell</i></b> <b><i>2 Active cells</i></b>	
<b><i>ISO plus L-NNA</i></b>	<b><i>3 Resting cells</i></b> <b><i>5 Active cells</i></b>	<b><i>6 Active cells</i></b>	<b><i>1 Resting cell</i></b>

**Table 3.1:** Abnormal electrical activity occurrence; alternans, EADs, and DADs in the two time period myocytes.

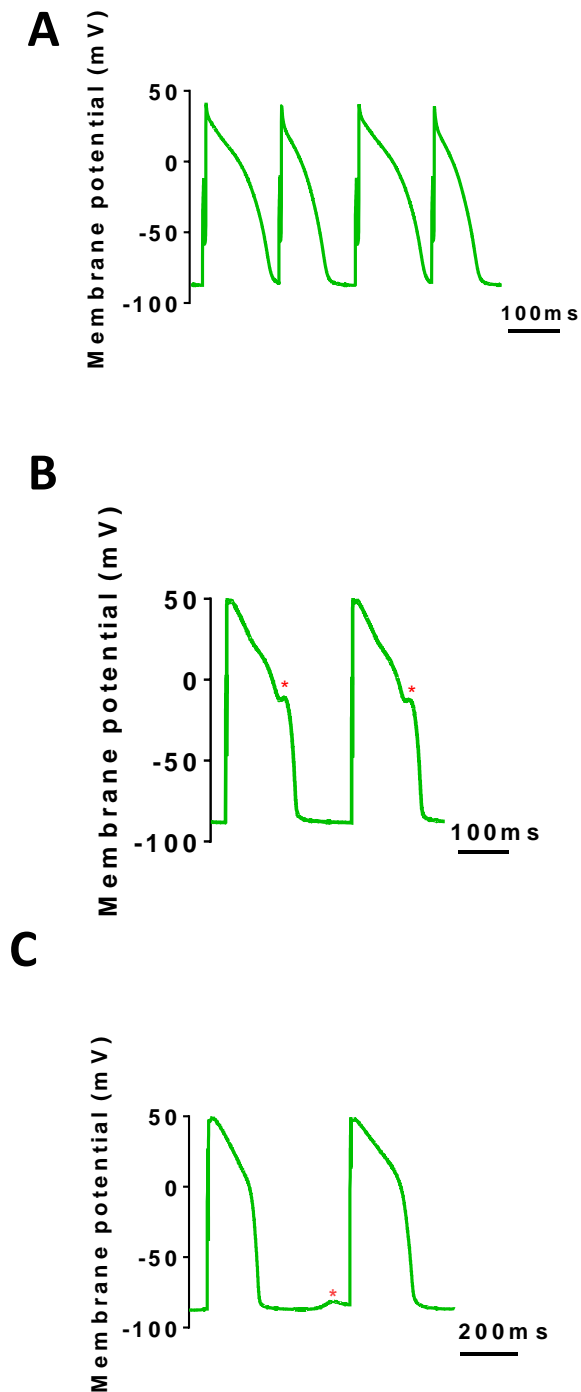


**Figure 3.15: Representative APs illustrating alternans, EADs, or DADs. A)** Representative example of alternans at 10 Hz from active period myocyte in the presence of 10 nM ISO and 500  $\mu$ M L-NNA. **B)** Representative example of EAD recorded at 2 Hz from a resting period myocyte in the presence of ISO and L-NNA. **C)** Representative example of DAD at 2 Hz from an active period myocyte in response to ISO and L-NNA. The red stars indicate the abnormality in the AP.

### **3.4 Discussion**

It was previously thought that diurnal variations in physiological functions were just responses to environmental influences. However, more recent evidence indicates that they result from a complex interplay between extracellular stimuli such as autonomic function and the intrinsic circadian clock (Collins and Rodrigo, 2010). For example Bexton *et al.* (1986) showed that the circadian pattern of QT intervals corrected for heart rate (QTc) differed between innervated and denervated hearts. Pacemaker patients with normally innervated hearts displayed distinct diurnal changes in the QTc interval, with a profound shortening between 6 and 9 AM. Furthermore, Hohnloser *et al.* (1993) found that uncorrected QT intervals peaked a few hours prior to 6 AM, decreased thereafter and started to increase at 6 PM. Hence, QT intervals are longer during sleep.

The current study investigated whether there is diurnal variation of repolarization at different stimulation frequencies and electrical restitution properties of acutely isolated guinea-pig left ventricular cardiac under basal conditions and in response to ISO. Moreover, our study investigated whether NO signalling played a role in the response to ISO by inhibiting NOS activity with L-NNA.

#### **3.4.1 Diurnal variation of APD<sub>90</sub>**

##### **3.4.1.1 APD<sub>90</sub> values are similar in active and resting period myocytes under basal conditions**

Mean APD<sub>90</sub> at each stimulation frequency was similar in active and resting period myocytes under basal conditions when the cells were perfused with normal Tyrode. The overall finding was that under basal conditions, there was no diurnal variation in mean APD<sub>90</sub> at each stimulation frequency or change of AP morphology between active and resting period myocytes.

Many cardiac arrhythmias have their own characteristic circadian variations. One of the proposed underlying mechanisms is an alteration of cardiac electrophysiological properties due to a variation in ion channel gene expression during the day. Yamashita *et al.* (2003) found that K<sub>v</sub>1.5 which mediates I<sub>Kur</sub>, and K<sub>v</sub>4.2 subunits that contribute to I<sub>to, fast</sub> are exceptional in their fluctuating circadian patterns of gene expression in the rat heart, with K<sub>v</sub>1.5 increases during the active period, and K<sub>v</sub>4.2

increases during the resting period. Jeyaraj *et al.* (2003) studied the molecular evidence which links circadian rhythms to susceptibility in ventricular arrhythmias in mice. They showed that cardiac ion channel expression and QT-interval duration exhibit circadian rhythmicity under the control of a clock-dependent oscillator, kruppel-like factor 15 (Klf15). Klf15 transcriptionally controls rhythmic expression of  $K_v$  channel interacting protein 2 (KChIP2), a critical subunit for generating  $I_{to}$ . Modulation of the level of Klf15 caused loss of rhythmic QT variation, abnormal repolarization and enhanced susceptibility to ventricular arrhythmias.

Unlike the above studies on repolarising currents in rat and mice myocytes, in the current study on guinea-pig myocytes there was no diurnal variation in  $APD_{90}$  or AP morphology under control conditions which indicates species differences. This suggests that ion channel expression is unchanged in active and resting period myocytes in guinea-pig ventricular myocytes. The previous diurnal variation studies concentrated on  $I_{to}$  and  $I_{Kur}$ , which are not expressed in guinea pigs ventricular myocytes and, instead, are more reliant of delayed rectifier  $K^+$  currents.

#### **3.4.1.2 $APD_{90}$ responses to ISO are larger in resting than active period myocytes**

The effects of 10 nM ISO on APD or AP shape were very modest despite strong contractions of the cells when ISO was applied. However, resting period myocytes were more responsive to 10 nM ISO than active period myocytes as  $APD_{90}$  was shorter at different stimulation frequency in response to ISO compared to control but this shortening was only significant at 1 Hz and 2 Hz. Previous work by Rachel Caves in our laboratory showed significant shortening of ISO on APD when 30 nM ISO has been used while modest effect with 10 nM ISO and almost nothing with 3 nM concentrations. I did not use higher concentrations of ISO as my study protocol stimulates the cell until it reaches maximum stimulation frequency and applying higher concentration ISO affected the viability and increased arrhythmogenicity of the cells as seen by others when ISO was used at higher concentrations (e.g. Collins and Rodrigo, 2010). In the literature, ISO has differential effects on APD depending on the experimental conditions and the concentration used. In dog cardiomyocytes,

low concentrations of ISO (0.001 and 0.01  $\mu\text{M}$ ), shortened the cardiac action potential, in contrast to a relative prolongation with high (1 and 10  $\mu\text{M}$ ) concentrations of ISO (Charpentier and Rosen, 1994). The length of the cardiac action potential is largely determined by the interplay between the amount of inward  $I_{\text{Ca,L}}$  and outward  $I_{\text{Kr}}$  and  $I_{\text{Ks}}$  (Karle *et al.*, 2002). Enhancement of  $I_{\text{Ks}}$ , due to PKA-dependent phosphorylation of  $\text{K}_{\text{v}}7.1$  subunits, is fundamental in the shortening of APD during  $\beta$ -AR stimulation in guinea pig ventricular myocytes (Silva and Rudy, 2005). ). The reason for the net absence of effect of ISO on  $\text{APD}_{90}$  maybe that, despite an expected increase in both  $I_{\text{Ca,L}}$  and  $I_{\text{Ks}}$  (the main ion currents likely to be affected by 10 nM ISO), the influences on APD of these two ion currents may have cancelled each other out. The effect of L-NNA, in the continued presence of ISO, to shorten APD below the ISO value, suggests that NO may have exerted an anti-adrenergic influence on the ISO-dependent increase in  $I_{\text{Ks}}$  (i.e.  $I_{\text{Ks}}$ -increase wins) that was larger than it's anti-adrenergic influence on the ISO-dependent increase in  $I_{\text{Ca,L}}$ . This complex scenario would be consistent with a net APD-shortening effect on  $\text{APD}_{90}$ .

ISO is generally considered to shorten myocardial repolarisation in canine ventricle, with a reduction in the  $\text{APD}_{95}$  in isolated tissues (Volders *et al.*, 2003) and cells (Stengl *et al.*, 2006). However, in human ventricle ISO lengthened repolarisation in isolated tissues or cells (Eckel *et al.*, 1982; Mitchell *et al.*, 1986; Koumi *et al.*, 1995;). This means that ISO effect is species dependent and this may also depend on isolated cells versus tissues.

Whether there are diurnal variation in how  $I_{\text{Kr}}$  and  $I_{\text{Ks}}$  are regulated by  $\beta$ -AR stimulation has not been determined, but  $I_{\text{Ca,L}}$  responses have been investigated.

Collins and Rodrigo (2010) studied diurnal variation of left ventricular myocytes isolated from rat hearts at two opposing time points, equivalent to the animals resting (Day time) or active (night time). They found that the increase in systolic  $\text{Ca}^{2+}$  transient amplitude, when ISO was applied alone, was significantly greater in resting versus active period myocytes, reflecting a greater SR  $\text{Ca}^{2+}$  load at this time. This is consistent with my finding as resting period myocytes showed more responsiveness to ISO in terms of  $\text{APD}_{90}$  changes although these changes were modest. They did not find any diurnal variation in SERCA-2A, phospholamban, or ryanodine receptor

mRNA levels, suggesting a posttranslational modification of SR activity, possibly involving NO signalling (see next section).

### **3.4.2 Blocking NO production in the continued presence of ISO shortens APD<sub>90</sub> and this effect was more pronounced in the active period myocytes**

The active period myocytes showed more significant shortening in APD<sub>90</sub> than resting period myocytes when L-NNA was applied in the continued presence of ISO. The effect was more pronounced at 4 Hz and 5 Hz. Furthermore, L-NNA made the AP plateau more positive and this effect was more significant in active period myocytes. This suggests that the APs of active period myocytes were more affected by inhibiting NO production in the continued presence of ISO. In other words, active period myocytes were more responsive to the presence of ISO, in terms of APD and AP morphology, when NO production was inhibited.

In rat myocyte studies, it has been found that inhibiting nNOS during  $\beta$ -AR stimulation with ISO, further increased  $I_{Ca,L}$  in comparison to ISO alone, and the effect was significantly greater in active than resting period myocytes (Collins and Rodrigo, 2010). This was due to a diurnal variation in nNOS signalling. Quantitative PCR analysis revealed a 2.65-fold increase in nNOS mRNA levels in active over resting period myocytes. This increase in nNOS activity in the active time period might be the reason why active period myocytes showed less SR  $Ca^{2+}$ -loading and decreased L-type  $Ca^{2+}$  current density when ISO was applied, compared to the resting period (Collins and Rodrigo, 2010). My findings are consistent with the previously mentioned studies as the active period myocytes showed more shortening in APD<sub>90</sub> and a significantly more depolarized AP plateau when NOS was inhibited. While the molecular basis has not been studied, my results are consistent with higher  $I_{Ca,L}$  and more responsiveness to ISO when NOS was inhibited with L-NNA. The shortening of the AP is also likely to be due to an increased response of  $I_{Ks}$  to ISO, although this needs further investigation.

A study conducted on left ventricular rat tissue by Zhou *et al.*, (2011) found that mRNA and protein levels of  $\beta$ 3-AR exhibited a distinctive circadian rhythm. Expression was highest in the resting period and lowest during the active period. Likewise, the  $\beta$ 3-AR specific agonist BRL37344 decreased contractile force

substantially during the resting period with minimal effects in the active period, providing evidence that  $\beta$ 3-AR signalling is higher during resting periods and lower during active periods. Whether there is a similar diurnal variation of expression of  $\beta$ 3-AR in guinea pig myocytes is unknown, but our results are consistent with this since we observed active period myocytes to be more responsive to ISO in the presence of L-NNA than resting period cells and to be more arrhythmogenic.

### **3.4.3 The molecular basis for NO regulation of cardiac APD**

#### **3.4.3.1 NO signalling is known to be linked to $\beta$ -AR pathway**

NO signalling is known to be linked to the  $\beta$ -adrenergic signalling pathway. ISO stimulates  $\beta$ 1,  $\beta$ 2, and  $\beta$ 3-AR (Imanishi *et al.*, 2006). eNOS is coupled to  $\beta$ 3-AR and activation of  $\beta$ 3-AR by ISO is reported to increase NO production from eNOS (Wang *et al.*, 2008). The  $\beta$ 3-AR stimulation is negatively inotropic, involving a complex interaction with the NO/cGMP dependent pathway. Although the exact mechanism is not clear yet,  $\beta$ 3-AR stimulation stimulates NO generation from eNOS, leading to sGC activation, synthesis of cGMP, and activation of PDE2 by cGMP which then reduces cAMP levels and decreases  $I_{Ca,L}$  amplitude in rat left ventricular myocytes (Mongillo *et al.*, 2006). The effect of PDE2 inhibition of contractility was dramatically reduced in myocytes obtained from mice in which the expression of eNOS had been knocked out (Shesely *et al.*, 1996). Therefore, eNOS plays a role in the negative inotropic and protective effect of ISO mediated by the  $\beta$ 3-AR stimulation. However, it remains to be determined whether nNOS is also involved in the negative inotropism of  $\beta$ 3-AR signaling in the heart (Sterin-Borda *et al.*, 2006).

In the literature a lot of studies have concentrated on the link between NO and  $\beta$ -AR. Abi-Gerges *et al.* (2001) found that NO inhibits ISO enhanced  $I_{Ca,L}$  in rat ventricular myocytes. Matsumoto *et al.* (2000) have shown that inhibition of NOS non-specifically by L-NMMA can increase the effect of adenylyl cyclase activation by forskolin on L-type  $Ca^{2+}$  current in rat ventricular myocytes. These enhancements of  $I_{Ca,L}$  are consistent with the more depolarised AP plateau observed in guinea-pig left ventricular myocytes in the current study. Despite many studies on the effect of NO

signalling on  $\text{Ca}^{2+}$  current, very little has been made on the effect on APD and AP shape in acutely isolated myocytes. Applying L-NNA in the continued presence of ISO would be predicted to block NO synthesis from nNOS and eNOS and abolishes the protective effect of eNOS when stimulated by  $\beta_3$ -AR. At the same time, ISO would still activate  $\beta_1$  and  $\beta_2$ -ARs and stimulate cAMP synthesis, and PKA activation, which would increase  $I_{\text{Ca,L}}$ . This effect was more significant in active period myocytes, and thus associated with more cellular arrhythmic events, including DADs, EADs, and alternans.

NO signalling and the QT interval have recently been linked through genetic variants in CAPON. Recent genome-wide association studies have identified CAPON (also known as the nNOS adapter protein NOS1AP) as a regulator of cardiac repolarization and sequence variations in CAPON are associated with baseline QT interval and subsequent risk for sudden cardiac death (Arking *et al.*, 2006; Post *et al.*, 2007). Chang *et al.* (2008) found that adenoviral-mediated overexpression of CAPON in guinea-pig ventricular myocytes resulted in a shortening of APD through a mechanism involving inhibition of  $I_{\text{Ca,L}}$  and enhancement of  $I_{\text{Kr}}$ . Pre-treatment with the NOS inhibitor (L-NAME) reversed these effects. Furthermore, CAPON overexpression was also associated with an up-regulation of nNOS protein levels, an enhancement of nNOS activity and increase in NO generation (Chang *et al.*, 2008).

#### **3.4.3.2 Ionic currents other than $I_{\text{Ca,L}}$ that regulate APD**

In guinea-pig ventricular myocytes, the  $\text{Ca}^{2+}$  ionophore, A23187, induced suppression of  $I_{\text{Ca,L}}$  and enhancement of  $I_{\text{Ks}}$ . At a low stimulation rate,  $I_{\text{Ca,L}}$  suppression and  $I_{\text{Ks}}$  enhancement contributed to the A23187-induced APD shortening with a similar magnitude, whereas at a high stimulation rate,  $I_{\text{Ks}}$  enhancement made the dominant contribution to APD shortening (Bai *et al.*, 2005). Viswanathan *et al.* (1999) studied the different currents contributing to the APD adaptation during computer simulations of dynamic restitution in guinea pig cells at 37°C in computer stimulation cell model study.  $I_{\text{Ca,L}}$  is an inward current, which would prolong APD if it was potentiated, rather than shorten it. However, at short cycle lengths,  $I_{\text{Na/Ca}}$  is predominantly outward during the plateau phase.  $I_{\text{Na/Ca}}$  is regulated

by transmembrane concentrations of  $\text{Ca}^{2+}$  and  $\text{Na}^+$  and by membrane potential. Elevation of intracellular  $\text{Ca}^{2+}$  increases inward  $I_{\text{Na/Ca}}$ , whereas elevation of intracellular  $\text{Na}^+$  increases outward  $I_{\text{Na/Ca}}$ . Stimulating the cell at high frequencies results in accumulation of  $\text{Ca}^{2+}$  and  $\text{Na}^+$  in the cell. However, the net effect of ion accumulation, according to the model, was a larger outward  $I_{\text{Na/Ca}}$  which will shorten the APD at high stimulation frequencies. Therefore, outward  $I_{\text{Na/Ca}}$  contributes to the observed rate-dependent shortening of the APD not  $I_{\text{Ca,L}}$  which plays a more important role in the plateau. The effect of NO on  $I_{\text{Na/Ca}}$  needs further investigation.

Repolarizing  $\text{K}^+$  currents play a crucial role in determining APD. It is well known that blocking  $I_{\text{Ks}}$  or  $I_{\text{Kr}}$  would prolong APD (Viswanathan *et al.*, 1999; Sanguinetti *et al.*, 1996). Very little is known about the effect of NO on  $I_{\text{Ks}}$  and  $I_{\text{Kr}}$ . However, in one study NO donors inhibited  $I_{\text{Kr}}$  in hamster ovarian cells irrespective of sGC activation (Gomez *et al.*, 2008), while enhancing  $I_{\text{Ks}}$  in a cGMP-independent manner (Asada *et al.*, 2009). However, the effect of NO signalling pathway on  $I_{\text{Kr}}$  and  $I_{\text{Ks}}$  ionic currents in the presence of  $\beta$ -AR needs further research.

### **3.4.4 Diurnal variation of electrical restitution parameters**

#### **3.4.4.1 Active period myocytes are more arrhythmogenic under basal conditions**

Electrical restitution parameters showed evidence of diurnal variation and the active period myocytes were more susceptible to arrhythmic episodes. The electrical restitution hypothesis predicts that a steep maximum slope of the restitution curve can produce large fluctuations of APD, refractoriness and alternans. In this study,  $\tau$  values were significantly shorter and maximum slopes steeper for active versus resting period myocytes under basal conditions. Maximum stimulation frequency values were significantly higher, thus ERP was also shorter, in active than resting period myocytes. These results suggest that active period myocytes electrical restitution curves are indicative of a more unstable phenotype than resting period myocytes. Arrhythmic events (alternans, DADs, and EADs) were detected more in the active period myocytes. These events were observed under basal conditions, in response to ISO, and when L-NNA was applied in the continued presence of ISO.

DADs and EADs were more frequently encountered in response to ISO alone or ISO and L-NNA.

Interestingly, there was more responsiveness to  $\beta$ -AR stimulation in the resting period myocytes.  $APD_{90Max}$  was shortened more, slope values were increased more,  $\tau$  values were shortened more and there were higher maximum stimulation frequencies in response to ISO in resting compared to active period myocytes. L-NNA increased the maximum stimulation frequency of both active and resting period myocytes, suggesting a further shortening of ERP.

In the literature single cell electrical restitution was studied by some research groups (Goldhaber et al., 2005; Qu et al., 1999; Tolkacheva et al., 2006). Almost all of the previous single cell studies investigated the role of  $I_{Ca,L}$  in APD restitution which was discussed in chapter 1. Clearly diurnal variation of restitution has not been investigated in whole heart or single cells before. This study is the first to investigate diurnal variation in restitution parameters in single cells. The percentage of arrhythmic myocytes was higher in active than resting period myocytes.

Higher sympathetic nervous system activity occurs during active periods and higher parasympathetic nervous system activity occurs during resting periods (Honda *et al.*, 2013). NO signalling has been reported to play an important role in the parasympathetic nervous system, in terms of mediating the protective effects of vagus nerve stimulation against the induction of VF in whole heart studies (Brack *et al.*, 2007). Thus, it is possible that NO may be a fundamental signalling molecule in the parasympathetic control of the heart. The precise cellular mechanisms have not yet been determined. Nevertheless, there is now a lot of evidence that an imbalance in the autonomic regulation of the heart and, in particular, the loss of vagal tone, is associated with an increased risk of arrhythmias (Brack *et al.*, 2013; Zhao *et al.*, 2012).

## **Chapter 4. How is action potential repolarization regulated by Nitric oxide signalling pathways in acutely isolated guinea-pig active ventricular myocytes:**

### **4.1 Introduction:**

NO signalling has two distinctive signalling pathways; a cGMP-dependent pathway and a cGMP-independent pathway. In cGMP-dependent signalling, NO binds to the haem group of sGC activating guanylyl cyclase activity, which causes an increase in cGMP levels (Ziolo *et al.*, 2008). The NO dependent activation of sGC and the synthesis of cGMP is a key step in the NO/cGMP pathway. The main cGMP-independent mechanism through which NO can regulate physiological functions is S-nitrosylation. S-nitrosylation is a reversible protein modification in which the thiol group (RSH) in the amino acid cysteine/ or tyrosine is converted into S-nitrosothiol (SNO). The RSH group has a sulphur-hydrogen bond. During S-nitrosylation; NO replaces the hydrogen atom (Sun and Murphy, 2010).

L-NNA is a widely used non-specific inhibitor of NOS. As shown in chapter 3, L-NNA shortened APD<sub>90</sub> significantly in the presence of  $\beta$ -AR stimulation by 10 nM ISO. The effects of L-NNA were more pronounced in active than resting period myocytes. The main aim of the work in this chapter was to investigate the underlying physiological mechanisms.

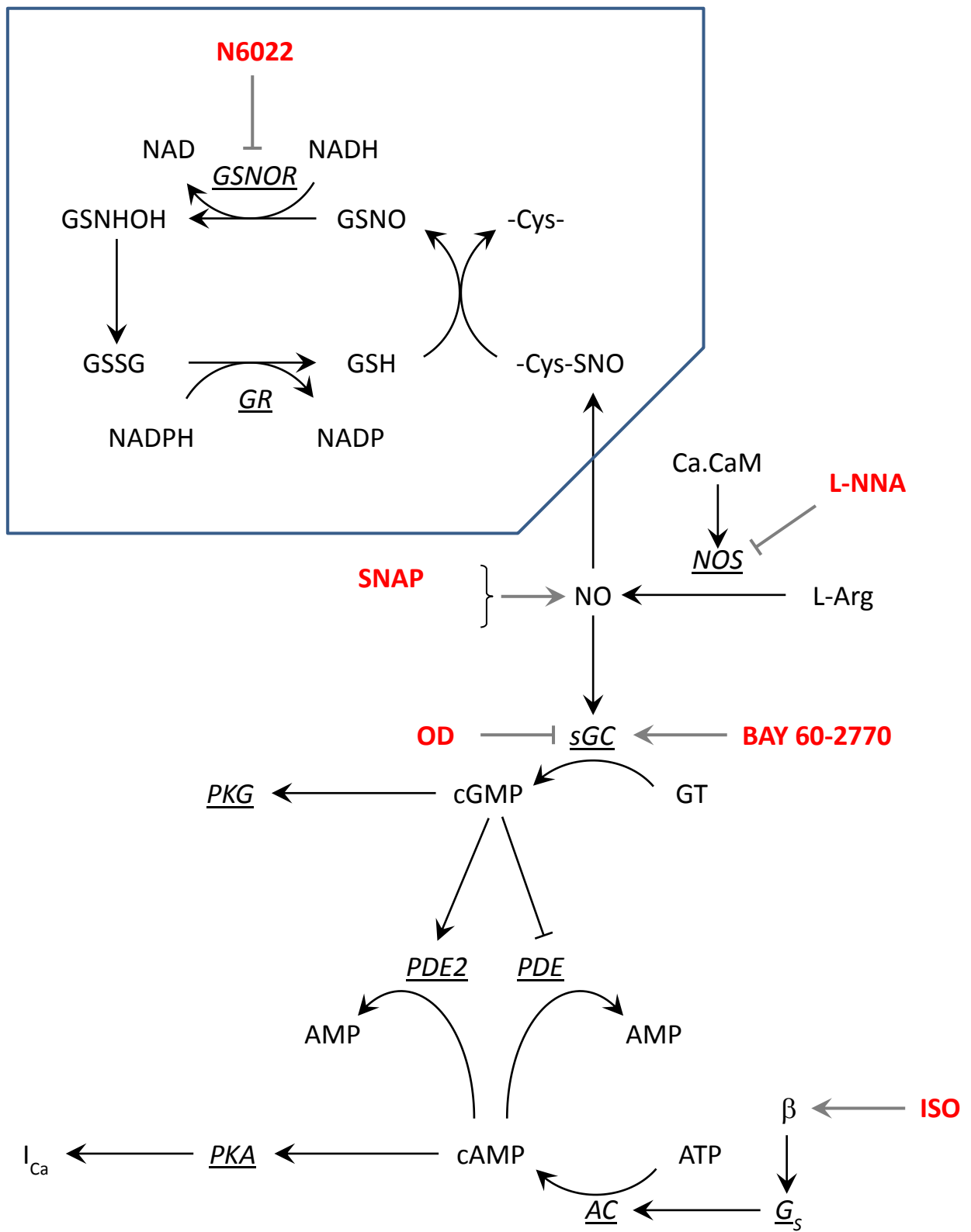
The NO donor SNAP has been commonly used to release NO, consequently stimulating the NO-signalling pathways. However, the use of NO donors will stimulate both the cGMP-dependent and cGMP-independent pathways which will make it hard to discriminate through which pathway the effect of NO has occurred. The concentrations of NO released by NO donors can also be difficult to determine and may not be physiological relevant concentrations. Moreover, the NO donors depend on the presence of reduced haem to activate sGC (Hammond and Balligand, 2012). It has been suggested that under certain conditions sGC haem can become oxidised especially under pathophysiological conditions, preventing the activation of the cGMP-dependent pathway (Schmidt *et al.*, 2009). To circumvent this problem, haem- independent sGC activators have been developed recently. An example is BAY 60-2770 which activates oxidised/haem-free NO-insensitive sGC (Knorr *et al.*, 2008).

Selective inhibitors of sGC enable discrimination of sGC-mediated signalling from other signalling pathways. One of these selective inhibitors is 1H-[1, 2, 4] oxadiazolo-[4, 3-a] quinoxalin-1-one (ODQ), which binds to the haem group of sGC in competition with NO and inhibits sGC by oxidising the haem group (Lies *et al.*, 2013). Interestingly, and paradoxically, ODQ has a synergistic effect on sGC potentiated by BAY 60-2770 (Krieg *et al.*, 2009). ODQ and BAY 60-2770 substantially increase the activation of sGC by more than BAY 60-2770 applied on its own.

The main cGMP-independent pathway is the S-nitrosylation pathway. It has recently become clear that S-nitrosylation is a dynamic and reversible process. S-nitrosylation can be reversed by a number of denitrosylase enzymes; s-nitrosoglutathione reductase (GSNOR) and thioredoxin reductase (Trx) (Gonzalez *et al.*, 2009). The primarily denitrosylation enzyme in the cardiac myocytes is GSNOR although recently a role of Trx has been implicated (Lima *et al.*, 2010). Denitrosylation has been shown to play a major role in controlling cellular S-nitrosylation of many target proteins (Benhar *et al.*, 2009). In this study denitrosylation was inhibited using N6022, a blocker of GSNOR (S-Nitrosoglutathion reductase) (Green *et al.*, 2012).

In this chapter we investigated the role of NO signalling pathways on the AP repolarization of active period guinea pig cardiac myocytes. sGC/cGMP dependent signalling pathways were activated by BAY 60-2770 on its own or in combination with ODQ. sGC was inhibited by ODQ. S-nitrosylation was enhanced by using N6022 to inhibit denitrosylation. A schematic of the NO signalling pathways to include the inhibitors and activators of the NO signalling pathways used is illustrated in Figure 4.1.

Figure 4.1: Schematic of the NO signalling pathways to include the inhibitors and activators of the NO signalling pathways used.



## **4.2 Results**

### **4.2.1 Does the shortening effect of L-NNA depend on the presence of $\beta$ -AR stimulation?**

The first experiments performed investigated if L-NNA applied without  $\beta$ -AR stimulation had any effects on its own. This tested if L-NNA had nonspecific effects on cardiac APs or effects due to inhibiting NOS under basal conditions. The experimental cells were stimulated starting from 1 Hz and up to the maximum stimulation frequency using the dynamic restitution protocol explained earlier. The results are shown in Figure 4.2. No significant change was observed in the electrical restitution curve when 500  $\mu$ M L-NNA was applied on its own (Figure 4.2A). Moreover, no significant change ( $p > 0.05$ ) on mean  $APD_{90}$  at different stimulation frequencies (Figure 4.2B). Maximum stimulation frequency and the shape of AP was in different with L-NNA compared to control. Therefore, the significant shortening effect of L-NNA which was explained in chapter 3 requires  $\beta$ -AR stimulation and does not occur in naive (untreated) cells.

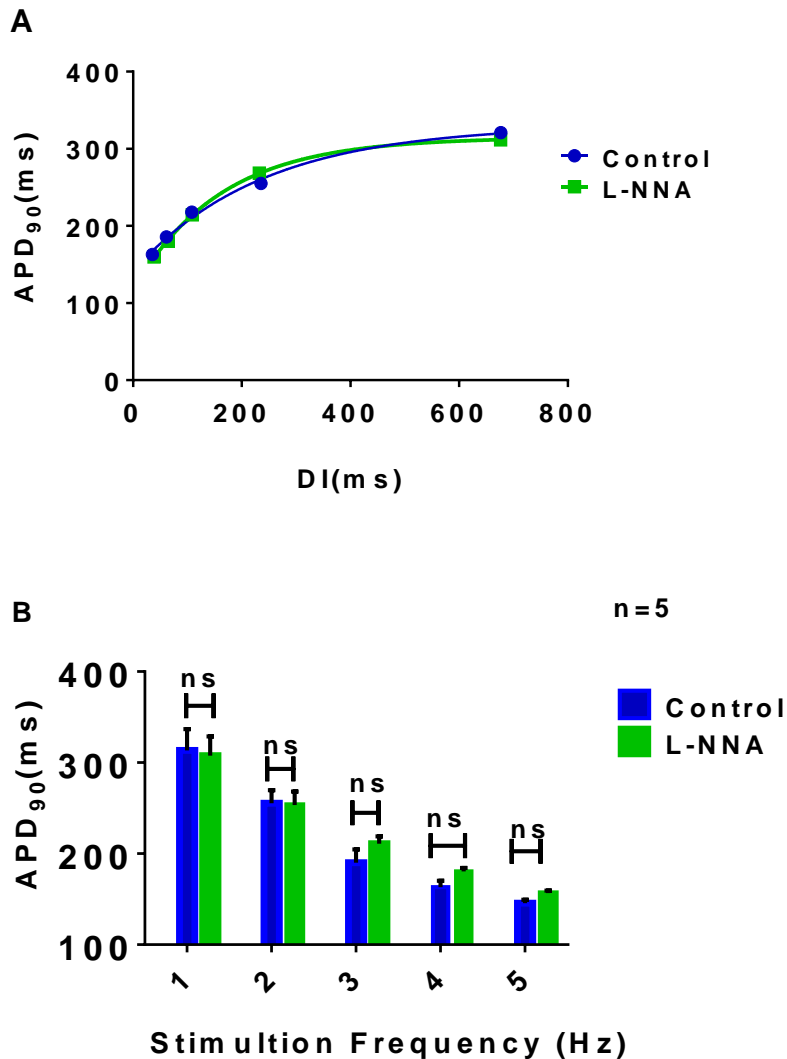


**Figure 4.2: The effect of NOS inhibition by 500  $\mu$ M L-NNA on electrical restitution curve and APD in the absence of  $\beta$ -AR stimulation.** Ventricular myocytes were stimulated at different frequencies using DYRT. **A)** Representative electrical restitution curve in response to control conditions and during application of 500  $\mu$ M L-NNA. **B)** Mean APD<sub>90</sub> at different stimulation frequencies before and during L-NNA application. Data are presented as mean  $\pm$  SEM. Paired t-test as used to obtain this data (n=5).

#### **4.2.2 Is there any effect of the NO donor SNAP on the APD or the electrical restitution parameters?**

The S-Nitroso-N-acetyl-DL-penicillamine (SNAP) is a widely used NO donor. Rachel Caves, a previous PhD student in the Mitcheson laboratory, has shown that 100  $\mu$ M SNAP results in a 20-40 fold increase of cGMP levels in cardiac myocytes (Caves *et*

*al.*, 2015). To test whether NO, released by SNAP, has effects on AP and electrical restitution parameters, cells were electrically stimulated using DYRT and initially exposed to Tyrode solution and then 100 $\mu$ M SNAP. SNAP was prepared in normal Tyrode freshly for each cell; it takes  $\sim$  1 minute for the agents to reach the recording chamber. Figure 4.3A shows representative electrical restitution curves under basal conditions and when 100  $\mu$ M SNAP was applied. No difference was noticed in the curves. Figure 4.3B shows mean data of the electrical restitution parameters. Mean APD<sub>90Max</sub> was decreased from  $318.4 \pm 17.1$  ms in control to  $292.1 \pm 12.1$  ms with SNAP but this change was not significant ( $p > 0.05$ ). Furthermore, SNAP decreased the mean  $\tau$  value from  $239.6 \pm 17.3$  ms in control to  $206.3 \pm 17.8$  ms in SNAP but this was not significant difference ( $p > 0.05$ ,  $n=6$ ). Slope at maximum stimulation frequency was also unchanged in both conditions (Control:  $0.75 \pm 0.07$ ; SNAP:  $0.79 \pm 0.09$ ,  $n=6$ ). Moreover, no significant difference was measured in the maximum stimulation frequency (Control:  $6.5 \pm 0.21$ ; SNAP  $6.3 \pm 0.22$ ,  $n=6$ ). SNAP also failed to modulate APD<sub>90</sub> at different stimulation frequencies (1 Hz – 5 Hz) (Figure 4.4). Wash off SNAP with normal Tyrode data is not plotted in the Figures as no any effect of SNAP, neither wash off, was seen.

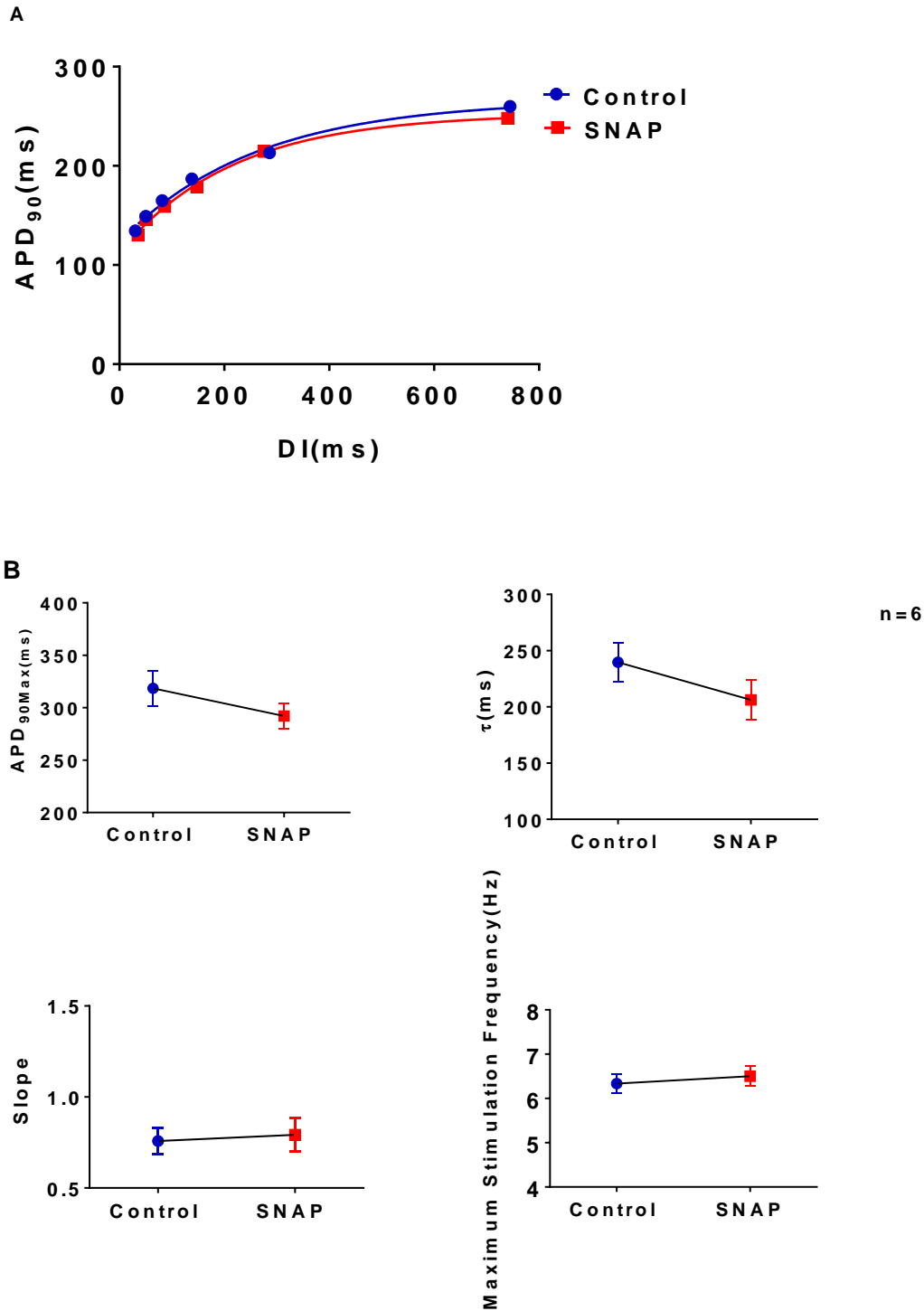


**Figure 4.3: The Effect of the NO donor 100  $\mu$ M SNAP on the Electrical restitution curve.** **A)** Representative electrical restitution curve under basal conditions, and in response to 100  $\mu$ M SNAP. **B)** The Effect of SNAP on  $APD_{90Max}$ ,  $\tau$ , maximum slope, and maximum stimulation frequency. The scale of the Y axis of some parameters is different to have a closer view on the changes of the parameters. Data are presented as mean  $\pm$  SEM (n=6).

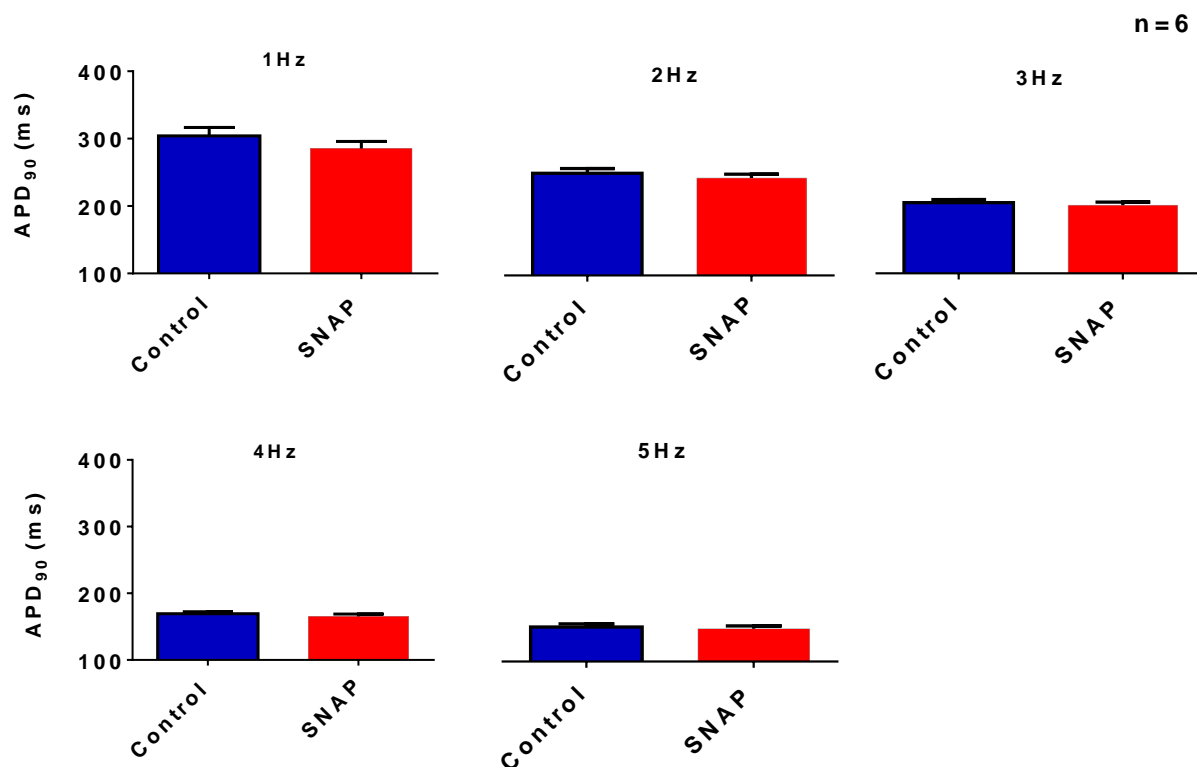


**Figure 4.4: Mean APD<sub>90</sub> at different stimulation frequencies (1 Hz – 5 Hz) under basal conditions, and in response to 100  $\mu$ M SNAP. Data are presented as mean  $\pm$  SEM (n=6).**

To confirm that NO was being released by SNAP under our recording conditions we measured NO production from SNAP, with a NO-sensitive probe. The NO metre was used to measure the NO released from 100  $\mu$ M SNAP at 35-37°C in the perfusion lines. SNAP breaks down to NO and a disulphide by-product. The rate of NO released is condition dependent. In particular it depends on pH and temperature. NO release is catalysed by copper sulphate so that theoretically the concentration of NO generated in the presence of copper sulphate is equal to the concentration of SNAP added. To calibrate the probe, two solutions were prepared. In solution 1, 5 mg EDTA was added to 250ml of distilled water followed by 5 mg SNAP to generate a standard SNAP solution that degrades slowly. In solution 2, 0.1 M copper sulphate was added to 250 ml of distilled water. The NO probe was immersed into 10 ml of solution 2. As soon as the background current became stable three aliquots of SNAP stock solution (5  $\mu$ l, 10  $\mu$ l and 20  $\mu$ l) were injected into the solution containing copper sulphate. Figure 4.5A shows the NO probe current generated. The currents increased rapidly upon addition of the first aliquot and reached a plateau within a few

seconds. The second aliquot was then added increasing the peak currents further. Finally a third aliquot was added. The currents increased each time, reached a peak in < 1 minute and then slowly declined as the NO was oxidised to nitrite and nitrate, which are not detected by the probe. The concentration of NO released from these three aliquots of SNAP was calculated as 45.3, 79.5 and 181.19 nM for application of the three aliquotes respectively. From this output a linear calibration curve can then be created by plotting the changes in current (pA) against the concentration of NO produced from each aliquot (Figure 4.5B). After calibration, NO release with 100  $\mu$ M solutions of SNAP added to physiological Tyrode solution at 35-37  $^{\circ}$ C was measured. The NO probe current peaked at around 1250 pA, which corresponds to  $\sim$  2  $\mu$ M NO (Figure 4.5C). Therefore SNAP was giving off NO but it did not modulate AP properties when used in my experiments. The actual amounts of NO are likely to be less than 2  $\mu$ M, because even with copper sulphate; not all the SNAP decomposes and some NO is likely to be oxidised rapidly. We also calculated the half-life for NO release from SNAP ( $t_{1/2}$ ), which is the time needed until the NO level decreased to 50% after SNAP application, to be  $\sim$ 2 minutes.

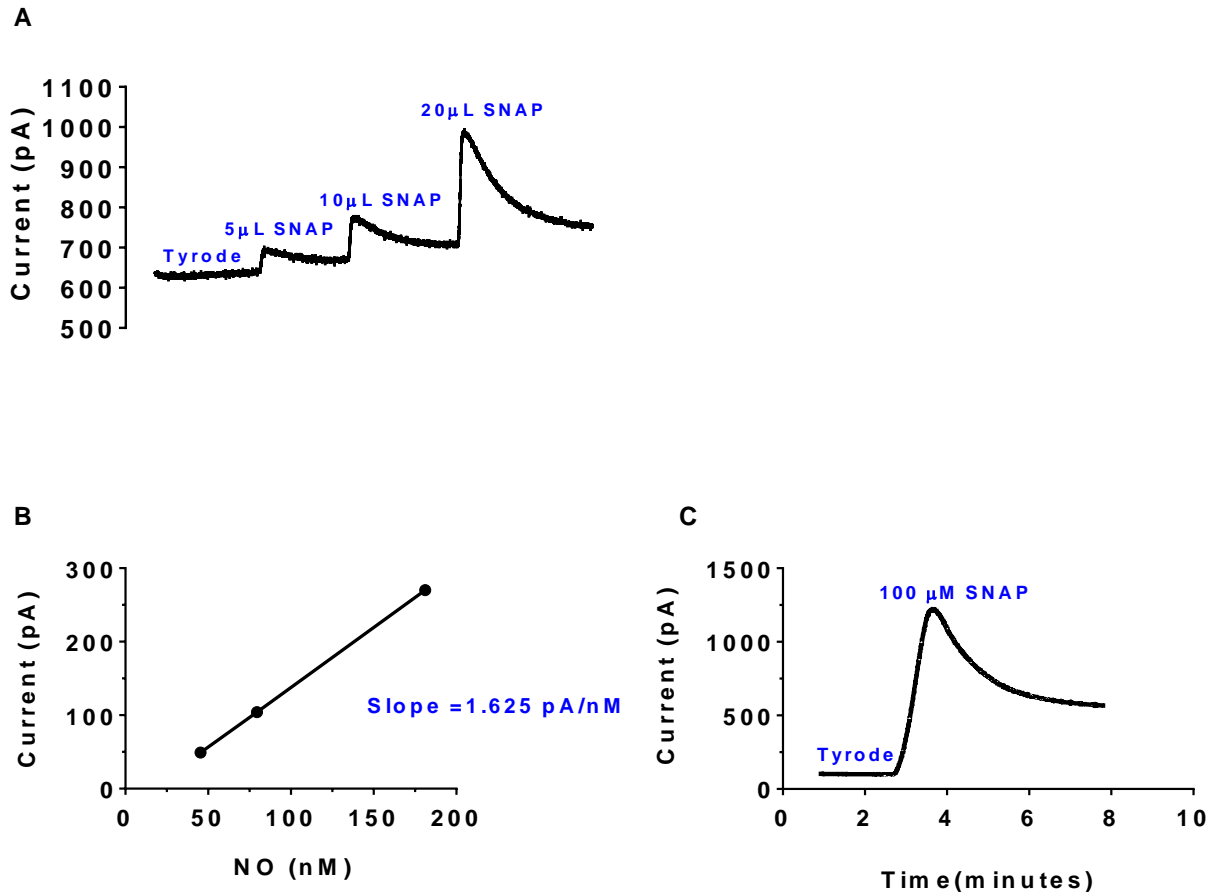


**Figure 4.5: NO meter readings.** **A)** NO meter current traces in response to applications of 5  $\mu$ l, 10  $\mu$ l, and 20  $\mu$ l SNAP in a copper sulphate containing solution that catalyses NO release. **B)** Plot of the calibration curve of NO meter by plotting the changes in current (pA) against the changes in NO concentration (nM). **C)** NO release curves from 100  $\mu$ M SNAP applied to physiological Tyrode solution at 35-37°C. The measurement was made in the input perfusion line, close to the recording chamber.

#### **4.2.3 The effect of soluble guanylyl cyclase activators on electrical restitution:**

BAY 60-2770 (BAY) is a haem-independent sGC activator. Therefore, BAY selectively activates sGC in the cGMP-dependent pathway. The aim of this experiment was to investigate the effect of increasing the activity of sGC on electrical restitution using BAY and ODQ. ODQ has been widely used as a selective inhibitor of sGC. Yet, previous studies have demonstrated that ODQ acts synergistically with BAY to potentiate the activation of sGC (Knorr *et al.*, 2008). Therefore, the effect of

BAY on its own and when added with ODQ on the electrical restitution curve was studied.

Representative AP traces and electrical restitution curves are shown in Figures 4.6A and B respectively. No change in the AP trace morphology or electrical restitution curves was noticed when 1  $\mu\text{M}$  BAY on its own was applied or when 10  $\mu\text{M}$  ODQ in the continued presence of BAY. Looking at the mean data of the electrical restitution parameters (Figure 4.7);  $\tau$  values were statistically not significantly different ( $p>0.05$ ,  $n=6$ ) between control ( $184.3 \pm 14.5$  ms) and when 1  $\mu\text{M}$  BAY was applied ( $192 \pm 8.9$  ms). Adding 10  $\mu\text{M}$  ODQ to BAY showed a significant decrease ( $166 \pm 11.2$  ms,  $p\leq 0.05$ ,  $n=6$ ) in mean  $\tau$  value in comparison to BAY alone ( $192.2 \pm 8.9$  ms) consistent with a small but not statistically significant increase of slope. There was no significant effect on the  $\text{APD}_{90\text{Max}}$  or maximum stimulation frequency between the three different experimental conditions. Previous experiments in the Mitcheson laboratory, using a competitive cGMP radioimmunoassay on isolated guinea-pig ventricular myocytes had measured the effect of BAY and ODQ on cGMP levels. 1  $\mu\text{M}$  and 10  $\mu\text{M}$  BAY increased cGMP by  $2.2 \pm 0.29$  ( $n=8$ ) and  $2.7 \pm 0.22$  ( $n=4$ ) folds respectively. This compares with  $19 \pm 3.7$  fold increases ( $n=8$ ) with 100  $\mu\text{M}$  SNAP. All responses were profoundly potentiated by inhibiting phosphodiesterases with IBMX. 10  $\mu\text{M}$  ODQ potentiated the response of 1  $\mu\text{M}$  BAY, resulting in a  $28 \pm 9.6$  fold increase of cGMP ( $n=8$ ). Overall, these results suggest that a combination of BAY and ODQ failed to modulate electrical restitution parameters, despite known effects on cellular cGMP levels.

The effect of BAY and ODQ on  $\text{APD}_{90}$  while stimulating the experimental cells at different frequencies has also been studied (Figure 4.8). Neither BAY, nor BAY and ODQ showed any significant change on  $\text{APD}_{90}$  at 1 Hz – 5 Hz stimulation frequencies ( $p>0.05$ ).

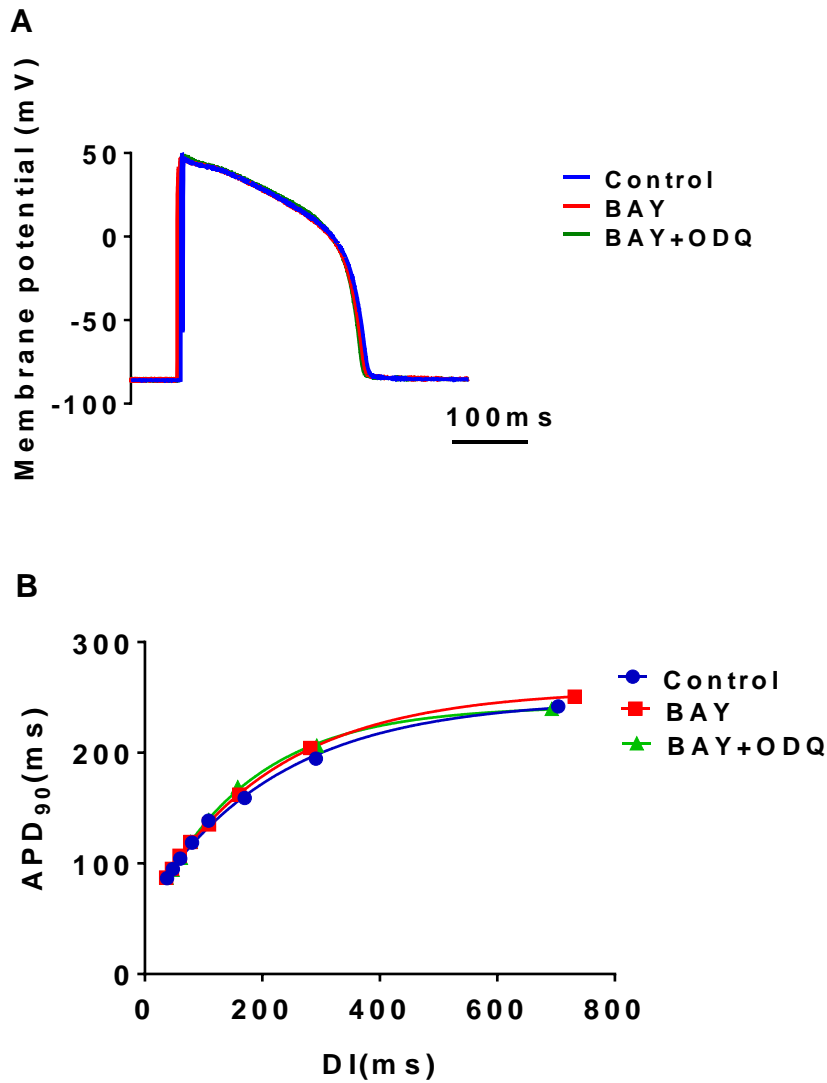


**Figure 4.6: The effect of the sGC activation by 1  $\mu$ M BAY on its own and 10  $\mu$ M ODQ in the continued presence of BAY on AP and electrical restitution curve. **A)** Representative AP traces in control conditions, in response to BAY, and in response to ODQ in the continued presence of BAY at 1 Hz. **B)** Representative electrical restitution curves of the three experimental conditions.**

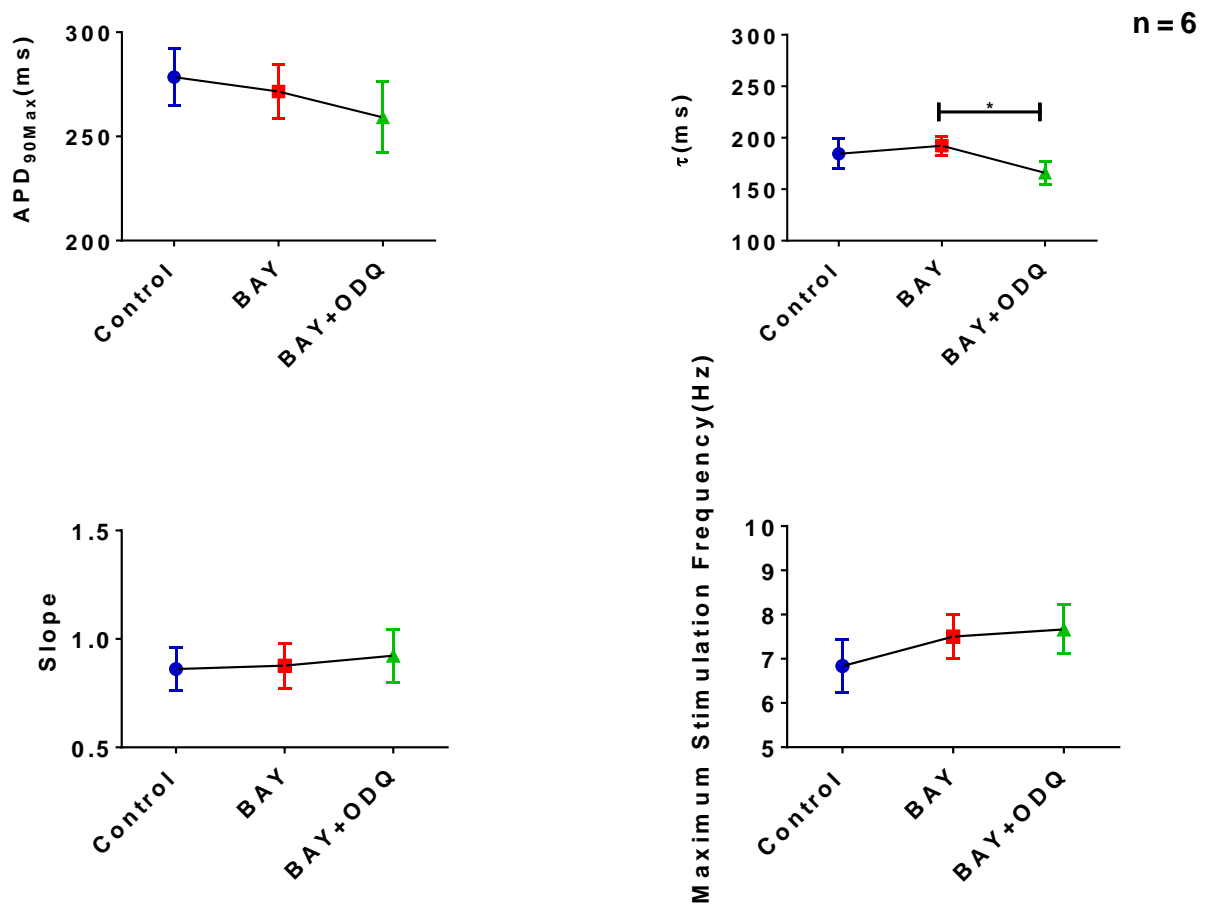


**Figure 4.7:** The effect of 1  $\mu\text{M}$  BAY on its own and 10  $\mu\text{M}$  ODQ in the continued presence of 1  $\mu\text{M}$  BAY on APD<sub>90Max</sub>,  $\tau$ , maximum slope, and maximum frequency of the cells. Data are presented as mean  $\pm$  SEM (n=6).

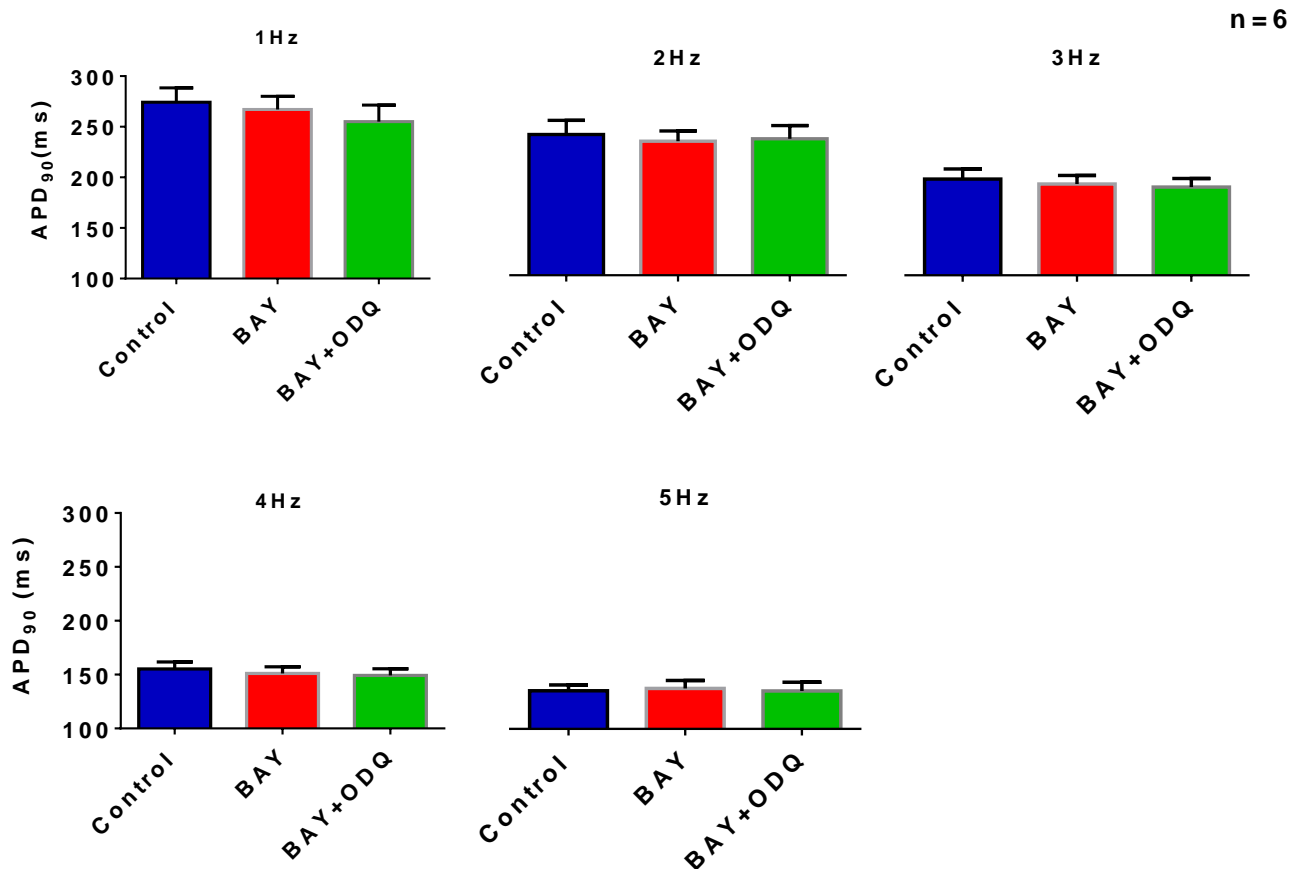


**Figure 4.8: Mean APD<sub>90</sub> at different stimulation frequencies (1 Hz – 5 Hz) in basal conditions, in response to 1  $\mu$ M BAY and in response to 10  $\mu$ M ODQ in the continued presence of BAY. Data are presented as mean  $\pm$  SEM (n=6).**

The results so far show that L-NNA, SNAP, and BAY do not show any significant effect on AP properties under basal conditions. The next experiments were designed to modulate the NO signalling pathways of cells that had additional exposure to  $\beta$ -AR stimulation with ISO.

It is well known that the  $\beta$  signalling pathway and NO signalling are linked through the  $\text{Ca}^{2+}$ -CaM dependent regulation of eNOS and nNOS. NOS is activated by  $\text{Ca}^{2+}$ -CaM, so increases in intracellular  $\text{Ca}^{2+}$  with ISO could also activate NOS. Application of ISO may stimulate  $\beta$ 1,  $\beta$ 2, and  $\beta$ 3-ARs. As mentioned in the previous chapter, eNOS is coupled to  $\beta$ 3-AR and activation of  $\beta$ 3-AR by ISO is reported to increase NO production (Barouch *et al.*, 2002; Ziolo, 2008). Therefore, the objective was to pre-treat the cells with ISO and then apply the NO signalling modulators and investigate the effects on cardiac AP repolarization.

The cells were stimulated at constant frequency of 2 Hz, and mean APD<sub>90</sub> was determined from the last 20 APs at each experimental condition. The stimulation frequency of 2 Hz was chosen because it is a frequency in the downward slope of the restitution curve, and a frequency that is well tolerated for prolonged periods of time. With constant pacing more information about the effect of different drugs on APD<sub>90</sub> can be obtained and experiments can be kept shorter without exposing the cell to higher frequency of stimulation of the dynamic restitution protocol.

Control experiments at 2 Hz constant pacing were conducted to confirm that the APs were stable under control conditions and that results were due to the agents used and not due to a time dependent effect. Figure 4.9A shows the time course of a representative cell with APD<sub>90</sub> plotted against experimental time. APD<sub>90</sub> of individual APs is plotted against time after starting the constant stimulation at 2 Hz. APD<sub>90</sub> was initially long (~300 ms) and declined to a steady-state level in the first 1-2 minutes, and remained stable for the rest of the recording. There was no change in APD<sub>90</sub> or AP shape during the experiment. Figure 4.9B shows average APD<sub>90</sub> of 20 APs when APD<sub>90</sub> stabilized at 2, 4, 6, and 8 minutes (n=5, from 5 different hearts). Mean ADP<sub>90</sub> at each time point was different in each cell, but did not vary during the course of the experiment. The stimulation protocol was left for ~ 20-25 minutes and APD was stable over this time.

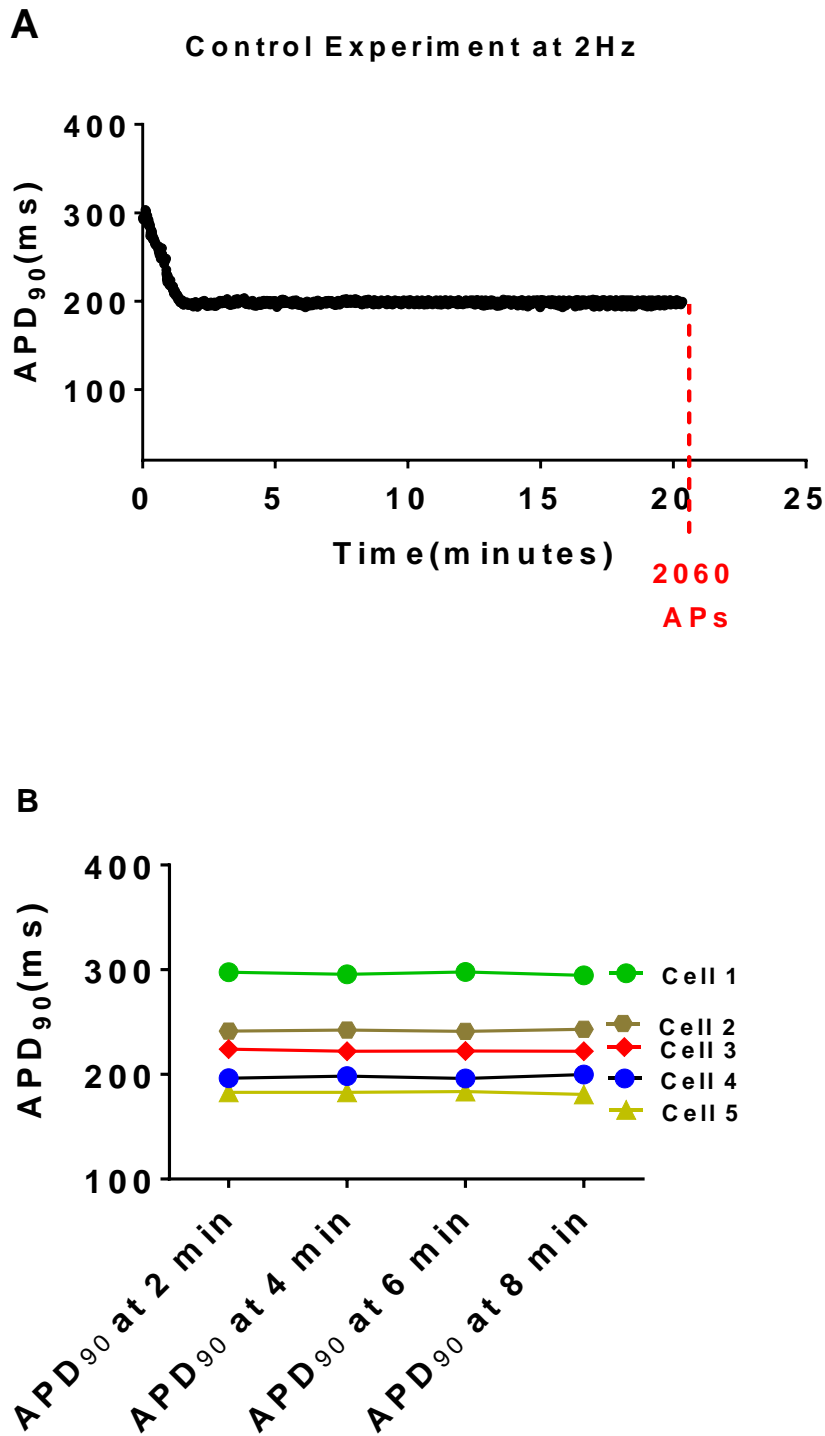


**Figure 4.9: Recordings of APD<sub>90</sub> with constant electrical stimulation at 2 Hz in control tyrode at 35-37°C. A)** The time course of a representative cell with APD<sub>90</sub> plotted against experimental time at 2 Hz stimulation frequency. **B)** Average APD<sub>90</sub> of 20 APs when APD<sub>90</sub> stabilized at 2, 4, 6, and 8 minutes (n=5).

#### **4.2.4 Does L-NNA shorten APD<sub>90</sub> in the presence of ISO while stimulating at constant frequency (2 HZ)**

As discussed in chapter 3, L-NNA shortened APD<sub>90</sub> in the presence of the non-specific  $\beta$ -AR agonist (ISO) and this effect was larger in the active than resting period myocytes. The effect of applying L-NNA in the continued presence of ISO was investigated while stimulating the guinea-pig left ventricular myocytes at a constant frequency of stimulation of 2 Hz. Stimulating at constant frequency enabled investigation of different NO signalling pathway modulators without exposing the myocytes to higher frequencies of stimulation which might lead to cell instability and frequency related effects on signalling pathways. The mean APD<sub>90</sub> was determined from the last 20 APs at each experimental condition.

Figure 4.10A shows representative AP traces from a single myocyte exposed to control, 10 nM ISO, and 500  $\mu$ M L-NNA in the continued presence of ISO. L-NNA shortened APD and changed the early plateau phase to become more positive which is consistent with what has been described in section 3.4.2. Figure 4.10B shows the time course of a representative cell with APD<sub>90</sub> plotted against experimental time in response to the experimental conditions. Applying L-NNA shortened APD<sub>90</sub> in comparison to control and ISO.

Figure 4.10C shows the mean APD<sub>90</sub> data at 2 Hz in response to ISO on its own and when L-NNA was applied in the presence of ISO. Applying 10 nM ISO did not significantly change APD<sub>90</sub> in comparison to control (Control,  $213.1 \pm 5.6$  ms; ISO,  $208.3 \pm 4.6$  ms,  $p > 0.05$ ,  $n = 5$ ); this might be due to the net increment effect of ISO on  $I_{Ca,L}$  and  $I_{Ks}$  to lengthen and shorten APD, respectively and may have cancelled each other out. However, adding 500  $\mu$ M L-NNA in the presence of 10 nM ISO shortened mean APD<sub>90</sub> to  $195.2 \pm 4.9$  ms ( $n = 5$ ), which was significantly shorter than in control or ISO only ( $p < 0.05$ ,  $n = 5$ ). Paired t-test was used to statistically analyse this data.

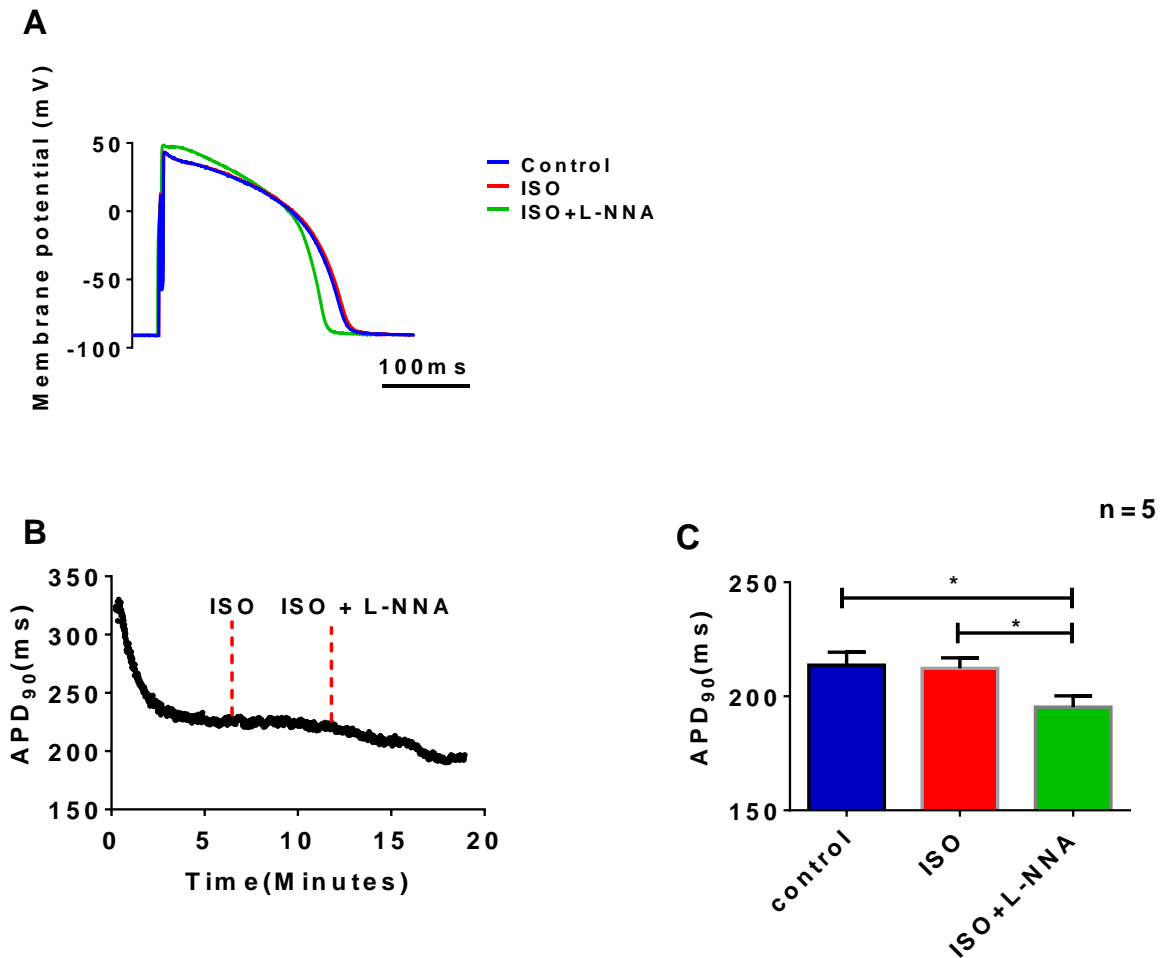


**Figure 4.10: The effect of applying 500  $\mu$ M L-NNA in the continued presence of 10 nM ISO at constant stimulation frequency of 2 Hz. A) Representative AP traces from a single cell in control, ISO, and ISO and L-NNA. B) Representative time course of the designed experiment from the same myocyte in panel A. C) Mean APD<sub>90</sub> at the three experimental conditions. Data are presented as mean  $\pm$  SEM (n=5).**

#### **4.2.5 Is there any effect of potentiating sGC with BAY on AP properties measured in the presence of ISO?**

Since inhibiting NO synthesis in the presence of ISO shortened APD<sub>90</sub>, the next question we addressed was the effect of potentiating NO activation of sGC and whether this increased APD<sub>90</sub>. Constant pacing experiments were done using BAY in the presence of ISO.

Application of 1  $\mu\text{M}$  BAY in the presence of 10 nM ISO, did not make a significant change in the mean  $\text{APD}_{90}$  (ISO,  $209.6 \pm 3.7$  ms; ISO + BAY,  $210.7 \pm 3.3$  ms;  $p > 0.05$ ,  $n = 4$ ) (Figure 4.11A). However, when we increased the concentration of ISO to 30 nM,  $\text{APD}_{90}$  showed a modest but highly significant elongation from  $215.9 \pm 3.6$  ms in 30 nM ISO to  $235.4 \pm 5.1$  ms when BAY was added ( $p \leq 0.01$ ,  $n = 7$ , see Figure 4.11B). In addition, the membrane potential of the early plateau phase changed modestly and became more positive in the presence of 30 nM ISO and ISO plus BAY (Figure 4.11B). These results suggest that potentiation of sGC with BAY can cause a modest lengthening of  $\text{APD}_{90}$ , but only at higher concentrations of ISO.

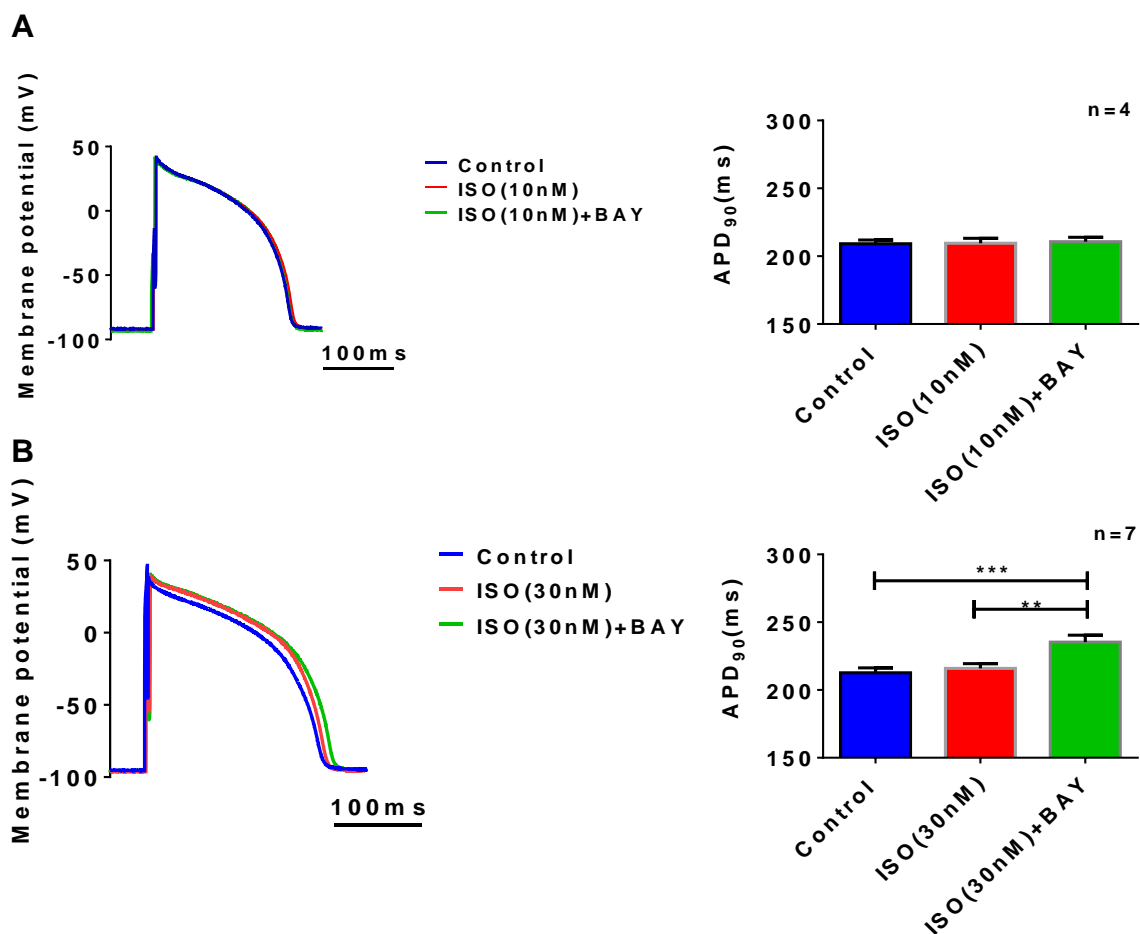


**Figure 4.11: The effect of the sGC activator 1  $\mu\text{M}$  BAY in the presence  $\beta$ -AR simulation (ISO).** **A)** Application of in the presence of 10 nM ISO. Representative AP traces on the left hand side of the panel, mean  $\text{APD}_{90}$  data on the right hand side ( $n = 4$ ). **B)** Application of in the presence of 30 nM ISO. Representative AP traces on the left side of the panel, mean data on the right hand side ( $n = 7$ ). Data are presented as mean  $\pm$  SEM.

#### **4.2.6 What is the effect of blocking the cGMP-dependent NO signalling pathway on APD in the presence of ISO?**

Blocking the cGMP-dependent NO signalling pathway was the next objective. ODQ is a selective sGC inhibitor, which binds to the haem group of sGC in competition with NO and inhibits sGC by oxidising the haem group (Lies *et al.*, 2013). 10  $\mu\text{M}$  ODQ was applied to myocytes electrically stimulated at 2 Hz and in the presence of 10 nM ISO. Our hypothesis was that ISO increases production of NO by activating  $\text{Ca}^{2+}$ -dependent NOSs. Therefore, the aim was to investigate the role of NO on AP duration while blocking the cGMP-dependent pathway and leaving any potential cGMP- independent pathways intact.

Figure 4.12A shows AP traces from a representative cell that was electrically stimulated at 2 Hz under basal conditions, in response to 10 nM ISO, and then in response to 10  $\mu\text{M}$  ODQ in the continued presence of ISO. Applying 10  $\mu\text{M}$  ODQ in the presence of ISO shortened APD and also changed the plateau to a slightly more depolarised potential. Figure 4.12B illustrates the time course of the experiment. The shortening effect when 10  $\mu\text{M}$  ODQ was applied took several minutes to develop and then stabilised at a new level. Figure 4.11C shows the mean  $\text{APD}_{90}$  data. Application of the 10 nM ISO did not make a significant change in the mean  $\text{APD}_{90}$  (Control,  $214.1 \pm 8.3$  ms; ISO,  $210.3 \pm 8.1$  ms,  $p > 0.05$ ,  $n=7$ ), however, application of 10  $\mu\text{M}$  ODQ (in the presence of the 10 nM ISO) significantly shortened  $\text{APD}_{90}$  in comparison to both control (Control,  $214.1 \pm 8.3$  ms; ISO + ODQ,  $201.5 \pm 8.2$  ms,  $p \leq 0.01$ ,  $n=7$ ) and ISO alone (ISO,  $210.3 \pm 8.1$  ms; ISO + ODQ,  $201.5 \pm 8.2$  ms,  $p \leq 0.05$ ,  $n=7$ ). These results, together with the results on selectively activating sGC with BAY, indicate that stimulating the cGMP-dependent pathway increases APD whereas inhibiting it resulted in a shortening of APD. The next section investigates how selectively modulating S-nitrosylation influences AP repolarization.

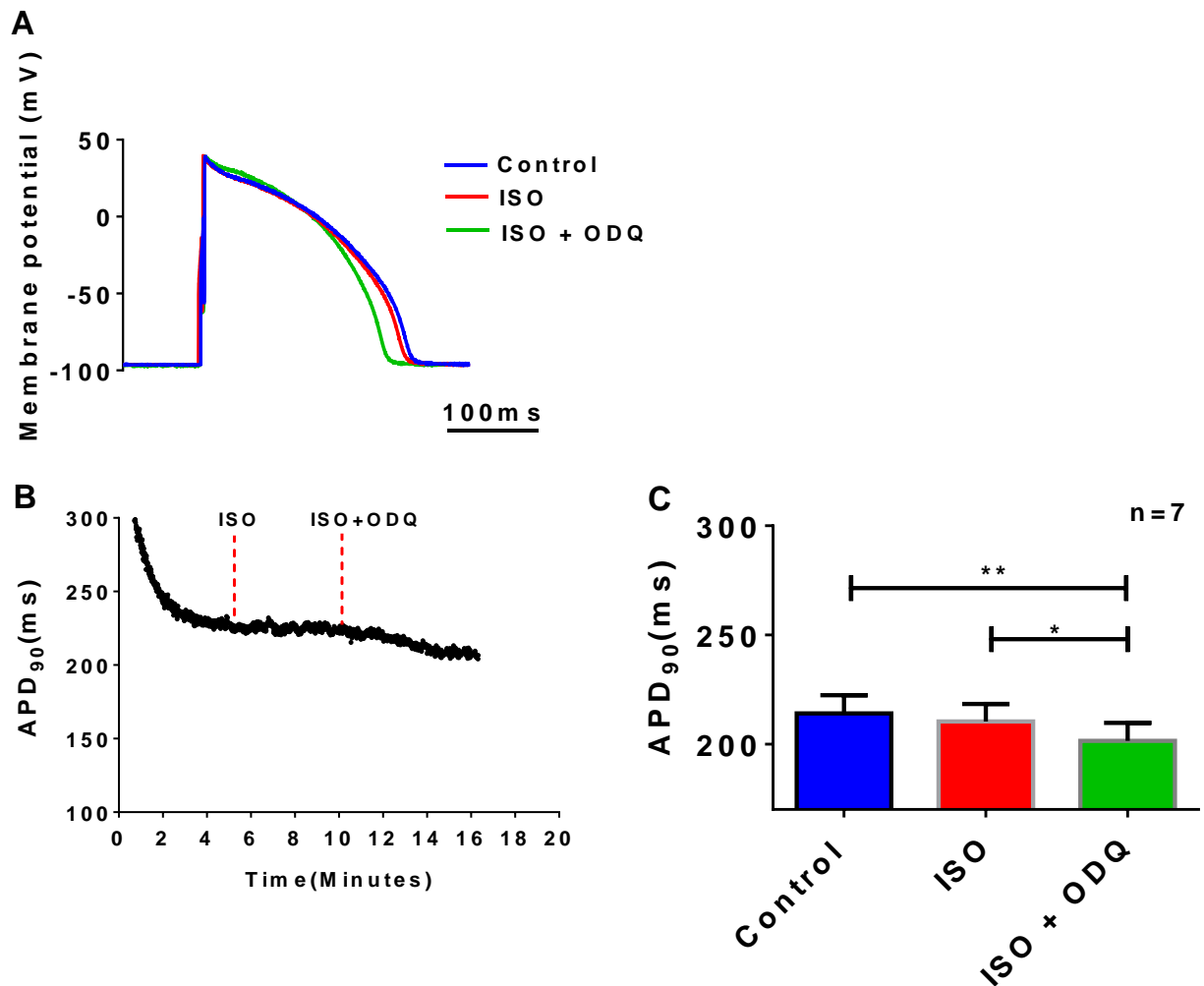


**Figure 4.12: The effect of the sGC inhibitor 10  $\mu$ M OQD on APD<sub>90</sub> in the presence  $\beta$ -AR stimulation (10 nM ISO) at constant pacing (2 Hz). **A**) Representative AP traces recorded after APD had stabilized at new levels in indicated recording solutions; in control conditions, in response to ISO, and when ODQ was applied in the presence of ISO. **B**) Representative time course of the designed experiment from the same myocyte in panel A. **C**) Mean Data at different experimental conditions. Data are presented as mean  $\pm$  SEM (n=7).**

#### 4.2.7 Does modulating S-nitrosylation affect AP repolarization?

The cGMP-independent pathway occurs mainly via S-nitrosylation, which is the post-translational modification wherein NO covalently attaches to thiol groups of cysteine residues on proteins to generate an S-nitrosothiol (Qin *et al.*, 2013). S-nitrosylation can be reversed by a number of denitrosylase enzymes, including S-

nitrosoglutathione reductase (GSNOR) which removes NO groups from nitrosothiols through metabolism of S-nitrosoglutathione, which is in dynamic equilibrium with nitrosylated proteins (Lima *et al.*, 2010). To investigate the S-nitrosylation pathway, denitrosylation was inhibited using N6022, a blocker of GSNOR.

The reported IC<sub>50</sub> of N6022 is 8 nM (Green *et al.*, 2012), so to ensure a good block occurred, a 200 nM concentration was applied to the myocytes in the presence of 10 μM ODQ and 10 nM ISO. ODQ was applied to block the cGMP-dependent pathway, and ISO was applied to increase the activity of the Ca<sup>2+</sup> dependent NOS. Application of N6022 showed significant shortening of the APD and the membrane potential of the early plateau became more positive (Figure 4.13A), and this change in the AP shape was consistent in all recordings. Figure 4.13B illustrates the time course of changes in APD<sub>90</sub> in a representative experiment. After N6022 reached the recording chamber it took around 1 minute to start shortening AP and then rapidly decreased APD over time until a new steady-state APD was reached after 3 minutes.

Applying N6022 in the presence of ODQ and ISO shortened the mean APD<sub>90</sub> to 143.3 ± 3.7 ms in comparison to the mean APD<sub>90</sub> in the presence of ODQ plus ISO of 192.5 ± 9.4 ms, a difference of 49.2 ms (p≤0.01, n=6) (Figure 4.13C).

Figure 4.13D represents mean APD<sub>90</sub> at two minute time points after N6022 was applied. N6022 started shortening APD<sub>90</sub> after 1-2 minutes from reaching the recording chamber. However, the shortening of APD<sub>90</sub> starts to be significant, compared to the mean APD<sub>90</sub> with ODQ and ISO, at 4 minutes.

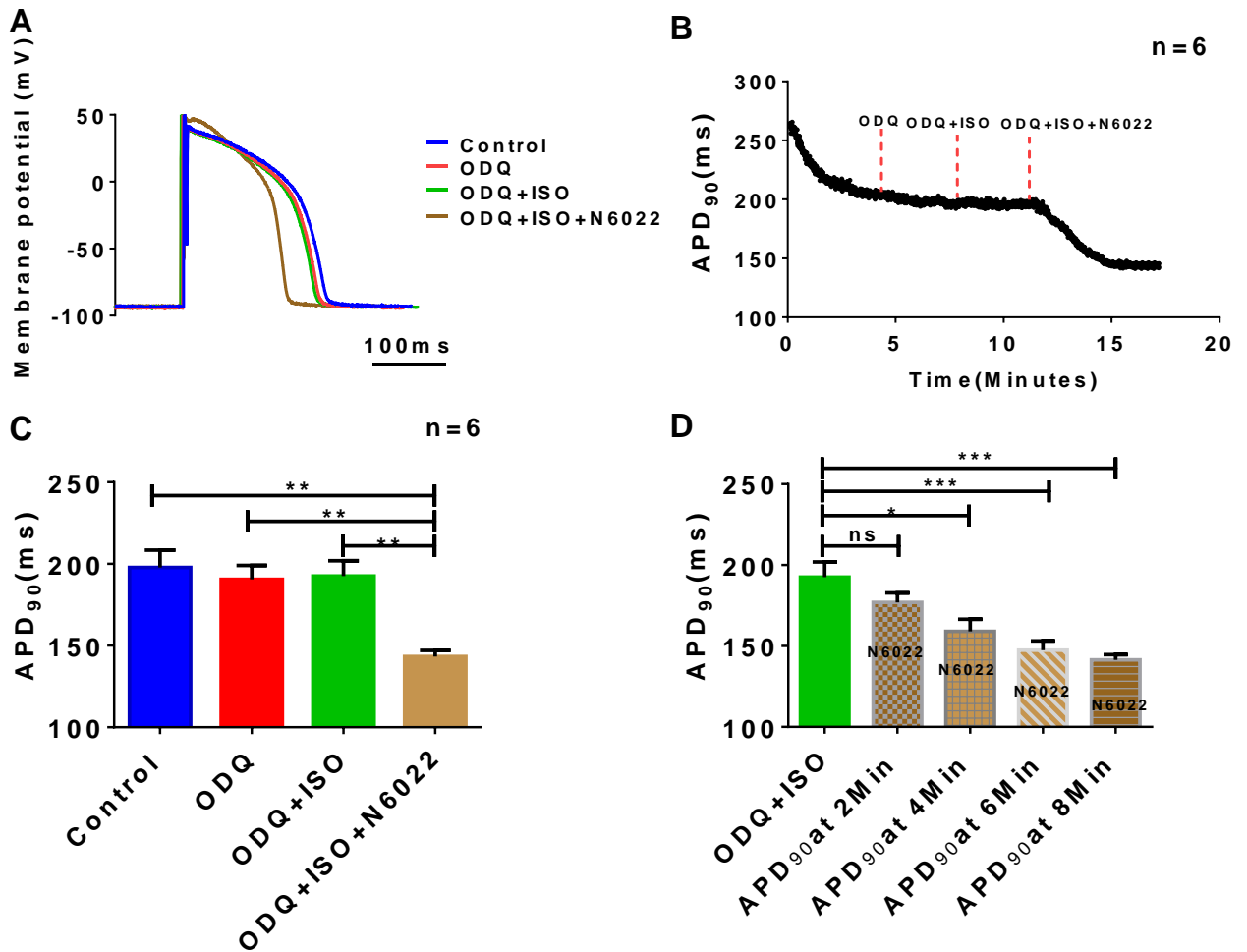


**Figure 4.13: The effect of the GSNOR inhibitor 200nM N6022 on APD<sub>90</sub> in the presence of  $\beta$ -AR stimulation (10 nM ISO). A) Representative AP traces recorded after APD had stabilized at new levels in indicated recording solutions, the stimulation frequency was 2 Hz. B) Representative time course illustrating changes to APD<sub>90</sub> during experiment. C) Mean APD<sub>90</sub> in experimental conditions. D) Mean APD<sub>90</sub> at different time points after N6022 was applied compared to mean APD<sub>90</sub> before N6022 was applied. Data are presented as mean  $\pm$  SEM (n=6).**

#### **4.2.7.1 Are the effects of N6022 specific and NO mediated?**

From the previous results it has been shown that adding N6022 to the cell when pre-treated with ODQ and ISO shortened APD<sub>90</sub> and elevated the AP plateau, which suggests complex effects on different currents by N6022. To confirm that the effects shown on AP properties were due to an increase in protein S-nitrosylation by N6022, two control experiments were performed.

If the effects of N6022 are due to changes in S-nitrosylation then they should be reduced by inhibiting NO synthesis with the non-specific NOS inhibitor L-NNA. The experiments were performed as described for N6022 in the previous section, except that 500  $\mu$ M L-NNA was applied first to decrease the physiological NO production in the cell and was present throughout the rest of the experiment. Experimental cells were stimulated at a constant frequency of 2 Hz, and mean APD<sub>90</sub> was determined from the last 20 APs in each experimental condition. Figure 4.14A shows representative AP traces. N6022 did not shorten APD significantly or change the AP shape compared to the previous experiments without L-NNA. Figure 4.14B illustrates the time course of a representative experiment. Applying N6022 in the continued presence of L-NNA and ISO started to shorten APD<sub>90</sub> about 3 minutes after reaching the recording chamber and reached steady state after 5 minutes. The amplitude of shortening was reduced compared to the previous experiment without L-NNA.

The mean steady state APD<sub>90</sub> results in each recording solution are shown in Figure 4.14C. Applying N6022 to the L-NNA and ISO pre-treated cells shortened the mean APD<sub>90</sub> by 34 ms, which was less than without L-NNA (49.2 ms) and not significant ( $p > 0.05$ ,  $n = 5$ ). Figure 4.14D represents mean APD<sub>90</sub> at different time points after N6022 was applied in the continued presence of L-NNA and ISO. N6022 shortened APD<sub>90</sub>, but it was never statistically significant and the effect of N6022 was far slower than without NOS inhibition. Therefore, applying L-NNA before N6022 attenuated most of the effects of N6022.

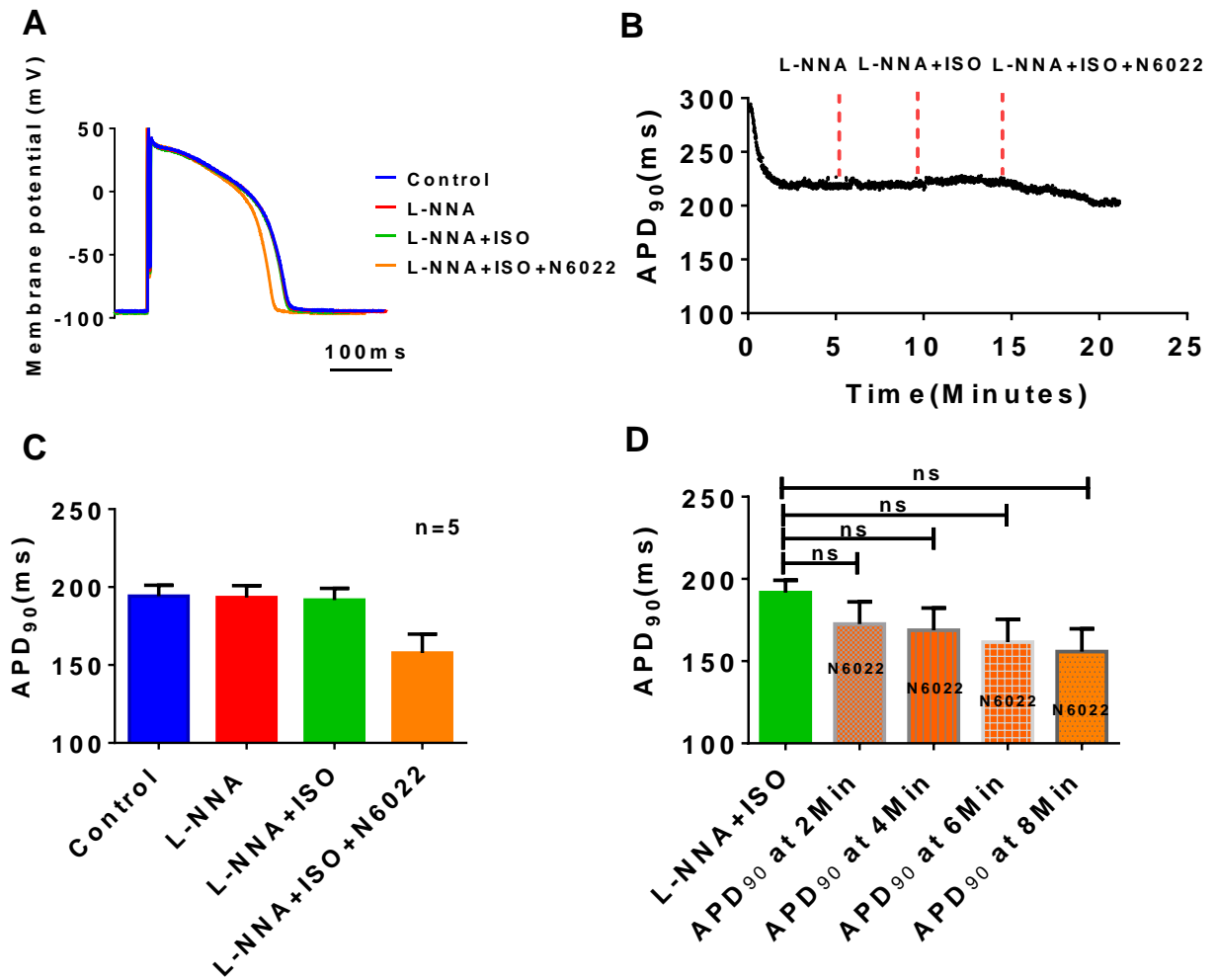


**Figure 4.14: Effect of pre-treating myocytes with 500  $\mu$ M L-NNA before applying 200 nM N6022 in the presence of  $\beta$ -AR stimulation (10 nM ISO). **A**) Representative AP traces recorded after APD had stabilized at new levels in indicated recording solutions, the stimulation frequency was 2 Hz. **B**) Representative time course of the designed experiment. **C**) Mean APD<sub>90</sub> at different experimental conditions. **D**) Mean APD<sub>90</sub> at different time points after N6022 was applied in the presence of L-NNA and ISO compared to mean APD<sub>90</sub> before N6022 was applied. Data are presented as mean  $\pm$  SEM (n=5).**

Next, 4-hydroxy-2, 2, 6, 6-tetramethylpiperidin-1-oxyl (Tempol) was used as an alternative approach to inhibiting S-nitrosylation before adding N6022. Tempol is a superoxide scavenger that is reported to decrease S-nitrosylation process by decreasing the availability of nitrosylates free radicals (see chapter 1). Therefore, it was expected that Tempol would decrease S-nitrosylation of target proteins that mediate APD shortening, and thus when N6022 was applied on Tempol pre-treated

myocytes it would have smaller effects on APs. Tempol was used at a concentration of 100  $\mu\text{M}$ , a physiological relevant concentration of Tempol (Lombard and Peric, 2004).

Myocytes were stimulated at 2 Hz under basal conditions and mean  $\text{APD}_{90}$  was determined from the last 20 APs in each experimental condition. 10  $\mu\text{M}$  ODQ was applied first to block the cGMP-dependent pathway, and 10 nM ISO was applied to increase the activity of the  $\text{Ca}^{2+}$  dependent NOS. Figure 4.15A shows representative AP traces. Applying N6022 on 100  $\mu\text{M}$  Tempol pre-treated myocytes shortened the APD also made the AP plateau more negative; an effect that was not observed in the earlier L-NNA experiment. Figure 4.15B illustrates the time course of a representative experiment and shows that  $\text{APD}_{90}$  was not significantly altered after applying N6022 to Tempol pre-treated myocytes. The N6022 reduced mean  $\text{APD}_{90}$  by 15.3 ms in the Tempol pre-treated myocytes (Figure 4.15C). Figure 4.15D represents mean  $\text{APD}_{90}$  before and at different time points after N6022 was applied in Tempol-treated cells and shows that N6022 did not significantly change  $\text{APD}_{90}$  ( $p > 0.05$ ,  $n = 5$ ). Therefore using a superoxide scavenger to reduce nitrosylation or blocking NOS production with L-NNA were both able to inhibit the actions of N6022 on APD shortening.

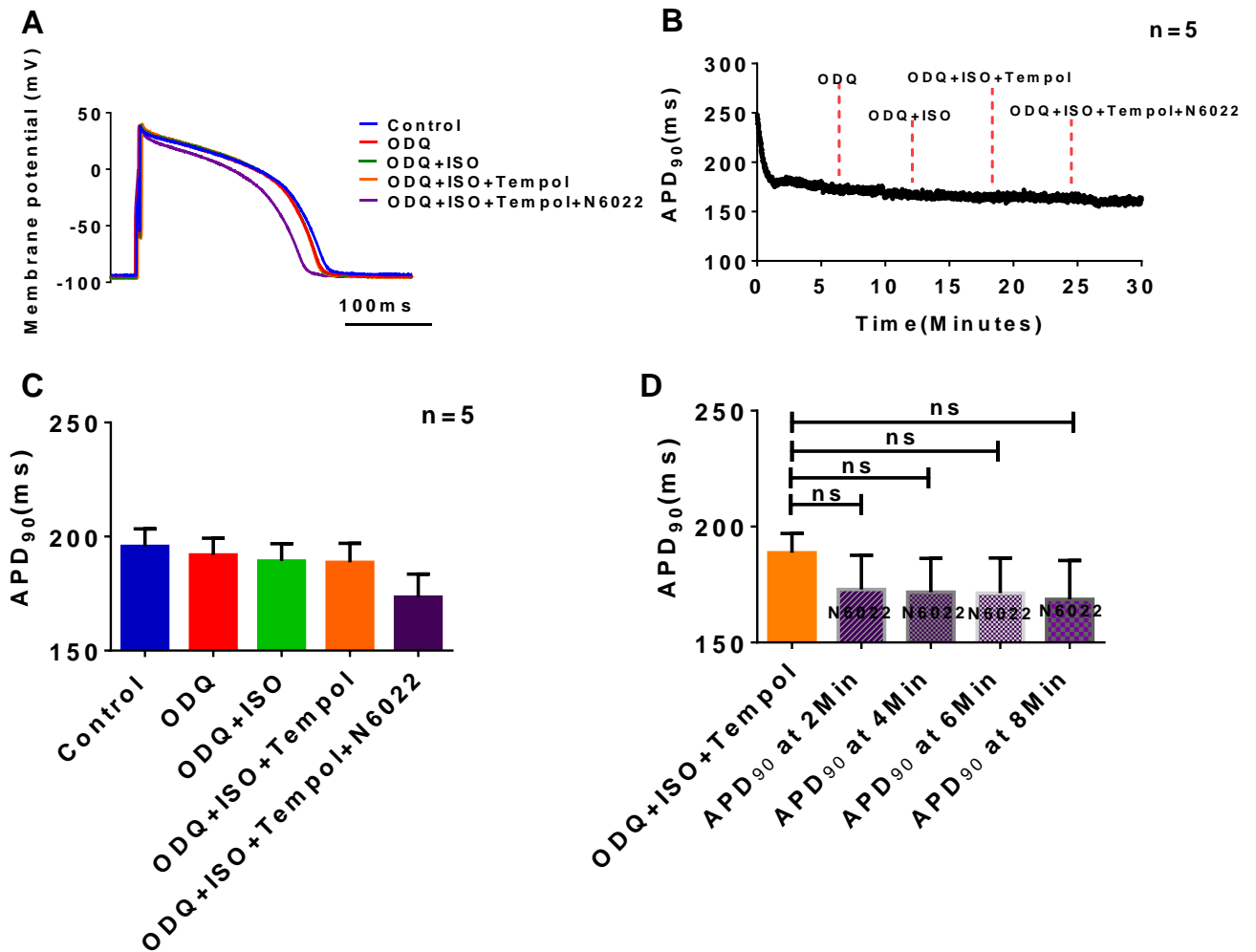


**Figure 4.15: The effect of pre-treating the myocytes with the oxygen free radical scavenger 100  $\mu$ M Tempol before applying 200 nM N6022 in the presence of 10  $\mu$ M ODQ and 10 nM ISO. **A)** Representative AP traces in response to the different experimental conditions. **B)** Representative time course of the designed experiment. APD<sub>90</sub> of individuals APs plotted against time from beginning of the experiment. **C)** Mean APD<sub>90</sub> at different experimental after reaching steady state level. **D)** Mean APD<sub>90</sub> at different time points after N6022 was applied in the presence of Tempol, ODQ, and ISO compared to mean APD<sub>90</sub> before applying N6022. Data are presented as mean  $\pm$  SEM (n=5).**

From the previous data we can conclude that increasing S-nitrosylation by inhibiting the de-nitrosylation enzyme GSNOR with N6022 shortened APD<sub>90</sub> when the cGMP-dependent pathway was inhibited by ODQ and the NOS activity was boosted by ISO. Moreover, the time course of this shortening was fast (Figure 4.12D). Pre-treating

myocytes with L-NNA before adding N6022 attenuated the effect of N6022 on AP duration and morphology. Some shortening was still seen, but its rate of development was slow (Figure 4.13D). Finally, applying the nitrosylation inhibitor Tempol also reduced the effect of N6022 on AP duration, shape, and slowed the response (Figure 4.14D). Therefore, the effect of N6022 is likely to be due to increased S-nitrosylation of different protein moieties that affect the shape and the duration of AP.

### **4.3 Discussion**

The work presented in this chapter investigated the effect of NO signalling pathway modulators, L-NNA, SNAP, BAY 60-2770, ODQ, or N6022 on AP properties and the dependency of this effect on the  $\beta$ -AR stimulation in guinea pig left ventricular active period myocyte using perforated patch clamp technique and physiologically relevant temperature.

NO/cGMP dependent and NO/cGMP independent pathways have been studied to highlight the effect of each pathway on AP properties using either a dynamic restitution protocol or constant pacing method.

#### **4.3.1 The electrophysiological effect of L-NNA on APs is dependent on the presence of $\beta$ -AR stimulator (ISO)**

Adding L-NNA without pre-treating the cell with ISO showed no significant change on APD<sub>90</sub> at different stimulation frequencies or on the shape of the APs. Thus L-NNA on its own did not change the APs properties. Therefore, the significant effect of L-NNA, which was described in chapter 3 is dependent on the presence of  $\beta$ -AR stimulation.

The link between the autonomic nervous system and the NO signalling pathways has been a focus of attention of many studies. Wang *et al.* (2008) studied signalling via eNOS and the I<sub>Ca,L</sub> was directly measured by the whole cell ruptured patch clamp technique. Myocytes were isolated from wild-type and eNOS knock-out mice. Results showed that eNOS limits the heart's response to  $\beta$ -AR stimulation by ISO as the Ca<sup>2+</sup> transient amplitudes were significantly greater in myocytes from eNOS knock-out than wild-type mice. Moreover, eNOS knock-out myocytes exhibited a

larger incidence of ISO-induced EADs and DADs. They suggested eNOS function may be protective against arrhythmias. However, mechanistic data are limited. A role of PDE2 has been proposed by Mongillo *et al.* (2006). Selective inhibition of PDE2 with erythro-9-(2-hydroxy-3-nonyl) adenine (EHNA) attenuated the negative inotropic effect of  $\beta$ 3-AR signalling and positively influenced cardiac performance in rat ventricular cardiac myocytes. Selective activation of  $\beta$ 3-AR was obtained with a combination of noradrenaline plus the  $\beta$ 1-AR antagonist CGP20712A and the  $\beta$ 2-antagonist ICI118,551. Selective blockade of  $\beta$ 3-AR was attained with the selective  $\beta$ 3-AR antagonist SR59230A.

The conclusion was that  $\beta$ 3-AR is involved in the noradrenaline induced NO generation. Thus sGC activation resulted in cGMP increases and then activation of PDE2, which reduced cAMP dependent signalling.

Notably, the effect of PDE2 inhibition on contractility was dramatically reduced in myocytes obtained from mice in which the expression of eNOS had been knock-out (Shesely *et al.*, 1996). Likewise, the antagonistic effects induced by  $\beta$ 3-AR stimulation on  $\beta$ 1 and  $\beta$ -AR stimulation were initially linked to NO release via eNOS (Aragon *et al.*, 2010) as pre-treatment with either an inhibitor of sGC or an inhibitor of the cGMP-activated PKG, abolished the  $\beta$ 3-AR dependent negative inotropism in whole heart preparations of guinea-pig (Kitamura *et al.*, 2000). Therefore, the protective effect of NO on contractility and calcium handling of cardiac tissue was mediated, at least in part by eNOS, and sGC and stimulation of PDE2.

The literature on the effect of NOS modulation on APD is sparse. A study on guinea-pig ventricular myocytes showed that activation of eNOS by  $Ca^{2+}$ /Calmodulin dependent activation while inhibiting nNOS, caused depression of  $I_{Ca,L}$ , enhancement of  $I_{Ks}$ , and shortening of APD using perforated patch clamp technique at 37°C in the presence of  $Ca^{2+}$  loading agent such as digitalis (Bai *et al.*, 2005).

#### **4.3.2 SNAP has no effect on ventricular action potentials**

SNAP activates sGC by releasing NO and increases cGMP levels over control, in rat and human cardiac tissue, without modulating APD (Ebihara and Karmazyn, 1996; Ross *et al.*, 2005; Rozmaritsa *et al.*, 2014). Kotlo *et al.* (2011) also demonstrated that SNAP increased cGMP in a concentration-dependent manner in human vascular smooth muscle. Furthermore, SNAP increased cGMP in other tissues,

including kidney and platelets (Lu *et al.*, 1998; Kottenberg-Assenmacher *et al.*, 2003; Monteiro *et al.*, 2012). Surprisingly, few studies have investigated the modulation of APs by SNAP. Cameron *et al.* (2003) reported that SNAP shortened APD in goldfish ventricular myocytes at 21°C, by enhancing  $K_{ATP}$  channel activation, while Abramochkin *et al.* (2012) concluded that SNAP prolonged APD in rat atrial tissue at 37°C using in situ microelectrode examination. However, my overall finding was that SNAP failed to modulate APD or electrical restitution curve properties. This was consistent with what Abi-Gerges *et al.* (2001) reported on  $I_{Ca,L}$ . They found increases in NO levels with multiple NO donors, including SNAP, which had no effect on basal  $I_{Ca,L}$  in rat ventricular myocytes. These findings were also involving  $\beta$ -AR stimulation. Abi-Gerges *et al.* (1997) showed that SNAP inhibited ISO-stimulated  $I_{Ca,L}$  in frog ventricular myocytes. Wahler and Dollinger, (1995) also reported inhibitory effects of SNAP on  $I_{Ca,L}$  in guinea pig ventricular myocytes pre-treated cells with 10 nM ISO.

In the current study, the results from the NO sensor showed high NO release from SNAP and previous results from biochemical assays showed that cGMP levels are also elevated and yet there was no effect on guinea pig ventricular APs. The explanation may be that PDEs are important not only in the degradation of cyclic nucleotides but also in compartmentalising cyclic nucleotide signalling pathways in specific microdomains inside the cell (Fischmeister *et al.*, 2006). cGMP signalling also appears to be compartmentalised (Castro *et al.*, 2006).

Compartmentalisation has been studied indirectly using recombinant rat olfactory system cyclic nucleotide-gated (CNG) channels, which open in response to cyclic nucleotides. Cardiac myocytes were infected with adenovirus which encodes CNG channel expression at the plasma membrane resulting in a cyclic nucleotide-gated current ( $I_{CNG}$ ) in response to the increase in level of cyclic nucleotide-cGMP (Castro *et al.*, 2006; Castro *et al.*, 2010). Therefore, CNG channels were acting as real-time sensor of cGMP concentration underneath the plasma membrane (Fischmeister *et al.*, 2006). Castro *et al.* (2006) studied the compartmentalisation of cGMP-dependent NO signalling in rat ventricular myocytes under room temperature and using ruptured patch clamp technique, and found no effect of 100  $\mu$ M SNAP alone or IBMX (non-selective PDEs inhibitor) alone on  $I_{CNG}$ , but  $I_{CNG}$  increased when SNAP was added in combination with IBMX. This indicates that SNAP-derived cGMP was not detected at the plasma membrane unless PDEs were inhibited. So, the high level of cGMP

induced by the high level of NO released from SNAP was unable to reach the plasma membrane and affect ion channels unless PDEs were inhibited. This is consistent with my results that SNAP on its own could not modulate APD despite the high level of NO released and detected by the NO sensor.

#### **4.3.3 Activation of sGC lengthens cardiac APs, whereas inhibiting sGC shortens APD; but effects are only observed in the presence of $\beta$ -AR stimulation**

There is very little literature about the effect of NO on APD and how different sGC modulators affect APD. Our study is the first to study the effect of sGC modulators on AP repolarization in single ventricular myocytes. BAY 60-2770 was used as a useful pharmacological tool to activate sGC selectively and investigate the role of cGMP-dependent signalling. BAY showed differential effects depending on the experimental conditions and protocol used.

Neither BAY alone, nor BAY and ODQ, significantly modulated the electrical restitution curve or APD<sub>90</sub> at different stimulation frequency. Other studies have also shown that BAY alone or when applied with ODQ, increases cGMP level in ventricular myocytes using biochemical cGMP assays (Bice *et al.* 2014). Therefore, high cGMP levels are not sufficient on their own to have an impact on AP properties. Other factors must be involved, including the important role of PDEs as previously mentioned.

Applying 10 nM ISO and BAY and stimulating the cell at 2 Hz did not modulate APs, therefore we decided to apply BAY in the presence of 30 nM ISO. Although not all the cells tolerated the 30 nM ISO, stable APs could be recorded from 7 cells and a significant. Elongation of APD<sub>90</sub> occurred with BAY in the presence of 30 nM ISO. This is a novel finding and not too much is known about the effect of BAY on the heart relative to the vascular system (Lasker *et al.*, 2013).

In the reverse experiment, sGC was inhibited by ODQ in the presence of ISO. The result was a modest shortening in APD<sub>90</sub> when ODQ was applied. Overall, the results suggest a cGMP-dependent signalling pathway has a net inhibitory effect on repolarizing K<sup>+</sup> current as repolarization was altered without effects on the AP plateau. As guinea-pig ventricular myocytes lack I<sub>to</sub>; I<sub>Ks</sub> and I<sub>Kr</sub> are the predominant

repolarising currents. Mewe *et al.* (2010) reported that a membrane permeant analogue of cGMP, 8-Br-cGMP, inhibited  $I_{Kr}$  in atrial mouse myocytes but had no effect on  $I_{Kr}$  recorded from ventricular mouse myocytes. Rachel Caves, from Mitcheson group, also found no effect of cGMP on  $I_{Kr}$ .

NO signalling has been reported to enhance  $I_{Ks}$ . Bai *et al.* (2004) demonstrated that the application of the NO donor nitroprusside enhanced  $I_{Ks}$  in guinea pig ventricular myocytes.  $I_{Ks}$  enhancement was barely suppressed by ODQ but was reversed by a reducing agent. This suggests that a cGMP-independent signalling pathway mediated the enhancement of  $I_{Ks}$ . NO signalling appears to differentially regulate the ionic currents underlying the ventricular AP and is dependent on whether NO follows cGMP-dependent or cGMP-independent signalling pathways. Previous work in Mitcheson's laboratory by Rachel Caves found that BAY 60-2770 applied under basal conditions, failed to modulate  $I_{Ks}$  or  $I_{Kr}$ . When PDEs were inhibited, BAY 60-2770 inhibited  $I_{Ks}$  (but not  $I_{Kr}$ ). The mechanism for inhibition of  $I_{Ks}$  did not involve protein kinase G. These results demonstrate that PDE activity suppresses elevations of cGMP in response to sGC activation, and also compartmentalises cGMP-dependent signalling. The effect of cGMP-independent pathways, such as S-nitrosylation, on  $I_{Ks}$  needs to be further investigated.

The majority of research investigating the effect of NO signalling on cardiac ionic currents has focused on  $I_{Ca,L}$ . ODQ markedly and consistently increased basal  $I_{Ca,L}$  in murine embryonic stem cells that had differentiated into spontaneously beating cardiomyocytes (Bloch *et al.*, 1999). Likewise, Gallo *et al.* (2001) demonstrated that application of ODQ also enhanced  $I_{Ca,L}$  in guinea-pig ventricular myocytes an effect mimicked by an NO scavenger. Gallo *et al.* (1998) demonstrated that the application of NOS inhibitors enhanced basal  $I_{Ca,L}$  in guinea-pig ventricular myocytes and this effect was blocked in the presence of L-arginine. ISO increases  $I_{Ca,L}$ , but it seems that having ODQ there and blocking the cGMP-dependent pathway may increase  $I_{Ca,L}$  to a level that affects AP shape. Furthermore, the application of the cGMP analogue 8-Br-cGMP, also inhibited basal  $I_{Ca,L}$  in ferret ventricular myocytes (Campbell *et al.*, 1996).

#### **4.3.4 APD is substantially shortened by upregulating cGMP-independent NO signalling pathways**

After investigating the effect of NO through cGMP-dependent pathways it was crucial to study the effect of the cGMP-independent NO signalling pathway in modulating APD. When investigating the S-nitrosylation pathway I obtained very interesting findings. Applying N6022, which inhibits protein denitrosylation, shortened APD<sub>90</sub> significantly and changed the shape of the APs by making the plateau more positive. These results indicated that S-nitrosylation has an important role in modulating APD. N6022 is reported to increase S-nitrosylation of target proteins by inhibiting GSNOR, an enzyme important for de-nitrosylation. N6022 had the largest effect of any reagent tested (Green *et al.*, 2012). The evidence that N6022 inhibits GSNOR was mentioned in chapter 1.

Applying L-NNA, to inhibit NO synthesis, largely attenuated the profound shortening by N6022. This makes sense as L-NNA will non selectively inhibit NOS thus decreasing the production of NO, which will decrease the amount of protein S-nitrosylation and thus N6022 inhibition of denitrosylation will have less effect. Some shortening was still seen but the kinetics was slowed, probably because L-NNA did not block all NOS production.

Tempol had a similar effect to L-NNA. Tempol scavenges superoxide free radicals and is a mimetic of superoxide dismutase, an enzyme that catalyses the dismutation reaction, and converts superoxide into O<sub>2</sub> or hydrogen peroxide. Tempol has been used to decrease S-nitrosylation by decreasing superoxide availability (Ziolo *et al.*, 2008). Decreasing S-nitrosylation by adding Tempol also reduced the shortening in APD by N6022.

Another control experiment was done by applying N6022 on its own and comparing it's effect to control Tyrode – this data is not shown due to low n numbers. The result was a slow not significant shortening of APD<sub>90</sub>, without a change in shape of the plateau of the AP. This experiment shows that N6022 does not have a non-selective effect on APs, for example by directly and pharmacologically influencing ionic currents. N6022 requires NO synthesis and NO bioavailability for its effects on AP repolarization.

It is well known that applying S-nitrosothiol NO donors increased  $I_{Ca,L}$  when sGC is inhibited (Campbell *et al.*, 1996). It has also been reported that S-nitrosylation increases  $I_{Ks}$  in guinea-pig cardiomyocytes (Bai *et al.*, 2004; Bai *et al.*, 2005) which might explain the shortening of the action potential duration seen with N6022. All the previous studies confirm the shortening of APD in a cGMP-independent manner which is consistent with my APs when N6022 was applied in the presence of ODQ and ISO (to direct the effect of NO through cGMP independent pathway). Gomez *et al.* (2009) demonstrated that  $K_{ir2.1}$  current which is a major channel subunit for  $I_{K1}$  in ventricular myocytes, (expressed in Chinese hamster ovary cells), was enhanced by the application of the NO donor SNAP.  $K_{ir2.1}$  current enhancement was found to be due to an increase in the opening probability of the channels as a result of S-nitrosylation of Cys76 using biotin switch assay.

In summary, NO signalling appears to differentially regulate the ionic currents underlying the ventricular AP and is dependent on whether NO is exerting its action through cGMP-dependent or cGMP-independent signalling pathways. The overall data suggests  $I_{Ca,L}$  to be inhibited by cGMP-dependent NO signalling and enhanced by cGMP-independent NO signalling.  $I_{To}$  and  $I_{Kr}$  may also be inhibited by NO signalling but the mechanism is unclear. On the other hand,  $I_{Ks}$  and  $I_{K1}$  appear to be enhanced by NO signalling, in particular by cGMP-independent signalling pathways. Therefore activating sGC elongated APD while inhibiting sGC or increasing s-nitrosylation shorten APD which means that APs are affected and modulated by both signalling pathways.

## **Chapter 5. Electrophysiological effects of ivabradine in guinea pig left ventricular myocytes**

### **5.1 Introduction**

Ivabradine is an anti-anginal agent that lowers heart rate through inhibition of sinoatrial nodal HCN (hyperpolarization activated cyclic nucleotide gated non-selective cation) channels, and thus inhibits the pacemaker current  $I_f$ . In sinoatrial node (SAN) cells, HCN4 appears to be the most important contributor to  $I_f$  (Bucchi *et al.*, 2006). The HCN family is closely related to the ether-a-go-go (EAG) family of  $K^+$  channels. One member of this family is the protein product of human ether-a-go-go-related gene 1 (hERG1), which encodes the pore-forming subunits of channels that conduct  $I_{Kr}$ . Blockade of hERG1 channels can produce Torsades de Pointes (TdP) and sudden cardiac death.

The  $IC_{50}$  for Ivabradine to inhibit  $I_f$  in rabbit isolated SAN cells are between 1.5 and 3  $\mu M$  (Captan and Desai, 2012). Ivabradine was considered to be safe and causing no significant side effects on the heart rate or QT interval (Savelieva *et al.*, 2006). Nevertheless, some concerns regarding cardiac safety of ivabradine have recently been raised. Martin *et al.* (2014) recently concluded that ivabradine is associated with risk of atrial fibrillation, though the underlying mechanism for this is not clear. In April 2014, ivabradine was added to the list of the drugs that have potential risk of TdP and prolonged QT interval (<https://www.crediblemeds.org>). Almost all drugs associated with QT interval prolongation and TdP can inhibit cardiac  $I_{Kr}$ , and its recombinant equivalent hERG (Zeltser *et al.*, 2003; Hancox *et al.*, 2008).

Melgari *et al.* (2015) investigated the tendency of ivabradine to inhibit hERG1 potassium channels, which strongly influence ventricular repolarization and susceptibility to TdP arrhythmia. Patch clamp recordings of hERG current ( $I_{hERG}$ ) were made from hERG expressing human embryonic kidney cells at 37°C. They demonstrated that ivabradine can inhibit  $I_{hERG}$ , with an  $IC_{50}$  of ~ 2 to 3  $\mu mol/L$ . Moreover, in the same study, the effect of 0.1 - 0.5  $\mu M$  ivabradine (a therapeutically relevant concentration) on monophasic action potentials (MAP) recorded from

guinea-pig Langendorff-perfused hearts during constant ventricular pacing at 200-ms cycle length was also investigated. Ivabradine prolonged ventricular repolarization and altered electrical restitution properties at concentrations relevant to the upper therapeutic range. So, ivabradine does not discriminate between hERG and HCN channels. These are surprising findings and may have important implications both clinically and for the future design of HCN-selective bradycardic agents based on ivabradine structure (Miller *et al.*, 2015; Melgari *et al.*, 2015).

The aim of my study was to bridge the gap between the whole heart and the recombinant channel studies by investigating the effect of ivabradine on APs recorded using the perforated patch clamp technique at physiologically relevant temperature, in acutely isolated guinea-pig left ventricular myocytes. Electrical restitution experiments using the dynamic protocol, and constant pacing experiments were performed to determine if ivabradine had unexpected effects on ventricular repolarization.

## **5.2 Results**

### **5.2.1 What is the effect of 0.5 and 1 $\mu$ M ivabradine on the single cell electrical restitution curve**

To test whether ivabradine has effects on electrical restitution; 0.5 and 1  $\mu$ M ivabradine were applied in cells stimulated using the dynamic restitution protocol. These ivabradine concentrations were chosen as these are therapeutically relevant concentrations of drug and were the same as those being used at the time by collaborators in Prof A. Ng's group in their whole heart experiments. Figure 5.1 shows representative electrical restitution curves under basal conditions, when 0.5  $\mu$ M ivabradine was applied, and after drug wash-off with control Tyrode. Three different electrical restitution curves from three cells are shown to represent the variability. The electrical restitution curves of the cells were variable.  $APD_{90Max}$  values, slope and  $\tau$  values showed either no change in  $APD_{90}$ , increases, or decreases it. Figure 5.2 represents the effect of 0.5  $\mu$ M ivabradine on the parameters of the electrical restitution curve.  $APD_{90Max}$  was decreased to  $317 \pm 25.7$  ms with 0.5  $\mu$ M ivabradine in comparison to  $335.8 \pm 30.01$  ms in control, but this change was not significant ( $p > 0.05$ ,  $n = 5$ ). The maximum slope was unchanged in both conditions

(Control,  $0.69 \pm 0.2$ ;  $0.5 \mu\text{M}$  ivabradine,  $0.63 \pm 0.1$ ). Moreover, no significant difference was detected in the maximum stimulation frequency, which was  $5.8 \pm 0.4$  Hz in both cases.  $0.5 \mu\text{M}$  ivabradine decreased the  $\tau$  value to  $221.8 \pm 30.5$  ms, which compares to  $253.3 \pm 16.5$  ms in control; however, this reduction was not significant because of the high variation in values. Trying to washout ivabradine with normal Tyrode did not show further changes in the curve in comparison to  $0.5 \mu\text{M}$  ivabradine. Therefore,  $0.5 \mu\text{M}$  ivabradine did not modulate electrical restitution parameters in a statistically significant way, but effects on individual cells were observed and these were variable.

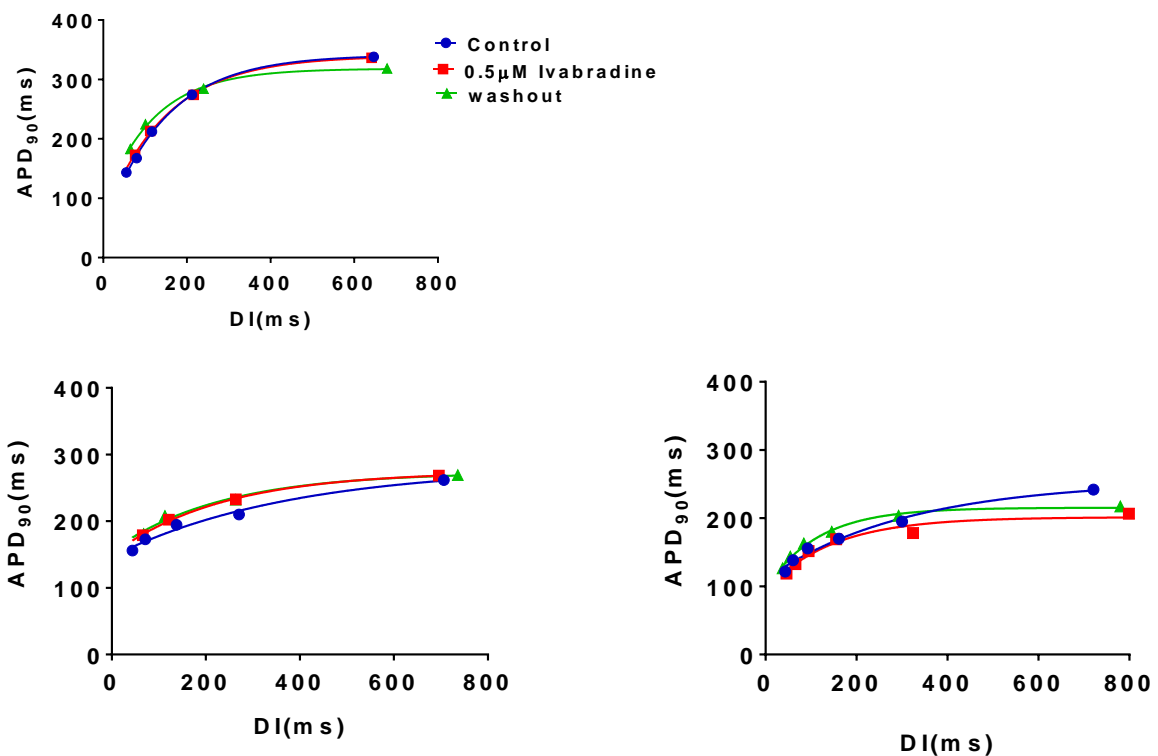


**Figure 5.1: The effect of  $0.5 \mu\text{M}$  ivabradine on electrical restitution curves.** Electrical restitution curves from three different cells in control and ivabradine solutions and after wash-off with control Tyrode.

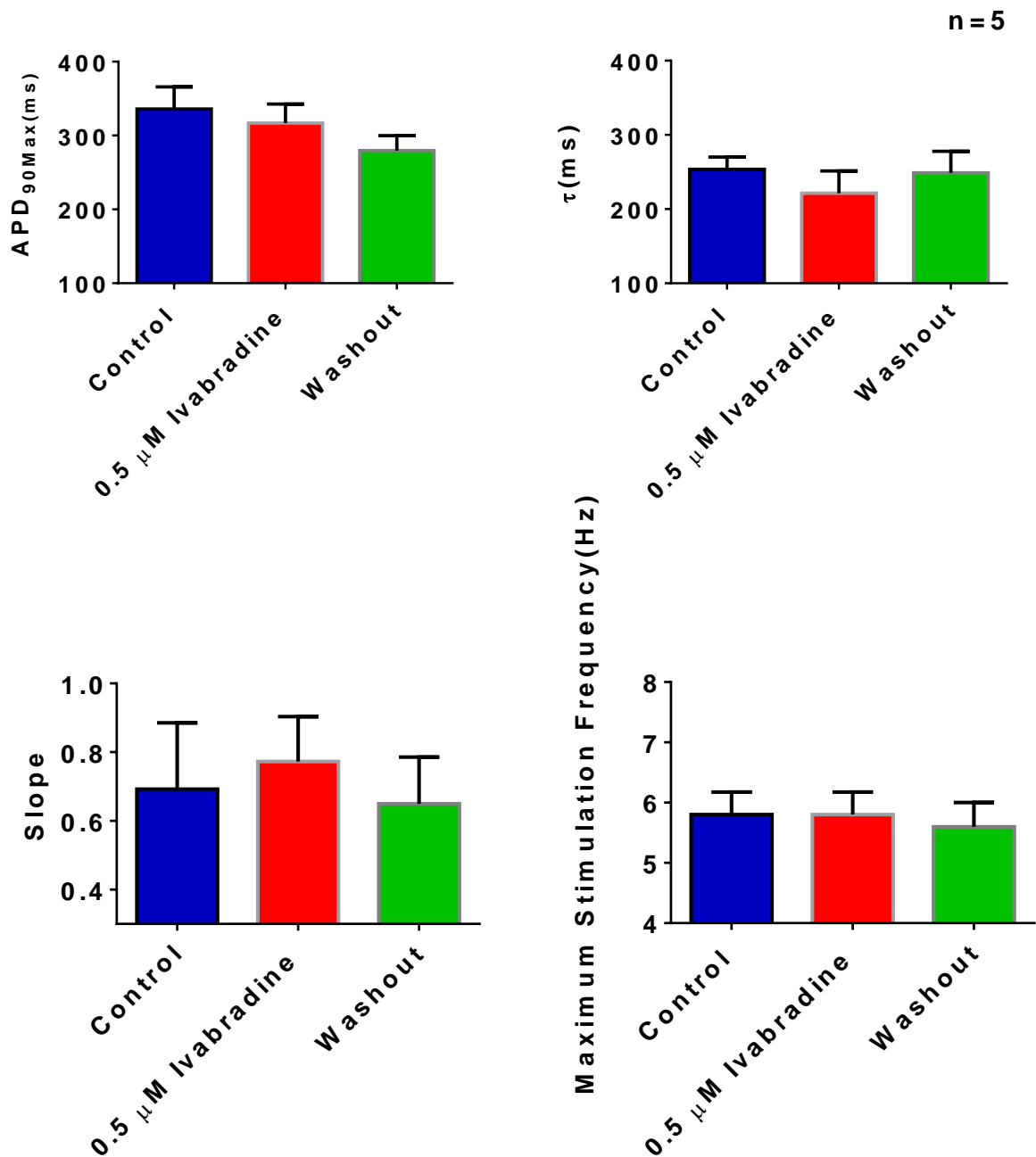


**Figure 5.2: The effect of 0.5  $\mu\text{M}$  ivabradine on electrical restitution curve parameters.** Mean maximum APD<sub>90</sub> (APD<sub>90Max</sub>),  $\tau$ , maximum slope, and mean maximum stimulation frequency. Data are presented as mean  $\pm$  SEM (n=5).

Figure 5.3 shows mean APD<sub>90</sub> from 20 APs at each frequency once APD had stabilized to a steady state level. Mean APD<sub>90</sub> at 5 Hz is not shown as 4 Hz was the maximum stimulation frequency observed in all cells before and during 0.5  $\mu\text{M}$

ivabradine. 0.5  $\mu\text{M}$  ivabradine did not significantly modulate mean  $\text{APD}_{90}$  at different stimulation frequencies (1 Hz - 4 Hz).

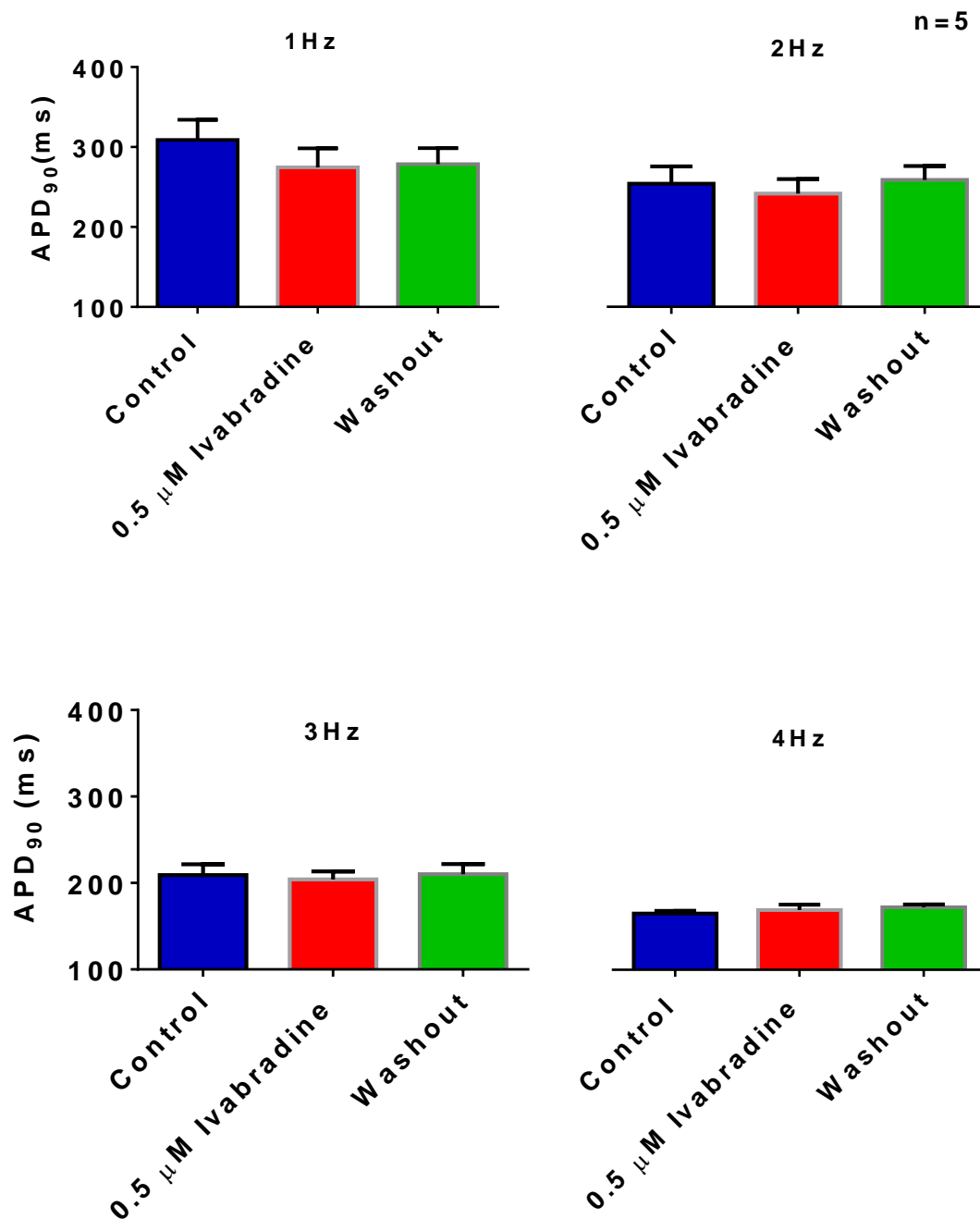


**Figure 5.3: Mean  $\text{APD}_{90}$  at different stimulation frequencies (1 Hz - 4 Hz) in control conditions, in response to 0.5  $\mu\text{M}$  ivabradine, and after wash-off with control Tyrode. The  $\text{APD}_{90}$  of 20 consecutive APs under each condition in each single cell was averaged and used to calculate the mean  $\pm$  SEM (n=5).**

0.5  $\mu\text{M}$  ivabradine did not show any consistent or reproducible effects on electrical restitution curves and  $\text{APD}_{90}$  values. A higher concentration of 1  $\mu\text{M}$  ivabradine was applied and the dynamic protocol used to obtain the electrical restitution data.

Figure 5.4A represents AP traces from representative cells at 1 Hz stimulation frequency, in control conditions, in response to 1  $\mu\text{M}$  ivabradine, and after washout with control Tyrode. It was decided to represent AP traces at 1 Hz because it was the only frequency at which 1  $\mu\text{M}$  ivabradine modulated APD significantly. Moreover, the effect on the AP shape less variable at 1 Hz stimulation frequency. Other frequencies show less effect on APD, but variable effect on AP shape. Figure 5.4B shows representative electrical restitution curve under basal condition, when 1  $\mu\text{M}$  ivabradine was applied, and during the washout with control Tyrode. The electrical restitution curves of the cells were less variable and almost all the cells showed the same findings.

Figure 5.5 represents the effect of 1  $\mu\text{M}$  ivabradine on the mean values of the parameters of the electrical restitution curve.  $\text{APD}_{90\text{Max}}$  was decreased to  $290.8 \pm 17.1$  ms with 1  $\mu\text{M}$  ivabradine in comparison to  $342.8 \pm 24.5$  ms in control, and this change was significant ( $p \leq 0.05$ ,  $n=7$ ). The maximum slope was higher in response to 1  $\mu\text{M}$  ivabradine but not significant (Control,  $0.84 \pm 0.16$ ; 1  $\mu\text{M}$  Ivabradine,  $0.96 \pm 0.18$ ,  $p > 0.05$ ,  $n=7$ ). Moreover, no significant difference was detected in the maximum stimulation frequency ( $5.7 \pm 0.4$ ) in comparison to control ( $5.5 \pm 0.4$ ). 1  $\mu\text{M}$  ivabradine significantly decreased  $\tau$  in comparison with control (Control,  $229.4 \pm 28.1$  ms; 1  $\mu\text{M}$  Ivabradine,  $138 \pm 19.4$  ms,  $p \leq 0.05$ ,  $n=7$ ). Therefore, 1  $\mu\text{M}$  ivabradine decreased the mean values of the time constant and  $\text{APD}_{90\text{Max}}$  significantly, while increasing the maximum slope insignificantly.

Trying to washout ivabradine with normal Tyrode did not show further changes in the curve in comparison to 1  $\mu\text{M}$  ivabradine.

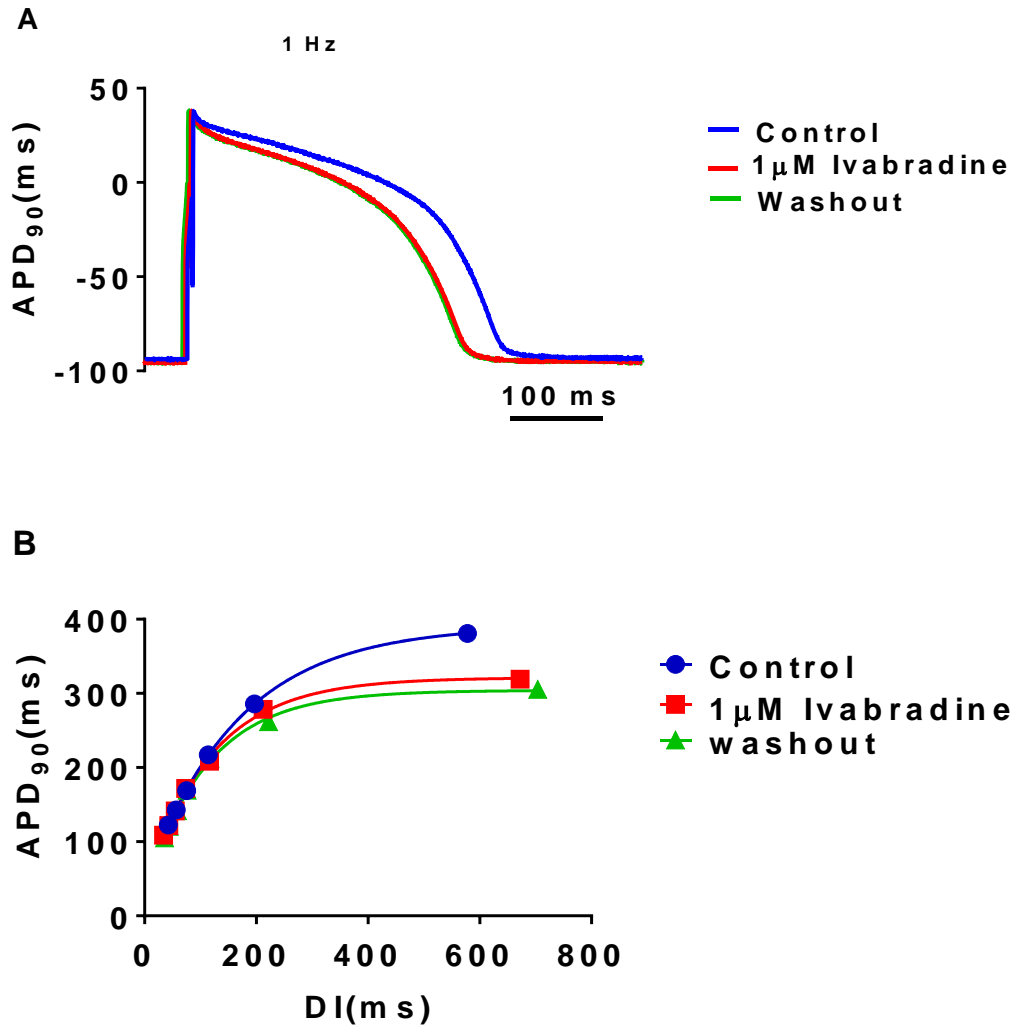


**Figure 5.4: The effect of 1  $\mu\text{M}$  ivabradine on the electrical restitution curve. A)** Representative AP traces from a representative cell in response to control, ivabradine, and after wash-off with control Tyrode at 1 Hz. **B)** Electrical restitution curve from the same cell shown in panel A.

n=7

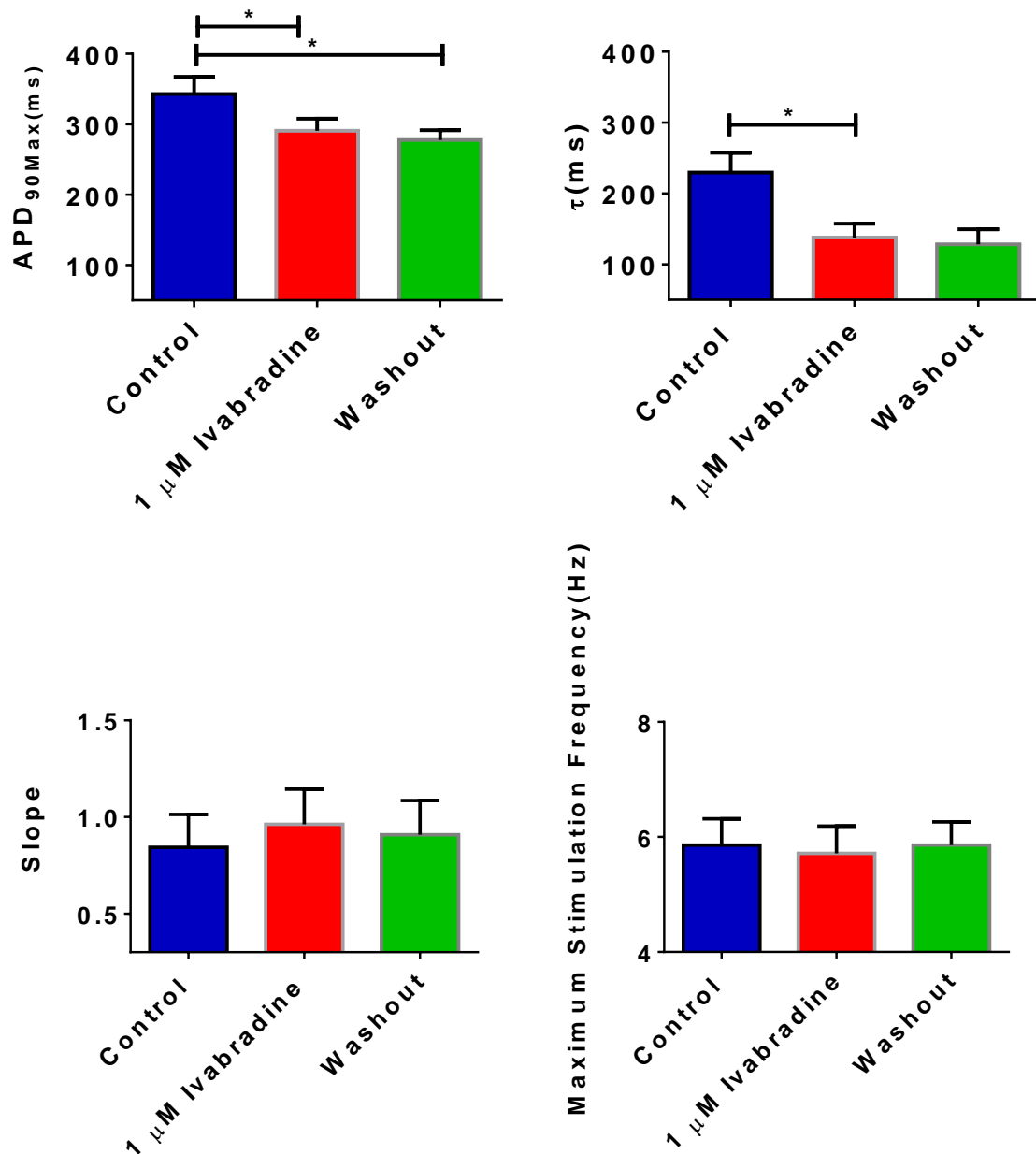


**Figure 5.5: The effect of 1 μM ivabradine on the electrical restitution curve parameters.** The effect of ivabradine on APD<sub>90Max</sub>, τ, maximum slope, and maximum stimulation frequency. Data are presented as mean ± SEM (n=7).

Figure 5.6 shows mean APD<sub>90</sub> of 20 APs at each frequency, once APD had stabilized. Mean APD<sub>90</sub> at 1 Hz stimulation frequency was significantly shorter with 1 μM ivabradine (289.5 ± 16.8 ms) in comparison to control (327.8 ± 21.2 ms) (p≤0.05,

n=7). It is consistent with the effect of 1  $\mu\text{M}$  ivabradine on  $\text{APD}_{90\text{Max}}$  explained earlier. However, 1  $\mu\text{M}$  ivabradine did not show significant changes to the mean  $\text{APD}_{90}$  at other stimulation frequencies. Mean  $\text{APD}_{90}$  did not recover with washout with normal Tyrode suggesting the effect of ivabradine is irreversible in short term experiments.

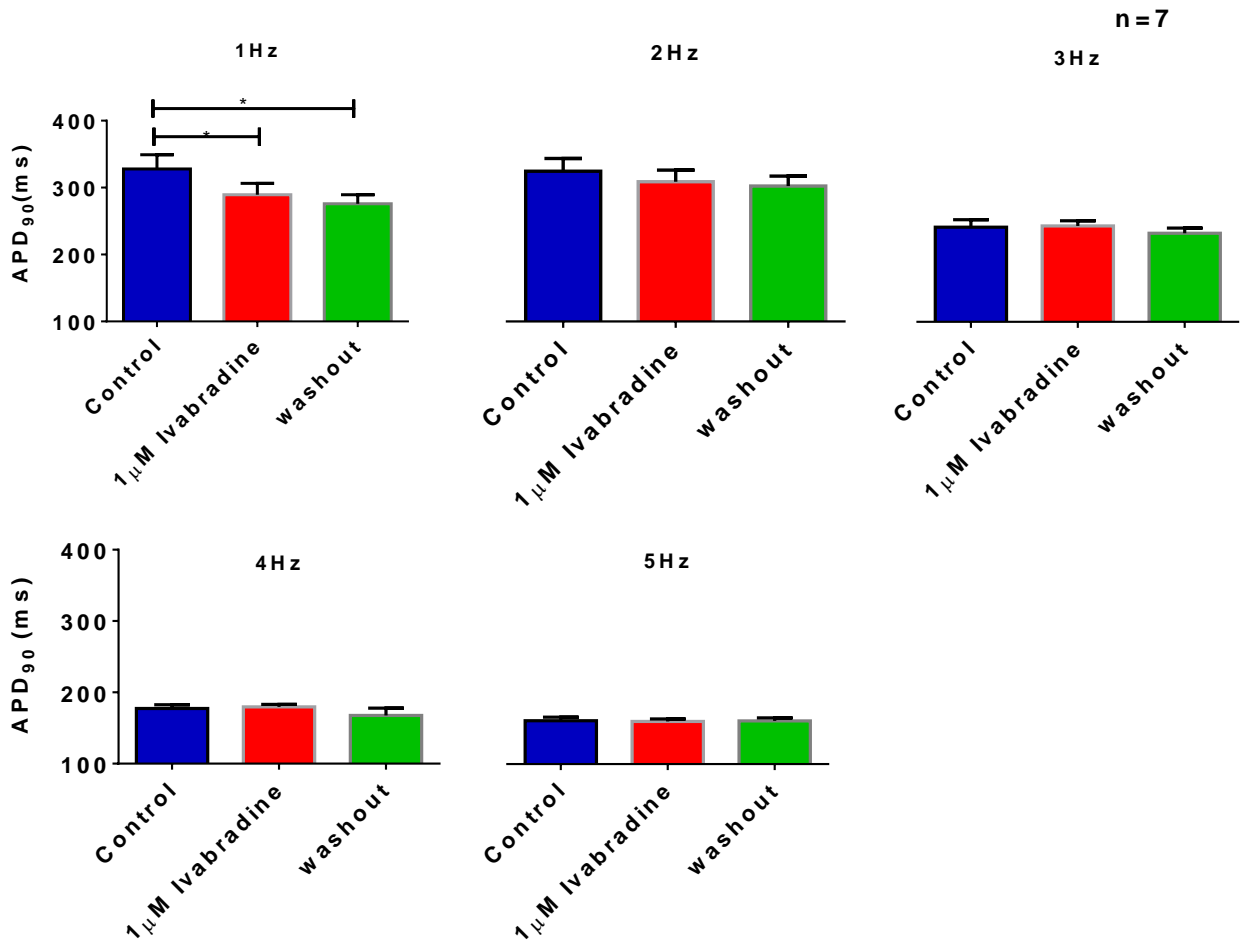


**Figure 5.6: Mean  $\text{APD}_{90}$  at different stimulation frequencies (1 Hz – 5 Hz) under control conditions, in response to 1  $\mu\text{M}$  ivabradine, and after wash-off with control Tyrode. Data are presented as mean  $\pm$  SEM (n=7).**

### **5.2.2 The effect of 1 and 3 $\mu\text{M}$ ivabradine on $\text{APD}_{25}$ , $\text{APD}_{50}$ , and on $\text{APD}_{90}$ with constant pacing at 2 Hz**

At this point we concluded that the effect of ivabradine on the acutely isolated guinea-pig left ventricular myocytes was variable and heterogeneous. Following

discussion with collaborators Prof. Andre Ng and Dr. Kieran Brack (Glenfield hospital, Leicester) we decided to do constant pacing (2 Hz) experiments, which are shorter and more controlled. In addition, at this time we also had access to further information from Prof. Jules Hancox and Dr. Melgari (University of Bristol) on the concentration-response relationship for ivabradine inhibition of hERG currents. They had measured the  $IC_{50}$  for ivabradine inhibition of hERG1 was 2.07  $\mu\text{M}$  which compares to 1.5 – 3  $\mu\text{M}$  for HCN currents. Based upon all these considerations, we switched to using 1 and 3  $\mu\text{M}$  ivabradine for the constant pacing experiments. Figure 5.7A presents APs from three cells in control, 1  $\mu\text{M}$  ivabradine, and then 3  $\mu\text{M}$  ivabradine to illustrate the variability in responses. As before, ivabradine did not washout. 1  $\mu\text{M}$  ivabradine caused either no change or shortening in APD. Moreover, the effect on AP morphology was also variable. Adding 3  $\mu\text{M}$  ivabradine did not cause a further change in APD or AP morphology. Figure 5.7B shows time course data of one of the representative cells. The  $APD_{90}$  of individual APs is plotted against time from the beginning of the experiment. Notice the shortening of  $APD_{90}$  when 1  $\mu\text{M}$  ivabradine was applied. 3  $\mu\text{M}$  ivabradine caused a negligible amount of additional shortening of  $APD_{90}$ .

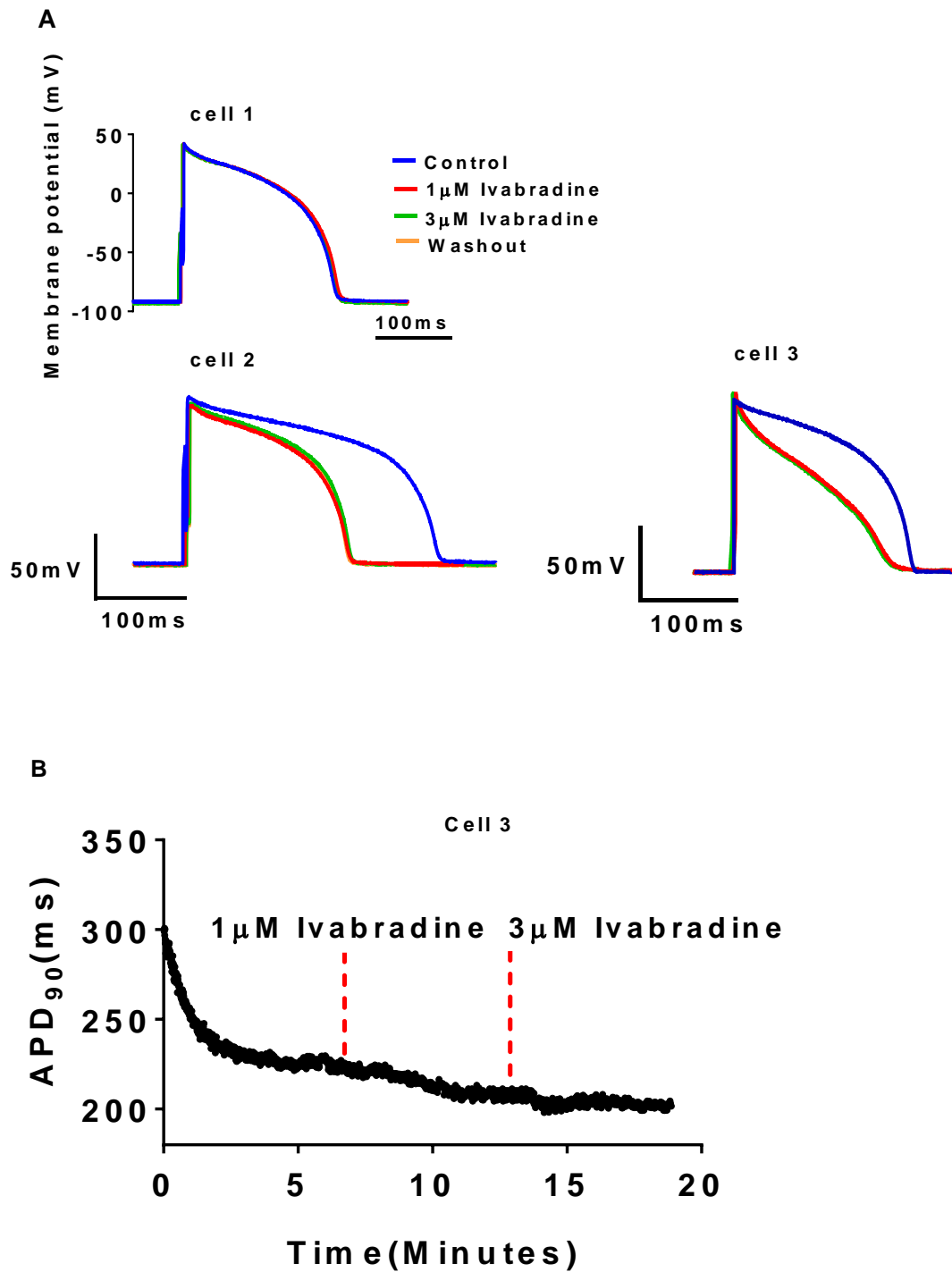


**Figure 5.7: The effect of 1 and 3  $\mu$ M ivabradine on APD and AP morphology in constant pacing experiments. A) Representative action potentials from three different cells to illustrate the variability in AP duration and shape when ivabradine was applied at 2 different concentrations. B) Time course data of cell 3 at 2 Hz. APD<sub>90</sub> of individual APs plotted against time from beginning of the experiment.**

1 and 3  $\mu\text{M}$  ivabradine changed the shape of the APs in many recordings and to capture this  $\text{APD}_{25}$  and  $\text{APD}_{50}$  as well as  $\text{APD}_{90}$  were calculated using the Tracan software. Figure 5.8A shows  $\text{APD}_{25}$ ,  $\text{APD}_{50}$ , and  $\text{APD}_{90}$  of individual cells under basal conditions and when ivabradine was applied at 1 and 3  $\mu\text{M}$  concentrations. Mean data of APD to different repolarization percentages is shown in Figure 5.8B. Mean  $\text{APD}_{25}$  with 1  $\mu\text{M}$  ivabradine ( $102.2 \pm 24$  ms) was not statistically significant ( $p > 0.05$ ,  $n=6$ ) from mean  $\text{APD}_{25}$  in control conditions ( $103.6 \pm 13.6$  ms). However, if you look at the changes to  $\text{APD}_{25}$  of individual cells in Figure 5.8A there is considerable variability. In some cells  $\text{APD}_{25}$  got longer, in others it got shorter and in others it was unchanged. This emphasizes the heterogeneous effect of ivabradine on  $\text{APD}_{25}$ . The mean  $\text{APD}_{25}$  with 3  $\mu\text{M}$  ivabradine was also not significantly different ( $p > 0.05$ ,  $n=6$ ). Mean  $\text{APD}_{25}$  in control conditions was  $103.6 \pm 13.6$  ms, and with 3  $\mu\text{M}$  ivabradine was  $110.7 \pm 27.3$  ms. While the effect on individual cells was variable; either lengthening, shortening or no effect.

Mean  $\text{APD}_{50}$  with 1  $\mu\text{M}$  ivabradine was  $147.4 \pm 24.5$  ms, which is shorter in comparison to in control conditions ( $155.3 \pm 6.8$  ms), but this shortening was not statistically significant ( $p > 0.05$ ,  $n=6$ ), although  $\text{APD}_{50}$  of individual cells was also variable. This again emphasizes the heterogeneous effect of ivabradine on AP morphology. Similarly, mean  $\text{APD}_{50}$  with 3  $\mu\text{M}$  ivabradine ( $144.6 \pm 25$  ms) was also shorter than control ( $155.3 \pm 6.8$  ms), but this was not significantly different ( $p > 0.05$ ,  $n=6$ ). The effect of 3  $\mu\text{M}$  ivabradine on  $\text{APD}_{50}$  of individual cells was variable. Again, no significant difference ( $p > 0.05$ ) was measured in mean  $\text{APD}_{50}$  between 1 and 3  $\mu\text{M}$  ivabradine.

The trend with  $\text{APD}_{90}$  was similar to  $\text{APD}_{25}$  and  $\text{APD}_{50}$ . Different myocytes responded in a variety of ways to application of ivabradine, but the net effect was no significant difference in mean  $\text{APD}_{90}$ . As observed in all other experiments, none of the responses were altered when ivabradine was washed out, suggesting ivabradine is having effects, and the actions of the drug are not reversible or are slow to reverse.

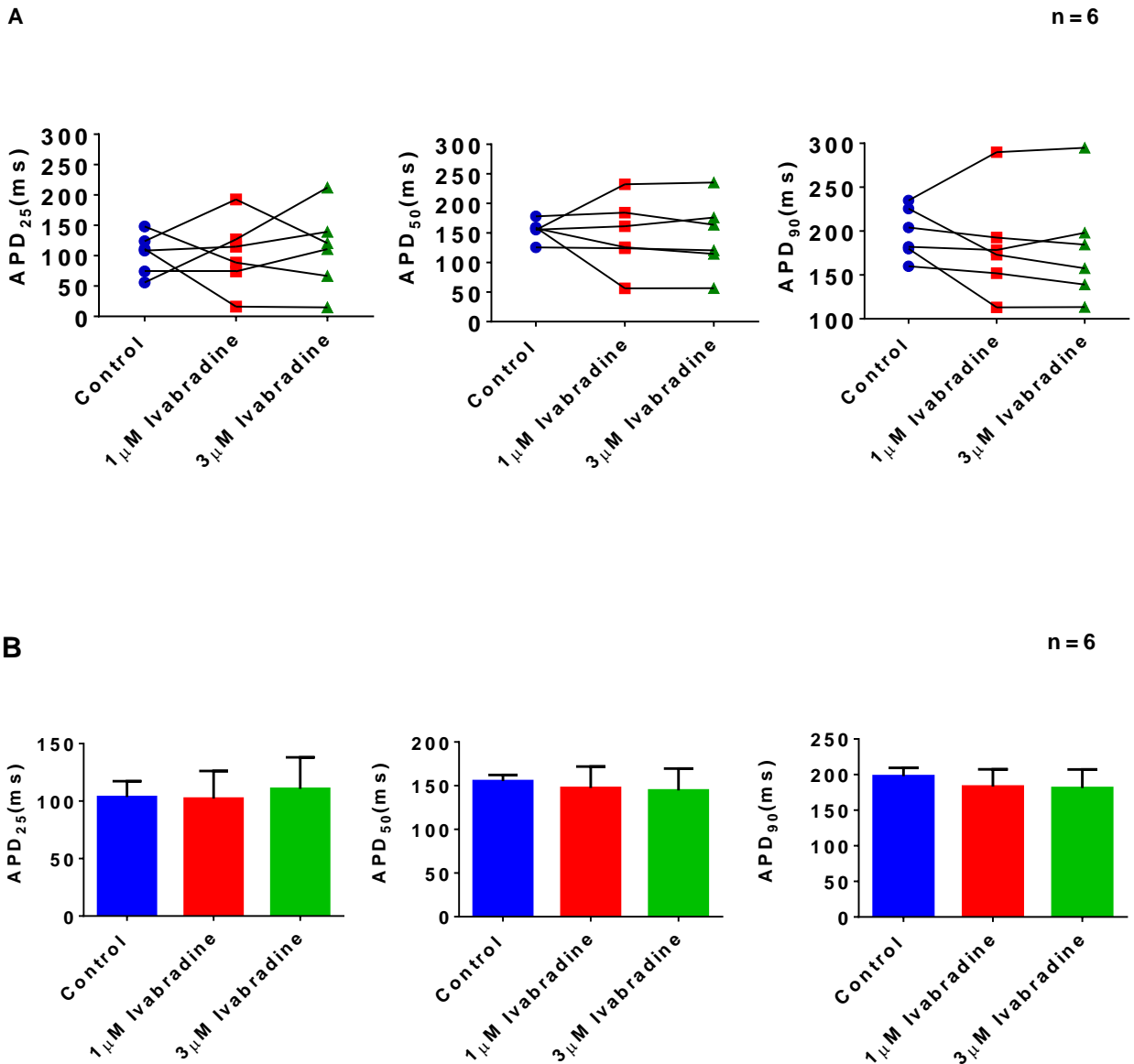


**Figure 5.8: The effect of 1 and 3  $\mu$ M ivabradine on mean APD<sub>25</sub>, APD<sub>50</sub>, and on APD<sub>90</sub> in constant pacing experiments. A) The effect of 1 and 3  $\mu$ M ivabradine on action potential duration with 25% repolarization (APD<sub>25</sub>), 50% repolarization (APD<sub>50</sub>), and 90% repolarization (APD<sub>90</sub>). Each symbol represents the data point from a single cell and the data points from a single cell are connected by a solid black line. Note, the APD<sub>90</sub> scale is different from the APD<sub>25</sub> and APD<sub>50</sub> scales to get a closer view. B) Mean data of APD<sub>25</sub>, APD<sub>50</sub>, and APD<sub>90</sub> with 1 and 3  $\mu$ M ivabradine at 2 Hz stimulation frequency. Data are presented as mean  $\pm$  SEM (n=6).**

### **5.2.3 The effect of applying the $I_{Kr}$ inhibitor E4031 before 1 and 3 $\mu$ M ivabradine on $APD_{25}$ , $APD_{50}$ , and on $APD_{90}$ in constantly paced cells**

It has been found that ivabradine prolongs ventricular repolarization and alters electrical restitution properties in whole heart studies, and that ivabradine inhibits hERG currents with similar potency to that reported for HCN currents/ $I_f$  (Melgari *et al.*, 2015). As described above, ivabradine caused variable effects on electrical restitution properties AP morphology. A possible explanation is that ivabradine has complex effects on several ionic currents and that's why the change of the shape and duration of APs was heterogeneous. To test this hypothesis, 1  $\mu$ M of the  $I_{Kr}$  inhibitor E4031 was applied to block  $I_{Kr}$  before applying Ivabradine. Applying ivabradine in the presence of E4031 should not cause a further change in AP shape or duration if ivabradine exerts all its effects through inhibition of  $I_{Kr}$ .

Figure 5.9A shows AP traces from a representative cell. Applying 1  $\mu$ M E4031 lengthen APD. Applying ivabradine in the continued presence of E4031 did not significantly modulate the AP shape or duration. Figure 5.9B represents the effect of pre-treating cells with the  $I_{Kr}$  blocker E4031 before applying ivabradine on  $APD_{25}$ ,  $APD_{50}$ , and on  $APD_{90}$  in individual cells. E4031 decreased  $APD_{25}$  almost in all cells, while applying ivabradine in the continued presence of E4031 caused no additional effect. E4031 increased  $APD_{50}$  in almost all the cells; applying E4031 caused lengthening or no change in  $APD_{50}$ . The effect of E4031 on  $APD_{90}$  was also consistent; applying E4031 caused lengthening in  $APD_{90}$  in almost all cells. However, applying ivabradine in the continued presence of E4031 did not change  $APD_{90}$  or AP morphology of individual cells.

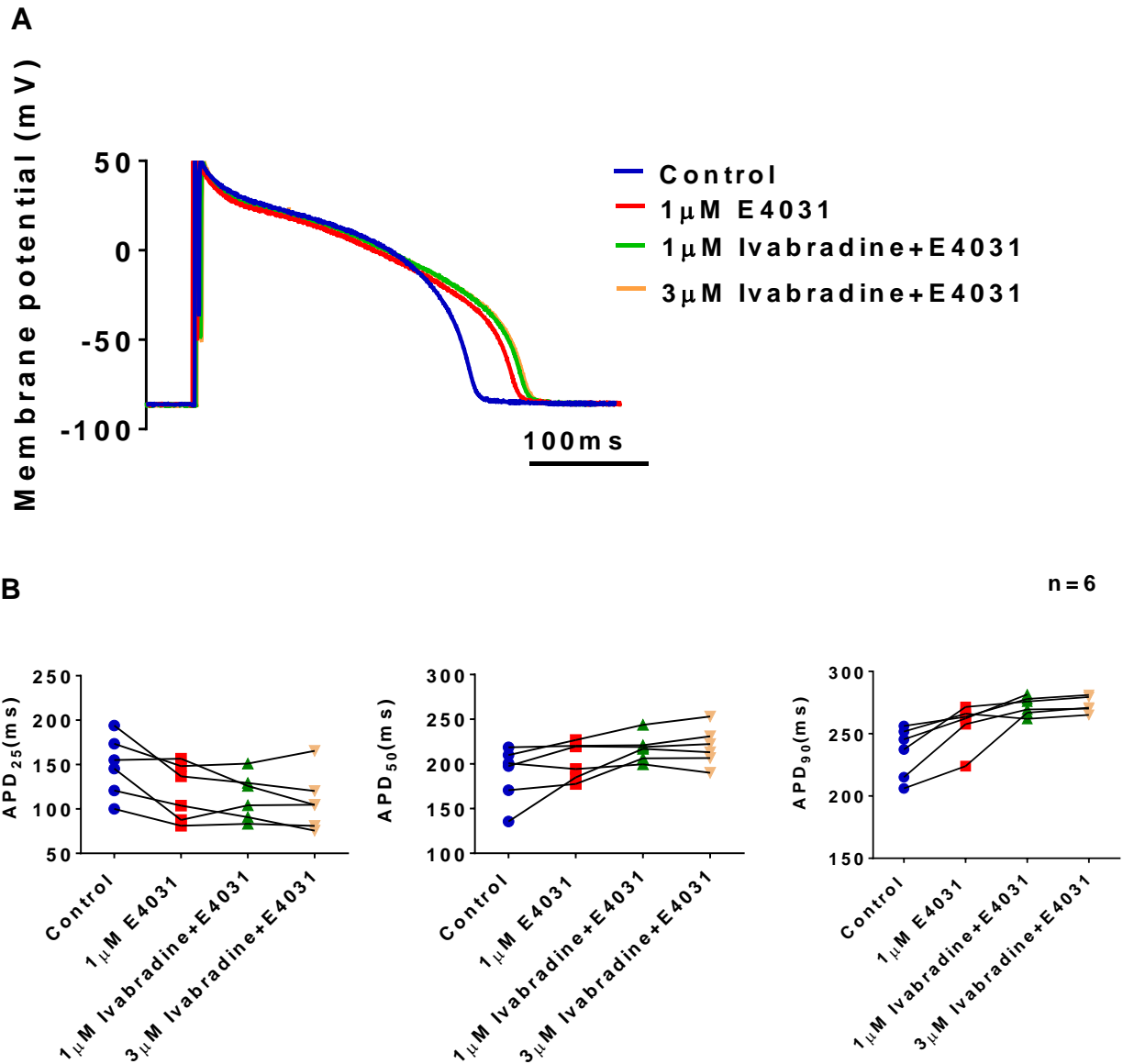


**Figure 5.9: The effect of pre-treating cells with the  $I_{Kr}$  blocker 1  $\mu$ M E4031 before applying 1 and 3  $\mu$ M ivabradine. A)** Representative APs traces in control conditions, in response to E4031, and when ivabradine was applied in the continued presence of E4031. **B)** The effect of pre-treating cells with the  $I_{Kr}$  blocker E4031 before applying ivabradine on APD<sub>25</sub>, APD<sub>50</sub>, and APD<sub>90</sub>. The results are presented as described in Figure 5.8A. Cells were paced at 2 Hz. Note; the scale is different in the three data plots. Data are presented as mean  $\pm$  SEM (n=6).

Figure 5.10 represents the mean data of APD<sub>25</sub>, APD<sub>50</sub>, and APD<sub>90</sub> to look at AP responses before and during ivabradine application when I<sub>Kr</sub> has been inhibited. Application of 1 and 3 μM ivabradine had minimal effects on APD<sub>25</sub> (p>0.05, n=6), and markedly less variable responses than seen in the absence of E4031. APD<sub>50</sub> and APD<sub>90</sub> showed a trend of being prolonged, but the changes were not statistically significant. So applying ivabradine in the presence of E4031 did not cause further significant changes in AP shape or duration.

n = 6

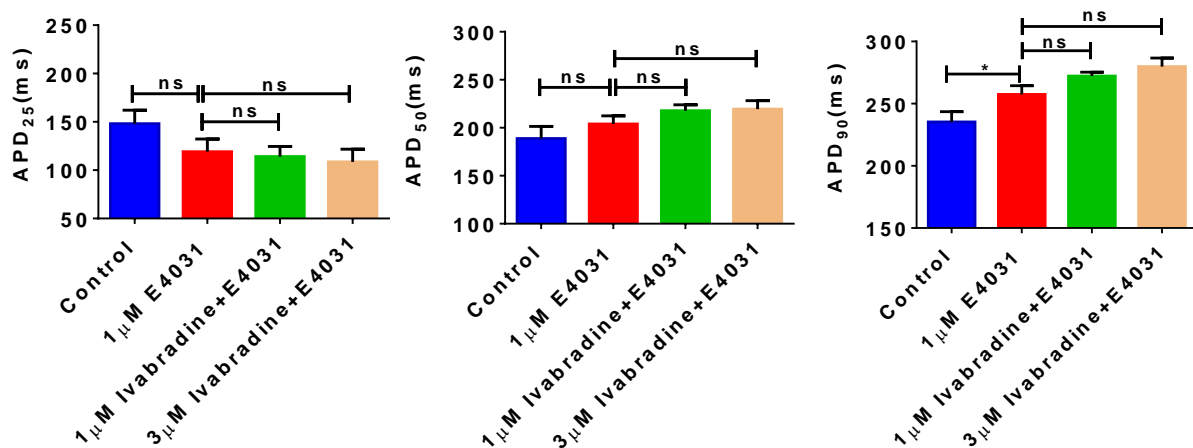


**Figure 5.10: Mean data of APD<sub>25</sub>, APD<sub>50</sub>, and APD<sub>90</sub> when pre-treating cells with the I<sub>Kr</sub> blocker 1 μM E4031 before applying 1 and 3 μM ivabradine. Data are presented as mean ± SEM (n=6).**

### **5.3 Discussion**

Ivabradine is an anti-anginal agent that lowers heart rate through inhibition of sinoatrial nodal HCN-channels, and thus inhibits the pacemaker current I<sub>f</sub>. Melagi *et al.* (2015) found that ivabradine can also inhibit I<sub>hERG</sub> in human embryonic kidney cells, as well as prolong ventricular repolarization, and alter electrical restitution properties in guinea pig whole heart studies. The aim of the current study was to investigate the effect of ivabradine on APs recorded in acutely isolated guinea pig left ventricular myocytes using the perforated patch clamp technique and physiologically relevant temperature.

### **5.3.1 Ivabradine showed variable effects on AP properties**

Data obtained from the dynamic restitution protocol found that 0.5  $\mu\text{M}$  ivabradine caused no significant change on electrical restitution curve parameters, and failed to modulate  $\text{APD}_{90}$  at different stimulation frequencies. Similarly, 1  $\mu\text{M}$  ivabradine only shortened mean  $\text{APD}_{90}$  at 1 Hz, but otherwise did not modulate mean  $\text{APD}_{90}$  at the other stimulation frequencies. The effect of 1  $\mu\text{M}$  ivabradine on electrical restitution curve parameters was variable. However, mean values of  $\tau$  and  $\text{APD}_{90\text{Max}}$  were shortened significantly. Nevertheless, the variable effect on individual cells makes it difficult to draw conclusions on the effect of 0.5 and 1  $\mu\text{M}$  ivabradine on electrical restitution curves. Collaborators at Glenfield hospital found that ivabradine prolonged ERP and prolonged MAP in guinea pig whole heart experiments when applied at concentrations from 0.1 – 0.5  $\mu\text{M}$ . However, in the current study ivabradine failed to modulate maximum stimulation frequency, which is an indicator of ERP, and the effect on APD was variable (either APD was not changed or shortened).

Applying 1 and 3  $\mu\text{M}$  ivabradine while pacing the cells at 2 Hz showed variable effects on  $\text{APD}_{90}$  and AP morphology. The variability in affecting individual cells makes the mean data not statistically significant. Ivabradine did not wash off in any of the experiments, which is consistent with data from other laboratories (Melgari *et al.*, 2015), thus the effect of ivabradine were sustained and unlikely to be due to an experimental artefact.

Different regions of the heart have different distributions of ionic currents. Likewise different layers of the left ventricle have different distributions of ionic currents (Wickenden *et al.*, 1999; Schram *et al.*, 2002). In guinea pigs,  $I_{Kr}$  and  $I_{Ks}$  are smaller in ventricular endocardial cells than in epicardial cells (Main *et al.*, 1998). A smaller  $I_{Ks}$  in left ventricular apex versus basal myocytes may underlie the longer apical APD. In the rabbit,  $I_{Kr}$  appears larger at the ventricular apex in isolated ventricular myocytes than the base (Cheng *et al.*, 1999). Therefore, one potential contributor to the variable effects of ivabradine observed in the present study may be that the cells have originated from different regions of the ventricle. Koncz *et al.* (2011) studied the electrophysiological effects of ivabradine in dog and human cardiac preparations and

concluded that significant prolongation of repolarization was only observed at 10  $\mu\text{M}$  ivabradine. This is in contrast to more recent reports. It is unclear why there are such differences, but variations in species type and recording conditions may be important. In addition, ivabradine is well-known to be a class V (HCN channel blocker) antiarrhythmic drug and to have class I ( $\text{Na}^+$  channels blocker) and Class III ( $\text{K}^+$  channels blocker) antiarrhythmic properties (Tavazzi and Mugelli, 2006). This may be advantageous in the treatment of patients with ischemic heart disease who are liable to disturbances of cardiac rhythm. It might also explain the distinct effect of ivabradine on different cells. Different regions of the left ventricle have different ionic current distributions and as ivabradine affects different ionic currents, this could underlie the variable changes in AP morphology. Note that APD-shortening was observed (statistically significant) despite such heterogeneity.

### **5.3.2 Blocking $I_{\text{Kr}}$ with E4031 and then applying ivabradine obliterated the variable effect of ivabradine on APD**

Ivabradine blocks HCN channels and inhibits the  $I_f$  current. However, HCN channels are predominantly in the SAN and AVN cells and not expressed outside the conduction system. The variable effect of ivabradine on the APD and AP morphology may be mediated by blocking  $\text{K}^+$  currents, particularly  $I_{\text{Kr}}$ . Many studies have found that ivabradine blocks  $I_{\text{Kr}}$  (Miller *et al.*, 2015; Konz *et al.*, 2011; Melgari *et al.*, 2015). Konz *et al.* (2011) reported no significant effect of ivabradine on rabbit ventricular  $I_{\text{K1}}$ , while suggesting that the drug inhibits rabbit ventricular  $I_{\text{Kr}}$ . Miller *et al.* (2015) found that ivabradine prolongs action potentials in mouse cardiac myocytes and blocks the hERG current over a range of concentrations overlapping with those required to block HCN. HERG1 mutations that disrupt C-type inactivation also suppressed block of hERG1 by ivabradine demonstrating the state dependence of block. The most recent study by Melgari *et al.*, (2015) concluded that ivabradine prolongs ventricular repolarization in perfused guinea-pig hearts by blocking hERG/ $I_{\text{Kr}}$  channels. Both studies identified ivabradine as a potent blocker of hERG current with  $\text{IC}_{50}$  in low micro-molar range. The  $\text{IC}_{50}$  for ivabradine block of hERG was 2.07  $\mu\text{M}$  (Melgari *et al.*, 2015) compared to 6.8  $\mu\text{M}$  (Miller *et al.*, 2015). The

difference in  $IC_{50}$  in both studies may be due to differences in temperature and voltage protocols used in the two studies.

My results are consistent with the wider literature. When  $I_{Kr}$  was blocked by E4031 and then ivabradine was applied this abolished the variability in APD and AP shape observed previously, and resulted in there being no additional effect on APD and AP morphology. This suggests that  $I_{Kr}$  is a target for mediating the effects of ivabradine but it is not the only target as ivabradine showed shortening in  $APD_{90}$  when used alone. My data suggest that ivabradine, in addition to inhibiting  $I_{Kr}$ , also affects other currents in ventricular myocytes.

### **5.3.3 Ivabradine shortens APD in some cells**

In the current study, one of the more surprising findings was that ivabradine caused APD shortening in the majority of the cells. This is not consistent with ivabradine only inhibiting a repolarising current, such as  $I_{Kr}$ . What is also difficult to explain is that when  $I_{Kr}$  was blocked, ivabradine had a trend to prolong APD rather than shorten it. These findings may suggest that ivabradine has uncharacterised effects on other cardiac currents. This type of “promiscuity” of pharmacological activity is common in many low affinity channel blockers such as flecanide.

## **Chapter 6. Conclusions, clinical significance, and future works**

### **6.1 Conclusions**

Nitric oxide (NO) signalling has been recently linked with cardiac repolarisation. A number of whole heart studies have suggested a protective role of NO. However, the cellular mechanisms and signalling pathways mediating this effect are largely unknown. A role for NO signalling has also been described in the diurnal variation of cardiac muscle responses to sympathetic stimulation. The current study found that the active period myocytes were more prone to arrhythmias than the resting period myocytes under basal conditions. Moreover, blocking NO synthesis (L-NNA) in the continued presence of  $\beta$ -AR agonist (ISO) shortened APD<sub>90</sub> significantly in the active period myocytes. This suggests that APs of active period myocytes were more affected by inhibiting NO production in the continued presence of ISO. In other words, active period myocytes were more responsive to the presence of ISO, in terms of APD, when NO production was inhibited. These effects are consistent with NO having a protective effect by inhibiting effects of ISO on cardiac repolarisation. NO exerts its effects on AP properties through both cGMP-dependent and cGMP-independent pathways. Each pathway had differential effects. Enhancing the effect of cGMP-dependent pathway by the sGC activator BAY 60-2770 prolonged APD<sub>90</sub> while increasing S-nitrosylation by the denitrosylation inhibitor N6022 shortened APD<sub>90</sub>. However, NO signalling pathway modulators did not show significant effect on the slope of the single cells electrical restitution curves as it did in whole heart studies from previous studies.

Eventually, NO signalling pathways modulate the effects of  $\beta$ -AR stimulation of cardiac repolarisation and electrical restitution through a complex interplay of both cGMP-dependent and nitrosylation dependent mechanisms. Based on the literature and these findings, NO signalling may be a potential therapeutic target for diseases such as LQTS. However, further research is necessary to fully elucidate the regulation of ventricular repolarisation by NO signalling pathways. In this study we also investigated the effect of the bradycardic drug ivabradine on ventricular cardiac repolarization. Ivabradine had variable effect on AP repolarization. However, pretreating myocytes with the I<sub>Kr</sub> blocker E4031 before applying ivabradine abolished

the variable effects of ivabradine on AP repolarization. Suggesting this drug mediates its effects on AP repolarization, in large part, by inhibiting  $I_{Kr}$ .

## **6.2 Clinical significance of the findings in the heart**

Arking *et al.* (2006) identified that extremely long or short QT intervals were associated with a common genetic variant in the NOS1AP gene that encodes carboxy-terminal PDZ ligand of nNOS (CAPON). CAPON is an adaptor protein that binds to the post-synaptic density-protein, discs-large, ZO-1 (PDZ) domain located in the oxygenase domain of nNOS (Zhou and Zhu, 2009). LQTS 1 and 2 are life-threatening cardiac conditions that predispose to Torsade de Pointes (TdP), especially during high sympathetic activity. The underlying mechanism is thought to be linked to the reduced repolarisation capacity of the ventricles as a result of genetic mutations in components of the delayed rectifier  $K^+$  current. LQTS types 1 and 2 are due to mutations in  $I_{Ks}$  and  $I_{Kr}$  respectively.

Crotti *et al.* (2009) reported that in a LQTS population, the occurrence of symptoms and a greater probability of sudden cardiac death were linked with NOS1AP variants. These studies suggested that NO signalling could play a role in the regulation of the QT interval and cardiac repolarisation. Furthermore, Chang *et al.* (2008) found that adenoviral-mediated overexpression of CAPON in guinea pig ventricular myocytes caused shortening of APD through a mechanism involving inhibition of  $I_{Ca,L}$  and enhancement of  $I_{Kr}$ . Pre-treating the myocytes with the NOS inhibitor L-NAME reversed these effects. In addition, CAPON overexpression was also associated with an up-regulation of nNOS protein levels, an enhancement of nNOS activity and a modest increase in NO generation. Consequently, it is likely that the effects of CAPON overexpression were mediated by a nNOS signalling pathway. The role of CAPON under conditions of  $\beta$ -AR stimulation has not yet been investigated.

Current LQTS therapies include  $\beta$ -AR blockers, cardiac sympathetic denervation, and defibrillators (Chang *et al.*, 2008). The use of  $\beta$ -blockers is a highly effective therapy for LQT1 patients, but less effective for LQT2 or 3 (Vincent *et al.*, 2009). NO signalling is known to modulate  $\beta$ -AR signalling and may therefore be a target for therapeutic agents aimed at treating LQTS. The findings in the current study provide

evidence for an important role of NO signalling pathways in regulating cardiac ventricular repolarisation under conditions of sympathetic stimulation. Along with other studies, the work contributes to evidence that NO signalling pathways have a protective function, dampening the effects of  $\beta$ -AR stimulation on cardiac repolarisation and contractility and reducing the risk of arrhythmias.

NO signalling has recently been shown to play a protective role against arrhythmias such as ventricular fibrillation (VF). Susceptibility to VF can be predicted from electrical restitution properties of the heart. The maximum slope of the restitution curve is used to predict the risk of arrhythmia, with a steeper slope associated with a greater chance of VF (Ng *et al.*, 2007). Brack *et al.* (2007) have shown that NO signalling plays an important role in the protective effect of vagus nerve stimulation (VS) against induction of VF in an isolated Langendorff perfused rabbit heart with intact dual autonomic innervation. VS flattened the slope of the restitution curve and increased the threshold for inducing VF. However, the slope became steeper with VS in the presence of the NOS inhibitor L-NNA. In addition, an increase in the VF threshold was no longer observed. In summary, the protective effects of VS were absent by inhibiting NO synthesis, suggesting these effects are likely mediated by NO signalling. Moreover, Brack *et al.* (2009) found that NO was released and detected in the ventricle during VNS, using the NO fluorescent indicator 4,5-diaminofluorescein diacetate (DAF-2 DA). DAF-2 DA fluorescence increased during VS and was inhibited in the presence of L-NNA or a nNOS-specific inhibitor. These studies provide evidence that VS increases NO in the ventricles and this plays an essential role in the protection against arrhythmia. Thus it appears likely that NO signalling is important in both parasympathetic and sympathetic regulation of cardiac function.

Moreover, ivabradine has now been associated with an increased risk of TdP and sudden death. Recent findings suggest that ivabradine blocks  $I_{Kr}$  at similar concentrations to the intended target – HCN channels in SAN (Melgari *et al.*, 2015). My results suggest that there are highly variable effects of cardiac AP repolarisation. Not just AP prolongation (as expected from  $I_{Kr}$  inhibition) but also AP shortening and AP triangulation. This may indicate an increased risk of a greater dispersion of

repolarisation, which is thought to be a major mechanism in establishing conditions for re-entrant circuits and VF.

### **6.3 Future work:**

To further investigate the mechanisms underlying the regulation of repolarisation by NO signalling pathways in guinea-pig isolated left ventricular myocytes, I suggests conducting the following experiments:

-Perform voltage clamp and calcium imaging studies to investigate the molecular aspects of diurnal variation behind the effects of NO on cardiac contractility.

-Investigate diurnal variation of repolarisation currents and their responses to  $\beta$ -AR stimulation.

- Investigate the effect of NO signalling pathways in modulating  $\beta$ -AR effects on  $I_{Ca,L}$ ,  $I_{NCX}$  and the repolarization currents  $I_{Kr}$  and  $I_{Ks}$ .

- Investigate the role of PDEs in NO signalling on Isoprenaline stimulated  $I_{Ca,L}$  and  $I_{Ks}$

-Investigate the S-nitrosylation pathway further by detecting and quantifying S-nitrosylated proteins using biotin-switch techniques.

## **Chapter 7:**

### **Bibliography**

Aarnoudse, A.J.L., Newton-Cheh, C., de Bakker, P.I., Straus, S.M., Kors, J.A., Hofman, A., Uitterlinden, A.G., Witteman, J.C. and Stricker, B.H., 2007. Common NOS1AP variants are associated with a prolonged QTc interval in the Rotterdam Study. *Circulation*, 116(1), pp.10-16.

Abi-Gerges, N., Fischmeister, R. and Méry, P.F., 2001. G protein-mediated inhibitory effect of a nitric oxide donor on the L-type Ca<sup>2+</sup> current in rat ventricular myocytes. *The Journal of Physiology*, 531(1), pp.117-130.

Abi-Gerges, N., Hove-Madsen, L., Fischmeister, R. and Méry, P.F., 1997. A comparative study of the effects of three guanylyl cyclase inhibitors on the L-type Ca<sup>2+</sup> and muscarinic K<sup>+</sup> currents in frog cardiac myocytes. *British journal of pharmacology*, 121(7), pp.1369-1377.

Abramochkin, D.V., Makarenko, E.Y., Mitrochin, V.M., Tian, B., Kalugin, L.Y., Sutyagin, P.V. and Kamkin, A.G., 2012. Effect of Nitric Oxide on Mechanoelectric Feedback in Rat Right Atrium. *Bulletin of experimental biology and medicine*, 153(1), pp.32-35.

Ahern, G.P., Hsu, S.F., Klyachko, V.A. and Jackson, M.B., 2000. Induction of persistent sodium current by exogenous and endogenous nitric oxide. *Journal of Biological Chemistry*, 275(37), pp.28810-28815.

Ahmed, G.U., Xu, Y., Dong, P.H., Zhang, Z., Eiserich, J. and Chiamvimonvat, N., 2001. Nitric oxide modulates cardiac Na<sup>+</sup> channel via protein kinase A and protein kinase G. *Circulation research*, 89(11), pp.1005-1013.

Alderton, W.K., Cooper, C.E. and Knowles, R.G., 2001. Nitric oxide synthases: structure, function and inhibition. *Biochemical Journal*, 357(3), pp.593-615.

Alexander, S., Peters, J., Mead, A. and Lewis, S., 1999. TiPS receptor and ion channel nomenclature supplement 1999. *Trends in Pharmacological Sciences*, 19, p.1.

Andreopoulos, S. and Papapetropoulos, A., 2000. Molecular aspects of soluble guanylyl cyclase regulation. *General Pharmacology: The Vascular System*, 34(3), pp.147-157.

Angelone, T., Filice, E., Quintieri, A.M., Imbrogno, S., Recchia, A., Pulerà, E., Mannarino, C., Pellegrino, D. and Cerra, M.C., 2008.  $\beta_3$ -Adrenoceptors modulate left

ventricular relaxation in the rat heart via the NO-cGMP-PKG pathway. *Acta physiologica*, 193(3), pp.229-239.

Aragon, J.P., Elston, M., Grinsfelder, D.B., Lavu, M., Calvert, J.W., Wright, H.M., Barouch, L.A. and Lefer, D.J., 2010. Role of eNOS and nNOS in Beta3-Adrenergic Receptor Mediated Cardioprotection. *Circulation*, 122(21 Supplement), p.A12052.

Arking, D.E., Pfeufer, A., Post, W., Kao, W.L., Newton-Cheh, C., Ikeda, M., West, K., Kashuk, C., Akyol, M., Perz, S. and Jalilzadeh, S., 2006. A common genetic variant in the NOS1 regulator NOS1AP modulates cardiac repolarization. *Nature genetics*, 38(6), pp.644-651.

Asada, K., Kurokawa, J. and Furukawa, T., 2009. Redox-and calmodulin-dependent S-nitrosylation of the KCNQ1 channel. *Journal of Biological Chemistry*, 284(9), pp.6014-6020.

Axon Instruments, I., 1999. Axopatch 200B Patch Clamp Theory and Operation. Axon Instruments, Inc.

Bai, C.X., Namekata, I., Kurokawa, J., Tanaka, H., Shigenobu, K. and Furukawa, T., 2005. Role of nitric oxide in Ca<sup>2+</sup> sensitivity of the slowly activating delayed rectifier K<sup>+</sup> current in cardiac myocytes. *Circulation research*, 96(1), pp.64-72.

Bai, C.X., Takahashi, K., Masumiya, H., Sawanobori, T. and Furukawa, T., 2004. Nitric oxide-dependent modulation of the delayed rectifier K<sup>+</sup> current and the L-type Ca<sup>2+</sup> current by ginsenoside Re, an ingredient of Panax ginseng, in guinea-pig cardiomyocytes. *British journal of pharmacology*, 142(3), pp.567-575.

Balligand, J.L., Kobzik, L., Han, X., Kaye, D.M., Belhassen, L., O'Hara, D.S., Kelly, R.A., Smith, T.W. and Michel, T., 1995. Nitric oxide-dependent parasympathetic signaling is due to activation of constitutive endothelial (type III) nitric oxide synthase in cardiac myocytes. *Journal of Biological Chemistry*, 270(24), pp.14582-14586.

Balligand, J.L., Ungureanu-Longrois, D., Simmons, W.W., Pimental, D., Malinski, T.A., Kapturczak, M., Taha, Z., Lowenstein, C.J., Davidoff, A.J. and Kelly, R.A., 1994. Cytokine-inducible nitric oxide synthase (iNOS) expression in cardiac myocytes. Characterization and regulation of iNOS expression and detection of iNOS activity in single cardiac myocytes in vitro. *Journal of Biological Chemistry*, 269(44), pp.27580-27588.

Banville, I. and Gray, R.A., 2002. Effect of action potential duration and conduction velocity restitution and their spatial dispersion on alternans and the stability of arrhythmias. *Journal of cardiovascular electrophysiology*, 13(11), pp.1141-1149.

Banville, I., Gray, R.A. and Ideker, R.E., 1998. Optimization of high-resolution video imaging system to study cardiac spatiotemporal patterns. *Ann Biomed Eng*, 26(suppl 1), p.S19.

Barouch, L.A., Harrison, R.W., Skaf, M.W., Rosas, G.O., Cappola, T.P., Kobeissi, Z.A., Hobai, I.A., Lemmon, C.A., Burnett, A.L., O'Rourke, B. and Rodriguez, E.R., 2002. Nitric oxide regulates the heart by spatial confinement of nitric oxide synthase isoforms. *Nature*, 416(6878), pp.337-339.

Barouch, L.A., Harrison, R.W., Skaf, M.W., Rosas, G.O., Cappola, T.P., Kobeissi, Z.A., Hobai, I.A., Lemmon, C.A., Burnett, A.L., O'Rourke, B. and Rodriguez, E.R., 2002. Nitric oxide regulates the heart by spatial confinement of nitric oxide synthase isoforms. *Nature*, 416(6878), pp.337-339.

Beigi, F., Gonzalez, D.R., Minhas, K.M., Sun, Q.A., Foster, M.W., Khan, S.A., Treuer, A.V., Dulce, R.A., Harrison, R.W., Saraiva, R.M. and Premer, C., 2012. Dynamic denitrosylation via S-nitrosoglutathione reductase regulates cardiovascular function. *Proceedings of the National Academy of Sciences*, 109(11), pp.4314-4319.

Bellamy, T.C. and Garthwaite, J., 2002. The receptor-like properties of nitric oxide-activated soluble guanylyl cyclase in intact cells. *Molecular and cellular biochemistry*, 230(1-2), pp.165-176.

Benhar, M., Forrester, M.T. and Stamler, J.S., 2009. Protein denitrosylation: enzymatic mechanisms and cellular functions. *Nature reviews Molecular cell biology*, 10(10), pp.721-732.

Bers, D.M. and Perez-Reyes, E., 1999. Ca channels in cardiac myocytes: structure and function in Ca influx and intracellular Ca release. *Cardiovascular research*, 42(2), pp.339-360.

Bers, D.M., 2002. Cardiac excitation–contraction coupling. *Nature*, 415(6868), pp.198-205.

Best, J.M. and Kamp, T.J., 2012. Different subcellular populations of L-type Ca<sup>2+</sup> channels exhibit unique regulation and functional roles in cardiomyocytes. *Journal of molecular and cellular cardiology*, 52(2), pp.376-387.

Bexton, R.S., Vallin, H.O. and Camm, A.J., 1986. Diurnal variation of the QT interval-influence of the autonomic nervous system. *British heart journal*, 55(3), pp.253-258.

Bice, J.S., Keim, Y., Stasch, J.P. and Baxter, G.F., 2014. NO-independent stimulation or activation of soluble guanylyl cyclase during early reperfusion limits infarct size. *Cardiovascular research*, 101(2), pp.220-228.

Bickley, L. and Szilagyi, P.G., 2012. *Bates' guide to physical examination and history-taking*. Lippincott Williams & Wilkins.

Bloch, W., Fleischmann, B.K., Lorke, D.E., Andressen, C., Hops, B., Hescheler, J. and Addicks, K., 1999. Nitric oxide synthase expression and role during cardiomyogenesis. *Cardiovascular research*, 43(3), pp.675-684.

Blonder, J.P., Mutka, S.C., Sun, X., Qiu, J., Green, L.H., Mehra, N.K., Boyanapalli, R., Suniga, M., Look, K., Delany, C. and Richards, J.P., 2014. Pharmacologic inhibition of S-nitrosoglutathione reductase protects against experimental asthma in BALB/c mice through attenuation of both bronchoconstriction and inflammation. *BMC pulmonary medicine*, 14(1), p.1.

Bolaños, J.P., Almeida, A., Stewart, V., Peuchen, S., Land, J.M., Clark, J.B. and Heales, S.J., 1997. Nitric oxide-mediated mitochondrial damage in the brain: Mechanisms and implications for neurodegenerative diseases. *Journal of neurochemistry*, 68(6), pp.2227-2240.

Brack, K.E., Patel, V.H., Coote, J.H. and Ng, G.A., 2007. Nitric oxide mediates the vagal protective effect on ventricular fibrillation via effects on action potential duration restitution in the rabbit heart. *The Journal of physiology*, 583(2), pp.695-704.

Brack, K.E., Patel, V.H., Mantravardi, R., Coote, J.H. and Ng, G.A., 2009. Direct evidence of nitric oxide release from neuronal nitric oxide synthase activation in the left ventricle as a result of cervical vagus nerve stimulation. *The Journal of physiology*, 587(12), pp.3045-3054.

Brack, K.E., Winter, J. and Ng, G.A., 2013. Mechanisms underlying the autonomic modulation of ventricular fibrillation initiation—tentative prophylactic properties of vagus nerve stimulation on malignant arrhythmias in heart failure. *Heart failure reviews*, 18(4), pp.389-408.

Brahmajothi, M.V. and Campbell, D.L., 1999. Heterogeneous Basal Expression of Nitric Oxide Synthase and Superoxide Dismutase Isoforms in Mammalian Heart Implications for Mechanisms Governing Indirect and Direct Nitric Oxide-Related Effects. *Circulation Research*, 85(7), pp.575-587.

Brochet, D.X., Yang, D., Di Maio, A., Lederer, W.J., Franzini-Armstrong, C. and Cheng, H., 2005. Ca<sup>2+</sup> blinks: rapid nanoscopic store calcium signaling.

*Proceedings of the National Academy of Sciences of the United States of America*, 102(8), pp.3099-3104.

Bryant, S.M., Wan, X., Shipsey, S.J. and Hart, G., 1998. Regional differences in the delayed rectifier current (IKr and IKs) contribute to the differences in action potential duration in basal left ventricular myocytes in guinea-pig. *Cardiovascular research*, 40(2), pp.322-331.

Cameron, J.S., Hoffmann, K.E., Zia, C., Hemmett, H.M., Kronsteiner, A. and Lee, C.M., 2003. A role for nitric oxide in hypoxia-induced activation of cardiac KATP channels in goldfish (*Carassius auratus*). *Journal of experimental biology*, 206(22), pp.4057-4065.

Camm, A.J. and Lau, C.P., 2003. Electrophysiological effects of a single intravenous administration of ivabradine (S 16257) in adult patients with normal baseline electrophysiology. *Drugs in R & D*, 4(2), pp.83-89.

Campbell, D.L., Stamler, J.S. and Strauss, H.C., 1996. Redox modulation of L-type calcium channels in ferret ventricular myocytes. Dual mechanism regulation by nitric oxide and S-nitrosothiols. *The Journal of general physiology*, 108(4), pp.277-293.

Cao, J.M., Qu, Z., Kim, Y.H., Wu, T.J., Garfinkel, A., Weiss, J.N., Karagueuzian, H.S. and Chen, P.S., 1999. Spatiotemporal heterogeneity in the induction of ventricular fibrillation by rapid pacing importance of cardiac restitution properties. *Circulation research*, 84(11), pp.1318-1331.

Captan, H.P. and Desai, P.A., Heart Rate Slowing by If Inhibition.

Carmeliet, E., 2004. Intracellular Ca<sup>2+</sup> concentration and rate adaptation of the cardiac action potential. *Cell calcium*, 35(6), pp.557-573.

Castro, L.R., Schittl, J. and Fischmeister, R., 2010. Feedback control through cGMP-dependent protein kinase contributes to differential regulation and compartmentation of cGMP in rat cardiac myocytes. *Circulation research*, 107(10), pp.1232-1240.

Castro, L.R., Verde, I., Cooper, D.M. and Fischmeister, R., 2006. Cyclic guanosine monophosphate compartmentation in rat cardiac myocytes. *Circulation*, 113(18), pp.2221-2228.

Catterall, W.A., 1991. Functional subunit structure of voltage-gated calcium channels. *Science*, 253(5027), pp.1499-1500.

Catterall, W.A., 2000. Structure and regulation of voltage-gated Ca<sup>2+</sup> channels. *Annual review of cell and developmental biology*, 16(1), pp.521-555.

Catterall, W.A., Perez-Reyes, E., Snutch, T.P. and Striessnig, J., 2005. International Union of Pharmacology. XLVIII. Nomenclature and structure-function relationships of voltage-gated calcium channels. *Pharmacological reviews*, 57(4), pp.411-425.

Caves, R.E., 2015. *Nitric oxide signalling and the regulation of cardiac repolarisation* (Doctoral dissertation, Department of Cell Physiology and Pharmacology).

Cawley, S.M., Kolodziej, S., Ichinose, F., Brouckaert, P., Buys, E.S. and Bloch, K.D., 2011. sGC $\alpha$ 1 mediates the negative inotropic effects of NO in cardiac myocytes independent of changes in calcium handling. *American Journal of Physiology-Heart and Circulatory Physiology*, 301(1), pp.H157-H163.

Chan, N.N., Vallance, P. and Colhoun, H.M., 2000. Nitric oxide and vascular responses in Type I diabetes. *Diabetologia*, 43(2), pp.137-147.

Chang, K.C., Barth, A.S., Sasano, T., Kizana, E., Kashiwakura, Y., Zhang, Y., Foster, D.B. and Marbán, E., 2008. CAPON modulates cardiac repolarization via neuronal nitric oxide synthase signaling in the heart. *Proceedings of the National Academy of Sciences*, 105(11), pp.4477-4482.

Charpentier, F.L.A.V.I.E.N. and Rosen, M.R., 1994. Beta-adrenergic regulation of action potentials and automaticity in young and adult canine purkinje fibers. *American Journal of Physiology-Heart and Circulatory Physiology*, 266(6), pp.H2310-H2319.

Cheng, J., Kamiya, K., Liu, W., Tsuji, Y., Toyama, J. and Kodama, I., 1999. Heterogeneous distribution of the two components of delayed rectifier K<sup>+</sup> current: a potential mechanism of the proarrhythmic effects of methanesulfonanilideclass III agents. *Cardiovascular research*, 43(1), pp.135-147.

Cheng, J., Kamiya, K., Liu, W., Tsuji, Y., Toyama, J. and Kodama, I., 1999. Heterogeneous distribution of the two components of delayed rectifier K<sup>+</sup> current: a potential mechanism of the proarrhythmic effects of methanesulfonanilideclass III agents. *Cardiovascular research*, 43(1), pp.135-147.

Cherry, E.M. and Fenton, F.H., 2004. Suppression of alternans and conduction blocks despite steep APD restitution: electrotonic, memory, and conduction velocity restitution effects. *American Journal of Physiology-Heart and Circulatory Physiology*, 286(6), pp.H2332-H2341.

Cho, H.S., Takano, M. and Noma, A., 2003. The electrophysiological properties of spontaneously beating pacemaker cells isolated from mouse sinoatrial node. *The Journal of physiology*, 550(1), pp.169-180.

Choate, J.K. and Paterson, D.J., 1999. Nitric oxide inhibits the positive chronotropic and inotropic responses to sympathetic nerve stimulation in the isolated guinea-pig atria. *Journal of the autonomic nervous system*, 75(2), pp.100-108.

Choi, H., Tostes, R.C. and Webb, R.C., 2011. Thioredoxin reductase inhibition reduces relaxation by increasing oxidative stress and s-nitrosylation in mouse aorta. *Journal of cardiovascular pharmacology*, 58(5), p.522.

CHOWDHARY, S. and TOWNEND, J.N., 1999. Role of nitric oxide in the regulation of cardiovascular autonomic control. *Clinical science*, 97(1), pp.5-17.

Chowdhary, S., Vaile, J.C., Fletcher, J., Ross, H.F., Coote, J.H. and Townend, J.N., 2000. Nitric oxide and cardiac autonomic control in humans. *Hypertension*, 36(2), pp.264-269.

Colagiovanni, D.B., Drolet, D.W., Langlois-Forget, E., Piché, M.P., Looker, D. and Rosenthal, G.J., 2012. A nonclinical safety and pharmacokinetic evaluation of N6022: a first-in-class S-nitrosoglutathione reductase inhibitor for the treatment of asthma. *Regulatory Toxicology and Pharmacology*, 62(1), pp.115-124.

Collins, H.E. and Rodrigo, G.C., 2010. Inotropic Response of Cardiac Ventricular Myocytes to  $\beta$ -Adrenergic Stimulation With Isoproterenol Exhibits Diurnal Variation Involvement of Nitric Oxide. *Circulation research*, 106(7), pp.1244-1252.

Conlon, K. and Kidd, C., 1999. Neuronal nitric oxide facilitates vagal chronotropic and dromotropic actions on the heart. *Journal of the autonomic nervous system*, 75(2), pp.136-146.

Conrath, C.E. and Opthof, T., 2006. Ventricular repolarization: an overview of (patho) physiology, sympathetic effects and genetic aspects. *Progress in biophysics and molecular biology*, 92(3), pp.269-307.

Corbin, J.D., Turko, I.V., Beasley, A. and Francis, S.H., 2000. Phosphorylation of phosphodiesterase-5 by cyclic nucleotide-dependent protein kinase alters its catalytic and allosteric cGMP-binding activities. *European Journal of Biochemistry*, 267(9), pp.2760-2767.

Crotti, L., Celano, G., Dagradi, F. and Schwartz, P.J., 2008. Congenital long QT syndrome. *Orphanet journal of rare diseases*, 3(1), p.1.

Crotti, L., Monti, M.C., Insolia, R., Peljto, A., Goosen, A., Brink, P.A., Greenberg, D.A., Schwartz, P.J. and George, A.L., 2009. NOS1AP is a genetic modifier of the long-QT syndrome. *Circulation*, 120(17), pp.1657-1663.

Cutler, M.J., Wan, X., Laurita, K.R., Hajjar, R.J. and Rosenbaum, D.S., 2009. Targeted SERCA2a gene expression identifies molecular mechanism and therapeutic target for arrhythmogenic cardiac alternans. *Circulation: Arrhythmia and Electrophysiology*, 2(6), pp.686-694.

Decker, K.F., Heijman, J., Silva, J.R., Hund, T.J. and Rudy, Y., 2009. Properties and ionic mechanisms of action potential adaptation, restitution, and accommodation in canine epicardium. *American Journal of Physiology-Heart and Circulatory Physiology*, 296(4), pp.H1017-H1026.

Degaute, J.P., Van De Borne, P., Linkowski, P. and Van Cauter, E., 1991. Quantitative analysis of the 24-hour blood pressure and heart rate patterns in young men. *Hypertension*, 18(2), pp.199-210.

DiFrancesco, D., 2010. The role of the funny current in pacemaker activity. *Circulation research*, 106(3), pp.434-446.

Doyle, D.A., Cabral, J.M., Pfuetzner, R.A., Kuo, A., Gulbis, J.M., Cohen, S.L., Chait, B.T. and MacKinnon, R., 1998. The structure of the potassium channel: molecular basis of K<sup>+</sup> conduction and selectivity. *science*, 280(5360), pp.69-77.

Draijer, R., Vaandrager, A.B., Nolte, C., de Jonge, H.R., Walter, U. and van Hinsbergh, V.W., 1995. Expression of cGMP-dependent protein kinase I and phosphorylation of its substrate, vasodilator-stimulated phosphoprotein, in human endothelial cells of different origin. *Circulation research*, 77(5), pp.897-905.

Durgan, D.J., Hotze, M.A., Tomlin, T.M., Egbejimi, O., Graveleau, C., Abel, E.D., Shaw, C.A., Bray, M.S., Hardin, P.E. and Young, M.E., 2005. The intrinsic circadian clock within the cardiomyocyte. *American Journal of Physiology-Heart and Circulatory Physiology*, 289(4), pp.H1530-H1541.

Dutka, T.L., Mollica, J.P. and Lamb, G.D., 2011. Differential effects of peroxynitrite on contractile protein properties in fast-and slow-twitch skeletal muscle fibers of rat. *Journal of Applied Physiology*, 110(3), pp.705-716.

Ebihara, Y. and Karmazyn, M., 1996. Inhibition of  $\beta$ -but not a  $\alpha$ 1-mediated adrenergic responses in isolated hearts and cardiomyocytes by nitric oxide and 8-bromo cyclic GMP. *Cardiovascular research*, 32(3), pp.622-629.

Eckel, L., Gristwood, R.W., Nawrath, H., Owen, D.A. and Satter, P., 1982. Inotropic and electrophysiological effects of histamine on human ventricular heart muscle. *The Journal of physiology*, 330(1), pp.111-123.

- Edwards, J.N. and Blatter, L.A., 2014. Cardiac alternans and intracellular calcium cycling. *Clinical and Experimental Pharmacology and Physiology*, 41(7), pp.524-532.
- Eijgelsheim, M., Newton-Cheh, C., Aarnoudse, A.L., van Noord, C., Witteman, J.C., Hofman, A., Uitterlinden, A.G., Stricker, B.H., 2009. Genetic variation in NOS1AP is associated with sudden cardiac death: evidence from the Rotterdam Study. *Human Molecular Genetics*. **18**, 4213-4218.
- Eisner, D.A., Dibb, K.M. and Trafford, A.W., 2009. The mechanism and significance of the slow changes of ventricular action potential duration following a change of heart rate. *Experimental physiology*, 94(5), pp.520-528.
- Eldstrom, J. and Fedida, D., 2011. The voltage-gated channel accessory protein KCNE2: multiple ion channel partners, multiple ways to long QT syndrome. *Expert reviews in molecular medicine*, 13, p.e38.
- El-Sherif, N., Caref, E.B., Yin, H. and Restivo, M., 1996. The electrophysiological mechanism of ventricular arrhythmias in the long QT syndrome tridimensional mapping of activation and recovery patterns. *Circulation Research*, 79(3), pp.474-492.
- Fabiato, A., 1983. Calcium-induced release of calcium from the cardiac sarcoplasmic reticulum. *American Journal of Physiology-Cell Physiology*, 245(1), pp.C1-C14.
- Fakler, B., Brändle, U., Glowatzki, E., Weidemann, S., Zenner, H.P. and Ruppersberg, J.P., 1995. Strong voltage-dependent inward rectification of inward rectifier K<sup>+</sup> channels is caused by intracellular spermine. *Cell*, 80(1), pp.149-154.
- Feil, R., Lohmann, S.M., de Jonge, H., Walter, U. and Hofmann, F., 2003. Cyclic GMP-dependent protein kinases and the cardiovascular system insights from genetically modified mice. *Circulation research*, 93(10), pp.907-916.
- Fenton, F.H., Cherry, E.M., Hastings, H.M. and Evans, S.J., 2002. Multiple mechanisms of spiral wave breakup in a model of cardiac electrical activity. *Chaos: An Interdisciplinary Journal of Nonlinear Science*, 12(3), pp.852-892.
- Ferdinandy, P., 2006. Peroxynitrite: just an oxidative/nitrosative stressor or a physiological regulator as well?. *British journal of pharmacology*, 148(1), pp.1-3.
- Feron, O., Belhassen, L., Kobzik, L., Smith, T.W., Kelly, R.A. and Michel, T., 1996. Endothelial nitric oxide synthase targeting to caveolae specific interactions with caveolin isoforms in cardiac myocytes and endothelial cells. *Journal of Biological Chemistry*, 271(37), pp.22810-22814.

Fischmeister, R., Castro, L.R., Abi-Gerges, A., Rochais, F., Jurevičius, J., Leroy, J. and Vandecasteele, G., 2006. Compartmentation of cyclic nucleotide signaling in the heart the role of cyclic nucleotide phosphodiesterases. *Circulation research*, 99(8), pp.816-828.

Fleenor, B.S., Seals, D.R., Zigler, M.L. and Sindler, A.L., 2012. Superoxide-lowering therapy with TEMPOL reverses arterial dysfunction with aging in mice. *Aging cell*, 11(2), pp.269-276.

Fox, J.J., McHarg, J.L. and Gilmour, R.F., 2002. Ionic mechanism of electrical alternans. *American Journal of Physiology-Heart and Circulatory Physiology*, 282(2), pp.H516-H530.

Fozzard, H.A., Haber, E., Jennings, R.B., Katz, A.M. and Morgan, H.I., 1991. *The Heart and Cardiovascular System*, 2193 pp.

Francis, S.H. and Corbin, J.D., 1999. Cyclic nucleotide-dependent protein kinases: intracellular receptors for cAMP and cGMP action. *Critical reviews in clinical laboratory sciences*, 36(4), pp.275-328.

Francis, S.H., Busch, J.L. and Corbin, J.D., 2010. cGMP-dependent protein kinases and cGMP phosphodiesterases in nitric oxide and cGMP action. *Pharmacological reviews*, 62(3), pp.525-563.

Francis, S.H., Colbran, J.L., McAllister-Lucas, L.M. and Corbin, J.D., 1994. Zinc interactions and conserved motifs of the cGMP-binding cGMP-specific phosphodiesterase suggest that it is a zinc hydrolase. *Journal of Biological Chemistry*, 269(36), pp.22477-22480.

Gaborit, N., Le Bouter, S., Szuts, V., Varro, A., Escande, D., Nattel, S. and Demolombe, S., 2007. Regional and tissue specific transcript signatures of ion channel genes in the non-diseased human heart. *The Journal of physiology*, 582(2), pp.675-693.

Gallo, M.P., Ghigo, D., Bosia, A., Alloatti, G., Costamagna, C., Penna, C. and Levi, R.C., 1998. Modulation of guinea-pig cardiac L-type calcium current by nitric oxide synthase inhibitors. *The Journal of physiology*, 506(3), pp.639-651.

Gallo, M.P., Ghigo, D., Bosia, A., Alloatti, G., Costamagna, C., Penna, C. and Levi, R.C., 1998. Modulation of guinea-pig cardiac L-type calcium current by nitric oxide synthase inhibitors. *The Journal of physiology*, 506(3), pp.639-651.

Gallo, M.P., Malan, D., Bedendi, I., Biasin, C., Alloatti, G. and Levi, R.C., 2001. Regulation of cardiac calcium current by NO and cGMP-modulating agents. *Pflügers Archiv*, 441(5), pp.621-628.

Gauthier, C., Tavernier, G., Charpentier, F., Langin, D. and Le Marec, H., 1996. Functional beta3-adrenoceptor in the human heart. *Journal of Clinical Investigation*, 98(2), p.556.

Gauthier, C., Tavernier, G., Charpentier, F., Langin, D. and Le Marec, H., 1996. Functional beta3-adrenoceptor in the human heart. *Journal of Clinical Investigation*, 98(2), p.556.

Gidday, J.M., Shah, A.R., Maceren, R.G., Wang, Q., Pelligrino, D.A., Holtzman, D.M. and Park, T.S., 1999. Nitric oxide mediates cerebral ischemic tolerance in a neonatal rat model of hypoxic preconditioning. *Journal of Cerebral Blood Flow & Metabolism*, 19(3), pp.331-340.

Glitsch, H.G., 2001. Electrophysiology of the sodium-potassium-ATPase in cardiac cells. *Physiological Reviews*, 81(4), pp.1791-1826.

Goldhaber, J.I., Xie, L.H., Duong, T., Motter, C., Khuu, K. and Weiss, J.N., 2005. Action potential duration restitution and alternans in rabbit ventricular myocytes the key role of intracellular calcium cycling. *Circulation research*, 96(4), pp.459-466.

Gómez, R., Caballero, R., Barana, A., Amorós, I., Calvo, E., López, J.A., Klein, H., Vaquero, M., Osuna, L., Atienza, F. and Almendral, J., 2009. Nitric oxide increases cardiac IK1 by nitrosylation of cysteine 76 of Kir2. 1 channels. *Circulation research*, 105(4), pp.383-392.

Gómez, R., Núñez, L., Vaquero, M., Amorós, I., Barana, A., de Prada, T., Macaya, C., Maroto, L., Rodríguez, E., Caballero, R. and López-Farré, A., 2008. Nitric oxide inhibits Kv4. 3 and human cardiac transient outward potassium current (Ito1). *Cardiovascular research*, 80(3), pp.375-384.

Gonzalez, D.R., Beigi, F., Treuer, A.V. and Hare, J.M., 2007. Deficient ryanodine receptor S-nitrosylation increases sarcoplasmic reticulum calcium leak and arrhythmogenesis in cardiomyocytes. *Proceedings of the National Academy of Sciences*, 104(51), pp.20612-20617.

Gonzalez, D.R., Treuer, A., Sun, Q.A., Stamler, J.S. and Hare, J.M., 2009. S-Nitrosylation of cardiac ion channels. *Journal of cardiovascular pharmacology*, 54(3), p.188.

Grant, A.O., 2009. Cardiac ion channels. *Circulation: Arrhythmia and Electrophysiology*, 2(2), pp.185-194.

Green, L.S., Chun, L.E., Patton, A.K., Sun, X., Rosenthal, G.J. and Richards, J.P., 2012. Mechanism of inhibition for N6022, a first-in-class drug targeting S-nitrosogluthathione reductase. *Biochemistry*, 51(10), pp.2157-2168.

Grushin, K.S., Nenov, M.N., Dynnik, V.V., Semushina, S.G., Pakhomova, I.A., Murashev, A.N. and Kokoz, Y.M., 2008. Role of the NO-cGMP cascade in regulation of L-type Ca<sup>2+</sup> currents in isolated cardiomyocytes. *Biochemistry (Moscow) Supplement Series A: Membrane and Cell Biology*, 2(3), pp.243-252.

Gussak, I., Antzelevitch, C. and Wilde, A.A., 2008. Electrical diseases of the heart. *Genetics, mechanisms, treatment, prevention.//Springer.-2008.-520 pp.*

Haendeler, J., Hoffmann, J., Tischler, V., Berk, B.C., Zeiher, A.M. and Dimmeler, S., 2002. Redox regulatory and anti-apoptotic functions of thioredoxin depend on S-nitrosylation at cysteine 69. *Nature cell biology*, 4(10), pp.743-749.

Hall, J.E., 2015. *Guyton and Hall textbook of medical physiology*. Elsevier Health Sciences.

Hammond, J. and Balligand, J.L., 2012. Nitric oxide synthase and cyclic GMP signaling in cardiac myocytes: from contractility to remodeling. *Journal of molecular and cellular cardiology*, 52(2), pp.330-340.

Hammond, J. and Balligand, J.L., 2012. Nitric oxide synthase and cyclic GMP signaling in cardiac myocytes: from contractility to remodeling. *Journal of molecular and cellular cardiology*, 52(2), pp.330-340.

Han, X., Kobzik, L., Balligand, J.L., Kelly, R.A. and Smith, T.W., 1996. Nitric oxide synthase (NOS3)-mediated cholinergic modulation of Ca<sup>2+</sup> current in adult rabbit atrioventricular nodal cells. *Circulation Research*, 78(6), pp.998-1008.

Hancox, J.C., Levi, A.J. and Witchel, H.J., 1998. Time course and voltage dependence of expressed HERG current compared with native "rapid" delayed rectifier K current during the cardiac ventricular action potential. *Pflügers Archiv*, 436(6), pp.843-853.

Hancox, J.C., McPate, M.J., El Harchi, A. and hong Zhang, Y., 2008. The hERG potassium channel and hERG screening for drug-induced torsades de pointes. *Pharmacology & therapeutics*, 119(2), pp.118-132.

Harteneck, C., Wedel, B., Koesling, D. and Bo, E., 1991. Molecular cloning and expression of a new  $\alpha$ -subunit of soluble guanylyl cyclase Interchangeability of the  $\alpha$ -subunits of the enzyme. *FEBS letters*, 292(1), pp.217-222.

Herring, N. and Paterson, D.J., 2001. Nitric oxide-cGMP pathway facilitates acetylcholine release and bradycardia during vagal nerve stimulation in the guinea-pig in vitro. *The Journal of physiology*, 535(2), pp.507-518.

Herring, N., Golding, S. and Paterson, D.J., 2000. Pre-synaptic NO-cGMP pathway modulates vagal control of heart rate in isolated adult guinea pig atria. *Journal of molecular and cellular cardiology*, 32(10), pp.1795-1804.

Hibino, H., Inanobe, A., Furutani, K., Murakami, S., Findlay, I.A.N. and Kurachi, Y., 2010. Inwardly rectifying potassium channels: their structure, function, and physiological roles. *Physiological reviews*, 90(1), pp.291-366.

Hille, B., 2001. *Ion channels of excitable membranes* (Vol. 507). Sunderland, MA: Sinauer.

Hohnloser, S.H., Zabel, M., Just, H. and Raeder, E.A., 1993. Relation of diurnal variation of ventricular repolarization to ventricular ectopic activity and modification by sotalol. *The American journal of cardiology*, 71(5), pp.475-478.

Honda, M., Komatsu, R., Isobe, T., Tabo, M. and Ishikawa, T., 2013. Involvement of the autonomic nervous system in diurnal variation of corrected QT intervals in common marmosets. *Journal of pharmacological sciences*, 121(2), pp.131-137.

Horackova, M., Armour, J.A., Hopkins, D.A. and Huang, M.H., 1995. Nitric oxide modulates signaling between cultured adult peripheral cardiac neurons and cardiomyocytes. *American Journal of Physiology-Cell Physiology*, 269(2), pp.C504-C510.

Horner, S.M., Dick, D.J. and Murphy, C.F., 1996. Cycle length dependence of the electrophysiological effects of increased load on the myocardium. *Circulation*, 94(5), pp.1131-1136.

Htet Hlaing, K. and Clément, M.V., 2014. Formation of protein S-nitrosylation by reactive oxygen species. *Free radical research*, 48(9), pp.996-1010.

Ichinose, F., Hataishi, R., Wu, J.C., Kawai, N., Rodrigues, A.C.T., Mallari, C., Post, J.M., Parkinson, J.F., Picard, M.H., Bloch, K.D. and Zapol, W.M., 2003. A selective inducible NOS dimerization inhibitor prevents systemic, cardiac, and pulmonary

hemodynamic dysfunction in endotoxemic mice. *American Journal of Physiology-Heart and Circulatory Physiology*, 285(6), pp.H2524-H2530.

Ignarro, L.J. and Napoli, C., 2005. Novel features of nitric oxide, endothelial nitric oxide synthase, and atherosclerosis. *Current diabetes reports*, 5(1), pp.17-23.

Imanishi, M., Tomishima, Y., Itou, S., Hamashima, H., Nakajima, Y., Washizuka, K., Sakurai, M., Matsui, S., Imamura, E., Ueshima, K. and Yamamoto, T., 2008. Discovery of a novel series of biphenyl benzoic acid derivatives as potent and selective human  $\beta$ 3-adrenergic receptor agonists with good oral bioavailability. Part I. *Journal of medicinal chemistry*, 51(6), pp.1925-1944.

Irisawa, H., Brown, H.F. and Giles, W., 1993. Cardiac pacemaking in the sinoatrial node. *Physiological Reviews*, 73(1), pp.197-227.

Iwashita, E., Miyahara, T., Hino, K., Tokunaga, T., Wakisaka, H. and Sawazaki, Y., 1995. High nitric oxide synthase activity in endothelial cells in ulcerative colitis. *Journal of gastroenterology*, 30(4), pp.551-554.

Jalife, J., 2000. Ventricular fibrillation: mechanisms of initiation and maintenance. *Annual review of physiology*, 62(1), pp.25-50.

Janvier, N.C., McMorn, S.O., Harrison, S.M., Taggart, P. and Boyett, M.R., 1997. The Role of  $\text{Na}^{+}$ - $\text{Ca}^{2+}$  Exchange Current in Electrical Restitution in Ferret Ventricular Cells. *The Journal of physiology*, 504(2), pp.301-314.

Jarchau, T., Häusler, C., Markert, T., Pöhler, D., Vanderkerckhove, J., De Jonge, H.R., Lohmann, S.M. and Walter, U., 1994. Cloning, expression, and in situ localization of rat intestinal cGMP-dependent protein kinase II. *Proceedings of the National Academy of Sciences*, 91(20), pp.9426-9430.

Jeyaraj, D., Haldar, S.M., Wan, X., McCauley, M.D., Ripperger, J.A., Hu, K., Lu, Y., Eapen, B.L., Sharma, N., Ficker, E. and Cutler, M.J., 2012. Circadian rhythms govern cardiac repolarization and arrhythmogenesis. *Nature*, 483(7387), pp.96-99.

Jumrussirikul, P., Dinerman, J., Dawson, T.M., Dawson, V.L., Ekelund, U., Georgakopoulos, D., Schramm, L.P., Calkins, H., Snyder, S.H., Hare, J.M. and Berger, R.D., 1998. Interaction between neuronal nitric oxide synthase and inhibitory G protein activity in heart rate regulation in conscious mice. *Journal of Clinical Investigation*, 102(7), p.1279.

Kao, W.L., Arking, D.E., Post, W., Rea, T.D., Sotoodehnia, N., Prineas, R.J., Bishe, B., Doan, B.Q., Boerwinkle, E., Psaty, B.M. and Tomaselli, G.F., 2009. Genetic

variations in nitric oxide synthase 1 adaptor protein are associated with sudden cardiac death in US white community-based populations. *Circulation*, 119(7), pp.940-951.

Kao, W.L., Arking, D.E., Post, W., Rea, T.D., Sotoodehnia, N., Prineas, R.J., Bishe, B., Doan, B.Q., Boerwinkle, E., Psaty, B.M. and Tomaselli, G.F., 2009. Genetic variations in nitric oxide synthase 1 adaptor protein are associated with sudden cardiac death in US white community-based populations. *Circulation*, 119(7), pp.940-951.

Karle, C.A., Zitron, E., Zhang, W., Kathöfer, S., Schoels, W. and Kiehn, J., 2002. Rapid component IKr of the guinea-pig cardiac delayed rectifier K<sup>+</sup> current is inhibited by  $\beta$ 1-adrenoreceptor activation, via cAMP/protein kinase A-dependent pathways. *Cardiovascular research*, 53(2), pp.355-362.

Kay, A.R., Sugimori, M. and Llinás, R., 1998. Kinetic and stochastic properties of a persistent sodium current in mature guinea pig cerebellar Purkinje cells. *Journal of neurophysiology*, 80(3), pp.1167-1179.

Kaye, D.M., Wiviott, S.D. and Kelly, R.A., 1999. Activation of nitric oxide synthase (NOS3) by mechanical activity alters contractile activity in a Ca<sup>2+</sup>-independent manner in cardiac myocytes: role of troponin I phosphorylation. *Biochemical and biophysical research communications*, 256(2), pp.398-403.

Kaye, D.M., Wiviott, S.D., Kobzik, L.E.S.T.E.R., Kelly, R.A. and Smith, T.W., 1997. S-nitrosothiols inhibit neuronal norepinephrine transport. *American Journal of Physiology-Heart and Circulatory Physiology*, 272(2), pp.H875-H883.

Kelly, C.J. and Gold, D.P., 1999, May. Nitric oxide in interstitial nephritis and other autoimmune diseases. In *Seminars in nephrology* (Vol. 19, No. 3, pp. 288-295).

Kelly, R.A., Balligand, J.L. and Smith, T.W., 1996. Nitric oxide and cardiac function. *Circulation Research*, 79(3), pp.363-380.

Kitamura, T., Onishi, K., Dohi, K., Okinaka, T., Isaka, N. and Nakano, T., 2000. The negative inotropic effect of  $\beta$ 3-adrenoceptor stimulation in the beating guinea pig heart. *Journal of cardiovascular pharmacology*, 35(5), pp.786-790.

Klabunde, R., 2011. *Cardiovascular physiology concepts*. Lippincott Williams & Wilkins.

Knorr, A., Hirth-Dietrich, C., Alonso-Alija, C., Härter, M., Hahn, M., Keim, Y., Wunder, F. and Stasch, J.P., 2007. Nitric oxide-independent activation of soluble guanylate

cyclase by BAY 60-2770 in experimental liver fibrosis. *Arzneimittel-Forschung*, 58(2), pp.71-80.

Knorr, A., Hirth-Dietrich, C., Alonso-Alija, C., Härter, M., Hahn, M., Keim, Y., Wunder, F. and Stasch, J.P., 2007. Nitric oxide-independent activation of soluble guanylate cyclase by BAY 60-2770 in experimental liver fibrosis. *Arzneimittel-Forschung*, 58(2), pp.71-80.

Koesling, D., 1999. Studying the structure and regulation of soluble guanylyl cyclase. *Methods (San Diego, Calif.)*, 19, 485-493.

Koller, M.L., Riccio, M.L. and Gilmour Jr, R.F., 1998. Dynamic restitution of action potential duration during electrical alternans and ventricular fibrillation. *American Journal of Physiology-Heart and Circulatory Physiology*, 275(5), pp.H1635-H1642.

Koncz, I., Szél, T., Bitay, M., Cerbai, E., Jaeger, K., Fülöp, F., Jost, N., Virág, L., Orvos, P., Tálosi, L. and Kristóf, A., 2011. Electrophysiological effects of ivabradine in dog and human cardiac preparations: potential antiarrhythmic actions. *European journal of pharmacology*, 668(3), pp.419-426.

Kotlo, K.U., Hesabi, B. and Danziger, R.S., 2011. Implication of microRNAs in atrial natriuretic peptide and nitric oxide signaling in vascular smooth muscle cells. *American Journal of Physiology-Cell Physiology*, 301(4), pp.C929-C937.

Kottenberg-Assenmacher, E., Weber, M. and Kojda, G., 2003. The effect of hypercholesterolemia on platelet soluble guanylyl cyclase. *Vascular pharmacology*, 40(3), pp.141-147.

Koumi, S.I., Backer, C.L., Arentzen, C.E. and Sato, R., 1995. beta-Adrenergic modulation of the inwardly rectifying potassium channel in isolated human ventricular myocytes. Alteration in channel response to beta-adrenergic stimulation in failing human hearts. *Journal of Clinical Investigation*, 96(6), p.2870.

Krieg, T., Liu, Y., Rütz, T., Methner, C., Yang, X.M., Dost, T., Felix, S.B., Stasch, J.P., Cohen, M.V. and Downey, J.M., 2009. BAY 58-2667, a nitric oxide-independent guanylyl cyclase activator, pharmacologically post-conditions rabbit and rat hearts. *European heart journal*, 30(13), pp.1607-1613.

Kubalova, Z., 2003. Inactivation of L-type calcium channels in cardiomyocytes. Experimental and theoretical approaches. *Gen Physiol Biophys*, 22(4), pp.441-54.

Kumar P, Clark M (2012). Kumar & Clark's Clinical Medicine. 8th ed. London UK: Saunders Elsevier Limited. Chapter 14, Cardiac Arrhythmias; p.709, Figure 14.47.

Lapp, H., Mitrovic, V., Franz, N., Heuer, H., Buerke, M., Wolfertz, J., Mueck, W., Unger, S., Wensing, G. and Frey, R., 2009. Cinaciguat (BAY 58–2667) improves cardiopulmonary hemodynamics in patients with acute decompensated heart failure. *Circulation*, 119(21), pp.2781-2788.

Lasker, G.F., Pankey, E.A., Frink, T.J., Zeitzer, J.R., Walter, K.A. and Kadowitz, P.J., 2013. The sGC activator BAY 60-2770 has potent erectile activity in the rat. *American Journal of Physiology-Heart and Circulatory Physiology*, 304(12), pp.H1670-H1679.

Laurita, K.R. and Rosenbaum, D.S., 2008. Cellular mechanisms of arrhythmogenic cardiac alternans. *Progress in biophysics and molecular biology*, 97(2), pp.332-347.

Ledbetter, M.W., Preiner, J.K., Louis, C.F. and Mickelson, J.R., 1994. Tissue distribution of ryanodine receptor isoforms and alleles determined by reverse transcription polymerase chain reaction. *Journal of Biological Chemistry*, 269(50), pp.31544-31551.

Lees-Miller, J.P., Guo, J., Wang, Y., Perissinotti, L.L., Noskov, S.Y. and Duff, H.J., 2015. Ivabradine prolongs phase 3 of cardiac repolarization and blocks the hERG1 (KCNH2) current over a concentration-range overlapping with that required to block HCN4. *Journal of molecular and cellular cardiology*, 85, pp.71-78.

Levick, J.R., 2000. Initiation of heart beat and nervous control. *An Introduction to Cardiovascular Physiology*, pp.51-65.

Levick, J.R., 2010. Overview of the cardiovascular system. *An Introduction to Cardiovascular Physiology*, pp.1-13.

Lies, B., Groneberg, D., Gambaryan, S. and Friebe, A., 2013. Lack of effect of ODQ does not exclude cGMP signalling via NO-sensitive guanylyl cyclase. *British journal of pharmacology*, 170(2), pp.317-327.

Lies, B., Groneberg, D., Gambaryan, S. and Friebe, A., 2013. Lack of effect of ODQ does not exclude cGMP signalling via NO-sensitive guanylyl cyclase. *British journal of pharmacology*, 170(2), pp.317-327.

Lima, B., Forrester, M.T., Hess, D.T. and Stamler, J.S., 2010. S-nitrosylation in cardiovascular signaling. *Circulation research*, 106(4), pp.633-646.

Lincoln, T.M., Dills, W.L. and Corbin, J.D., 1977. Purification and subunit composition of guanosine 3': 5'-monophosphate-dependent protein kinase from bovine lung. *Journal of Biological Chemistry*, 252(12), pp.4269-4275.

Liu, D.W. and Antzelevitch, C., 1995. Characteristics of the Delayed Rectifier Current (IKr and IKs) in Canine Ventricular Epicardial, Midmyocardial, and Endocardial Myocytes A Weaker IKs Contributes to the Longer Action Potential of the M Cell. *Circulation research*, 76(3), pp.351-365.

Liu, Q.H., Li, X.L., Xu, Y.W., Lin, Y.Y., Cao, J.M. and Wu, B.W., 2012. A novel discovery of IK1 channel agonist: zacopride selectively enhances IK1 current and suppresses triggered arrhythmias in the rat. *Journal of cardiovascular pharmacology*, 59(1), pp.37-48.

Long, S.B., Campbell, E.B. and MacKinnon, R., 2005. Crystal structure of a mammalian voltage-dependent Shaker family K<sup>+</sup> channel. *Science*, 309(5736), pp.897-903.

Lu, M., Wang, X. and Wang, W., 1998. Nitric oxide increases the activity of the apical 70-pS K<sup>+</sup> channel in TAL of rat kidney. *American Journal of Physiology-Renal Physiology*, 274(5), pp.F946-F950.

Lu, Z., Kamiya, K., Opthof, T., Yasui, K. and Kodama, I., 2001. Density and kinetics of IKr and IKs in guinea pig and rabbit ventricular myocytes explain different efficacy of IKs blockade at high heart rate in guinea pig and rabbit implications for arrhythmogenesis in humans. *Circulation*, 104(8), pp.951-956.

MacMicking, J., Xie, Q.W. and Nathan, C., 1997. Nitric oxide and macrophage function. *Annual review of immunology*, 15(1), pp.323-350.

Mahmoud, K.D., de Smet, B.J., Zijlstra, F., Rihal, C.S. and Holmes, D.R., 2011. Sudden cardiac death: epidemiology, circadian variation, and triggers. *Current problems in cardiology*, 36(2), pp.56-80.

Main, M.C., Bryant, S.M. and Hart, G., 1998. Regional differences in action potential characteristics and membrane currents of guinea-pig left ventricular myocytes. *Experimental physiology*, 83(06), pp.747-761.

Marks, A.R., Tempst, P., Hwang, K.S., Taubman, M.B., Inui, M., Chadwick, C., Fleischer, S. and Nadal-Ginard, B., 1989. Molecular cloning and characterization of the ryanodine receptor/junctional channel complex cDNA from skeletal muscle sarcoplasmic reticulum. *Proceedings of the National Academy of Sciences*, 86(22), pp.8683-8687.

Maron, B.J., Kogan, J., Proschan, M.A., Hecht, G.M. and Roberts, W.C., 1994. Circadian variability in the occurrence of sudden cardiac death in patients with hypertrophic cardiomyopathy. *Journal of the American College of Cardiology*, 23(6), pp.1405-1409.

Martin, R.I., Pogoryelova, O., Koref, M.S., Bourke, J.P., Teare, M.D. and Keavney, B.D., 2014. Atrial fibrillation associated with ivabradine treatment: meta-analysis of randomised controlled trials. *Heart*, 100(19), pp.1506-1510.

Marx, S.O., Kurokawa, J., Reiken, S., Motoike, H., D'Armiento, J., Marks, A.R. and Kass, R.S., 2002. Requirement of a macromolecular signaling complex for  $\beta$  adrenergic receptor modulation of the KCNQ1-KCNE1 potassium channel. *Science*, 295(5554), pp.496-499.

Massion, P.B. and Balligand, J.L., 2003. Modulation of cardiac contraction, relaxation and rate by the endothelial nitric oxide synthase (eNOS): lessons from genetically modified mice. *The Journal of physiology*, 546(1), pp.63-75.

Massion, P.B., Dessy, C., Desjardins, F., Pelat, M., Havaux, X., Belge, C., Moulin, P., Guiot, Y., Feron, O., Janssens, S. and Balligand, J.L., 2004. Cardiomyocyte-restricted overexpression of endothelial nitric oxide synthase (NOS3) attenuates  $\beta$ -adrenergic stimulation and reinforces vagal inhibition of cardiac contraction. *Circulation*, 110(17), pp.2666-2672.

Massion, P.B., Feron, O., Dessy, C. and Balligand, J.L., 2003. Nitric oxide and cardiac function ten years after, and continuing. *Circulation research*, 93(5), pp.388-398.

Matsuda, H. and Iyanagi, T., 1999. Calmodulin activates intramolecular electron transfer between the two flavins of neuronal nitric oxide synthase flavin domain. *Biochimica et Biophysica Acta (BBA)-General Subjects*, 1473(2), pp.345-355.

Matsumoto, S., Takahashi, T., Ikeda, M., Nishikawa, T., Yoshida, S. and Kawase, T., 2000. Effects of N<sup>G</sup>-Monomethyl-L-arginine on Ca<sup>2+</sup> Current and Nitric-Oxide Synthase in Rat Ventricular Myocytes. *Journal of Pharmacology and Experimental Therapeutics*, 294(1), pp.216-223.

Maurice, D.H., Palmer, D., Tilley, D.G., Dunkerley, H.A., Netherton, S.J., Raymond, D.R., Elbatarny, H.S. and Jimmo, S.L., 2003. Cyclic nucleotide phosphodiesterase activity, expression, and targeting in cells of the cardiovascular system. *Molecular pharmacology*, 64(3), pp.533-546.

Melgari, D., Brack, K.E., Zhang, C., Zhang, Y., El Harchi, A., Mitcheson, J.S., Dempsey, C.E., Ng, G.A. and Hancox, J.C., 2015. hERG potassium channel blockade by the HCN channel inhibitor bradycardic agent ivabradine. *Journal of the American Heart Association*, 4(4), p.e001813.

Mery, P.F., Hove-Madsen, L.E.I.F., Chesnais, J.M., Hartzell, H.C. and Fischmeister, R.O.D.O.L.P.H.E., 1996. Nitric oxide synthase does not participate in negative inotropic effect of acetylcholine in frog heart. *American Journal of Physiology-Heart and Circulatory Physiology*, 270(4), pp.H1178-H1188.

Mery, P.F., Lohmann, S.M., Walter, U. and Fischmeister, R., 1991. Ca<sup>2+</sup> current is regulated by cyclic GMP-dependent protein kinase in mammalian cardiac myocytes. *Proceedings of the National Academy of Sciences*, 88(4), pp.1197-1201.

Mewe, M., Mauerhöfer, M., Wulfsen, I., Szlachta, K., Zhou, X.B., Schwarz, J.R. and Bauer, C.K., 2010. Modulation of cardiac ERG1 K<sup>+</sup> channels by cGMP signaling. *Journal of molecular and cellular cardiology*, 49(1), pp.48-57.

Miller, C., 2000. An overview of the potassium channel family. *Genome Biol*, 1(4), pp.1-5.

Miller, C.L. and Yan, C., 2010. Targeting cyclic nucleotide phosphodiesterase in the heart: therapeutic implications. *Journal of cardiovascular translational research*, 3(5), pp.507-515.

Mitchell, M.R., Powell, T., Sturridge, M.F., Terrar, D.A. and Twist, V.W., 1986. Electrical properties and response to noradrenaline of individual heart cells isolated from human ventricular tissue. *Cardiovascular research*, 20(12), pp.869-876.

Miyauchi, Y., Zhou, S., Okuyama, Y., Miyauchi, M., Hayashi, H., Hamabe, A., Fishbein, M.C., Mandel, W.J., Chen, L.S., Chen, P.S. and Karagueuzian, H.S., 2003. Altered atrial electrical restitution and heterogeneous sympathetic hyperinnervation in hearts with chronic left ventricular myocardial infarction implications for atrial fibrillation. *Circulation*, 108(3), pp.360-366.

Moens, A.L., Yang, R., Watts, V.L. and Barouch, L.A., 2010. Beta 3-adrenoreceptor regulation of nitric oxide in the cardiovascular system. *Journal of molecular and cellular cardiology*, 48(6), pp.1088-1095.

Mongillo, M., Tocchetti, C.G., Terrin, A., Lissandron, V., Cheung, Y.F., Dostmann, W.R., Pozzan, T., Kass, D.A., Paolocci, N., Houslay, M.D. and Zaccolo, M., 2006. Compartmentalized phosphodiesterase-2 activity blunts  $\beta$ -adrenergic cardiac inotropy via an NO/cGMP-dependent pathway. *Circulation research*, 98(2), pp.226-234.

Monken, C.E. and Gill, G.N., 1980. Structural analysis of cGMP-dependent protein kinase using limited proteolysis. *Journal of Biological Chemistry*, 255(15), pp.7067-7070.

Monteiro, P.F., Morganti, R.P., Delbin, M.A., Calixto, M.C., Lopes-Pires, M.E., Marcondes, S., Zanesco, A. and Antunes, E., 2012. Platelet hyperaggregability in high-fat fed rats: a role for intraplatelet reactive-oxygen species production. *Cardiovasc Diabetol*, 11(5).

Morris, C.J., Yang, J.N. and Scheer, F.A., 2012. The impact of the circadian timing system on cardiovascular and metabolic function. *Progress in brain research*, 199, p.337.

Münzel, T., Daiber, A., Ullrich, V. and Mülsch, A., 2005. Vascular consequences of endothelial nitric oxide synthase uncoupling for the activity and expression of the soluble guanylyl cyclase and the cGMP-dependent protein kinase. *Arteriosclerosis, thrombosis, and vascular biology*, 25(8), pp.1551-1557.

Myles, R.C., Burton, F.L., Cobbe, S.M. and Smith, G.L., 2008. The link between repolarisation alternans and ventricular arrhythmia: does the cellular phenomenon extend to the clinical problem?. *Journal of molecular and cellular cardiology*, 45(1), pp.1-10.

Naitoh, N., Tagawa, M., Yamaura, M., Taneda, K., Furushima, H. and Aizawa, Y., 1998. Comparison of electrophysiologic effects of intravenous E-4031 and MS-551, novel class III antiarrhythmic agents, in patients with ventricular tachyarrhythmias. *Japanese heart journal*, 39(4), pp.457-467.

Nathan, C. and Xie, Q.W., 1994. Nitric oxide synthases: roles, tolls, and controls. *Cell*, 78(6), pp.915-918.

Nerbonne, J.M. and Kass, R.S., 2005. Molecular physiology of cardiac repolarization. *Physiological reviews*, 85(4), pp.1205-1253.

Ng, G.A., Brack, K.E., Patel, V.H. and Coote, J.H., 2007. Autonomic modulation of electrical restitution, alternans and ventricular fibrillation initiation in the isolated heart. *Cardiovascular research*, 73(4), pp.750-760.

Niwa, N. and Nerbonne, J.M., 2010. Molecular determinants of cardiac transient outward potassium current (I<sub>to</sub>) expression and regulation. *Journal of molecular and cellular cardiology*, 48(1), pp.12-25.

Nuss, H.B., Kääb, S., Kass, D.A., Tomaselli, G.F. and Marbán, E., 1999. Cellular basis of ventricular arrhythmias and abnormal automaticity in heart failure. *American Journal of Physiology-Heart and Circulatory Physiology*, 277(1), pp.H80-H91.

Osadchii, O.E., 2012. Effects of ventricular pacing protocol on electrical restitution assessments in guinea-pig heart. *Experimental physiology*, 97(7), pp.807-821.

Paolocci, N., Ekelund, U.E., Isoda, T., Ozaki, M., Vandegaer, K., Georgakopoulos, D., Harrison, R.W., Kass, D.A. and Hare, J.M., 2000. cGMP-independent inotropic effects of nitric oxide and peroxyntirite donors: potential role for nitrosylation. *American Journal of Physiology-Heart and Circulatory Physiology*, 279(4), pp.H1982-H1988.

Park, D.S. and Fishman, G.I., 2011. Basic Science for Clinicians: The Cardiac Conduction System. *Circulation*, 123(8), p.904.

Paterson, D.J., 2001. Nitric oxide and the autonomic regulation of cardiac excitability. *Experimental physiology*, 86(01), pp.1-12.

Perozo, E., Cortes, D.M., Sompornpisut, P., Kloda, A. and Martinac, B., 2002. Open channel structure of MscL and the gating mechanism of mechanosensitive channels. *Nature*, 418(6901), pp.942-948.

Peterson, B.Z., DeMaria, C.D. and Yue, D.T., 1999. Calmodulin is the Ca<sup>2+</sup> sensor for Ca<sup>2+</sup>-dependent inactivation of L-type calcium channels. *Neuron*, 22(3), pp.549-558.

Picht, E., DeSantiago, J., Blatter, L.A. and Bers, D.M., 2006. Cardiac alternans do not rely on diastolic sarcoplasmic reticulum calcium content fluctuations. *Circulation research*, 99(7), pp.740-748.

Pinnell, J., Turner, S. and Howell, S., 2007. Cardiac muscle physiology. Continuing Education in Anaesthesia, Critical Care & Pain, 7(3), pp.85-88.

Pitt, G.S., Zühlke, R.D., Hudmon, A., Schulman, H., Reuter, H. and Tsien, R.W., 2001. Molecular basis of calmodulin tethering and Ca<sup>2+</sup>-dependent inactivation of L-type Ca<sup>2+</sup> channels. *Journal of Biological Chemistry*, 276(33), pp.30794-30802.

Post, W., Shen, H., Damcott, C., Arking, D.E., Kao, W.L., Sack, P.A., Ryan, K.A., Chakravarti, A., Mitchell, B.D. and Shuldiner, A.R., 2007. Associations between genetic variants in the NOS1AP (CAPON) gene and cardiac repolarization in the old order Amish. *Human heredity*, 64(4), pp.214-219.

Pruvot, E.J., Katra, R.P., Rosenbaum, D.S. and Laurita, K.R., 2004. Role of calcium cycling versus restitution in the mechanism of repolarization alternans. *Circulation research*, 94(8), pp.1083-1090.

Pueyo, E., Husti, Z., Hornyik, T., Baczkó, I., Laguna, P., Varró, A. and Rodríguez, B., 2010. Mechanisms of ventricular rate adaptation as a predictor of arrhythmic risk. *American Journal of Physiology-Heart and Circulatory Physiology*, 298(5), pp.H1577-H1587.

Qin, Y., Dey, A. and Daaka, Y., 2013. Protein s-nitrosylation measurement. *Methods Enzymol*, 522, pp.409-425.

Qu, Z., Weiss, J.N. and Garfinkel, A., 1999. Cardiac electrical restitution properties and stability of reentrant spiral waves: a simulation study. *American Journal of Physiology-Heart and Circulatory Physiology*, 276(1), pp.H269-H283.

Ramay, H.R., Liu, O.Z. and Sobie, E.A., 2011. Recovery of cardiac calcium release is controlled by sarcoplasmic reticulum refilling and ryanodine receptor sensitivity. *Cardiovascular research*, p.cvr143.

Riccio, M.L., Koller, M.L. and Gilmour, R.F., 1999. Electrical restitution and spatiotemporal organization during ventricular fibrillation. *Circulation Research*, 84(8), pp.955-963.

Richie-Jannetta, R., Francis, S.H. and Corbin, J.D., 2003. Dimerization of cGMP-dependent protein kinase I $\beta$  is mediated by an extensive amino-terminal leucine zipper motif, and dimerization modulates enzyme function. *Journal of Biological Chemistry*, 278(50), pp.50070-50079.

Robinson, R.B., Boyden, P.A., Hoffman, B.F. and Hewett, K.W., 1987. Electrical restitution process in dispersed canine cardiac Purkinje and ventricular cells. *American Journal of Physiology-Heart and Circulatory Physiology*, 253(5), pp.H1018-H1025.

Roden, D.M., 1998. Taking the "idio" out of "idiosyncratic": predicting torsades de pointes. *Pacing and Clinical Electrophysiology*, 21(5), pp.1029-1034.

Rolls, H.K., Stevenson, W.G., Strichartz, G.R. and Lilly, L.S., 2007. Mechanisms of cardiac arrhythmias. *Pathophysiology of heart disease. 4th ed. USA: Lippincott Williams & Wilkins*, pp.280-302.

Roman, L.J. and Masters, B.S.S., 2006. Electron transfer by neuronal nitric-oxide synthase is regulated by concerted interaction of calmodulin and two intrinsic regulatory elements. *Journal of Biological Chemistry*, 281(32), pp.23111-23118.

Rosati, B., Dong, M., Cheng, L., Liou, S.R., Yan, Q., Park, J.Y., Shiang, E., Sanguinetti, M., Wang, H.S. and McKinnon, D., 2008. Evolution of ventricular myocyte electrophysiology. *Physiological genomics*, 35(3), pp.262-272.

Rosati, B., Dong, M., Cheng, L., Liou, S.R., Yan, Q., Park, J.Y., Shiang, E., Sanguinetti, M., Wang, H.S. and McKinnon, D., 2008. Evolution of ventricular myocyte electrophysiology. *Physiological genomics*, 35(3), pp.262-272.

Ross, G., Engel, P., Abdallah, Y., Kummer, W. and Schluter, K.D., 2005. Tuberoinfundibular peptide of 39 residues: a new mediator of cardiac function via nitric oxide production in the rat heart. *Endocrinology*, 146(5), pp.2221-2228.

Rozmaritsa, N., Christ, T., Van Wagoner, D.R., Haase, H., Stasch, J.P., Matschke, K. and Ravens, U., 2014. Attenuated response of L-type calcium current to nitric oxide in atrial fibrillation. *Cardiovascular research*, 101(3), pp.533-542.

Sagami, I., Daff, S. and Shimizu, T., 2001. Intra-subunit and Inter-subunit Electron Transfer in Neuronal Nitric-oxide Synthase EFFECT OF CALMODULIN ON HETERODIMER CATALYSIS. *Journal of Biological Chemistry*, 276(32), pp.30036-30042.

Saladin, K.S., 2004. *Anatomy and Physiology*, 3th Edi.

Sanguinetti, M.C. and Jurkiewicz, N.K., 1990. Two components of cardiac delayed rectifier K<sup>+</sup> current. Differential sensitivity to block by class III antiarrhythmic agents. *The Journal of general physiology*, 96(1), pp.195-215.

Sanguinetti, M.C. and Tristani-Firouzi, M., 2006. hERG potassium channels and cardiac arrhythmia. *Nature*, 440(7083), pp.463-469.

Sanguinetti, M.C. and Tristani-Firouzi, M., 2006. hERG potassium channels and cardiac arrhythmia. *Nature*, 440(7083), pp.463-469.

Sanguinetti, M.C., Curran, M.E., Spector, P.S. and Keating, M.T., 1996. Spectrum of HERG K<sup>+</sup>-channel dysfunction in an inherited cardiac arrhythmia. *Proceedings of the National Academy of Sciences*, 93(5), pp.2208-2212.

Sanguinetti, M.C., Jurkiewicz, N.K., Scott, A. and Siegl, P.K., 1991. Isoproterenol antagonizes prolongation of refractory period by the class III antiarrhythmic agent E-4031 in guinea pig myocytes. Mechanism of action. *Circulation Research*, 68(1), pp.77-84.

Saraiva, R.M. and Hare, J.M., 2006. Nitric oxide signaling in the cardiovascular system: implications for heart failure. *Current opinion in cardiology*, 21(3), pp.221-228.

Sato, D., Despa, S. and Bers, D.M., 2012. Can the sodium-calcium exchanger initiate or suppress calcium sparks in cardiac myocytes?. *Biophysical journal*, 102(8), pp.L31-L33.

Sato, D., Despa, S. and Bers, D.M., 2012. Can the sodium-calcium exchanger initiate or suppress calcium sparks in cardiac myocytes?. *Biophysical journal*, 102(8), pp.L31-L33.

Savelieva, I. and Camm, A., 2006. Novel If current inhibitor ivabradine: safety considerations.

Scheer, F.A., van Doornen, L.J. and Buijs, R.M., 2004. Light and diurnal cycle affect autonomic cardiac balance in human; possible role for the biological clock. *Autonomic neuroscience*, 110(1), pp.44-48.

Schmidt, H.H., Schmidt, P.M. and Stasch, J.P., 2009. NO-and haem-independent soluble guanylate cyclase activators. In *cGMP: Generators, Effectors and Therapeutic Implications* (pp. 309-339). Springer Berlin Heidelberg.

Schmidt, P.M., Schramm, M., Schröder, H., Wunder, F. and Stasch, J.P., 2004. Identification of residues crucially involved in the binding of the heme moiety of soluble guanylate cyclase. *Journal of Biological Chemistry*, 279(4), pp.3025-3032.

Schram, G., Pourrier, M., Melnyk, P. and Nattel, S., 2002. Differential distribution of cardiac ion channel expression as a basis for regional specialization in electrical function. *Circulation research*, 90(9), pp.939-950.

Schrammel, A., Gorren, A.C., Schmidt, K., Pfeiffer, S. and Mayer, B., 2003. S-nitrosation of glutathione by nitric oxide, peroxynitrite, and  $\bullet$ NO/O $2^{\bullet-}$ . *Free Radical Biology and Medicine*, 34(8), pp.1078-1088.

Schulman, I.H. and Hare, J.M., 2012. Regulation of cardiovascular cellular processes by S-nitrosylation. *Biochimica et Biophysica Acta (BBA)-General Subjects*, 1820(6), pp.752-762.

Schulz, R., Rassaf, T., Massion, P.B., Kelm, M. and Balligand, J.L., 2005. Recent advances in the understanding of the role of nitric oxide in cardiovascular homeostasis. *Pharmacology & therapeutics*, 108(3), pp.225-256.

Schwartz, P.J. and Ackerman, M.J., 2013. The long QT syndrome: a transatlantic clinical approach to diagnosis and therapy. *European heart journal*, 34(40), pp.3109-3116.

Schwarz, P., Diem, R., Dun, N.J. and Förstermann, U., 1995. Endogenous and exogenous nitric oxide inhibits norepinephrine release from rat heart sympathetic nerves. *Circulation Research*, 77(4), pp.841-848.

Scicchitano, P., Cortese, F., Ricci, G., Carbonara, S., Moncelli, M., Iacoviello, M., Cecere, A., Gesualdo, M., Zito, A., Caldarola, P. and Scrutinio, D., 2014. Ivabradine, coronary artery disease, and heart failure: beyond rhythm control. *Drug design, development and therapy*, 8, p.689.

Sears, C.E., Bryant, S.M., Ashley, E.A., Lygate, C.A., Rakovic, S., Wallis, H.L., Neubauer, S., Terrar, D.A. and Casadei, B., 2003. Cardiac neuronal nitric oxide synthase isoform regulates myocardial contraction and calcium handling. *Circulation Research*, 92(5), pp.e52-e59.

Sears, C.E., Choate, J.K. and Paterson, D.J., 1998. Effect of nitric oxide synthase inhibition on the sympatho-vagal control of heart rate. *Journal of the autonomic nervous system*, 73(1), pp.63-73.

Seddon, M., Shah, A.M. and Casadei, B., 2007. Cardiomyocytes as effectors of nitric oxide signalling. *Cardiovascular research*, 75(2), pp.315-326.

Sham, J.S., Hatem, S.N. and Morad, M., 1995. Species differences in the activity of the Na (+)-Ca<sup>2+</sup> exchanger in mammalian cardiac myocytes. *The Journal of Physiology*, 488(3), pp.623-631.

Shao, D., Oka, S.I., Brady, C.D., Haendeler, J., Eaton, P. and Sadoshima, J., 2012. Redox modification of cell signaling in the cardiovascular system. *Journal of molecular and cellular cardiology*, 52(3), pp.550-558.

Shaul, P.W., 2002. Regulation of endothelial nitric oxide synthase: location, location, location. *Annual review of physiology*, 64(1), pp.749-774.

Shen, M.J. and Zipes, D.P., 2014. Role of the autonomic nervous system in modulating cardiac arrhythmias. *Circulation research*, 114(6), pp.1004-1021.

Shesely, E.G., Maeda, N., Kim, H.S., Desai, K.M., Kregel, J.H., Laubach, V.E., Sherman, P.A., Sessa, W.C. and Smithies, O., 1996. Elevated blood pressures in mice lacking endothelial nitric oxide synthase. *Proceedings of the National Academy of Sciences*, 93(23), pp.13176-13181.

Shinagawa, Y., Satoh, H. and Noma, A., 2000. The sustained inward current and inward rectifier K<sup>+</sup> current in pacemaker cells dissociated from rat sinoatrial node. *The Journal of Physiology*, 523(3), pp.593-605.

Silva, J. and Rudy, Y., 2005. Subunit interaction determines IKs participation in cardiac repolarization and repolarization reserve. *Circulation*, 112(10), pp.1384-1391.

Singh, B.N., 1993. Arrhythmia control by prolonging repolarization: the concept and its potential therapeutic impact. *European heart journal*, 14(suppl H), pp.14-23.

Sipido, K.R., Callewaert, G. and Carmeliet, E., 1995. Inhibition and rapid recovery of Ca<sup>2+</sup> current during Ca<sup>2+</sup> release from sarcoplasmic reticulum in guinea pig ventricular myocytes. *Circulation Research*, 76(1), pp.102-109.

Stasch, J.P., Schmidt, P., Alonso-Alija, C., Apeler, H., Dembowski, K., Haerter, M., Heil, M., Minuth, T., Perzborn, E., Pleiss, U. and Schramm, M., 2002. NO-and haem-independent activation of soluble guanylyl cyclase: molecular basis and cardiovascular implications of a new pharmacological principle. *British journal of pharmacology*, 136(5), pp.773-783.

Stengl, M., Ramakers, C., Donker, D.W., Nabar, A., Rybin, A.V., Spätjens, R.L., van der Nagel, T., Wodzig, W.K., Sipido, K.R., Antoons, G. and Moorman, A.F., 2006. Temporal patterns of electrical remodeling in canine ventricular hypertrophy: Focus on IKs downregulation and blunted  $\beta$ -adrenergic activation. *Cardiovascular research*, 72(1), pp.90-100.

Sterin-Borda, L., Bernabeo, G., Ganzinelli, S., Joensen, L. and Borda, E., 2006. Role of nitric oxide/cyclic GMP and cyclic AMP in  $\beta$  3 adrenoceptor-chronotropic response. *Journal of molecular and cellular cardiology*, 40(4), pp.580-588.

Sun, J. and Murphy, E., 2010. Protein S-nitrosylation and cardioprotection. *Circulation Research*, 106(2), pp.285-296.

Sun, J., Steenbergen, C. and Murphy, E., 2006. S-nitrosylation: NO-related redox signaling to protect against oxidative stress. *Antioxidants & redox signaling*, 8(9-10), pp.1693-1705.

Taggart, P., Sutton, P., Chalabi, Z., Boyett, M.R., Simon, R., Elliott, D. and Gill, J.S., 2003. Effect of adrenergic stimulation on action potential duration restitution in humans. *Circulation*, 107(2), pp.285-289.

Taglialatela, M., Pannaccione, A., Iossa, S., Castaldo, P. and Annunziato, L., 1999. Modulation of the K<sup>+</sup> channels encoded by the human ether-a-gogo-related gene-1 (hERG1) by nitric oxide. *Molecular pharmacology*, 56(6), pp.1298-1308.

Takeshima, H., Nishimura, S., Matsumoto, T., Ishida, H., Kangawa, K., Minamino, N., Matsuo, H., Ueda, M., Hanaoka, M. and Hirose, T., 1989. Primary structure and

expression from complementary DNA of skeletal muscle ryanodine receptor. *Nature*, 339(6224), pp.439-445.

Takimoto, E., 2012. Cyclic GMP-dependent signaling in cardiac myocytes. *Circulation Journal*, 76(8), pp.1819-1825.

Tavazzi, L. and Mugelli, A., 2006. Can If inhibition help in congestive heart failure?. *Dialogues in cardiovascular medicine*, 11(1), pp.30-35.

Tolkacheva, E.G., Anumonwo, J.M. and Jalife, J., 2006. Action potential duration restitution portraits of mammalian ventricular myocytes: role of calcium current. *Biophysical journal*, 91(7), pp.2735-2745.

Tortora, G.J. and Derrickson, B.H., 2008. *Principles of anatomy and physiology*. John Wiley & Sons.

Trudeau, M.C., Warmke, J.W., Ganetzky, B. and Robertson, G.A., 1995. HERG, a human inward rectifier in the voltage-gated potassium channel family. *SCIENCE*. pp.92-92.

Trujillo, T.C. and Nolan, P.E., 2000. Antiarrhythmic agents. *Drug safety*, 23(6), pp.509-532.

Tseng, G.N., 1988. Calcium current restitution in mammalian ventricular myocytes is modulated by intracellular calcium. *Circulation Research*, 63(2), pp.468-482.

Uhler, M.D., 1993. Cloning and expression of a novel cyclic GMP-dependent protein kinase from mouse brain. *Journal of Biological Chemistry*, 268(18), pp.13586-13591.

Van Wagoner, D.R., Pond, A.L., McCarthy, P.M., Trimmer, J.S. and Nerbonne, J.M., 1997. Outward K<sup>+</sup> current densities and Kv1.5 expression are reduced in chronic human atrial fibrillation. *Circulation research*, 80(6), pp.772-781.

Vandelle, E. and Delledonne, M., 2011. Peroxynitrite formation and function in plants. *Plant Science*, 181(5), pp.534-539.

Vandenberg, J.I., Torres, A.M., Campbell, T.J. and Kuchel, P.W., 2004. The HERG K<sup>+</sup> channel: progress in understanding the molecular basis of its unusual gating kinetics. *European Biophysics Journal*, 33(2), pp.89-97.

Vega, A.L., Yuan, C., Votaw, V.S. and Santana, L.F., 2011. Dynamic changes in sarcoplasmic reticulum structure in ventricular myocytes. *BioMed Research International*, 2011.

Vincent, G.M., Schwartz, P.J., Denjoy, I., Swan, H., Bithell, C., Spazzolini, C., Crotti, L., Piippo, K., Lupoglazoff, J.M., Villain, E. and Priori, S.G., 2009. High Efficacy of  $\beta$ -Blockers in Long-QT Syndrome Type 1 Contribution of Noncompliance and QT-Prolonging Drugs to the Occurrence of  $\beta$ -Blocker Treatment "Failures". *Circulation*, 119(2), pp.215-221.

Viswanathan, P.C., Shaw, R.M. and Rudy, Y., 1999. Effects of IKr and IKs heterogeneity on action potential duration and its rate dependence a simulation study. *Circulation*, 99(18), pp.2466-2474.

Volders, P.G., Stengl, M., van Opstal, J.M., Gerlach, U., Spätjens, R.L., Beekman, J.D., Sipido, K.R. and Vos, M.A., 2003. Probing the Contribution of IKs to Canine Ventricular Repolarization Key Role for  $\beta$ -Adrenergic Receptor Stimulation. *Circulation*, 107(21), pp.2753-2760.

Volders, P.G., Vos, M.A., Szabo, B., Sipido, K.R., de Groot, S.M., Gorgels, A.P., Wellens, H.J. and Lazzara, R., 2000. Progress in the understanding of cardiac early afterdepolarizations and torsades de pointes: time to revise current concepts. *Cardiovascular research*, 46(3), pp.376-392.

Wahler, G.M. and Dollinger, S.J., 1995. Nitric oxide donor SIN-1 inhibits mammalian cardiac calcium current through cGMP-dependent protein kinase. *American Journal of Physiology-Cell Physiology*, 268(1), pp.C45-C54.

Walker, C.A. and Spinale, F.G., 1999. The structure and function of the cardiac myocyte: a review of fundamental concepts. *The Journal of thoracic and cardiovascular surgery*, 118(2), pp.375-382.

Walker, M.L., Wan, X., Kirsch, G.E. and Rosenbaum, D.S., 2003. Hysteresis effect implicates calcium cycling as a mechanism of repolarization alternans. *Circulation*, 108(21), pp.2704-2709.

Walter, U. and Gambaryan, S., 2009. cGMP and cGMP-dependent protein kinase in platelets and blood cells. In *cGMP: Generators, Effectors and Therapeutic Implications* (pp. 533-548). Springer Berlin Heidelberg.

Wang, D.W., Yazawa, K., George, A.L. and Bennett, P.B., 1996. Characterization of human cardiac Na<sup>+</sup> channel mutations in the congenital long QT syndrome. *Proceedings of the National Academy of Sciences*, 93(23), pp.13200-13205.

Wang, H., Kohr, M.J., Traynham, C.J., Wheeler, D.G., Janssen, P.M. and Ziolo, M.T., 2008. Neuronal nitric oxide synthase signaling within cardiac myocytes targets phospholamban. *American Journal of Physiology-Cell Physiology*, 294(6), pp.C1566-C1575.

Wang, H., Kohr, M.J., Wheeler, D.G. and Ziolo, M.T., 2008. Endothelial nitric oxide synthase decreases  $\beta$ -adrenergic responsiveness via inhibition of the L-type  $\text{Ca}^{2+}$  current. *American Journal of Physiology-Heart and Circulatory Physiology*, 294(3), pp.H1473-H1480.

Wang, H., Kohr, M.J., Wheeler, D.G. and Ziolo, M.T., 2008. Endothelial nitric oxide synthase decreases  $\beta$ -adrenergic responsiveness via inhibition of the L-type  $\text{Ca}^{2+}$  current. *American Journal of Physiology-Heart and Circulatory Physiology*, 294(3), pp.H1473-H1480.

Wang, H., Kohr, M.J., Wheeler, D.G. and Ziolo, M.T., 2008. Endothelial nitric oxide synthase decreases  $\beta$ -adrenergic responsiveness via inhibition of the L-type  $\text{Ca}^{2+}$  current. *American Journal of Physiology-Heart and Circulatory Physiology*, 294(3), pp.H1473-H1480.

Wang, J.C., Kiyosue, T., Kiriya, K. and Arita, M., 1999. Bepridil differentially inhibits two delayed rectifier  $\text{K}^{+}$  currents,  $\text{I}_{\text{Kr}}$  and  $\text{I}_{\text{Ks}}$ , in guinea-pig ventricular myocytes. *British journal of pharmacology*, 128(8), pp.1733-1738.

Wedel, B., Harteneck, C., Foerster, J., Friebe, A., Schultz, G. and Koesling, D., 1995. Functional domains of soluble guanylyl cyclase. *Journal of Biological Chemistry*, 270(42), pp.24871-24875.

Wedel, B.J. and Garbers, D.L., 1998. Guanylyl cyclases: approaching year thirty. *Trends in Endocrinology & Metabolism*, 9(6), pp.213-219.

Weiss, J.N., CHEN, P.S., Qu, Z., Karagueuzian, H.S., LIN, S.F. and Garfinkel, A., 2002. Electrical restitution and cardiac fibrillation. *Journal of cardiovascular electrophysiology*, 13(3), pp.292-295.

Weiss, J.N., CHEN, P.S., Qu, Z., Karagueuzian, H.S., LIN, S.F. and Garfinkel, A., 2002. Electrical restitution and cardiac fibrillation. *Journal of cardiovascular electrophysiology*, 13(3), pp.292-295.

Weiss, J.N., Garfinkel, A., Karagueuzian, H.S., Chen, P.S. and Qu, Z., 2010. Early afterdepolarizations and cardiac arrhythmias. *Heart rhythm*, 7(12), pp.1891-1899.

Weiss, J.N., Karma, A., Shiferaw, Y., Chen, P.S., Garfinkel, A. and Qu, Z., 2006. From pulsus to Pulseless the saga of cardiac alternans. *Circulation Research*, 98(10), pp.1244-1253.

Wickenden, A.D., Jegla, T.J., Kaprielian, R. and Backx, P.H., 1999. Regional contributions of  $\text{Kv}1.4$ ,  $\text{Kv}4.2$ , and  $\text{Kv}4.3$  to transient outward  $\text{K}^{+}$  current in rat

ventricle. *American Journal of Physiology-Heart and Circulatory Physiology*, 276(5), pp.H1599-H1607.

Wickenden, A.D., Jegla, T.J., Kaprielian, R. and Backx, P.H., 1999. Regional contributions of Kv1. 4, Kv4. 2, and Kv4. 3 to transient outward K<sup>+</sup> current in rat ventricle. *American Journal of Physiology-Heart and Circulatory Physiology*, 276(5), pp.H1599-H1607.

Wilcox, C.S., 2010. Effects of tempol and redox-cycling nitroxides in models of oxidative stress. *Pharmacology & therapeutics*, 126(2), pp.119-145.

Wildhirt, S.M., Weismueller, S., Schulze, C., Conrad, N., Kornberg, A. and Reichart, B., 1999. Inducible nitric oxide synthase activation after ischemia/reperfusion contributes to myocardial dysfunction and extent of infarct size in rabbits: evidence for a late phase of nitric oxide-mediated reperfusion injury. *Cardiovascular research*, 43(3), pp.698-711.

Wilson, L.D., Jeyaraj, D., Wan, X., Hoeker, G.S., Said, T.H., Gittinger, M., Laurita, K.R. and Rosenbaum, D.S., 2009. Heart failure enhances susceptibility to arrhythmogenic cardiac alternans. *Heart Rhythm*, 6(2), pp.251-259.

Wink, D.A., Vodovotz, Y., Laval, J., Laval, F., Dewhirst, M.W. and Mitchell, J.B., 1998. The multifaceted roles of nitric oxide in cancer. *Carcinogenesis*, 19(5), pp.711-721.

Xu, K.Y., Huso, D.L., Dawson, T.M., Bredt, D.S. and Becker, L.C., 1999. Nitric oxide synthase in cardiac sarcoplasmic reticulum. *Proceedings of the National Academy of Sciences*, 96(2), pp.657-662.

Xu, L., Eu, J.P., Meissner, G. and Stamler, J.S., 1998. Activation of the cardiac calcium release channel (ryanodine receptor) by poly-S-nitrosylation. *Science*, 279(5348), pp.234-237.

Yamamoto, A., Katou, S., Yoshioka, H., Doke, N. and Kawakita, K., 2004. Involvement of nitric oxide generation in hypersensitive cell death induced by elicitor in tobacco cell suspension culture. *Journal of General Plant Pathology*, 70(2), pp.85-92.

Yamashita, T., Sekiguchi, A., Iwasaki, Y.K., Sagara, K., Inuma, H., Hatano, S., Fu, L.T. and Watanabe, H., 2003. Circadian variation of cardiac K<sup>+</sup> channel gene expression. *Circulation*, 107(14), pp.1917-1922.

Yan, G.X., Rials, S.J., Wu, Y., Liu, T., Xu, X., Marinchak, R.A. and Kowey, P.R., 2001. Ventricular hypertrophy amplifies transmural repolarization dispersion and induces early afterdepolarization. *American Journal of Physiology-Heart and Circulatory Physiology*, 281(5), pp.H1968-H1975.

Yang, Y., Qi, M. and Mei, C., 2004. Endogenous salicylic acid protects rice plants from oxidative damage caused by aging as well as biotic and abiotic stress. *The Plant Journal*, 40(6), pp.909-919.

Young, M.E., 2003. Circadian rhythms in cardiac gene expression. *Current hypertension reports*, 5(6), pp.445-453.

Young, M.E., Razeghi, P. and Taegtmeier, H., 2001. Clock Genes in the Heart Characterization and Attenuation With Hypertrophy. *Circulation research*, 88(11), pp.1142-1150.

Zagotta, W.N., Olivier, N.B., Black, K.D., Young, E.C., Olson, R. and Gouaux, E., 2003. Structural basis for modulation and agonist specificity of HCN pacemaker channels. *Nature*, 425(6954), pp.200-205.

Zeltser, D., Justo, D., Halkin, A., Prokhorov, V., Heller, K. and Viskin, S., 2003. Torsade de pointes due to noncardiac drugs: most patients have easily identifiable risk factors. *Medicine*, 82(4), pp.282-290.

Zhang, C., 2014. *Exploring Factors that affect electrical restitution in the Guinea Pig ventricle* (Bsc dissertation, Department of cardiovascular sciences).

Zhang, M. and Kass, D.A., 2011. Phosphodiesterases and cardiac cGMP: evolving roles and controversies. *Trends in pharmacological sciences*, 32(6), pp.360-365.

Zhang, Y.H., Jin, C.Z., Jang, J.H. and Wang, Y., 2014. Molecular mechanisms of neuronal nitric oxide synthase in cardiac function and pathophysiology. *The Journal of physiology*, 592(15), pp.3189-3200.

Zhang, Y.H., Zhang, M.H., Sears, C.E., Emanuel, K., Redwood, C., El-Armouche, A., Kranias, E.G. and Casadei, B., 2008. Reduced phospholamban phosphorylation is associated with impaired relaxation in left ventricular myocytes from neuronal NO synthase-deficient mice. *Circulation research*, 102(2), pp.242-249.

Zhao, M., Sun, L., Liu, J.J., Wang, H., Miao, Y. and Zang, W.J., 2012. Vagal nerve modulation: a promising new therapeutic approach for cardiovascular diseases. *Clinical and Experimental Pharmacology and Physiology*, 39(8), pp.701-705.

Zhao, Y., Brandish, P.E., DiValentin, M., Schelvis, J.P., Babcock, G.T. and Marletta, M.A., 2000. Inhibition of soluble guanylate cyclase by ODC. *Biochemistry*, 39(35), pp.10848-10854.

Zhou, L. and Zhu, D.Y., 2009. Neuronal nitric oxide synthase: structure, subcellular localization, regulation, and clinical implications. *Nitric Oxide*, 20(4), pp.223-230.

Zhou, L., Zhang, P., Cheng, Z., Hao, W., Wang, R., Fang, Q. and Cao, J.M., 2011. Altered circadian rhythm of cardiac  $\beta$ 3-adrenoceptor activity following myocardial infarction in the rat. *Basic research in cardiology*, 106(1), pp.37-50.

Zicha, S., Moss, I., Allen, B., Varro, A., Papp, J., Dumaine, R., Antzelevich, C. and Nattel, S., 2003. Molecular basis of species-specific expression of repolarizing K<sup>+</sup> currents in the heart. *American Journal of Physiology-Heart and Circulatory Physiology*, 285(4), pp.H1641-H1649.

Ziolo, M.T. and Bers, D.M., 2003. The real estate of NOS signaling location, location, location. *Circulation research*, 92(12), pp.1279-1281.

Ziolo, M.T., 2008. The fork in the nitric oxide road: cyclic GMP or nitrosylation?. *Nitric oxide: biology and chemistry/official journal of the Nitric Oxide Society*, 18(3), p.153.

Ziolo, M.T., Kohr, M.J. and Wang, H., 2008. Nitric oxide signaling and the regulation of myocardial function. *Journal of molecular and cellular cardiology*, 45(5), pp.625-632.

Ziolo, M.T., Maier, L.S., Piacentino, V., Bossuyt, J., Houser, S.R. and Bers, D.M., 2004. Myocyte nitric oxide synthase 2 contributes to blunted  $\beta$ -adrenergic response in failing human hearts by decreasing Ca<sup>2+</sup> transients. *Circulation*, 109(15), pp.1886-1891.

Zipes, D.P., Camm, A.J., Borggrefe, M., Buxton, A.E., Chaitman, B., Fromer, M., Gregoratos, G., Klein, G., Moss, A.J., Myerburg, R.J. and Priori, S.G., 2006.

Zobel, C., Cho, H.C., Nguyen, T.T., Pekhletski, R., Diaz, R.J., Wilson, G.J. and Backx, P.H., 2003. Molecular dissection of the inward rectifier potassium current (IK1) in rabbit cardiomyocytes: evidence for heteromeric co-assembly of Kir2. 1 and Kir2. 2. *The Journal of physiology*, 550(2), pp.365-372.

Zucchi, R. and Ronca-Testoni, S., 1997. The sarcoplasmic reticulum Ca<sup>2+</sup> channel/ryanodine receptor: modulation by endogenous effectors, drugs and disease states. *Pharmacological reviews*, 49(1), pp.1-52.

Zweier, J.L. and Talukder, M.H., 2006. The role of oxidants and free radicals in reperfusion injury. *Cardiovascular research*, 70(2), pp.181-190.

## **Appendix:**

### **Action potential duration restitution in guinea-pig ventricular myocytes using Standard restitution protocol (STRT)**

#### **Introduction**

To investigate action potential duration (APD) restitution in response to 10 nM ISO alone and then ISO plus 500  $\mu$ M L-NNA using STRT protocol.

#### **Methods**

-Guinea-pig left ventricular myocytes were used.

-Action potentials (APs) were recorded using the perforated patch-clamp technique at 35-37°C

-x100 APs were stimulated to reach a steady-state APD

-S1-S2 restitution protocol

- S1 stimuli x20
- S2 stimulus typically applied 300 ms after the final S1 stimulus
- Interval between the final S1 stimulus and the S2 stimulus decreased by 2ms with each repeat of the protocol until AP failure
- Decrements later modified to 5 ms

-Experimental conditions:

- Control
- 10 nM ISO
- 10 nM ISO + 500  $\mu$ M L-NNA

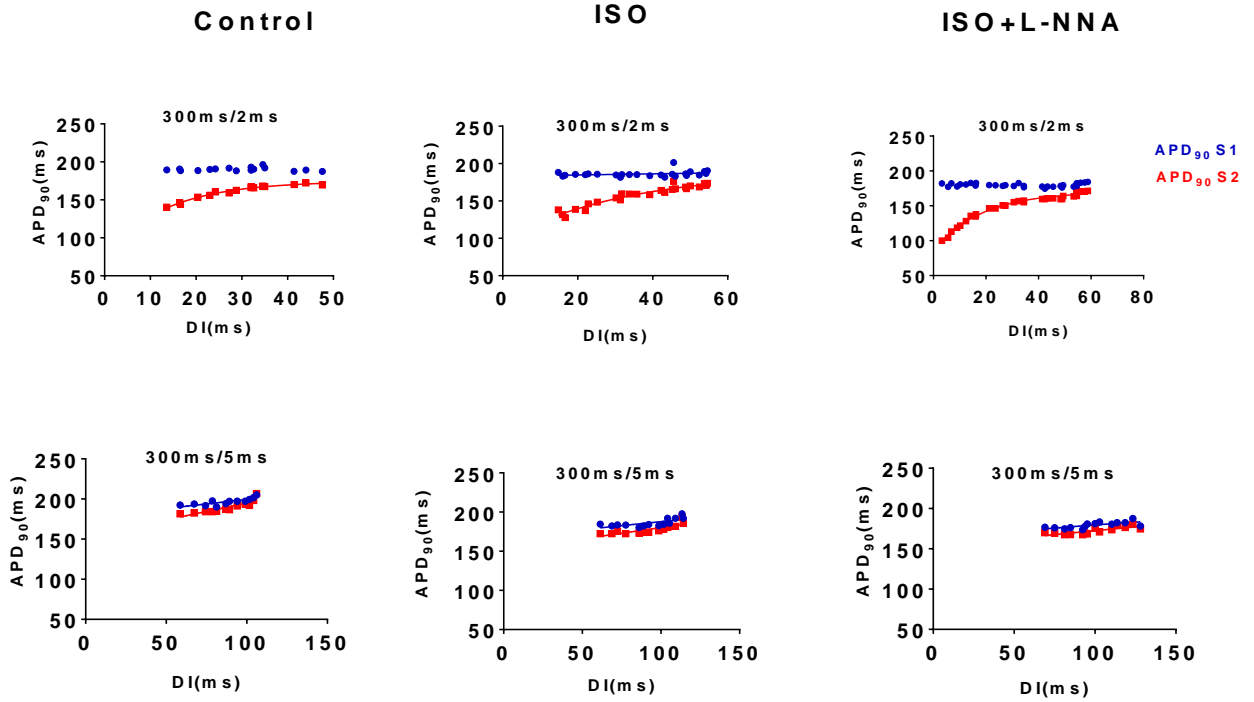
-AP failure was determined as >10% decrease in the AP peak amplitude

-S2 APD<sub>90</sub> data was curve fitted with a one phase decay equation

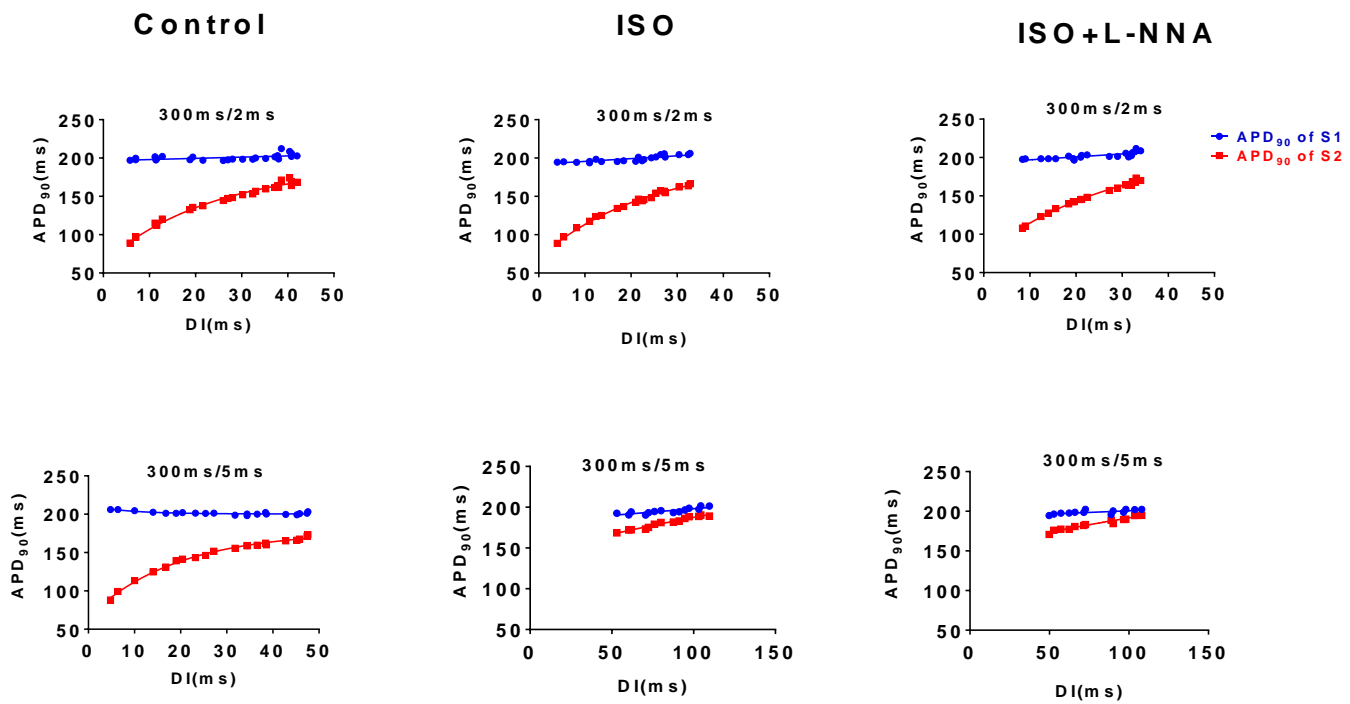
#### **Results:**

Data from 3 cells only was obtained. Roughly the cells did not show change in S2 APD<sub>90</sub> in response to L-NNA when applied in the continued presence of ISO. However, more cells should be obtained to make conclusions.

**Cell1:**

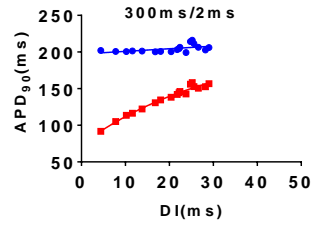


**Cell 2:**

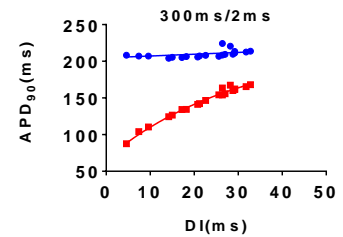


**Cell 3:**

**Control**



**ISO**



**ISO+L-NNA**

